U N I V E R S I T Y O F S U R R E Y

DEPARTMENT OF MECHANICAL ENGINEERING

''DEVELOPMENT OF AN ELECTRO-HYDRAULIC FLOATING DOUBLE-DISC VALVE''

by

AYO USMAN, BSc.

Thesis submitted for the Degree of Doctor of Philosophy in Mechanical Engineering

AUGUST 1984

SUMMARY

There is a need for low-cost switching and proportional electro-hydraulic valves with low contamination sensitivity and good reliability. In an attempt to meet this need, a novel electro-hydraulic floating double-disc valve has been developed to the stage where it can be used to control hydraulic cylinders or motors directly. As the valve is significantly underlapped, problems still remain in achieving adequate hydraulic stiffness in the proportional mode of operation.

The valve operation, which relies on the complex interaction between fluid and electro-magnetic forces acting on the valve discs, is described and a theoretical model of the fluid and electro-magnetic characteristics of the valve is presented. The theory shows satisfactory agreement with experimental data.

A pre-production version of the double-disc valve has been designed and manufactured and it incorporates ideas for manufacturing cost reduction while at the same time conforming to CETOP 3 international valve port standards. This valve has been successfully tested as a switching or proportional device when controlling two different cylinders. Proportional control of the valve is achieved using Pulse-Width-Modulation technique. British Technology Group and University of Surrey have applied for a patent on the valve. The patented floating-disc valve has the following features: (a) 3 way or 4 way 2-position or proportional action with minor changes to produce the two types of action, (b) cartridge construction with inter-changeable components, (c) low contamination sensitivity, (d) few critical dimensions, (e) no sliding surfaces, (f) CETOP valve port configuration and (g) potentially capable of operating with corrosive or non-lubricating fluids.

A. Usman AUGUST 1984

To My Parents

Acknowledgements

The author wishes to thank his supervisor, Professor G. A. Parker, for his help, guidance, invaluable suggestions and encouragement throughout the course of this research.

Thanks are also due to Mr G. Green, whose enthusiasm, patience, and machining skills made this research possible; Mr R. Warren, for fabricating the pre-production valve; Mr M. Jeffery, for his support with the computing system in the department and the author's colleagues, for their friendly attitude towards him.

The author is grateful to University of Surrey, for their studentship award for 1980/81 session; CVCP , for supplementing his school fees and Kwara State Government Scholarship Board of Nigeria, for their award that enabled him to complete this research.

Lastly, the financial support of the research by the Science and Engineering Research Council is gratefully acknowledged.

Table of Contents

APPENDICES

A_1, A_2, A_3, A_4 = curtain areas between nozzle and disc as denoted in Fig.6.1

A_c, A_{sn}, A_{nD} = cross-sectional areas of coil, supply and drain nozzles

$\bar{A}$ = non-dimensional area ratio ($=A_{nD}/A_{sn}$)

B_a, B_g, B_p, B_y = flux densities of armature (disc), working gap, pole core and yoke

B_f = transient flow force damping constant

b = passage height between the rod and drain nozzle

C_a, C_g, C_p, C_y = flux coefficients of disc, working gap, pole core and yoke

C_{FI}, C_{FX} = electro-magnetic force coefficients

C_{Dns}, C_{DnD} = supply and drain nozzle discharge coefficients

d_c = coil wire diameter

D_{ns1}, D_{ns2} = supply nozzle diameter with respect to disc 1 and 2

D, D_{nD}, D_R = disc, drain and rod diameters

f_s, f_L = space factor and coil leakage factor

F_m, F_f = electro-magnetic and fluid forces

$\bar{F}$ = non-dimensional fluid force ($=F_f/P_s.A_{sn}$)

F_{ft}, F_{rt}, F_{sd} = total fluid, transient flow and dynamic pressure forces

g = distance between the disc and the coil surface

$h_{1L}, h_{1R}, h_{2L}, h_{2R}$, = distance between disc and its chamber walls

H_a, H_p, H_y = magnetic intensities of armature, pole core and yoke

HG = holding gap

i, I = instantaneous current and current in the coil

K_q, K_c, K_p = flow gain, flow-pressure coefficient and pressure sensitivity

K_{qo}, K_{co}, K_{po} = valve null coefficients

K_f = steady state flow force spring constant

k = heat-dissipation coefficient

L = coil inductance

L_a, L_p, L_y	= magnetic circuit lengths of armature, pole core and yoke
L_t	= total magnetic circuit length
L_{snt}, L_{Dnt}	= supply and drain nozzle tube lengths
M_v	= mass of moving bodies with respect to the valve
N, NI	= number of coil turns and magnetomotive force
n_w	= number of working gaps
P	= pressure
$P_{b1}, P_{b2}, P_{u1}, P_{u2}$	= local pressures as defined in Fig.3.1
P(r)	= pressure at radius r
P_L	= load pressure ($=P_1-P_2$)
P_{te}, P_{ug}, P_u	= total effective, useful and total gap permeances
P_{fi}, P_{fo}, P_l	= inner, outer pole fringing and leakage permeances
Q, q	= flowrate
Q_1, Q_2, Q_3, Q_4	= flowrate through the four orifices denoted in Fig.6.1
r	= radius
r_{a1}, r_{a2}	= radius at which flow is assumed to be reattached with respect to discs 1 and 2 respectively
r_{t1}, r_{t2}	= mean radius of supply nozzle land with respect to discs 1 and 2
r_{dt}	= mean radius of drain nozzle land
r_{dG}	= radius at which the inward flow separate from the disc
r_o	= radius of hole through coil inner pole or the supply nozzle outer radius
r_1, r_2	= inner and outer wire bobbin radius
r_3	= outer coil body radius
r_{ns}, r_{nD}	= supply and drain nozzle radius
R_e	= local Reynolds number based on supply nozzle diameter
R	= disc radius
t	= time
t_a, t_p	= disc thickness and coil pole thickness

T_s, T_c = period of sawtooth waveform and coil time constant

T_D = total disc travel

u_1 = dynamic velocity of fluid through supply nozzle

x = disc displacement

$\underline{x}$ = non-dimensional disc displacement ($=x/T_D$)

X_g = gap between disc and coil surface

z = disc displacement from valve neutral position

z_{f1}, z_{f2} = distances between the supply and drain nozzle tips and the faces of the disc

θ_c = coefficient of linear expansion of the disc material

θ_f = final temperature rise of coil

θ_t = angle of tilt

μ = fluid viscosity

μ_g = permeability of gap

ρ = oil density

w = natural frequency

ζ = damping ratio

Suffices

d,D = drain

h = hydraulic

L,R = left-hand side and right-hand side

n = nozzle

s,S = supply

v = valve

1,2 = disc 1 or disc chamber 1 and disc 2 or disc chamber 2

1L,1R = left and right- hand sides of disc 1

2L,2R = left and right- hand sides of disc 2

List of Figures

List of Figures

List of Figures

List of Design drawings

List of Tables

CHAPTER 1

INTRODUCTION

1. Introduction

1.1 Servomechanisms

Servomechanisms can be used to control position, velocity, or force and have been used in practice for three to four decades in the industrial field of engineering [1].

A servomechanism is a feedback control system in which one or more of the system signals represent mechanical motion. The different types of servomechanisms are pneumatic, hydraulic, electric and electro-hydraulic.

1.1.1 Pneumatic servomechanisms

Pneumatic servomechanisms have received relatively little attention in comparison to other type of servomechanisms owing to the following disadvantages: (a) the fluid is compressible, the servomechanism will exhibit a lack of stiffness, especially to external load disturbances. (b) low efficiency. (c) it is difficult to achieve satisfactory low pressure sealing, and this puts a limit on system pressure.

However, owing to the constantly increasing temperature requirements for missile and aircraft components, high speed pneumatic control devices are being used [2].

1.1.2 Hydraulic servomechanisms

Hydraulic servomechanisms are widely in use in the machine tool industry for both the basic drive mechanism and the control of cutting tool [3,4]. In general, the advantages of hydraulic components are: (a) good stiffness characteristics, (b) ease of accurate control of working table position and velocity, (c) zero backlash, (d) rapid response to change in speed or direction and (e) low rate of wear.

In the aircraft industry hydraulic servomechanisms are used for power operated controls, autostabilisers and autopilots. In general industry it finds favour in speed control systems for prime movers, and in the operation of process control valves. The hydraulic servomechanism in its basic form has a hydraulic valve, actuator and a mechanical or electric feedback.

1.1.3 Electro-hydraulic servomechanisms

The increasing demands from modern control systems require greater flexibility between controlling elements. This has resulted in the combining of electrical signalling with fluid power actuators. The need to change from electrical to hydraulic control at some point in the loop has led to the development of an electric torque motor to actuate the hydraulic valve. The torque motor receives its inputs from an electronic amplifier. A block diagram of a typical electro-hydraulic servomechanism is shown in Figure 1.1.

In the last three decades, electro-hydraulic servomechanisms have been used for a wide variety of analogue control systems due primarily to their high power-to-weight ratio, inherent stiffness, compact construction, high accuracy, positive locking action, and fast dynamic response.

Recently, the rapid change in electronic technology and the development of microprocessors have presented an opportunity for the use of electro-hydraulic servomechanism in a digital mode. Now, microprocessors are being used in systems, either for presenting input data to the control system or as part of the control loop. As a result, there is considerable interest in hydraulic valves which are compatible with this concept.

Clearly, switching valves offer the best opportunity for digital electro-

hydraulic servomechanisms due primarily to their simple construction and cheapness. Digital electro-hydraulic servomechanisms have the following advantages over their analogue counterparts:

(a) Systems are generally cheaper and more reliable because of the simplicity of the basic two state element.

(b) Friction, non-linearities, and hysteresis have less influence on digital devices than on analogue systems.

(c) Control elements, such as valves of digital devices have switching functions and are therefore less sensitive to contamination.

(d) Switching states of digital control systems are less influenced by load changes and other disturbances compared to analogue systems.

(e) It is simple to programme digital systems.

Despite the above advantages, digital electro-hydraulic systems have the following undesirable and disadvantageous features:

(1) Input pulses may result in stepping and sometimes jerky movements of the output member.

(2) Resolution is not infinite.

(3) Dynamic response does not meet requirements in certain applications owing to the high data transmission rates required.

(4) Wear of valve seats.

(5) The additional cost of digital to analogue conversion where necessary.

(6) Pulsatile flow output may be a disadvantage in some applications.

(7) Problem of decoding digital data into analogue outputs (e.g. pressure).

Early development started with the adaptation of conventional servo-valves for a switching mode of operation [5,6]. Several investigators [6-13] have all looked into digital electro-hydraulic system in one form or the other. A brief discussion of digital electro-hydraulic control mechanisms are described by Günter [6] and Mansfeld [13]. Günter [6] also stressed that

digital electro-hydraulic control mechanisms require fast switching valves with low pressure drop. It is evident from their studies that the most important component for development in an electro-hydraulic servomechanism is the valve.

1.2 Electro-hydraulic valves

An electro-hydraulic valve, which is the most complex element in an electro-hydraulic control system, receives an electrical signal and converts it to an output flow to drive an actuator. Electro-hydraulic valves may be classified as a proportional (servo-valve) or digital (directional valve).

1.2.1 Servo-valves

Servo-valves are highly developed and sophisticated devices which provide control for a wide variety of analogue control systems [1]. They are designed so that the output flowrate is proportional to the electrical input signal under constant load conditions.

Servo-valves use an electric torque motor as their low power device to convert an electrical signal into hydraulic signal. For hydraulic power amplification purposes, servo-valves have at least two stages. The first stage has a flapper moving between two nozzles and the second stage has a conventional four-way sliding spool.

In spite of the advanced development of servo-valves, they have the following disadvantages:

(a) Precision components within the valve and caliberation requirements make the unit costs high. Typically the prices range from £700 to £2,000.

(b) Very small clearances, of the order 2.5 micrometer, within the valve make it very sensitive to fluid contamination. Hence, fine filteration of the hydraulic system and good maintenance is required for reliable operation.

(c) Jamming of the spool caused by silting when the valve has a period of inoperation.

Traditionally, servo-valves are used for analogue control applications but recently their use as switching devices have been investigated [14-18]. The major disadvantages of this approach are inertia limitations, increase wear and possible structural fatigue of the spool and its sleeve.

Murtaugh [18] was an early investigator of the pulse-width-modulation technique to operate an acceleration switching valve. The configuration of this valve was similar to that of a conventional electro-hydraulic flow control valve, except that the spool restraining springs were removed. Because of the double integration inherent in this two-stage valve, the no-load cylinder rod acceleration was proportional to the system error signal - hence the name 'acceleration switching valve'. The valve thus had a zero steady state velocity error. Levine [19] found that due to the removal of the restraining springs, the valve became sensitive to flow reaction forces, thus limiting the valve operation to a low flow range.

An intensive study made by Gorden [20] has shown that the PWM mode of operation does improve the stiction problem of the electro-hydraulic valve when compared to the conventional mode of operation.

1.2.2 Directional control valves

Directional control valves determine the flow path of the fluid in the system. They function to stop, start, check, divert, shuttle, proportion, the flow of oil in an actuator.

Traditionally, directional valves perform only switching functions and they operate on the on/off principle. Recently, solenoid proportional valves have been introduced in mobile applications. In these designs, either the armature position, or the force applied to it can be controlled.

With force controlled solenoids only a small movement results and these are normally used to operate a poppet valve which controls the flow of a pilot valve operating the main directional valve spool. With position controlling solenoids there is a closed loop control over the armature position and this is maintained irrespective of the opposing force. The electrical input current produces a movement of the armature which is transmitted directly to the valve spool. This movement is sensed by an inductive linear transducer, fedback to a servo amplifier and compared with the command input voltage. Using this form of closed loop positional control the valve spool can be operated remotely and moved to any desired position.

Depending on the flow capacity of these valves, they are used in either direct operated or pilot operated modes. To meet large flow rate requirements, most of the commercially available directional valves use a solenoid first stage and have a conventional 4-way spool type valve as the second stage. This may be augmented by a third stage spool valve for large flowrates.

Conventional directional valves are spool type valves and they have the following inherent disadvantages:

(a) jamming of the spool caused by contamination in the oil. This is mainly caused by silting when the valve has a period of inoperation.

(b) precision components within the valve increase the cost. Typically the prices range from 55 to 500 Pounds sterling for the directional control valves. The KG model of Sperry Vickers, for example, which is

essentially an electro-hydraulic directional control valve costs 1,300 Pounds sterling.

(c) relatively high power is required to operate these valves and their dynamic performances is very modest.

These disadvantages had led to a growing demand for directional valves with improved properties in respect to function reliability, longlife, leakproof end positions without increased production accuracy and extremely short switching times to increase the dynamic performance. These requirements could be met with seating valves. Seating valves use elements such as poppets, foils, balls, discs, etc.

In low-pressure pneumatic systems, fluidic seating valves with moving parts like the foil element [21] were developed for complex switching functions. Other fluidic elements, the ball element [22] and the disc element [23], may be used in high pressure hydraulic systems.

In 1971, Post [22] introduced the concept of a ball element valve into hydraulic systems. In his recent study [24], a switching valve system consisting of small diameter ball elements as the first stage, and fluid-controlled ball elements as the second stage was developed. He has shown that the complete switching times of multistage electro-hydraulic valves are in the range 1-20ms depending on system pressure and size of the desired output stage. The ball valves are being used in hone-machines, hydraulic break hammers and pile hammers applications. Mansfeld [25] has used ball elements in switching valves as digital control elements for an electro-hydraulic servo actuator used in flight-control systems.

The main disadvantage of a ball element valve is the problem of contamination. Although Post [24] pointed out that large particles in the convergent passage are pushed aside or impressed into the wall material by

the ball if it is operated with high pressures. This claim is doubtful in that this might lead to blockage after long use. Another major disadvantage of ball valves for direct actuation by an electro-magnetic field is that the flux density is poor thereby providing a low attracting force to overcome the fluid forces. Severe water hammer effects as the ball switches are also said to be a problem.

A simple geometric shape which overcomes these disadvantages is a free-floating disc valve element [23]. This type of disc was first considered by Schrenk [26] in his pioneering work on disc valves. Schrenk's interest was in the flow patterns and discharge coefficient of disc valves. His work has shown that if the valve land was large two major flow patterns would be possible. At low openings the flow clings to the land face and the discharge coefficient is high, at large openings the flow separates from the land and the discharge coefficient is smaller.

In 1965, Bahr [21] used a floating disc as a small fluidic logic element working on air with no electrical input signal. Later its use as a power device in an all pneumatic pulse-width-modulation scheme was investigated by Goldstein et el [27].

The flow around the nozzle land region of disc valves is similar to that of flapper valves. A vast number of papers [28-31] have been presented on the effect of discharge coefficient on flow and force characteristics of flapper valves. Takenaka et el [32] in their study of the dynamic and static characteristics of hydraulic control valves also pointed out that the main unknown factor in designing valves was the discharge coefficient. Lichtarowicz et el [33] also made some contribution on the discharge coefficient of valves. Later in 1975, Lichtarowicz [34] discussed the effect of valve land on flow and force characteristics of flapper valves.

Although many robots are now being produced for industrial use, capital costs of installing robots for new applications is high and as a result there is considerable interest in cheaper robots. Also in the hydraulic industry there is a great demand for cheap, simply constructed and reliable electro-hydraulic valves. One purpose of this investigation is to assess whether cheap hydraulic control systems have a role to play in these developments. As electro-hydraulic servo-valves are expensive and contamination sensitive, alternative types of cheap valve have been proposed which do not have these limitations [35].

The main objective of the present research is to develop two versions of a novel disc type electro-hydraulic valve to the stage where they can be used to control hydraulic cylinders. Such valve-cylinder combinations can be used for low-cost manipulators in the robotics and programmable automation fields. The valve can also be geared towards mobile plant and remote control applications. As a result of its simplicity in construction, the disc type valve is aimed to fill the gap between the highly sophisticated servo-valve and the normal digital on/off or directional valve.

1.3 Description of the disc valve

There are two versions of the valve that have been investigated in this thesis based on single- and double-disc configurations.

1.3.1 Single-disc valve

Figure 1.2 illustrates the main features of the single-disc valve which acts as a 4-way 2-position device. A free-floating disc moves axially between two opposing nozzles under the influence of electro-magnetic and fluid forces. The disc is constructed of magnetic material and forms a strong flux path with the magnetic material surrounding either coil when it

is energised. Each nozzle is connected to the hydraulic oil supply and load ports 1 and 2 are connected downstream of a restrictor but upstream of the tube through the coil. When, for example, coil 1 is energised and coil 2 de-energised the disc closes of the left-hand nozzle and the pressure P_1 in load port 1 rises to supply pressure, P_s. At the same time flow is discharged radially from the right-hand nozzle into an annular drain port so that P_2 in load port 2 falls to a value dependent on the relative restrictions of the restrictor and the coil tube. Hence a large load pressure difference (P_1-P_2) is generated which may be used to drive an actuator.

On the other hand if coil 1 is switched off and coil 2 switched on, the disc is attracted towards the right-hand nozzle by the attractive force of coil 2 and this force is augmented by the pressure gradient over the whole left-hand side of the disc until it seals off the right-hand nozzle. When this happens, the pressure P_2 rises to supply pressure P_s and P_1 falls to a value dependent on the relative restrictions of the restrictor and the coil tube. This generates a load pressure difference (P_2-P_1) to drive an actuator in the opposite direction.

The main use of the single-disc valve is probably as a pilot valve as there is no inherent facility for closing off supply flow in the switched state with a corresponding loss of power. Accordingly, the restrictors are quite small to limit the quiescent power loss thereby giving potential problem with contamination. However, the second variation of the valve employing a two disc arrangement does not have these limitations and may be used to control significant load flows as a single stage valve. The present research is concentrated on the double-disc valve configuration owing to these potential advantages.

1.3.2 Double-disc valve

The double-disc valve is shown in Figure 1.3 and has two single-disc chambers back-to-back with a loose push rod between the floating discs. The figure shows the valve fully switched to the right. In this position disc 2 closes off the drain nozzle and disc 1 closes off the supply nozzle. Coil 2 is de-energised and coil 1 is energised. Under these conditions disc 1 is held on the supply nozzle seat by the attracting force of coil 1, despite the axial pressure force exerted by the fluid in the supply nozzle tube trying to push the disc off its seat. On the other hand, disc 2 is held on the drain nozzle seat by the excess disc chamber pressure acting approximately over the drain nozzle area.

When the valve is switched the action is initiated by an electronic switching amplifier starting to de-energise coil 1 and at the same time energising coil 2. As the electro-magnetic force in coil 1 falls, disc 1 starts to move to the left owing to the excess pressure force from the supply. It is free to move until the axial clearance of the rod is taken up, (see Fig. 1.4), at which point disc 1, the rod, and disc 2 will start to move as a solid body if the total axial forces on the body produces a net force to the left. For the normal sizes of the supply and drain nozzles this net force will only give reliable switching under all load conditions if additional thrust can be generated over and above that available statically at the start of switching. By a careful choice of the rod clearance and its diameter, the radial flow outwards from the supply to load ports 1 is in a laminar, incompressible flow condition during the first movement of disc 1. This gives a pressure gradient over the whole disc chamber, rather than just the nozzle, thereby giving a thrust augmentation in a similar manner to a hydro-static thrust bearing.

The final stage of switching (Fig. 1.5) involves accelerating the two discs

and the rod to the left with the attracting force of coil 2 increasing as disc 2 approaches the supply nozzle. Just before disc 2 reaches the supply nozzle it ceases to be pushed by the rod as disc 1 has already sealed off the drain nozzle.

From Figures 1.3 to 1.5 it will be seen that the nozzles are not flush with the chamber end faces. The reasons for this are:

(a) it allows as much pressure balancing as possible round the disc in the steady-state conditions and

(b) the magnetic attraction force and remanence would be too large if the disc is allowed to adhere to the coil face.

Clearly, the correct choice of this gap, the disc travel, nozzle seat areas, diametric clearance between the disc and its chamber, and so on have to be carefully chosen for a successful design based on a wide range of operating conditions.

It is possible to operate the valve in a proportional mode as well and for this purpose pulse-width-modulation (PWM) techniques have been used to energise both coils to move the disc assembly around the mid-position without touching the nozzles. The feature which distinguishes the PWM mode of control from the conventional proportional control is that, instead of generating a signal proportional to the error, the amplifier generates a series of time width varying pulses which alternately drive the valve to its two extreme positions (see Fig. 1.6). A relaxation in machine tolerances is feasible with the use of PWM techniques. Several authors [20,27,36-43] have employed PWM techniques to linearise the non-linear characteristics of electro-hydraulic valves.

The frequency characteristics of a pulse-width-modulator was theoretically analysed in detail by Ikebe et el [41]. This was done from the viewpoint of

both the removal of the hysteresis characteristics and the use of the piezoelectric flapper type servo-valve they developed as the input member to the valve. It can be concluded from their work that for a sinusoidal input, the ratio of carrier frequency to the input frequency must not be less than 7, and the carrier frequency should be chosen to be high enough so that the amplitude of this frequency component can be ignored in a control system output and does not excite structural modes of the system.

Optimal control of hydraulic valves operating on the on-off principle have been considered by several workers [44-49].

1.4 Outline of project

As stated earlier, the aim of this research is to develop an electro-hydraulic double-disc valve to the stage where it can be used to control hydraulic cylinders. To achieve this objective, the internal operation of the valve needs to be accurately known. Experiments have to be carried out to verify any assumptions made in theoretical models of the valve.

The basic descriptions of the two types of experimental valves used in this work are described in Chapter 2. Also described are the associated electronic controllers.

The double-disc valve performances rely on the complex interaction between the fluid and electro-magnetic forces acting on the valve discs. Chapter 3 deals with the steady-state theoretical fluid and electro-magnetic characteristics of the valve.

In Chapter 4, the design of a physical model for the valve is described. Experiments carried out to determine the internal fluid mechanisms of the valve are presented. With the same experimental equipment, the electro-magnetic characteristics of the valve are also determined. The results are

compared to that of the theoretical model in Chapter 3.

The design considerations for the double-disc valve, based on the results of Chapters 3 and 4, are dealt with in Chapter 5. It is necessary to be able to establish the criteria for system stability and performance. To achieve this, dynamic equations of the valve are developed in Chapter 6 based on approximate lumped parameter concepts.

Chapter 7 deals with experiments carried out with the prototype and pre-production valves and possible applications of the valve are outlined. Chapter 8 draws conclusions and gives recommendations for further work.

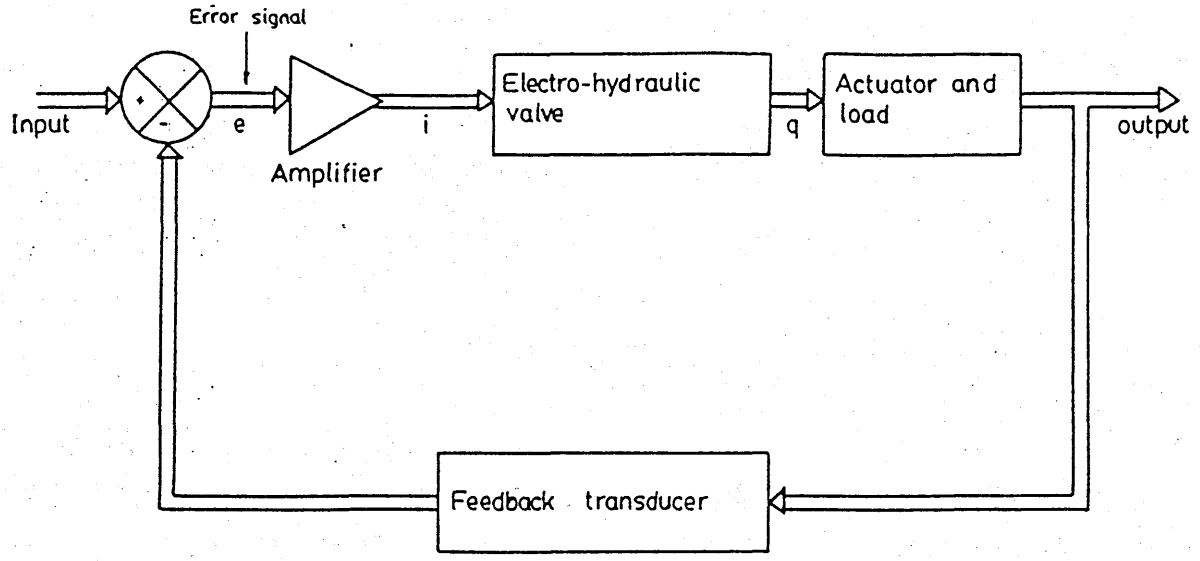

Fig-1-1 A block diagram of a typical electro-hydraulic servomechanism

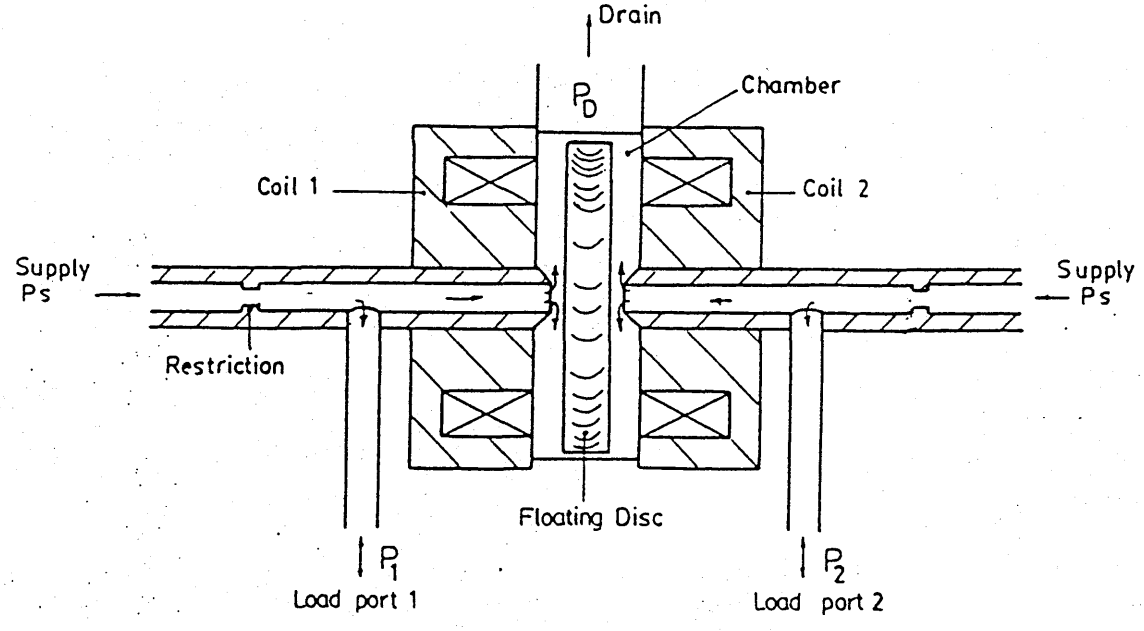

Fig-1-2 Single-disc valve

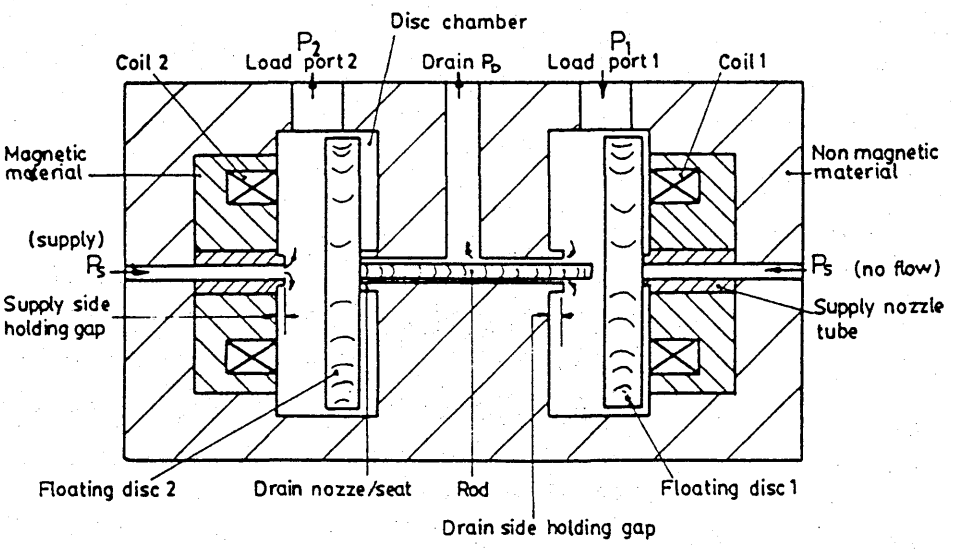

Fig. 1.3 Double-disc valve - at start of switching

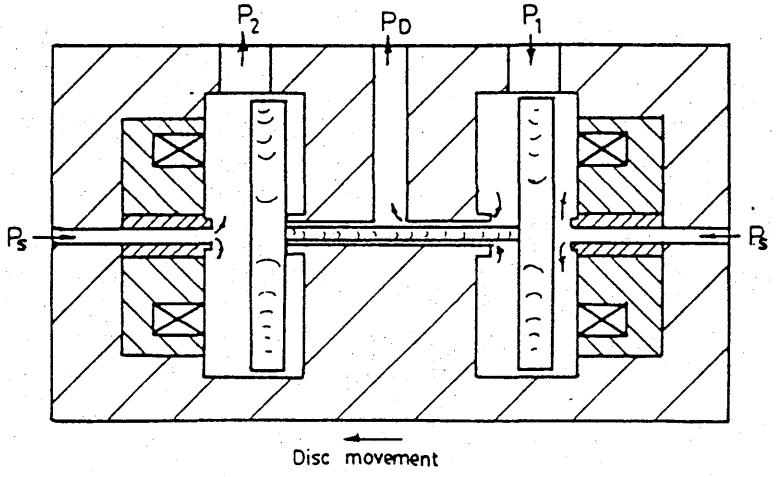

Fig. 1.4 Point of maximum thrust on disc 2 of a double-disc valve

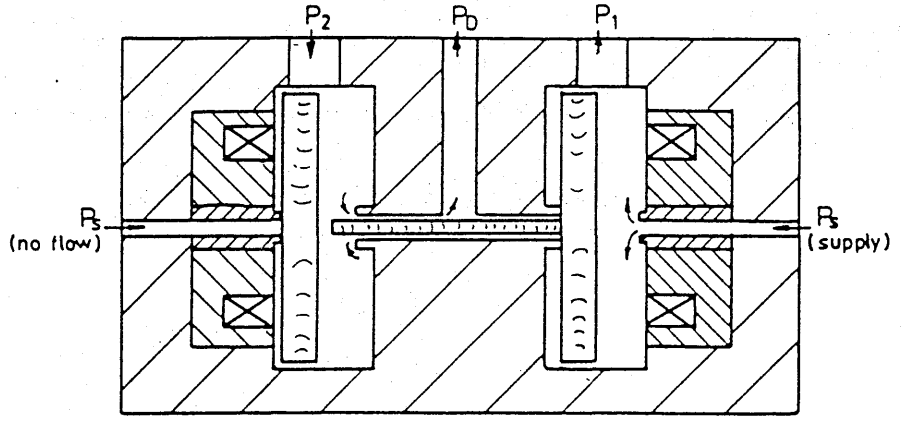

Fig. 1.5 Completion of switching of a double-disc valve

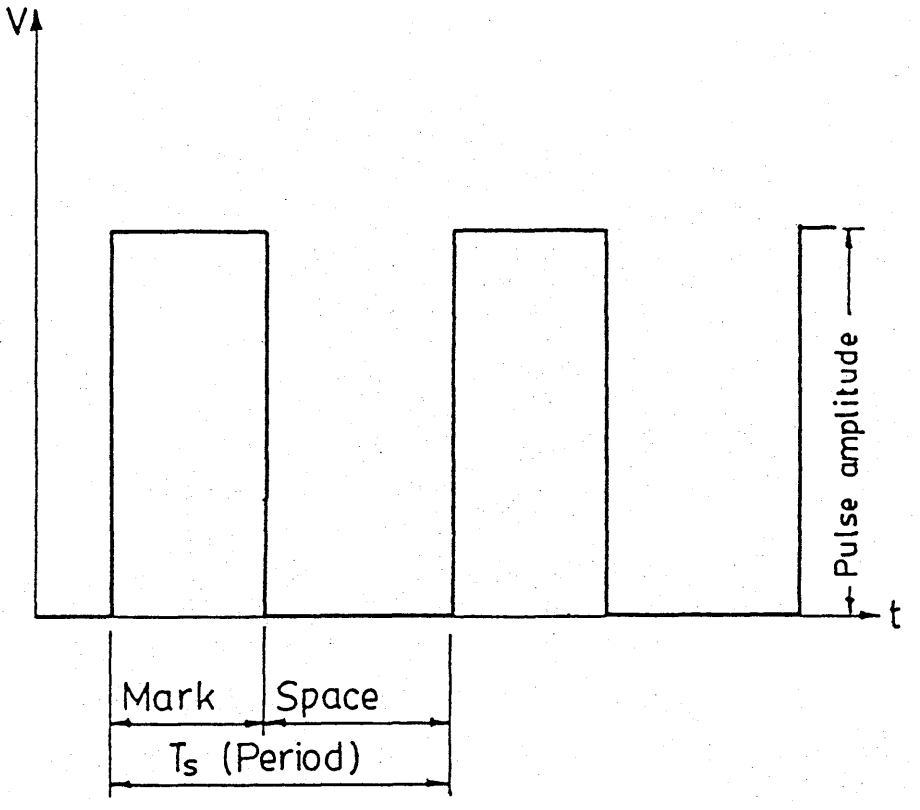

Fig. 1.6 A typical pulse-width-modulation signal

CHAPTER 2

EXPERIMENTAL VALVES AND CONTROLLERS

2 Experimental valves and controllers

During this study, two experimental double-disc valves were used. They were a prototype double-disc valve and the pre-production version of the valve. Extensive tests were carried out with the prototype valve to determine its characteristics and also to note the effect of parameter changes on its performance. In spite of several disadvantages of the prototype valve, the experience gained from experiments with it helped in the design and construction of the pre-production valve. This chapter describes the prototype valve and the design and production of the pre-production valve. The principle of operation of both valves, which remain the same, is as described in Chapter 1.

2.1 Description of a prototype double-disc valve

The prototype double-disc valve consists of three major components:- two identical valve end-covers and valve centre section. Fig. 2.1 shows an exploded view of the Prototype valve. The valve end cover incorporates the electro-magnetic coil assembly, supply nozzle tube, coil adaptor and a supply pipe fittings (see Fig. 2.2). The valve centre section has recesses for two disc chambers, two load ports and a drain port connections. For experimental purposes, the drain seats incorporating the drain nozzles, are screwed into the chamber faces of the centre section. This allows different drain nozzle configurations to be investigated.

Six radial slots are equally located around the disc chambers (see Fig. 2.2) which allows pressure balancing across the discs. There is also an annular groove in each valve end cover that links the radial slots in the valve centre section. Radial flow from each slot is collected in the annular grooves before it goes to the load ports. With this arrangement, the radial flow leaves the disc chamber to the load ports with low

hydraulic resistance and also ensures even flow distribution around the disc. The valve centre section incorporates two cross-drillings to allow miniature piezo-electric pressure transducers to be connected into the annular grooves to measure the load pressures in the two disc chambers.

The diameter of the disc chambers are slightly less than the outside diameter of the electro-magnetic coils to prevent the coils being pushed into the chambers by the flow through the supply nozzle tubes. The diameter of each of the disc chamber is 25.4 mm and the outside diameter of the coil is 27.0 mm. Both the supply and drain nozzles have projections (called the supply and drain side holding gaps respectively) into the disc chambers. The supply and drain side holding gaps are 0.13 mm and 0.38 mm respectively. The stops on the discs (see Fig. 2.3) associated with the holding gaps, are required to prevent the discs from damaging the nozzle seats. Initially, the depth of the stops on the discs is slightly less than that of the nozzle projections to ensure a good seal on the nozzle seats as it beds in with the disc after a few switching cycles. Damage to the soft iron disc is prevented by using a hard disc insert screwed into the disc. The supply nozzles are of diameter 2.54 mm and the drain nozzles are of diameter 3.80 mm. The drain nozzles are larger than the supply nozzles to accommodate the stainless steel rod of diameter 2.38 mm and length 38.0 mm. The floating disc is of thickness 3.60 mm and diameter 25.30 mm. The disc maximum travel in its chamber is 0.23 mm.

The valve housing and the nozzles are made of brass to reduce magnetic flux loss and remanence. The valve end covers and the coils are sealed by using 0 - rings. The coil has 380 turns of 34/35 SWG copper wire on a brass spool. It is sealed in the magnetic iron core with araldite cured by heating to 60^{o}C for 2 hours. The araldite seals two external wires to the coil and also provides a smooth face on the disc chamber end of the coil.

The core around the coil and discs are made of REMKO magnetic iron and heat treated after final machining operation to obtain good magnetic properties from the material. Owing to the difficulty of machining a narrow and deep annular housing for the coil windings, the magnetic core is made in two parts and pressed in afterwards to make a single body. The centre of the core is drilled for a supply nozzle tube used as a passage for oil from the supply. Copper coil windings around a brass spool are cemented into the housing of the core with apoxy resin. The winding terminals are brought out via a hole through the rear of the housing before being cemented.

2.2 Design and production of the pre-production valve

The prototype valve suffers the following disadvantages:

(1) wear of the nozzles and discs as the nozzles are made of soft brass. Shape not optimised to prevent cavitation.

(2) the clearance between the disc and the chamber diameters is not optimised and thus leading to disc jamming.

(3) the push rod is too long and buckling cannot be neglected.

(4) the disc thickness is not optimised.

(5) thermal effects are not taken into account in the rod dimension as well as non-optimal diametric clearance between the disc and its chamber.

(6) the two disc chambers cannot easily be made identical as the chambers are not accessible in the same way. They are also not interchangeable.

(7) oil leakage through the electro-magnetic coil assembly.

The supply and the drain nozzles of the prototype valve are not flush with the chamber end faces. This allows as much pressure balancing as possible round the disc in the steady-state condition and the attraction force and remanence would be too large if disc adhered to the coil surface. In consequence, the disc has to impact on the protruding nozzles, thus the

nozzles are prone to damage over a period of time. Damage could result in incomplete sealing on one side and hence lack of symmetry of performance. In addition, the push rod (made of silver steel) tends to dent the soft iron disc. This implies that the discs are also prone to wear. This wear problem in the prototype valve was overcome by making the following modifications:

(a) stops were added to the edge of the disc (see Fig. 2.3),

(b) having a silver steel disc insert in the disc (see Fig. 2.3) and

(c) replacing the brass nozzles with silver steel nozzles.

This implies that the central section of the valve is now made of hard material and that the push rod now impacts on the hard disc insert while the latter impacts on the hard protruding nozzles.

The wear problem becomes insignificant when operating the valve in a proportional mode using pulse-width-modulation techniques. With this mode of control, if the carrier frequency is high, the disc (armature) oscillates in the disc chamber without touching the nozzles.

The pre-production valve design is aimed at eliminating these disadvantages and the following are its advantages:

(a) The design is in cartridge form and is easy to assemble and dismantle.

(b) The valve is designed to suit both ISO and CETOP standards. The construction is simple and reduces pressure drop through the system to a minimum.

(c) There are few critical dimensions in the design. All the important components of the valve are produced by grinding or turning operations. With grinding operations, accuracy of $\pm$0.01 mm can be obtained.

(d) The stops on the discs of the prototype valve have now been removed from the pre-production valve. This means that the discs are now flat

and easy to produce. From the magnetic force-stroke characteristics, tests carried out with discs with stops indicate a highly non-linear behaviour which is less pronounced when the stops are removed.

(e) The stops on the discs of the prototype valve are now replaced with a stopping ring. The purpose of which is to prevent the hammering force of the disc on the protruding supply nozzle. The depth of the projection is important. It determines the amount of magnetic force available when the disc closes off the supply nozzle and also the pressure drop across the disc. The smaller the projection (supply holding gap), both the pressure drop and the magnetic force available increases. This holding gap can be altered by simply increasing or decreasing the thickness of the stopping ring and altering the length of the supply nozzle accordingly.

(f) Unlike the prototype valve, the drain nozzle and the drain seat are combined as one item. This item has four stops which are flush with the drain nozzle and thus the latter is protected from damaging. The drain seat is secured to the valve centre section with four 8BA screws. The outside diameter of the drain seat is slightly greater than that of the disc but less than that of the disc chamber diameter. To prevent internal leakage, an annular 'O' seal groove is provided. The amount of projection of the drain stops, which is called the drain holding gap (HG_D), can be altered at will in the pre-production valve by simply grinding the drain seat to suit the required depth. This is not possible with the prototype valve design. To adjust the holding gap in the prototype valve, the drain seat has to be unscrewed and turned to the required depth. This approach is unsatisfactory because there is no guarantee that the drain seat will be fully screwed to the required depth.

(g) The total disc travel in both disc chambers can easily be measured and

a correction made by grinding.

(h) For a given rod clearance, the length of the rod can easily be obtained without assembling the valve. The required dimensions are the total disc travel, the disc thickness, and the length of the valve centre section. These dimensions are available without assembling the valve. On the other hand, with the prototype valve, one side of the valve end cover, one disc and the centre section has to be assembled before the actual rod length could be obtained. In most cases, the other side of the valve has to be assembled and the rod length taken again. The average value then determines the rod length as the two disc chambers might not be identical. The drain diameter is greater than that of the rod and as such the measurement taken might not be accurate.

(i) The pre-production valve can be used as a switching or proportional device by simply changing any of the following items: (1) the push rod, (2) the drain seat, (3) the disc thickness and (4) the supply nozzle.

(j) The valve can be used for both high and low pressure applications by changing the quantities mentioned in (i) and making the necessary adjustments to the magnetic properties.

2.2.1 Design considerations

The design of the pre-production valve is as shown in the general assembly drawing number CDL3-1/1. Section D-D of the drawing is as shown in drawing number CDL3-2. Functionally, the valve has five major components: valve body, valve end cover, valve centre section, floating disc and flat-faced electro-magnetic coil.

(a) The valve body (13) made of dural aluminum alloy, incorporates the cross-drilling for the supply pressure P, drain T, service ports A and

B. The detail drawing of the valve body is given in drawing number CDL3-3. The port holes are counterbored for '0' seals (7). The load ports are at inclined angle to have CETOP 3 standard base mountings.

(b) The valve end cover (1) also made out of dural incorporates a recess to house a flat-faced electro-magnetic coil assembly and a coil adaptor. The detail drawing of the valve end cover is shown in drawing number CDL3-4. There are two identical valve end covers and they incorporate cross-drilling and annular grooves for supply of hydraulic oil into the valve chamber. The cross-drilling for the supply in the valve body links the annular grooves in the valve end cover. The valve end cover is fastened to the valve body with six M6 screws. Two holes tapped M6 are also provided in item (1) to be used when dismantling the valve assembly. A stopping ring (6) which is secured onto item (1) by four 8 BA screws acts as a stopping pad for the floating disc (10) and thus protect the protruding supply nozzle (2). The stops on item (6) flushes with the supply nozzle (2) tip. The stopping ring (6) is as shown in drawing number CDL3-7 and is made of non-magnetic stainless steel to reduce magnetic flux loss and remanence.

(c) The valve centre section (8), made of dural, incorporates cross-drilling for drain passage and annular grooves for the service ports and '0' seals. The valve centre section also have recesses for two drain seats (17) and two disc chambers that house the floating discs and the clearance left in the chamber for the disc movements. The push rod (15) made of stainless steel is also part of the valve centre section and is of length 24.89 mm and diameter 3.18mm. The detail features of the valve centre is shown in drawing number CDL3-5. Item (17), is shown in drawing no CDL3-7. Item (17) which is made of non-magnetic stainless steel, is secured into (8) with four 8BA screws. The drain nozzle is of diameter 3.81 mm and it accommodates the push

rod. The drain holding gap is 0.51 mm.

(d) The floating disc (10), made of REMKO soft magnetic material, incorporates a disc insert (16) which is made of harden silver steel. The detail feature of the disc and its insert is shown in drawing number CDL3-7/1. The disc form part of the electro-magnetic circuit of the valve. The floating disc is of thickness 0.38 mm and diameter 31.65 mm. The disc maximum travel in its chamber is 0.51 mm.

(e) The flat-faced electro-magnetic coil assembly has a supply nozzle (2), magnetic core (3), coil spool made of brass and a coil of copper wire type 34/35 SWG. The cross-section of the electro-magnetic coil assembly is shown in drawing numbers CDL3-6 and CDL3-6 MK2. The magnetic inner pole core and the outer pole core of drawing number CDL3-6 are combined as one item and made from REMKO soft magnetic iron. The detailed design procedure for the electro-magnetic coil is given in appendix A1. The supply nozzle is made of non-magnetic stainless steel. It has a diameter of 2.54 mm and it projects 0.13 mm into the disc chamber. The outside diameter of the electro-magnetic coil is 27 mm and the coil has 438 turns of copper wire of insulated diameter of 0.22 mm.

The pre-production valve was fabricated in the Mechanical Engineering Departmental workshop of University of Surrey, England. The exploded view of the valve is shown in Figure 2.4. Also shown in the figure is the CETOP size 3 sub-base mounting block which allows the complete valve assembly to be removed without disturbing the connecting pipes. Figure 2.5 shows the photograph of the assembled valve. The design was simple to construct and there were no problems experienced while fabricating the valve. The overall size of the valve is 70.0 mm x 76.0 mm x 127.0 mm long and weighs 1.8 Kg.

The electro-magnetic coil components are shown in Fig. 2.6. The magnetic cores of the electro-magnetic coils and the floating discs made of REMKO magnetic iron were heat treated after the final machining operation to obtain good magnetic properties from the material.

The strength of the bolts used to fasten the valve end cover to the valve body are established by BS84 standard [50] and Engineering Sciences Data Items No. 67019 and 72022 [51,52]. The result shows that six M6 socket head screws have sufficient strength with a factor of safety of 3.5.

2.3 Valve electronic controllers

Both switching and proportional modes of operation have been demonstrated in open and closed - loop position control modes. Chapter 7 deals with the experiments conducted with the valve in these modes. Digital and analogue pulse-width-modulator (PWM) and switching amplifiers have been constructed for use with the valves. The functions of the various amplifiers are presented below.

2.3.1 Four-level switching amplifier

The switching action of the valve is effected with a four-level switching amplifier. The current to each coil is controlled by the switching amplifier consisting of operational amplifiers, timers, diode wave clippers and a power transistor output stage. The detail design of this amplifier is given in appendix A2. The switching speed of the valve may be enhanced by using the established technique of overdriving the coil with a large amplitude pulse at the commencement of switching (see Fig. 2.7). The holding voltage provides enough electro-magnetic force to hold the disc on the supply nozzle seat after switching is completed. The input to the amplifier is a square wave and the timers in the amplifier provide the add-on pulse. The amplifier can generating a maximum current of 2 A when driven

by ±15 V power supply.

2.3.2 Analogue pulse-width-modulator

The proportional action of the disc valve may be achieved if a simple analogue pulse-width-modulator is used with the four-level amplifier. The analogue pulse-width-modulator has operational amplifiers and a comparator. The detail design of this amplifier is given in appendix A3. The principle of a pulse-width-modulation is described in appendix A4.

The constructed four-level switching amplifier has a limitation when used with the pulse-width-modulator (PWM) amplifier. The period of the add-on pulse from the monostable circuit of the four-level switching amplifier is constant at a set value. Under PWM mode, the add-on fixed time duration pulse from the monostable circuit dominates the control of the system at small mark/space ratios so that the PWM has no effect on the system. On the other hand, at large mark/space ratios, both the add-on pulse and the PWM controls the system. For a given carrier frequency, the add-on pulse width or duration remains constant when the mark/space ratio of the PWM changes. The effect of this is to create a hold-on (or step) current on one coil when the other coil current changes in a linear fashion with the mark/space ratio of the PWM. Typical results of an add-on pulse of duration 1.5 msec at a high carrier frequency are shown in Fig. 2.8. The figure shows that the add-on pulse introduces some non-linearity into the coil current as the d.c. input voltage of a PWM is varied for high carrier frequency. It also shows that the add-on pulse duration of 1.5 msec is too large for carrier frequency of 250 Hz. To operate the PWM at high carrier frequencies, the add-on pulse duration should be selected to be less than one-quarter of the maximum period of carrier signal. The add-on pulse duration can easily be altered by adjusting the timing resistor of the monostable circuit.

This limitation can be overcome by removing the add-on pulse from the switching amplifier. This implies that proportional control may be provided using the established pulse-width-modulation technique in which there is no over-driving of the coil with a large initial pulse. A special amplifier incorporating both pulse-width-modulator and switching amplifiers without add-on pulse is described in the next section.

2.3.3 Disc valve amplifier

The disc valve amplifier has an analogue PWM and a switching amplifier and the detail design is given in appendix A5. The pulse-width-modulation action of the amplifier is obtained with the aid of a built-in sawtooth waveform generator whose output is compared with an error signal to generate a PWM signal. This PWM signal drives the switching section of the disc valve amplifier. This amplifier can be used to provide both open and closed- loop control of the valve. The amplifier uses only one power supply as against two used in the four-level switching amplifier. With $\pm$15 V power supply, the amplifier can providing a maximum current of about 1.55 A.

2.3.4 Digital pulse-width-modulator amplifier

The valve can be controlled remotely via a microprocessor with the aid of a digital pulse-width-modulator. A 12-bit digital PWM amplifier, whose detail design is given in appendix A6, may be used with the switching section of the disc valve amplifier. To use the 12-bit digital PWM to control the valve, a 12-bit ADC (analogue to digital converter) board is required to convert the analogue command feedback signal to digital form for closed-loop operation. The 12-bit ADC board is also required to carry out the arithmetic summation of the command signal and the feedback signal.

An SBC-100 bus system was used as the micro-computer. The SBC-100 bus

system has a Cremenco board which has two serial and two parallel ports (the two parallel ports were used for the input/output transmission although only one serial port was used to communicate with an operator via a system console or VDU), ROM boards were used to store the computer software.

A computer program has been written in INTEL 8080 language to control the digital PWM. A flow chart of the computer program is shown in Fig. 2.9. PACL is the package command level and is the SBC-100 controller parameter access routine. The package can be loaded into read-only-memory (ROM) chips on the ROM board. To start the package power must be applied to the computer system when an automatic entry to the initialisation routines is made; if these procedures are successful an identification message is displayed on the system console.

PACL ddmmyy:
*

where ddmmyy/ is the day, the month, and the year of creation of the current version of PACL;

* is the package command request indicating that the system is ready to accept a command.

Alternatively, the package may be loaded from an external source into the RAM area of the computer system which enables the operator to undertake debugging, via the computer system monitor, during software development.

When the system is first activated, all system files are initialised with null arrays and the command level of package is entered. At this stage the user can ask for help by typing H or HELP and the following message will appear on the system console.

PACL FACILITIES AVAILABLE TO USER

DISPLAY	-	Display current values of controller parameter
RUN	-	Request to enter digital-pulse-width-modulator routine
EXIT	-	Request to jump to SBC-100 monitor level
HELP	-	Request for help
MSPT	-	Modify ''SPT''

where SPT holds the current values of controller parameter.

The control words to the digital PWM is initiated by the RUN command and the control words can be modified via MSPT command. The current content of the control words can be displayed via DISPLAY mode and EXIT stops any processing of the computer system and return command level to SBC-100 monitor. The package can trap errors and each error is displayed. All error service routines are treated as non-fatal and control is returned to the user.

This chapter has described the two experimental double-disc valves and their associated electronic controllers used in this work. The double-disc valve characteristics rely on the complex interaction between the fluid and electro-magnetic forces acting on the valve discs. The next chapter develops the steady-state theoretical fluid and electro-magnetic characteristics of the valve.

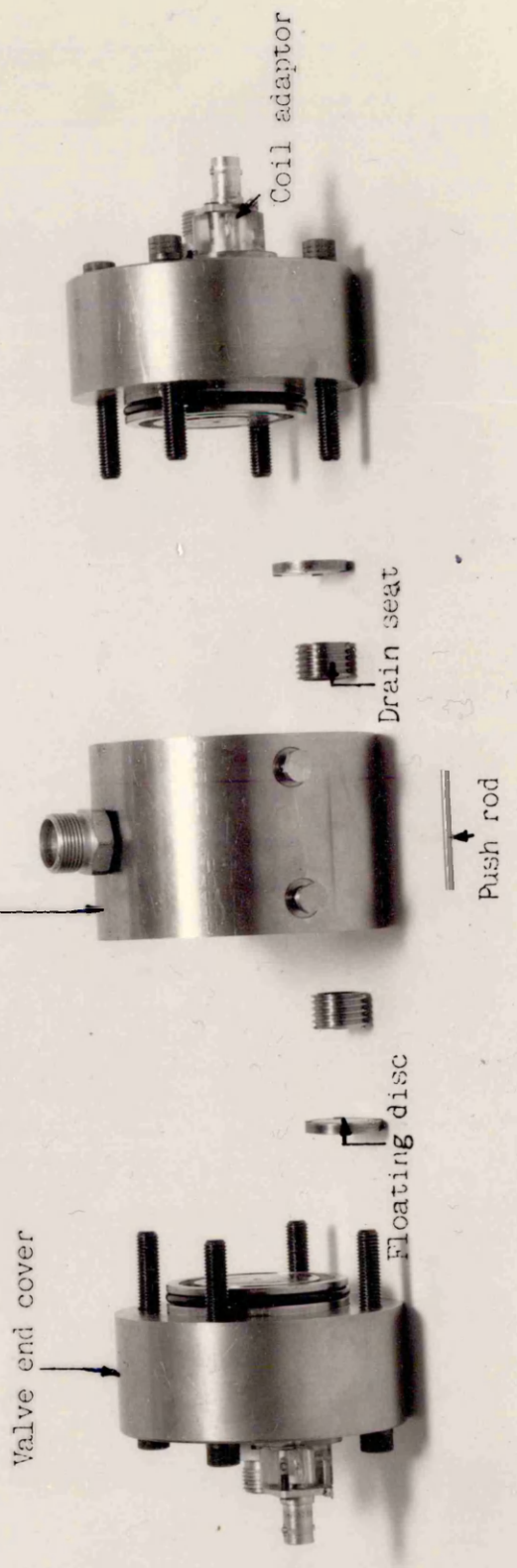

Fig. 2.1 Exploded view of a prototype double-disc valve.

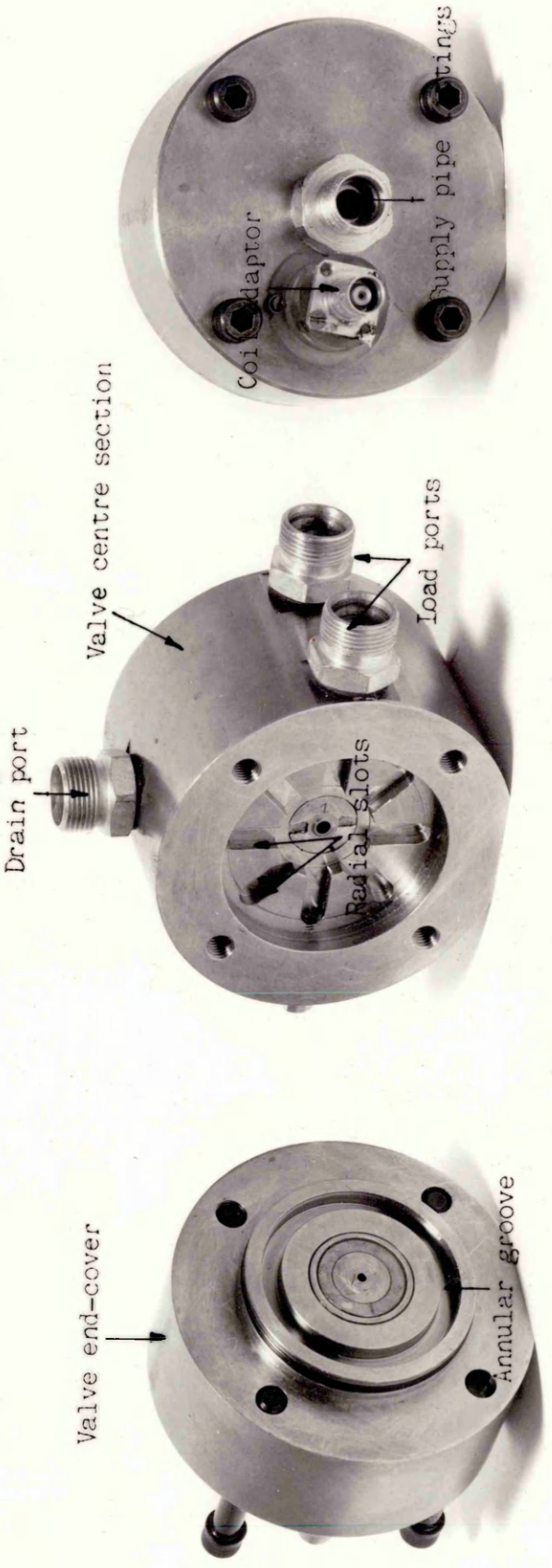

Fig. 2.2 Detail views of a prototype double-disc valve components.

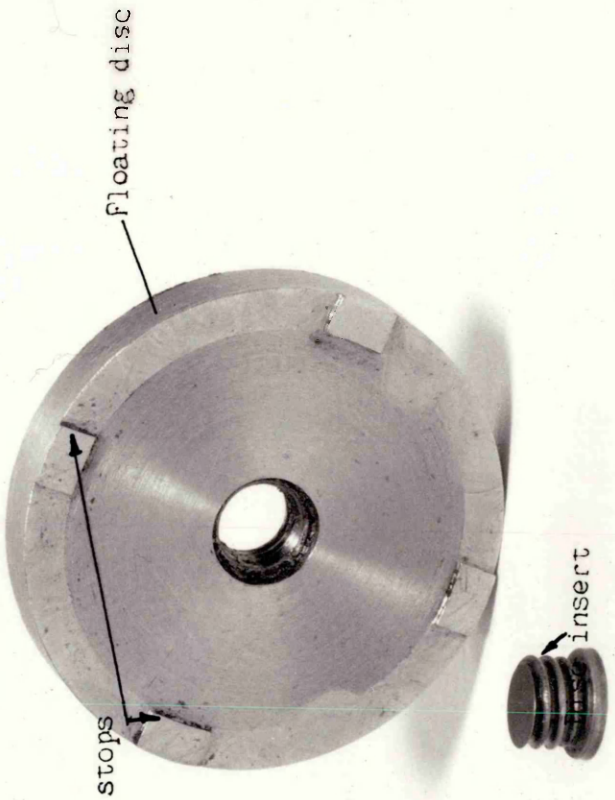

Fig. 2.3 Exploded view of a floating disc used with prototype valve.

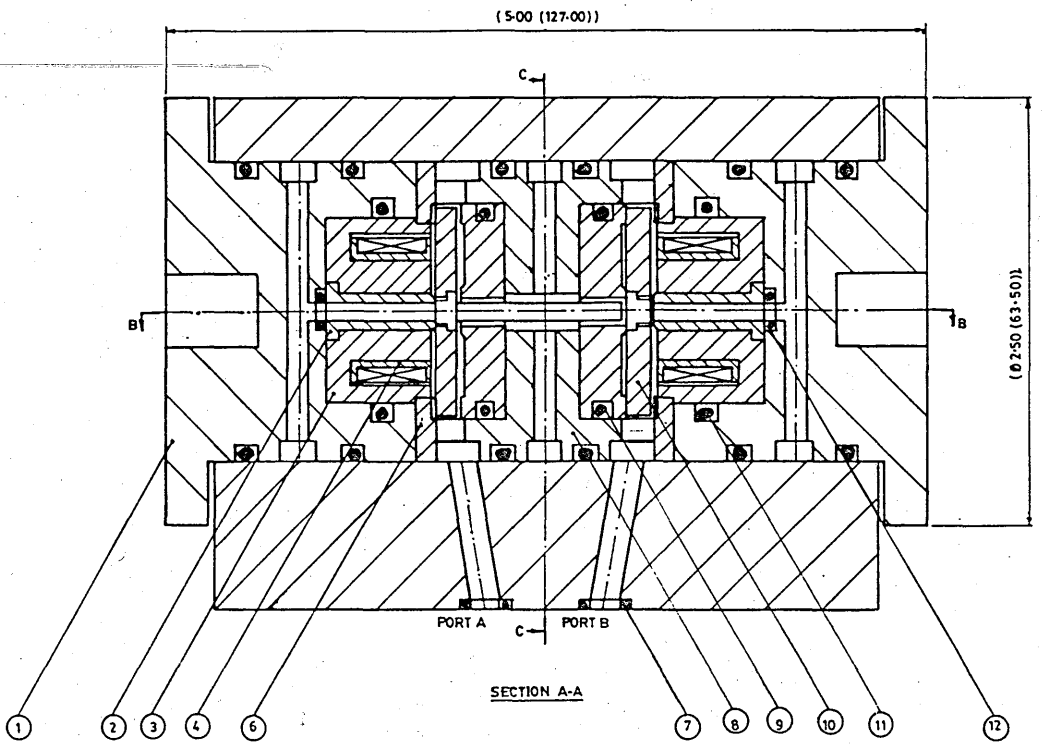

SECTION A-A

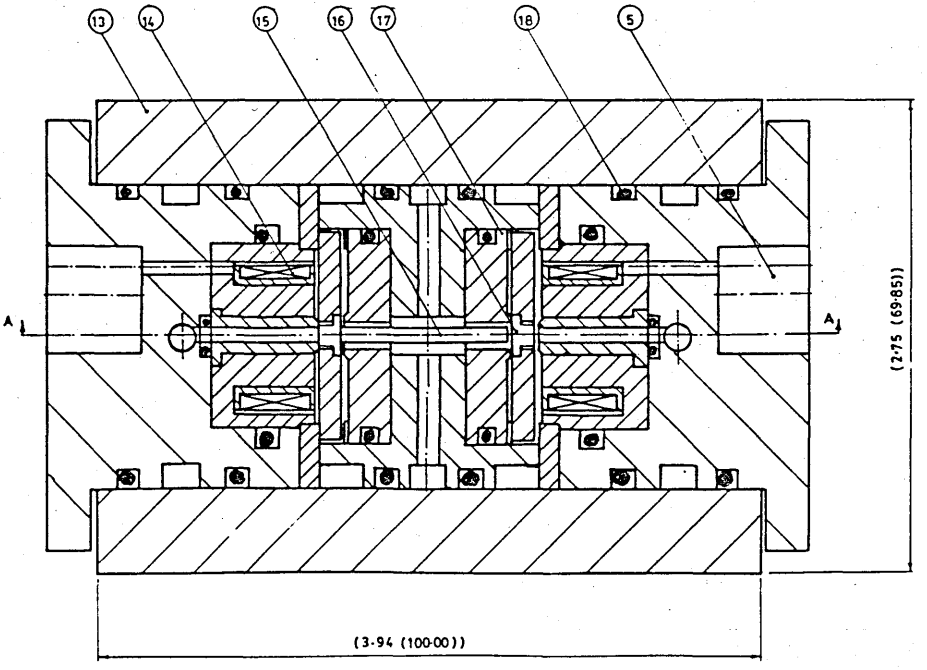

SECTION B-B

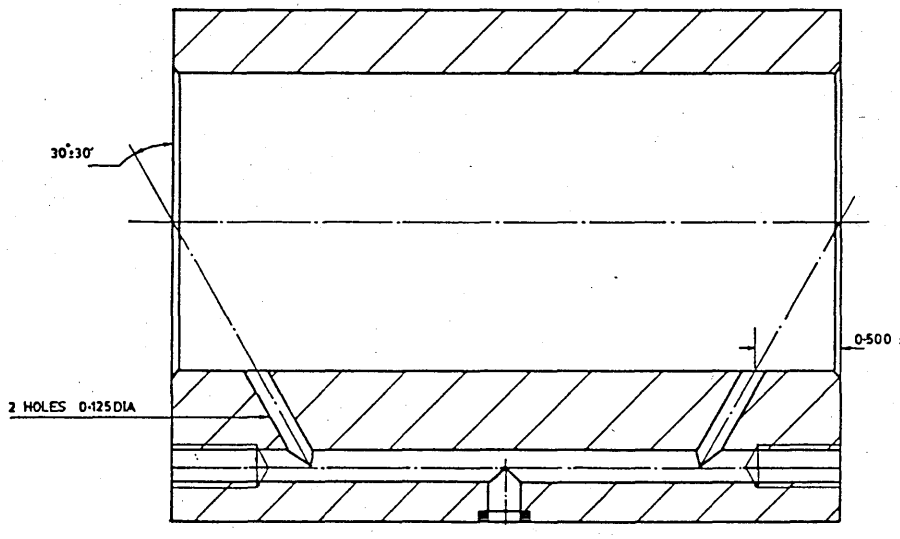
30°±30'
0·500 ±
2 HOLES 0·125 DIA

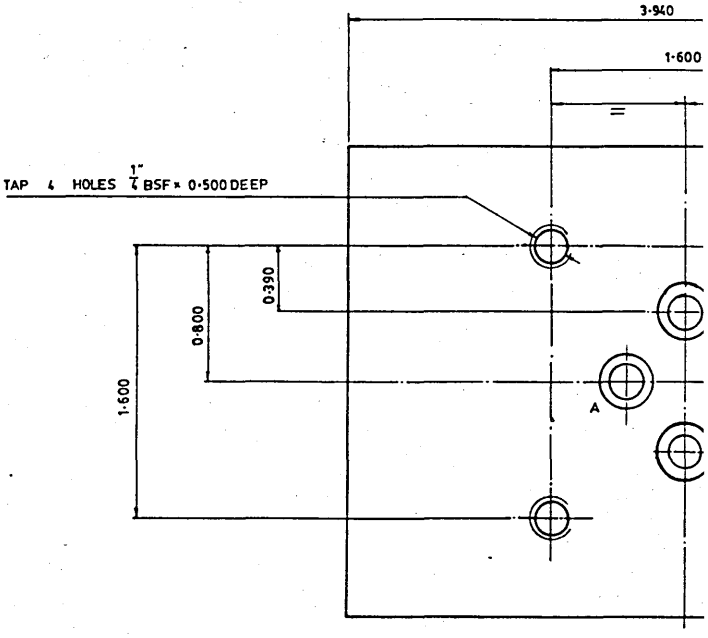

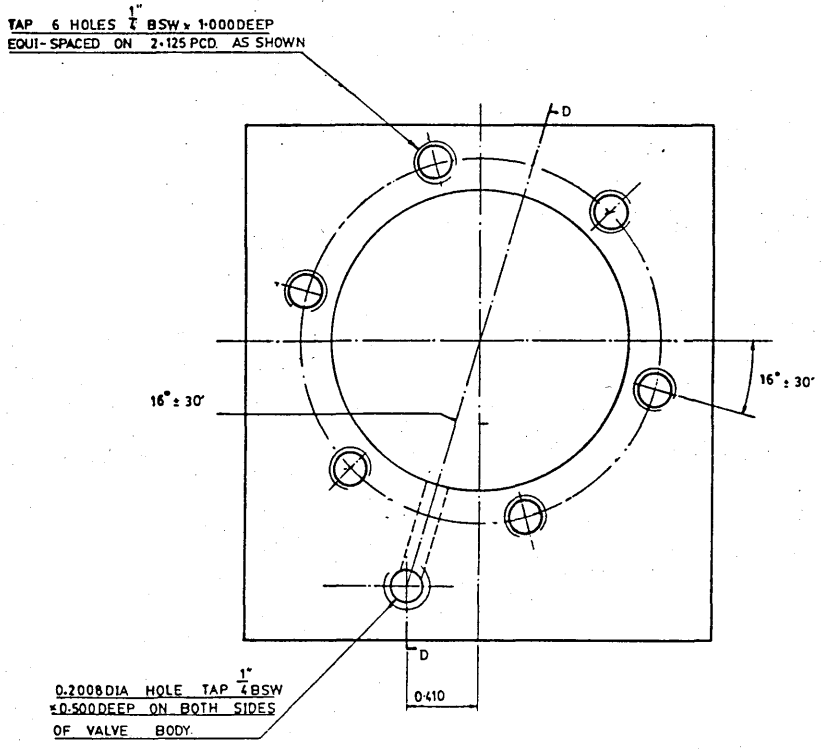

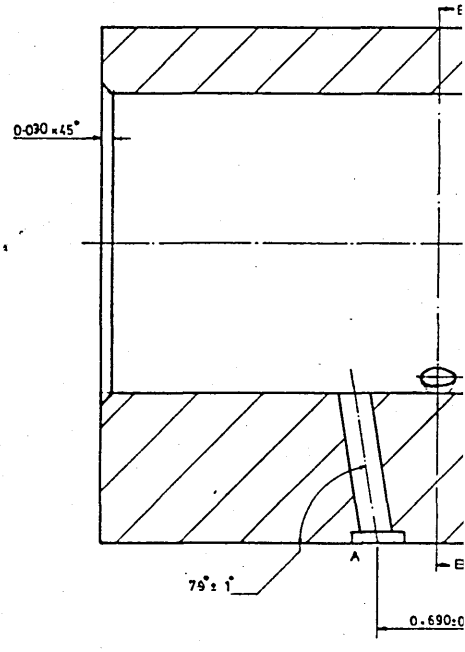

SECTION A

SEE DR'G. No. CDL3-2 FOR SECTION D-D

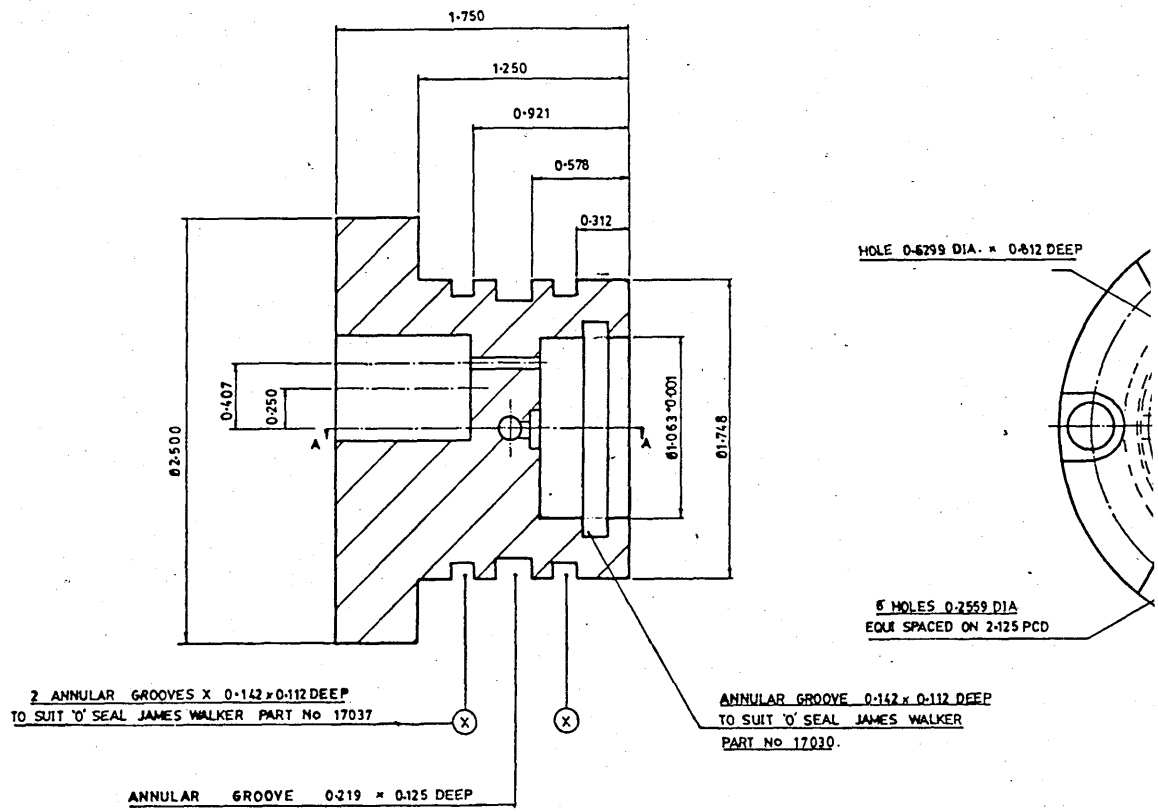

SECTION B-B

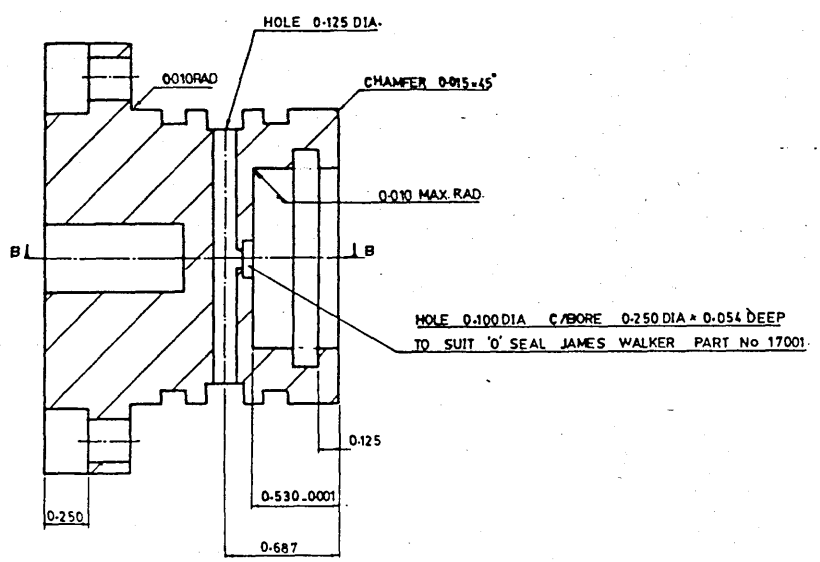

SECTION A-A

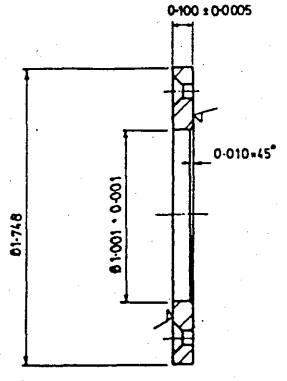

SECTION A-A

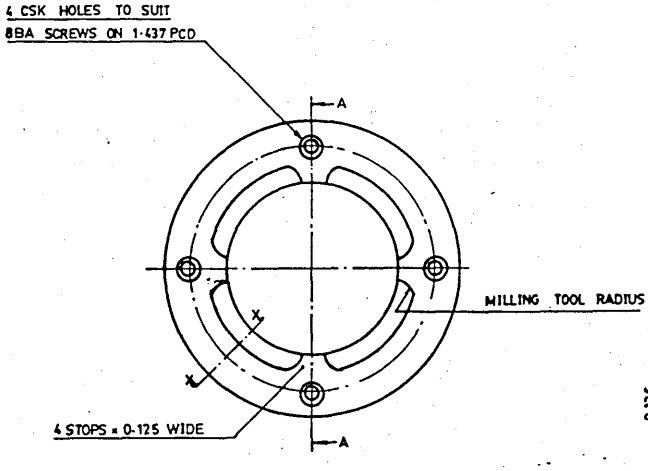

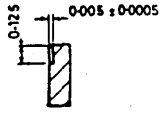

SECTION X-X

(6)

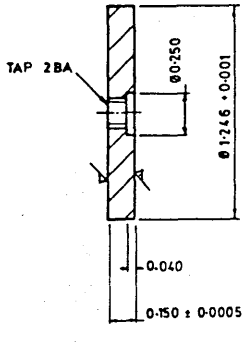

(10)

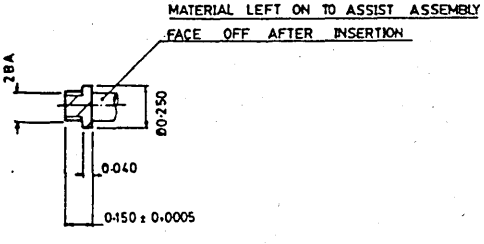

(16)

ASSEMBLE ITEMS (10) AND (16) WITH "LOCTITE"

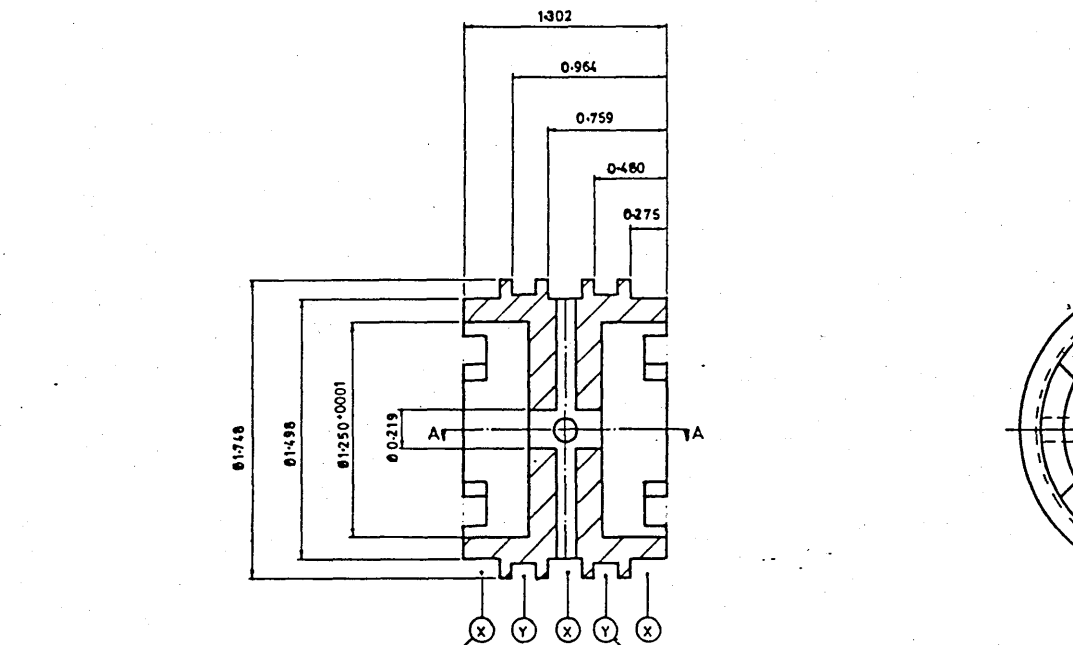

SECTION B-B

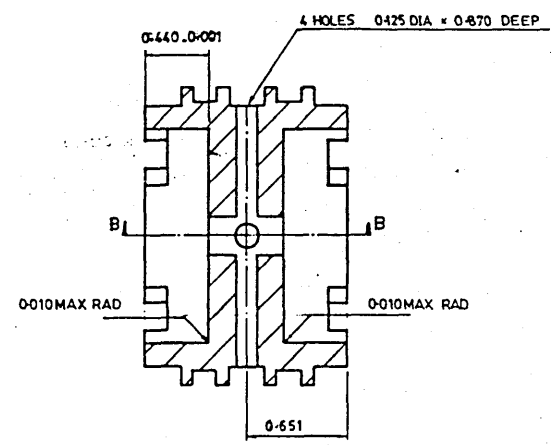

SECTION A-A

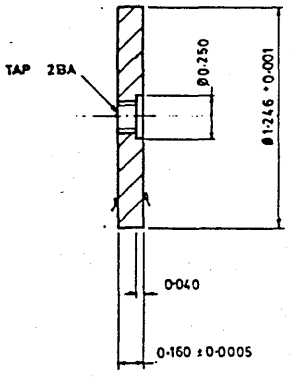

(10)

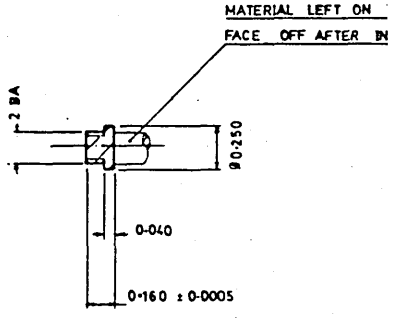

(16)

NOTES

1 ITEM (10) TO BE ANNEALED

2 ASSEMBLE ITEMS (10) AND (16) WITH "LOCTITE"

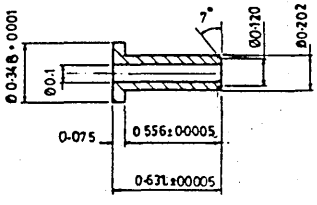

②

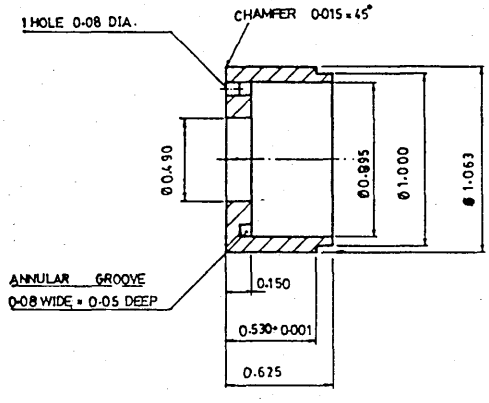

⑤

NOTES

1 TOLERANCE ON ALL DIMENSIONS ±0·001 UNLESS OTHERWISE STATED

2 ITEM (2) TO BE FORCE FITTED INTO ITEM (3)

3 THE ASSEMBLED ITEMS (2) AND (3) TO BE FORCE FITTED ITEM (5)

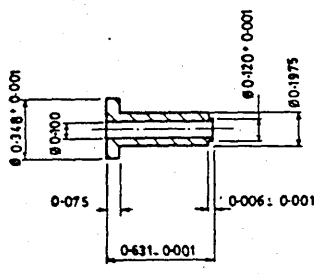

(2)

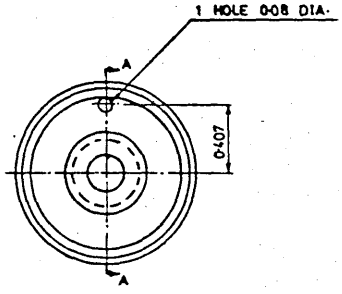

(3)

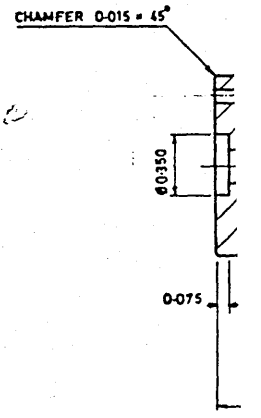

SECTI

NOTES

1 TOLERANCE ON ALL DIMENSIONS ±0·001 UNLESS OTHERWISE STATED
2 ITEM (2) TO BE HEAT TREATED
3 ITEM (2) TO BE FORCE FITTED INTO ITEM (3)

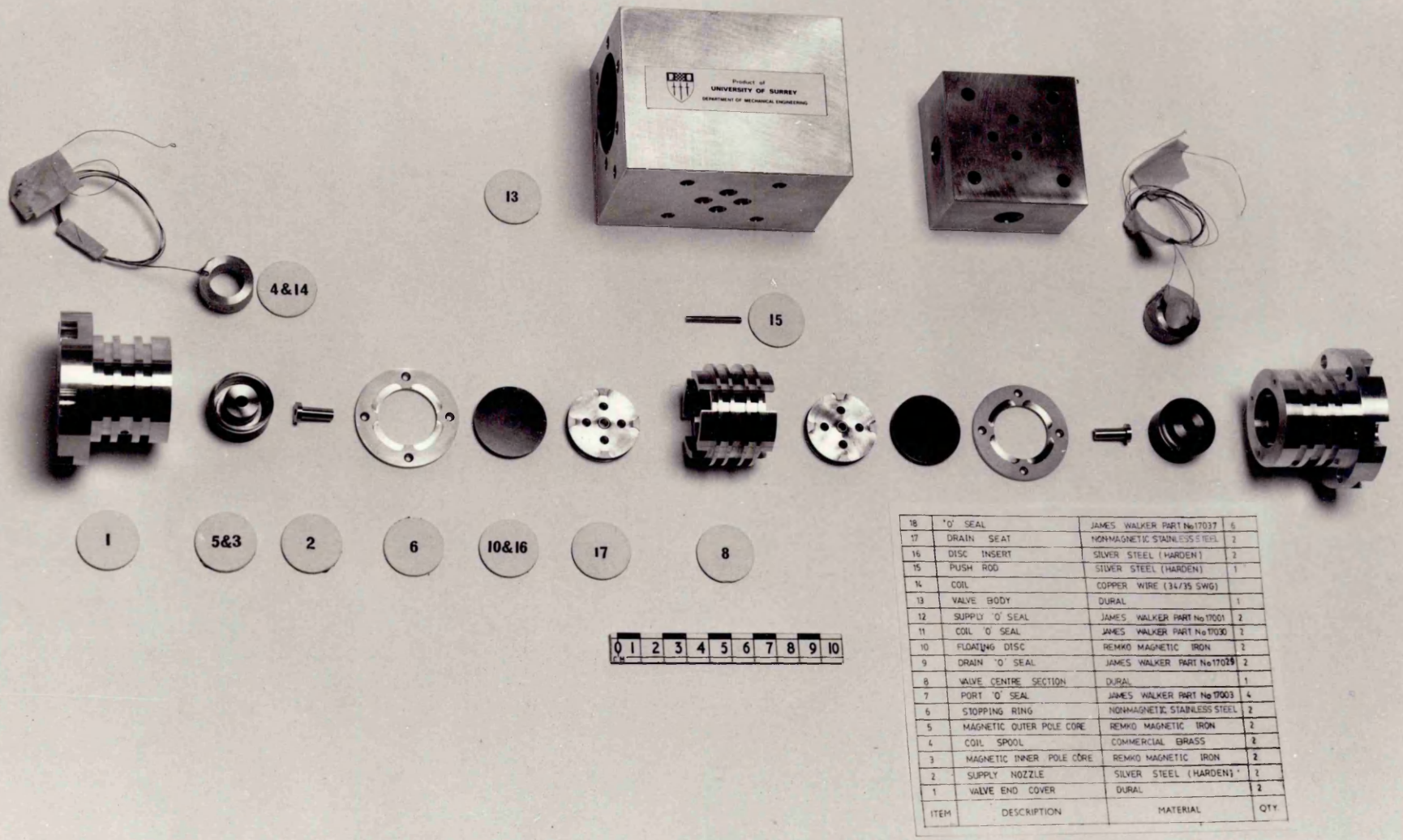

ITEM	DESCRIPTION	MATERIAL	QTY
18	'O' SEAL	JAMES WALKER PART No 17037	6
17	DRAIN SEAT	NONMAGNETIC STAINLESS STEEL	2
16	DISC INSERT	SILVER STEEL (HARDEN)	2
15	PUSH ROD	SILVER STEEL (HARDEN)	1
14	COIL	COPPER WIRE (34/35 SWG)	
13	VALVE BODY	DURAL	1
12	SUPPLY 'O' SEAL	JAMES WALKER PART No 17001	2
11	COIL 'O' SEAL	JAMES WALKER PART No 17030	2
10	FLOATING DISC	REMKO MAGNETIC IRON	2
9	DRAIN 'O' SEAL	JAMES WALKER PART No 17029	2
8	VALVE CENTRE SECTION	DURAL	1
7	PORT 'O' SEAL	JAMES WALKER PART No 17003	4
6	STOPPING RING	NONMAGNETIC STAINLESS STEEL	2
5	MAGNETIC OUTER POLE CORE	REMKO MAGNETIC IRON	2
4	COIL SPOOL	COMMERCIAL BRASS	2
3	MAGNETIC INNER POLE CORE	REMKO MAGNETIC IRON	2
2	SUPPLY NOZZLE	SILVER STEEL (HARDEN)	2
1	VALVE END COVER	DURAL	2

Fig. 2.4 Exploded view of a pre-production double-disc valve.

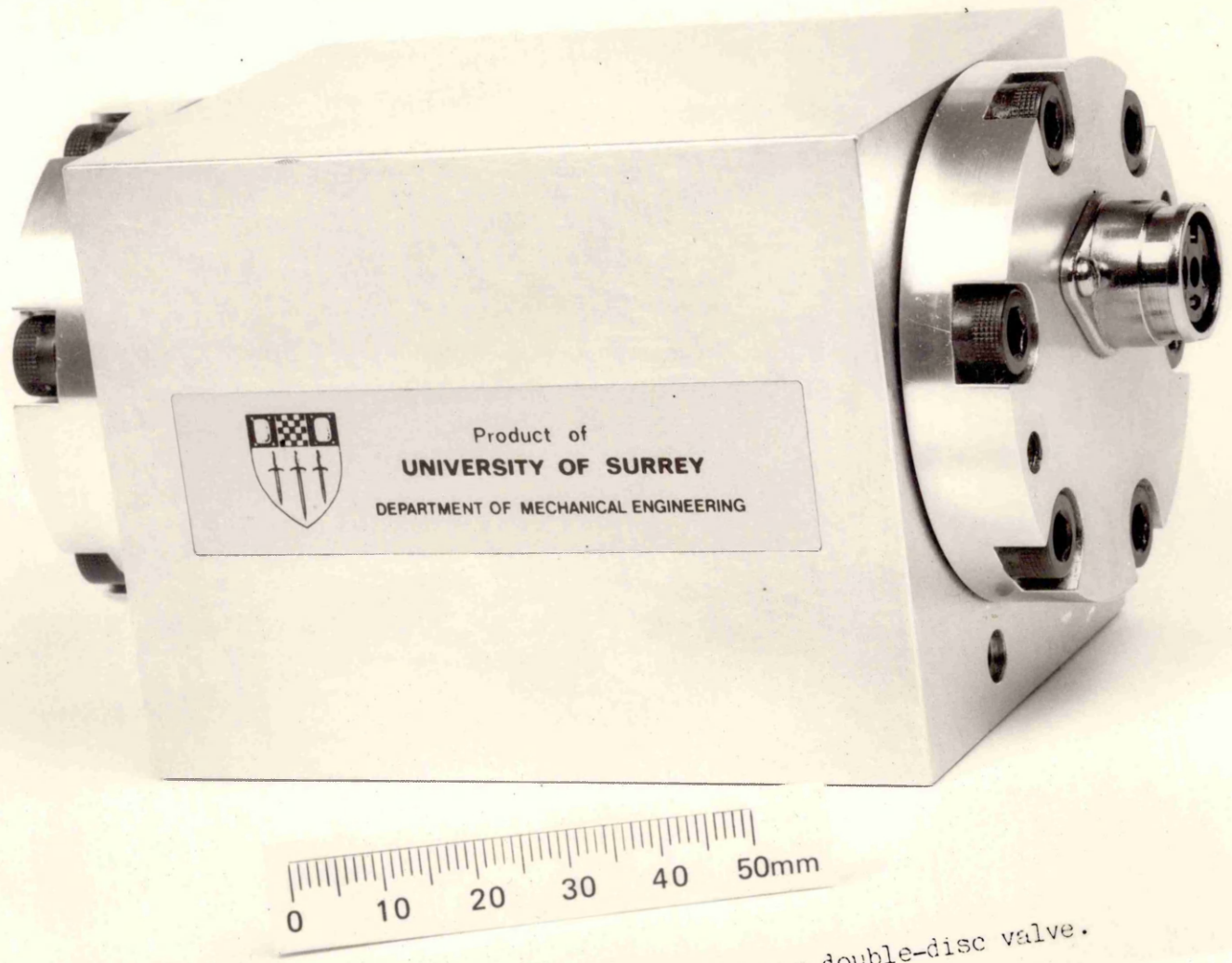

Fig. 2.5 Assembled view of a pre-production double-disc valve.

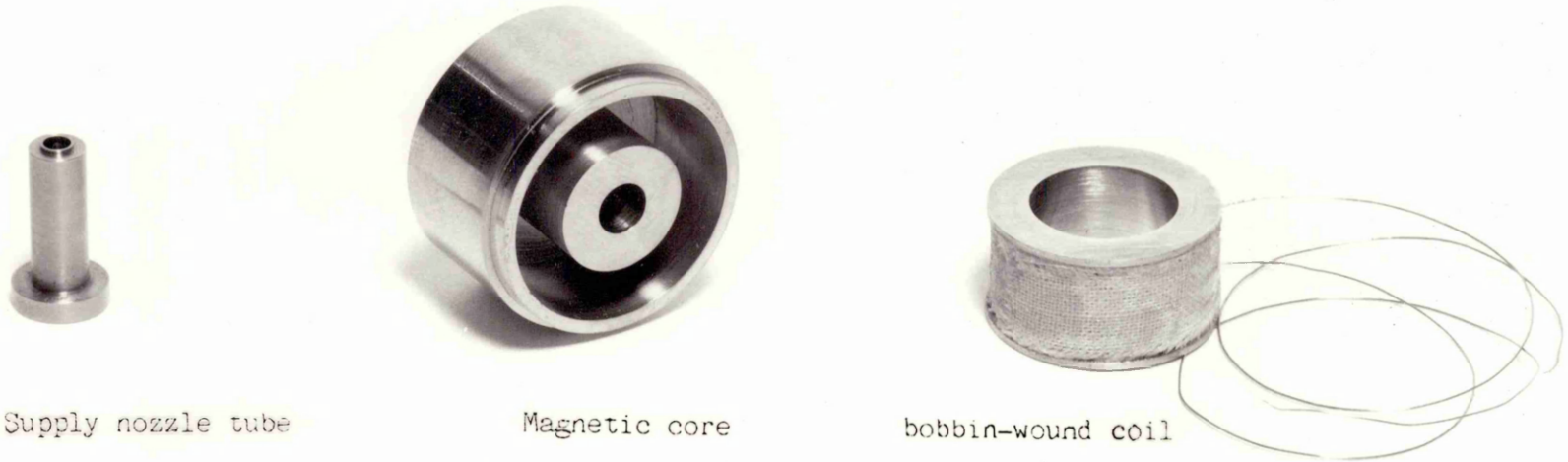

Fig. 2.6 Electro-magnetic coil components used in a pre-production double-disc valve.

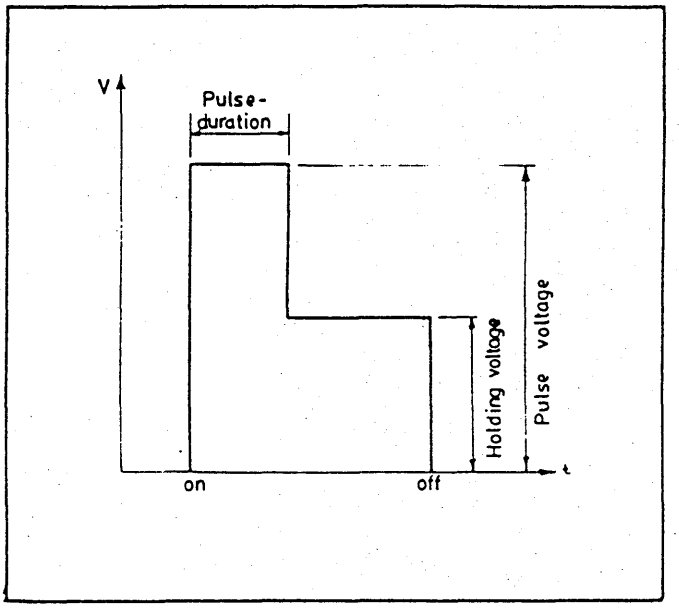

Fig. 2.7 A typical coil overdrive switching waveform.

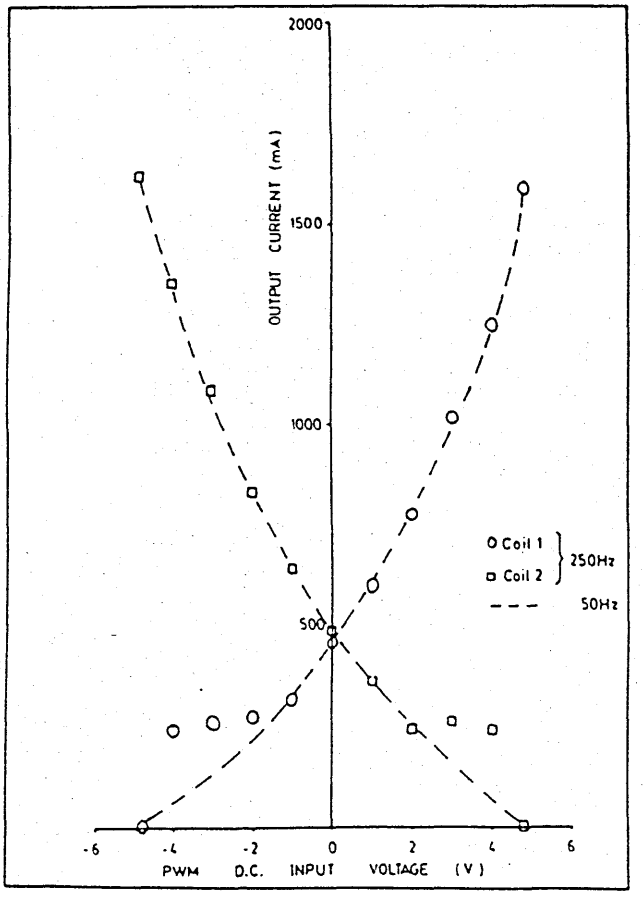

Fig. 2.8 Effect of coil overdriving pulse on valve proportional action with PWM.

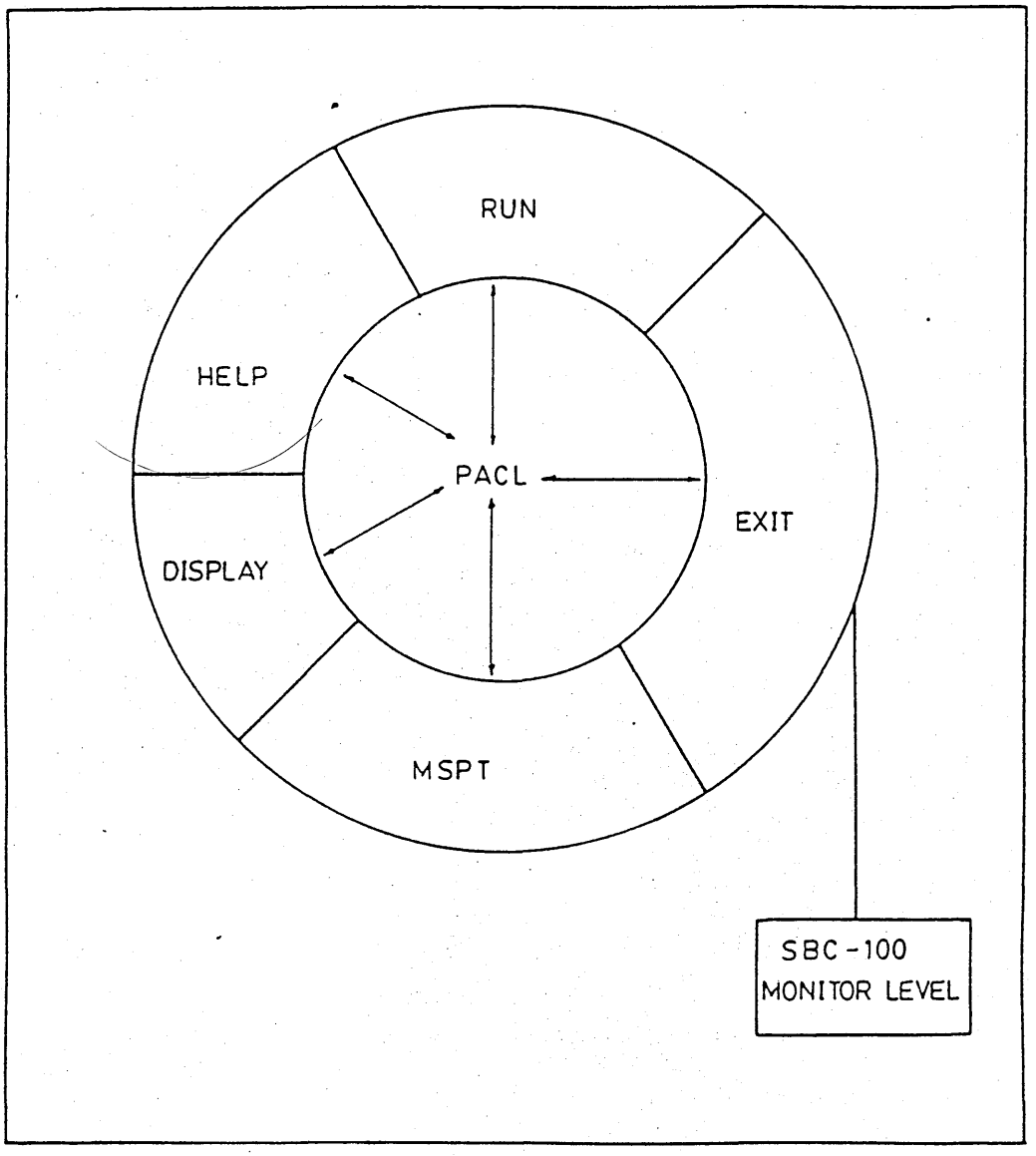

Fig. 2.9 A flow chart of a digital Pulse-Width-Modulator controller software.

CHAPTER 3

STEADY-STATE THEORETICAL MODEL OF A DOUBLE-DISC VALVE

3. Steady-state theoretical model of a double-disc valve

In this chapter, a steady-state theoretical model will be developed to predict both the fluid and electro-magnetic forces acting on the valve discs. The fluid mechanics of the valve will be dealt with first, followed by the electro-magnetic characteristics.

3.1 Steady-state fluid characteristics of valve

An understanding of radial flow between confined boundaries is of practical importance in the design of disc valves which employ the hydrostatic bearing principle. This study presents a combination of experimental data and a theoretical analysis of radial flow between the parallel space formed by the free-floating disc and its chamber wall using hydraulic oil.

Limited publications have been made of general radial flow between parallel discs. Their analyses, however, have been accomplished under different conditions, as the problems to which the results of their analyses are intended to apply are different. The characteristics of flat disc valves have been investigated by Oki [29] for the conditions that the region of a radial-flow is short and the clearance is wide. In 1964, Takenaka et el [28] also presented work on thrust on disc valves. Hagiwara [53] studied the characteristics of radial-flow nozzles. Moller [54] also investigated the radial flow between parallel discs.

In all these studies, the fluid from the source is supplied through a central tube or nozzle into the parallel space between the two discs and discharges to the atmosphere. In case of the double-disc valve under investigation, the free-floating disc is in contact with both an inward and outward radial flows. That is the free-floating disc is completely submerged.

Figure 3.1 shows the general geometry of the double-disc valve under investigation. The notation used through out this analysis is as shown in the figure, in which six distinct flow regions are defined. They are regions A, B and C denoted for the supply side of each of the disc elements, and regions D, E and F denoted for the drain side. Region A comprises the supply tube nozzle. Region B is defined for the supply nozzle land region and up to the point where the flow leaves the nozzle is assumed to be re-attached. Region C is the radial outward flow region formed between the floating disc and the supply side chamber wall. Region D is the radial inward flow region formed between the disc and the drain side chamber wall. Region E is defined for the curtain volume where the radial inward flow is affected by the drain nozzle protruding into the disc chamber. Region F is defined by the annular volume between the rod and the drain tube up to the drain port.

In Fig. 3.1, the flow from the supply, at pressure P_s, passes through both the curtain areas of the two supply nozzles into the supply side of the disc chambers. From the curtain areas, the flow is discharged radially outwards into annular grooves. The annular grooves link both the drain side of the disc chambers and the external load ports. From the annular grooves, either all or part of the flow discharges radially inwards into the drain side of the disc chambers. At the same time, some of the flow either passes into or comes from the external load into the disc chambers depending on the external load and the position of the discs. Finally, from the drain nozzles, the flow leaves the valve at drain pressure through an annular passage way formed by the drain nozzles and the push rod.

3.1.1 Pressure - flow equations

Region A : Assuming in this region that the flow is laminar, fully developed and incompressible, the flow through the supply nozzle tube is

given by

$$q_{LS} = \frac{\pi D_{ns1}^4}{128 \mu L_{snt1}} (P_s - P_{b1}) \qquad (3.1)$$

Region B : In this region, the valve is assumed to be operating on the orifice principle. The flow is further assumed to reattach at some distance of radius r_{a1} in a similar fashion to nozzle-flapper arm configuration. The flow is given by [55]

$$q_{1L} = C_{Dns}\, 2\pi r_{ns1}\, x \sqrt{\frac{2(P_{b1} - P_{1L}(r_{a1}))}{\rho}} \qquad (3.2)$$

This equation can be rewritten as

$$P_{1L}(r_{a1}) = P_{b1} - C_{12} \frac{q_{1L}^2}{x^2} \qquad (3.3)$$

where

$$C_{12} = \rho / (8\pi^2 C_{Dns}^2 r_{ns1}^2) \qquad (3.4)$$

As x is increased the annular curtain area ($\pi D_{ns1} x$) increases till $x = D_{ns1}/4$ when it is equal to the supply nozzle cross-sectional area. It can be seen therefore that the sensitivity of the valve will decrease since the importance of the nozzle resistance will increase as the disc travel (valve gap) is increased. At large openings the flow will be entirely controlled by the nozzle and changes in the disc travel will not influence the flow.

Owing to manufacturing constraints and because of the strength requirements the tip of the nozzle is not sharp and the land so produced can easily be greater than the disc travel or valve gap. Under such conditions, according to Lichtarowicz [34], the flow mechanism is no longer simple and considerable variations of the flow and force characteristics can be expected.

Region C : In this region, the following assumptions are made: (a) the flow is steady, (b) the flow is incompressible, (c) the flow is fully developed, (d) no rotation of the disc in its chamber, (e) the flow is only in the radial direction, (f) convective acceleration is negligible, (g) the disc is parallel to the chamber end walls and (h) the fluid films are so thin in relation to the dimensions of the components, measured within the plane of the surface, that the flow of fluid may be considered to be determined by viscous forces only, inertia effects being temporarily ignored.

Assumption (a)-(c) implies that laminar flow exist in this region. Under these conditions, the radial flow Navier-Stokes equation applies

$$\frac{\partial n}{\partial t} + n\frac{\partial n}{\partial r} + \frac{c}{r}\frac{\partial n}{\partial \theta} + w\frac{\partial n}{\partial t} - \frac{c^2}{r} = F_R - \frac{1}{\ell}\frac{\partial P}{\partial r} + \nu\left[\frac{1}{r}\frac{\partial}{\partial r}\left(r\frac{\partial n}{\partial r}\right) + \frac{1}{r^2}\frac{\partial^2 n}{\partial \theta^2} + \frac{\partial^2 n}{\partial z^2} - \frac{n}{r^2} - \frac{2}{r^2}\frac{\partial c}{\partial \theta}\right] \qquad (3.5)$$

The continuity equation is given by

$$\frac{1}{r}\frac{\partial}{\partial r}(nr) + \frac{1}{r}\frac{\partial c}{\partial \theta} + \frac{\partial w}{\partial t} = 0 \qquad (3.6)$$

If the fluid is assumed to be incompressible and uncavitated, then under assumptions (a)-(h) and from equations (3.5) and (3.6), the flow, q, across any annulus of radius r can be shown to be [56]

$$q = -\frac{\pi r h^3}{6\mu}\frac{dp}{dr} \qquad (3.7)$$

The negative sign signifying that flow will be outwards when dp/dr is negative and inwards when dp/dr is positive.

Integrating equation (3.7) and applying the boundary condition of $r = R_L$,

$p = P_1$ we have

$$P_{1L}(r) = P_1 + \frac{6 \mu q_{1L}}{\pi h_{1L}^3} \ln (R_L/r) \qquad (3.8)$$

where

$$h_{1L} = HG_s + x \qquad (3.9)$$

Equation (3.8) ignores inertia effects completely and represents, simply, a balance between pressure forces and viscous shear forces. In many low Reynolds number flows acceleration is present and inertia effects may be significant [57]. The most common field in which equation (3.8) is applied is that of hydrodynamic lubrication. Recent work in this field has focussed attention on inertia forces, and several workers [57-59] have indicated methods of analysing the viscous flow which include inertia effects. The methods described amount to solving the equation of motion approximately, in its integral form, as first suggested by Karman in his momentum-equation approach to boundary layer theory. Jackson et el [59] obtained an expression for the pressure distribution in a hydrostatic thrust bearing using an existing series expansion solution for radial flow between parallel planes.

The inertia term quoted by different authors are

$$\frac{0.150 \rho Q^2}{\pi^2 h^2} \left[\frac{1}{r_1^2} - \frac{1}{r_2^2} \right]$$ Liversey [57]

$$\frac{0.193 \rho Q^2}{\pi^2 h^2} \left[\frac{1}{r_1^2} - \frac{1}{r_2^2} \right]$$ Savage [58] and Jackson et el [59]

$$\frac{0.125 \rho Q^2}{\pi^2 h^2} \left[\frac{1}{r_1^2} - \frac{1}{r_2^2} \right]$$ McCandlish [60]

Savage [58] results agrees quite well with experimental data of Moller [54] using air as the fluid, except near the channel entrance where it falls below experimental data. Savage also agrees with that of Jackson et el [59]. It can be seen that the inertia effect predicted by Liversey [57] is some 23 per cent below that of Jackson et el [59] and Savage [58] and 17 per cent above that of McCandlish [60]. Jackson et el [59] results provide a reliable estimate of the pressure distribution in a hydrostatic thrust bearing taking account of inertia effects as well as viscous effects. Their result demonstrated that the inertia effect correction is underestimated by the momentum integral approach.

Using Jackson et el [59] inertia term, equation (3.8) becomes

$$P_{1L}(r) = P_1 + \frac{6\mu q_{1L}}{\pi h_{1L}^3} \ln (R_L/r) + \frac{0.193 \rho q_{1L}^2}{\pi^2 h_{1L}^2} \left[\frac{1}{R_L^2} - \frac{1}{r^2}\right] \qquad (3.10)$$

It can be seen that this is made up of a viscous pressure drop and an inertia contribution which is opposite in sense and which becomes progressively more important as the flowrate or the gap increases.

When $r = r_{a1}$, the radius at which the flow is assumed to be reattached to the disc, equation (3.10) becomes

$$P_{1L}(r_{a1}) = P_1 + \frac{6\mu q_{1L}}{\pi h_{1L}^3} \ln (R_L/r_{a1}) + \frac{0.193 \rho q_{1L}^2}{\pi^2 h_{1L}^2} \left[\frac{1}{R_L^2} - \frac{1}{r_{a1}^2}\right] \qquad (3.11)$$

The reattached radius r_{a1} is known from experiments to be equal to approximately 1.5 times the supply nozzle radius. That is

$$r_{a1} = 1.5\, r_{ns} \qquad (3.12)$$

Moller [54] theoretical and experimental results showed that with the flow separating at the channel inlet, the reattachment distance is a function of the channel width (distance between the disc and the channel wall) for a

given inlet nozzle diameter and is independent of Reynolds number and the diameter of the discs.

Region D : The flow in this region is similar to that of region C except that the flow is now inwards. Some work has been done on radial inward flow by Hagiwara [53] who carried out both theoretical and experimental investigations into radial outward and inward flow by using the Navier-Stokes equations. His results showed that the pressure loss as a result of inwards flow is greater than that of outward flow. The same inertia term but opposite in sense to that used in the outward flow is assumed to apply in this region. Therefore,

$$P_{1R}(r) = P_1 + \frac{6\mu q_{1R}}{\pi h_{1R}^3} \ln (r/R_L) + \frac{0.193 \rho q_{1R}^2}{\pi^2 h_{1R}^2} \left[\frac{1}{r^2} - \frac{1}{R_L^2} \right] \tag{3.13}$$

where

$$h_{1R} = HG_D + T_D - x \tag{3.14}$$

When $r = r_{dG}$, the radius at which the inward flow separate from the disc, equation (3.13) becomes

$$P_{1R}(r_{dG}) = P_1 + \frac{6\mu q_{1R}}{\pi h_{1R}^3} \ln (r_{dG}/R_L) + \frac{0.193 \rho q_{1R}^2}{\pi^2 h_{1R}^2} \left[\frac{1}{r_{dG}^2} - \frac{1}{R_L^2} \right] \tag{3.15}$$

Again r_{dG} is assumed to be 1.5 times the drain nozzle radius. That is

$$r_{dG} = 1.5\ r_{Dn} \tag{3.16}$$

Region E : In this region, the flow is assumed to follow an orifice type equation. The flow is given by

$$q_{1R} = C_{DnD}\ 2\pi\ r_{nD}\ (T_D - x) \sqrt{\frac{2(P_{1R}(r_{dG}) - P_{u1})}{\rho}} \tag{3.17}$$

Equation (3.17) can be rewritten as

$$P_{1R}(r_{dG}) = P_{u1} - C_{11} \frac{q_{1L}^2}{(T_D - X)^2} \tag{3.18}$$

where

$$C_{11} = \ell / (8\pi^2 C_{DnD}^2 r_{nD}^2) \tag{3.19}$$

Region F : In this region, the flow passes through the annular passage formed by the rod and the drain nozzle. The annular flow is by [55]

$$q_{1R} = \frac{\pi D_{nD} b^3 \left[1 + 1.5\left(\frac{\varepsilon}{b}\right)^3\right] \left[P_{u1} - P_D\right]}{12 \mu L_{Dnt1}} \tag{3.20}$$

where $b = (D_{nD} - D_R)/2$, passage height

ε = misalignment of rod from centre

If there is no misalignment (that is $\varepsilon = 0$) then equation (3.20) can be rewritten as

$$P_{u1} = P_D + \frac{12 \mu L_{Dnt1} q_{1R}}{\pi D_{nD} b^3} \tag{3.21}$$

Equating equations (3.15) and (3.18) and substituting for P_{u1} from equation (3.21) gives

$$P_1 = P_D + C_{18} q_{1R} + C_{11} \frac{q_{1R}^2}{(T_D - x)^2} - C_{15} \frac{q_{1R}}{h_{1R}^3} - C_{13} \frac{q_{1R}^2}{h_{1R}^2} \tag{3.22}$$

where

$$C_{13} = \frac{0.193 \ell}{\pi^2} \left[\frac{1}{R_L^2} - \frac{1}{r_{dG}^2}\right] \tag{3.23}$$

$$C_{15} = \frac{6 \mu}{\pi} \ln (r_{dG}/R_L) \tag{3.24}$$

$$C_{18} = \frac{12 \mu L_{Dnt1}}{\pi D_R b^3} \tag{3.25}$$

From equations (3.3) and (3.11) we have

$$P_1 = P_{b1} - C_{12} \frac{q_{1L}^2}{x^2} - C_{16} \frac{q_{1L}}{h_{1L}^3} - C_{14} \frac{q_{1L}^2}{h_{1L}^2} \tag{3.26}$$

where C_{12} is as defined in equation (3.4) and

$$C_{14} = \frac{0.193 \rho}{\pi^2} \left[\frac{1}{R_L^2} - \frac{1}{r_{a1}^2} \right] \tag{3.27}$$

$$C_{16} = \frac{6 \mu}{\rho} \ln (R_L / r_{a1}) \tag{3.28}$$

Equation (3.1) can be rewritten as

$$P_{b1} = P_s - C_{17} q_{LS} \tag{3.29}$$

where

$$C_{17} = \frac{128 \mu L_{snt1}}{\pi D_{ns1}^4} \tag{3.30}$$

Under no load condition,

$$q_{LS} = q_{1L} = q_{1R} = q_1 \tag{3.31}$$

From equations (3.22), (3.26), (3.29) and (3.31) we have

$$A_1 q_1^2 + B_1 q_1 - (P_s - P_D) = 0 \tag{3.32}$$

where

$$A_1 = \frac{C_{11}}{(T_D - x)^2} + \frac{C_{12}}{x^2} - \frac{C_{13}}{h_{1R}^2} + \frac{C_{14}}{h_{1L}^2} \tag{3.33}$$

$$B_1 = - \frac{C_{15}}{h_{1R}^3} + \frac{C_{16}}{h_{1L}^3} + C_{17} + C_{18} \tag{3.34}$$

Equation (3.32) can be solved for q_1 as

$$q_1 = \frac{- B_1 + \sqrt{B_1^2 + 4A_1 (P_s - P_D)}}{2 A_1} \qquad (3.35)$$

For a given value of disc displacement, x, equation (3.35) describes the flow through the disc chamber 1. Similar expressions apply to the valve disc chamber 2 with suffix 2 instead of 1, R instead of L, and x replaced by $(T_D - x)$.

The net flow q_T, through the valve is given by the sum of flows through the disc chambers 1 and 2 under blocked-load conditions. That is,

$$q_T = q_1 + q_2 \qquad (3.36)$$

The valve load pressure P_L is given by

$$P_L = P_1 - P_2 \qquad (3.37)$$

Dividing equation (3.37) by the supply pressure, P_s, give the non-dimensional load pressure characteristics of the valve.

3.1.2 Static fluid forces

The steady-state force acting on the supply side of disc 1 is given by

$$F_{1L} = \frac{\rho q_1^2}{2 A_{sn}} + \pi r_{t1}^2 P_{b1} + 2\pi \int_{r_{a1}}^{R_L} P_{1L}(r)\, r\, dr \qquad (3.38)$$

Substituting for $P_{1L}(r)$ from equation (3.10) and integrating we have

$$F_{1L} = \frac{\rho q_1^2}{2 A_{sn}} + \pi r_{t1}^2 P_{b1} + C_{11L} P_1 + (C_{12L} - C_{13L}) \frac{q_1^2}{h_{1L}^2} + C_{14L} \frac{q_1}{h_{1L}^3} \qquad (3.39)$$

where

$$C_{11L} = \pi \left[R_L^2 - r_{a1}^2 \right] \qquad (3.40)$$

$$C_{12L} = \frac{0.193\,\ell}{\pi}\left[1 - (r_{a1}/R_L)^2\right] \tag{3.41}$$

$$C_{13L} = \frac{0.386\,\ell}{\pi}\ln(R_L/r_{a1}) \tag{3.42}$$

$$C_{14L} = 3\mu\left[R_L^2 - r_{a1}^2\{2\ln(R_L/r_{a1}) + 1\}\right] \tag{3.43}$$

The fluid force acting on the drain side of disc 1 is given by

$$F_{1R} = 2\pi\int_{r_{dG}}^{R_L} P_{1R}(r)\, r\, dr \tag{3.44}$$

Substituting for $P_{1R}(r)$ from equation (3.13) and integrating we have

$$F_{1R} = C_{11R}\,P_1 + (C_{13R} - C_{12R})\frac{q_1^2}{h_{1R}^2} - C_{14R}\frac{q_1}{h_{1R}^3} \tag{3.45}$$

where coefficients C_{11R} to C_{14R} are the same with that of C_{11L} to C_{14L} with suffix dG instead of a1. Again similar expressions apply to the valve disc chamber 2 with suffix 2 instead of 1, R instead of L, and x replaced by $(T_D - x)$.

Now the resulting static fluid force F_f acting on the two discs and the push rod moving together as a rigid body is the difference of the net fluid forces F_1 and F_2 acting on the discs. Thus

$$F_f = F_1 - F_2 = (F_{1L} - F_{1R}) - (F_{2R} - F_{2L}) \tag{3.46}$$

The net fluid force can be expressed in non-dimensional form as $\bar{F}$ by dividing equation (3.46) by the static pressure force acting on the floating disc when it closes off the supply nozzle.

3.1.3 Boundary Conditions

As earlier stated, the steady state analysis of the valve fluid mechanics

is based on a blocked-load conditions. Under these conditions, when the disc displacement is zero, (that is the left-hand disc closes off the supply nozzle and the right-hand disc closes off the drain nozzle (see Fig.3.1) equations (3.47) through (3.53) applies.

$$q_1 = q_2 = P_1 = F_{1R} = 0 \tag{3.47}$$

$$F_{1L} = \pi r_{t1}^2 P_s \tag{3.48}$$

where $r_{t1} = (D_{snL1} + D_{ns1})/4$ (3.49)

$$F_{2L} = \pi (R_R^2 - r_{dt}^2) P_s \tag{3.50}$$

where $r_{dt} = (D_{nLD} + D_{nD})/4$ (3.51)

$$F_{2R} = \pi R_R^2 P_s \tag{3.52}$$

$$P_2 = P_s \tag{3.53}$$

Similarly when the disc displacement is equal to the total disc travel, (that is the left-hand disc closes off the drain nozzle and the right-hand disc closes off the supply nozzle) equations (3.54) through (3.59) applies.

$$q_1 = q_2 = P_2 = F_{2L} = 0 \tag{3.54}$$

$$F_{1L} = \pi R_L^2 P_s \tag{3.55}$$

$$F_{1R} = \pi (R_L^2 - r_{dt}^2) P_s \tag{3.56}$$

$$F_{2R} = \pi r_{t2}^2 P_s \tag{3.57}$$

where $r_{t2} = (D_{snL2} + D_{ns2})/4$ (3.58)

$$P_1 = P_s \tag{3.59}$$

In equations (3.48),(3.51),(3.57) and (3.58) it is assumed that the static pressure acts approximately on the projected area of the mean radius of the nozzle land on the floating disc.

3.1.4 Numerical computations of valve fluid characteristics and results

The basic steady-state fluid characteristics of the double-disc valve are as described by equations (3.1) to (3.59). In formulating these equations, it was assumed that the two disc chambers could be different and as such different notations were used for the two chambers. For example, the two

discs might have different diameters and thus making the valve unsymmetrical. For the symmetrical double-disc valve, all the corresponding parameters of the two disc chamber would be equal. This implies that the same equations could be used to simulate both symmetrical and non-symmetrical double-disc valve.

A computer programme has been written in FORTRAN 77 to determine the steady-state fluid characteristics of the double-disc valve model based on equations (3.1) to (3.59). These equations are solved numerically at a given disc displacements x using Shell Tellus R37 oil as the valve fluid medium. For a given total disc travel T_D, the disc is given an incremental displacement of one per cent of T_D and the valve discharge coefficients are obtained from the empirical formulae developed in Chapter 4. Using this discharge coefficient data, the chamber pressures, flowrates and the fluid forces acting on the floating discs are estimated. The computer programme is made highly interactive and several subroutines have been developed to display the package results graphically. To aid understanding of the steady-state characteristics of the double-disc valve, the programme has been made into a computer-aided design package. A flow chart of the package is given in appendix A7. The package displays all results graphically and the user may select which results are to be displayed.

The valve main parameters used in the package are: DSD, Disc diameter; TD, Total disc travel; HGS, Supply side nozzle holding gap; HGD, Drain side nozzle holding gap; SND, Supply nozzle diameter; SNLD, Supply nozzle land diameter; DNLD, Drain nozzle land diameter; SNTL, Supply nozzle tube length; PS, Supply pressure; CR, Rod clearance; RODD, Rod diameter; DND, Drain nozzle diameter; DNTL, Drain nozzle tube length; VSCO, Oil viscosity; VSCF, Valve linear scaling factor; CRNT Coil current. The values of these parameters used in the package are shown in Table 3.1.

Table 3.1 Physical constants of the valve main parameters

DSD = 31.65 mm	PS = 105.0 bar
TD = 0.51 mm	CR = 0.00 mm
HGS = 0.13 mm	RODD = 3.18 mm
HGD = 0.51 mm	DND = 3.81 mm
SND = 2.54 mm	DNTL = 3.81 mm
SNLD = 3.05 mm	VSCO = at 35 °C
DNLD = 4.57 mm	VSCF = 1.00
SNTL = 15.88 mm	CRNT = 0.00 A

The package allows any of the main parameters governing the valve performance to be varied independently. The package will be used to show the effect of the main parameter changes in Chapter 5.

Figure 3.2 shows a typical fluid forces acting on a single disc chamber as the disc moves from the supply nozzle land to drain nozzle land. Noting that positive disc displacement is defined for disc movement from left to right in Fig 3.1 and positive fluid force are assumed to act in the same direction. In Figure 3.2, when the disc is given a small displacement, the fluid forces increases to a maximum and then decreases to a minimum near the mid-position of the disc travel. From the supply nozzle tip to the mid-position of disc travel, the supply nozzle curtain area dominates the control of the valve. The position where the maximum fluid forces first occur is about 10 per cent of the disc total travel T_D. When the disc displacement is further increased pass the mid-position, the drain nozzle now dominates the valve control and the fluid force rises to a maximum before it decreases to a value depending on the drain nozzle land diameter. The rise in the fluid force is due to flow restriction that occurs when the

disc approaches the drain nozzle.

The rise in fluid force that occurs when the disc is approaching the drain nozzle is disadvantageous in a double-disc valve operation as this will cause unstable valve performance near its null position. That is, there will be point of inflexion near the valve null which is not desirable in proportional operation of the valve (see Fig.3.3). The theoretical steady-state fluid model for the valve has shown that the ratio of the drain nozzle area to that of the supply nozzle influences the fluid forces acting on each disc in its chamber. The level of rise in the fluid forces when the disc approaches the drain nozzle can be controlled by the correct choice of drain nozzle geometry and drain holding gap.

Where the net fluid force curve crosses the displacement axis it corresponds to the position of zero net fluid force and the discs and the rod assembly is stationary at that point if the curve gradient is negative. From Fig.3.3 it is seen that when x=0, the net fluid force is negative and the disc will not lift from its supply nozzle seat. For this reason, a rod length is used with a clearance which is greater than the distance between the supply nozzle tip and the position where the fluid force cease to be negative.

Figure 3.4 shows typical total drain flow under blocked-load conditions. The leakage flow is maximum at the mid-position of the disc travel and decreases rapidly with disc displacement away from this position because the disc modulates the valve orifices. This curve is a measure of hydraulic power loss if the valve is modulated under blocked load conditions. Figure 3.5 shows a typical non-dimensional load pressure curve obtained from the theoretical model under blocked load conditions. The load pressure difference P_L exhibits reasonable linearity for small changes from the null condition although the hydraulic stiffness of the valve is low compared to

a conventional servo-valve.

3.2 Electro-magnetic characteristics of a flat-faced type coil

The flat-faced armature type of electro-magnetic coil used to actuate the double-disc valve is illustrated in Fig. 3.6. It has a flat-faced armature (disc) made from REMKO soft magnetic iron, and a magnetic core having a central hole. The central hole admits a supply nozzle tube through which hydraulic oil flows into the valve. The electro-magnetic coil has two working gaps that are mechanically in parallel but magnetically in series. This type of electro-magnetic coil produces a large force through a short stroke compared to the plunger type of magnet.

There is little literature on this type of electro-magnetic coil. However, the design and analysis is well covered in books by Roters [61] and Hazeltine [62]. Yüksel [35] uses this type of electro-magnetic coil in his study. The electro-magnetic characteristics of the coil based on the semi-empirical formulae of Roters [61] will now be developed.

3.2.1 Magnetic circuit calculation

Fig. 3.6 shows a section of a flat-faced electro-magnetic coil. The iron paths of the magnet are so designed that the cross-section of the inner pole core equals that of the outer, and the free-floating disc (armature) cross-section at the radius $(r_1 + r_2)/2$ is equal to that of the pole cores.

The force exerted by the coil is given by

$$F_m = \frac{n_w}{2} \frac{B_g^2 A_c}{\mu_g} \tag{3.60}$$

where n_w is the number of working gaps, B_g the flux density in the working gap, μ_g the permeability of the working gap and A_c is the cross-sectional

area of each of the working faces.

The exciting magnetic magnetomotive force NI, which provide the flux required for the given force and stroke, is determined by the magnetic circuit equation for the electro-magnetic coil. This equation is given by

$$NI = \frac{2\ B_g\ x_g}{\mu_g} + \sum H_i\ L_i \qquad (3.61)$$

where the first term represents the magnetomotive force necessary to establish the flux at a density of B_g across a working gap x_g, and the second term represents the magnetomotive force necessary to establish the flux in the iron paths of the circuit.

There are two working gaps in series in this type of electro-magnetic coil hence the factor of 2 in equation (3.61). This implies that n_w in equation (3.60) will take the value of 2. If it is assumed that $\sum H_i L_i$ is small compared to $2\ B_g\ x_g/\mu_g$ we have

$$NI = \frac{2\ B_g\ x_g}{\mu_g} \qquad (3.62)$$

Substitution of equation (3.62) into equation (3.60) with $n_w = 2$ gives

$$F_m = \mu_g\ A_c\ (NI)^2/(4\ x_g^2) \qquad (3.63)$$

Equation (3.60) takes into consideration both the magnetic leakage and iron saturation of the electro-magnetic coil while equation (3.63) ignored these factors. Therefore for a given magnetisation curves of a magnetic material used in the coil, equation (3.60) will describe the electro-magnetic force-stroke characteristics of the coil better than that obtained from equation (3.63).

The ratio of the magnetic forces in equations (3.60) and (3.63) can be expressed as the coil leakage factor as

$$f_L = \frac{1}{4}\left[\frac{\mu_g NI}{B_g x_g}\right]^2 \tag{3.64}$$

The flux distribution of the various parts of the magnetic circuit can only be determined from the coil leakage coefficient. To determine the leakage coefficient, the permeance of the various parts of the magnetic circuit had to be estimated. These permeances are given by the semi-empirical formulae of Roters [61] and they are quoted below.

The inner pole fringing permeance is given by

$$P_{fi} = 3.26\,\mu_g r_1 + 4\,\mu_g r_1 \ln\left[\frac{r_2 - r_1}{\pi x_g}\right] \tag{3.65}$$

The outer pole fringing permeance is given by

$$P_{fo} = 1.63\,\mu_g r_3 + 2\,\mu_g r_3 \ln\left[1 + \frac{r_1}{x_g}\right] + 3.26\,\mu_g r_2 + 4\,\mu_g r_2 \ln\left[\frac{r_2 - r_1}{\pi x_g}\right] \tag{3.66}$$

The useful gap permeance P_{ug} is given by

$$(P_{ug})_{inner} = (P_{ug})_{outer} = \pi u_g \left[\frac{(r_1 - r_o)^2}{x_g}\right] \tag{3.67}$$

The total effective permeance P_{te} through the disc between the inner and outer pole core, is

$$P_{te} = \frac{1}{\left[\frac{1}{P_{ug} + P_{fi}} + \frac{1}{P_{ug} + P_{fo}}\right]} \tag{3.68}$$

The leakage permeance P_L between pole cores, is

$$P_L = \mu_g \left[1.57\ h\ \frac{(r_2 + r_1)}{(r_2 - r_1)} - \frac{(r_2 + r_1)}{2} \left(1 - \frac{\pi x_g}{r_2 - r_1} \right) \right] \tag{3.69}$$

The total useful permeance P_u of the coil is given by

$$P_u = \frac{\pi \mu_g (r_1 - r_o)^2}{2 x_g} \tag{3.70}$$

The effective permeance of the pole cores is given by

$$P_{effp} = P_{te} + \frac{2}{3} P_L \tag{3.71}$$

The leakage coefficient C_{lk} which is the maximum flux linking with the exciting coil to the useful flux (i.e. flux in working gap) is given by

$$C_{lk} = \frac{P_{te} + P_L}{P_u} \tag{3.72}$$

The useful density of the various parts of magnetic circuit are obtained from the following semi-empirical formulae from Roters [61]. It has been assumed that the smallest value of the flux density is equal to that of the yoke, B_y.

The flux density of the working gap is given by

$$B_g = C_g B_y \tag{3.73}$$

where $C_g = 1/C_{lk}$

The flux density of the armature is

$$B_a = C_a B_y \tag{3.74}$$

where $C_a = P_{te}/(P_u C_{lk})$

The flux density of the pole core is given by

$$B_p = C_p B_y \tag{3.75}$$

where $C_p = P_{effp}/(P_u C_{lk})$

By definition, the flux of various paths of the magnetic circuit is obtained by multiplying the various flux densities by the appropriate

cross-sectional area.

The magnetomotive force NI, for the iron parts of the magnetic circuit are obtained from equation (3.61) with the following equation

$$\Sigma H_i L_i = H_a L_a + H_p L_p + H_y L_y \qquad (3.76)$$

The magnetic intensities (H) are obtained from the experimental magnetisation curves for the REMKO magnetic material used (see appendix A8). The exciting current can be obtained from equation (3.61) and knowledge of the total number of coil turns.

From Fig. 3.6, the total length L_t of the magnetic circuit is seen to be equal to the sum of twice the length of pole core (L_{pc}), the length of the armature L_a and the length of the yoke, L_y. That is

$$L_t = L_a + L_p + L_y \qquad (3.77)$$

The lengths L_p, L_a and L_y can all be express in terms of the electromagnetic coil geometry as follows

$$L_a = (r_3 + r_2 - r_1 - r_o)/2 \qquad (3.78)$$

$$L_y = L_a \qquad (3.79)$$

$$L_p = 2\,L_{pc} = 2(h + x_g) + t_p + t_a \qquad (3.80)$$

For a good coil design, the disc (armature) thickness t_a, must be equal to t_p, the coil pole thickness.

The cross-sectional area of each of the working surfaces is given by

$$A_c = \pi(r_1^2 - r_o^2) = \pi(r_3^2 - r_2^2) = \pi(r_1 + r_2)t_a = \pi(r_1 + r_2)t_p \qquad (3.81)$$

and the following inequality should hold for weight economy [61]

$$3 \leq h/(r_2 - r_1) \leq 4 \qquad (3.82)$$

3.2.2 Numerical computations of valve magnetic characteristics and results

From equations (3.60) through (3.82), it can be seen that the electro-magnetic characteristics of the coil are highly non-linear. These equations are best solved using a numerical technique. A FORTRAN 77 program has been written to compute the steady-state electro-magnetic characteristics of the coil. A flow chart of the program is given in appendix A9.

The method used involved an iterative approach in which the flux densities needed were obtained from the experimental magnetisation curves supplied by SKF REMKO magnetic iron manufacturer (see appendix A8). The B-H data were obtained from these curves and a polynomial function of the form HBN = f(B) was obtained using a Chebyshev series with a NAG library routine E02AEF [63]. The program whose flow chart is shown in appendix A9 is divided into two parts.

The first part of the program compute the relationship between an electro-magnetic force and magnetomotive force for various working gaps (disc displacements) in the range 0.13 to 0.64 mm. For each of the disc displacements, the coil permeances and the coil leakage flux coefficients are calculated. After which the flux density of the yoke of the REMKO magnetic iron is assumed and the flux densities of the armature (disc) and magnetic pole piece are calculated. From these flux densities, the flux intensities of the various part of the magnetic circuit are calculated from the function HBN. Finally, the electro-magnetomotive force and magnetic force are calculated. Fig. 3.7 shows the relationship between the electro-magnetic force and the magnetomotive force NI for various distances between the coil face and the disc. Each curve represents the magnetic force against ampere-turns for a constant gap between the coil and the disc. Curve OAB represents the case when the gap is a minimum which correspond to the point where the disc is touching the supply nozzle land. The supply

nozzle projects above the coil surface and the amount of projection is called the holding gap (see Fig. 1.3). Curve OCD represents the case when the gap is a maximum. That is the disc has moved its total travel and is touching the drain nozzle land. Curve OAB is seen to represent the force holding the disc against the supply nozzle before switching occurs while curve OCD represents the attracting force pulling the disc towards the coil immediately after switching is initiated. For magnetomotive force and gap values below the line marked AC, the gradient of the curves are much greater than when above the line. This is due to the transition in the B-H characteristics from the unsaturated region into the saturated region. Best results can be obtained from the electro-magnetic coil if it is operated in the unsaturated region. For a given coil size, the number of coil turns N, is constant and the minimum current I_{min} to operate the coil in the unsaturated region is given by $\frac{OE}{N}$ where distance OE is as shown in Fig. 3.7. The maximum current I_{max} is given by $\frac{OF}{N}$ where OF is as shown in the Figure.

The second part of the program computes both the magnetic force and the coil leakage factor f_1 as obtained from equations (3.60) and (3.64) respectively for a given coil current and various disc displacements. An iterative method is used and the approach is described below. For a given current and coil turns, NI is known. This is denoted as EMFT in the program. Based on the permeances and flux densities, the flux intensities of the various parts of the electro-magnetic circuit are obtained from the polynomial function HBN = f(B). This polynomial function describes the H-B relationship of the REMKO magnetic iron used to construct the electro-magnetic coil. From the flux intensities and the magnetic circuit lengths, NI is estimated (see equation (3.61)). This is denoted as EMFTC in the program. The difference between EMFTC and EMFT is calculated. If EMFTC <

EMFT, the flux density of the yoke is given an incremental value and EMFTC estimation process is repeated. This iterative process is carried out until the estimated value of NI ,EMFTC, is about equal to the known value, EMFT. The maximum iterative process is limited to 100. When the estimated NI (EMFTC) equal to the known value (EMFT), the magnetic force is calculated based on the flux density of the working gap.

The theoretical magnetic force-stroke curves of the coil are shown in Fig. 3.8. Each of the curves represent a magnetic force against disc displacement for a constant coil current, CRNT. The Figure shows that the magnetic force rises sharply as the disc approaches the coil surface. In practical applications of the electro-magnetic coil, the disc is not allowed to touch the coil surface to prevent excessive magnetic force remanence. For this purpose the holding gap is provided and the useable region of the force-stroke characteristics is shown in Fig. 3.8 as the total disc travel. Increasing the disc travel further than this region, might not provide enough magnetic force to pull the disc towards the supply nozzle.

The coil leakage factor f_L, as expressed in equation (3.64), is shown in Fig. 3.9 for various coil currents, CRNT and is the ratio of the magnetic force obtained from equation (3.60) to that from equation (3.63). The magnetic force as expressed in equation (3.60) takes care of iron saturation while that of equation (3.63) ignores iron saturation. From Fig.3.9 it can be seen that the coil leakage factor is high for small gaps between the coil surface and the disc. For a small coil current, the coil leakage factor approaches unity at a faster rate as compared to higher coil current. Decreasing the coil current from 1.5 to 0.5 mA, the coil leakage factor drops from about 77 to 10 for a working gap of 0.03 mm. As the disc displacement is increased beyond 0.30 mm, the coil leakage factor tends to

unity for all coil currents. It can therefore be concluded that equation (3.63), which ignores iron saturation, may be used to estimate the magnetic force-stroke characteristics of a flat-faced type electro-magnetic coil for disc displacement greater than 0.30 mm. However, as most disc displacements are below this value, equation (3.60) should be used to estimate the magnetic characteristics. For low magnetic hysteresis, the disc should not be operated close to the coil surface. Hence the correct selection of holding gap is critical in the valve design.

The steady-state theoretical fluid and electro-magnetic characteristics of the double-disc valve have been presented in this chapter. The experiments carried out, on a physical model of the valve, to validate both the theoretical fluid and electro-magnetic models are presented in the next chapter.

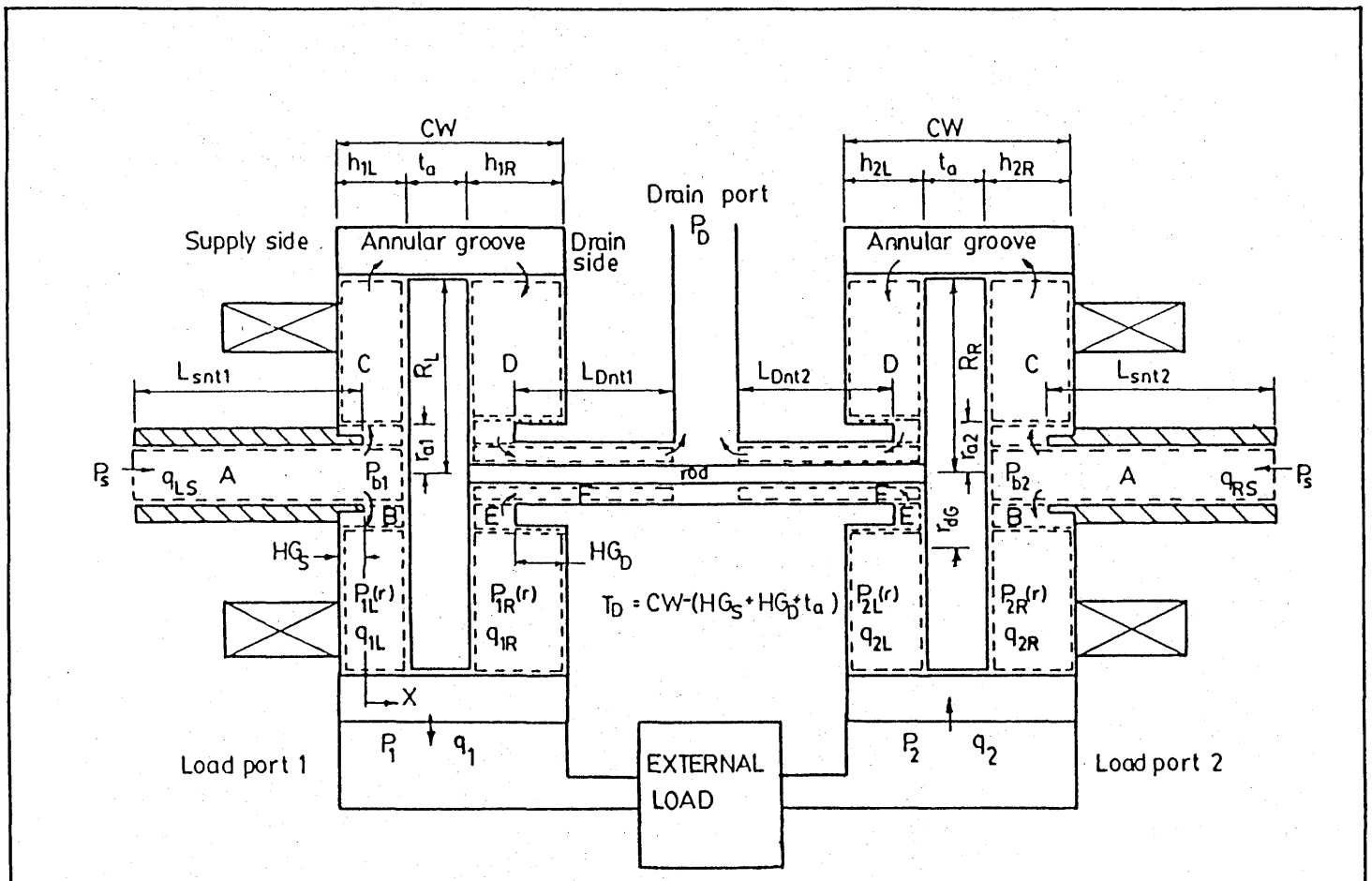

Fig. 3.1 Geometry and notation of a double-disc valve

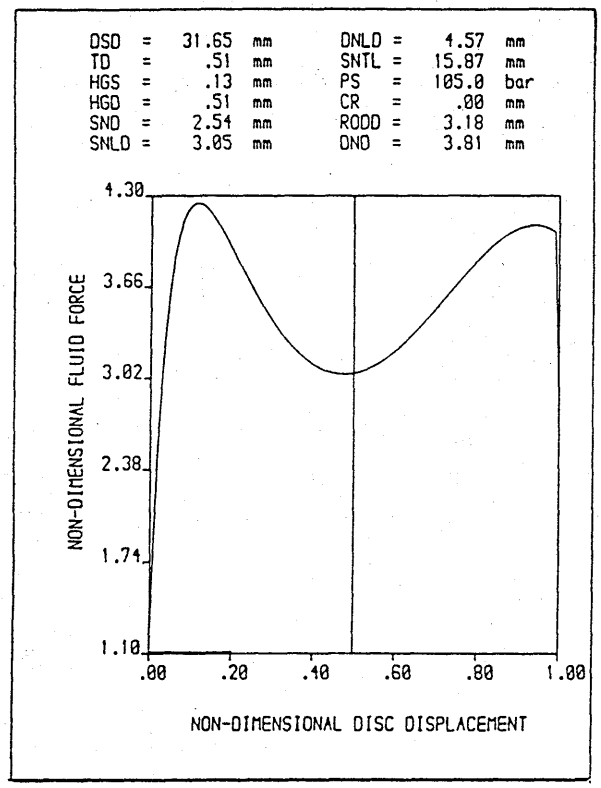

Fig. 3.2 Typical fluid forces acting on a single disc valve.

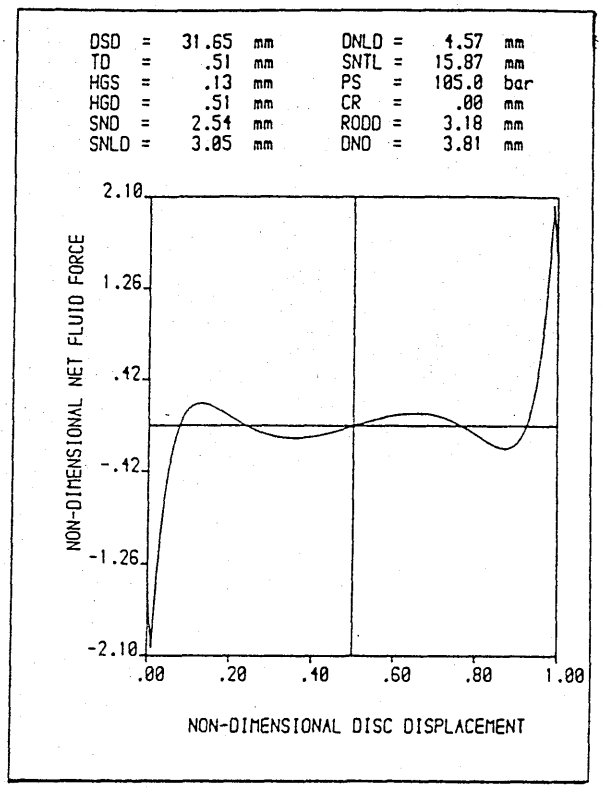

Fig. 3.3 Typical net fluid forces acting on a double-disc valve.

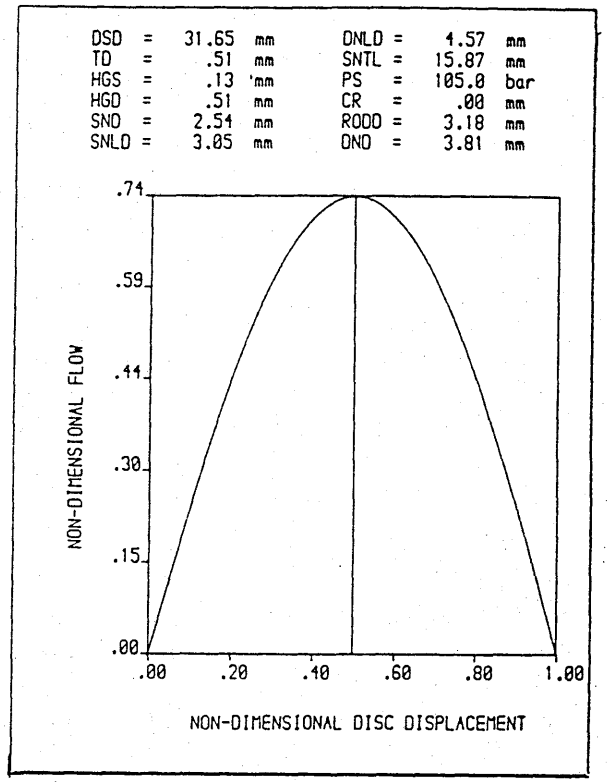

Fig. 3.4 Typical drain flow under blocked-load conditions.

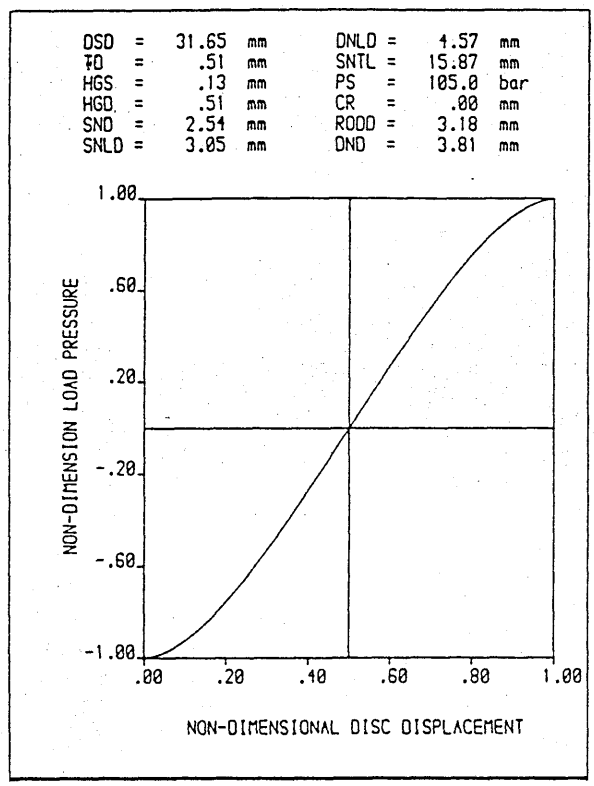

Fig. 3.5 Typical non-dimensional load pressure curve.

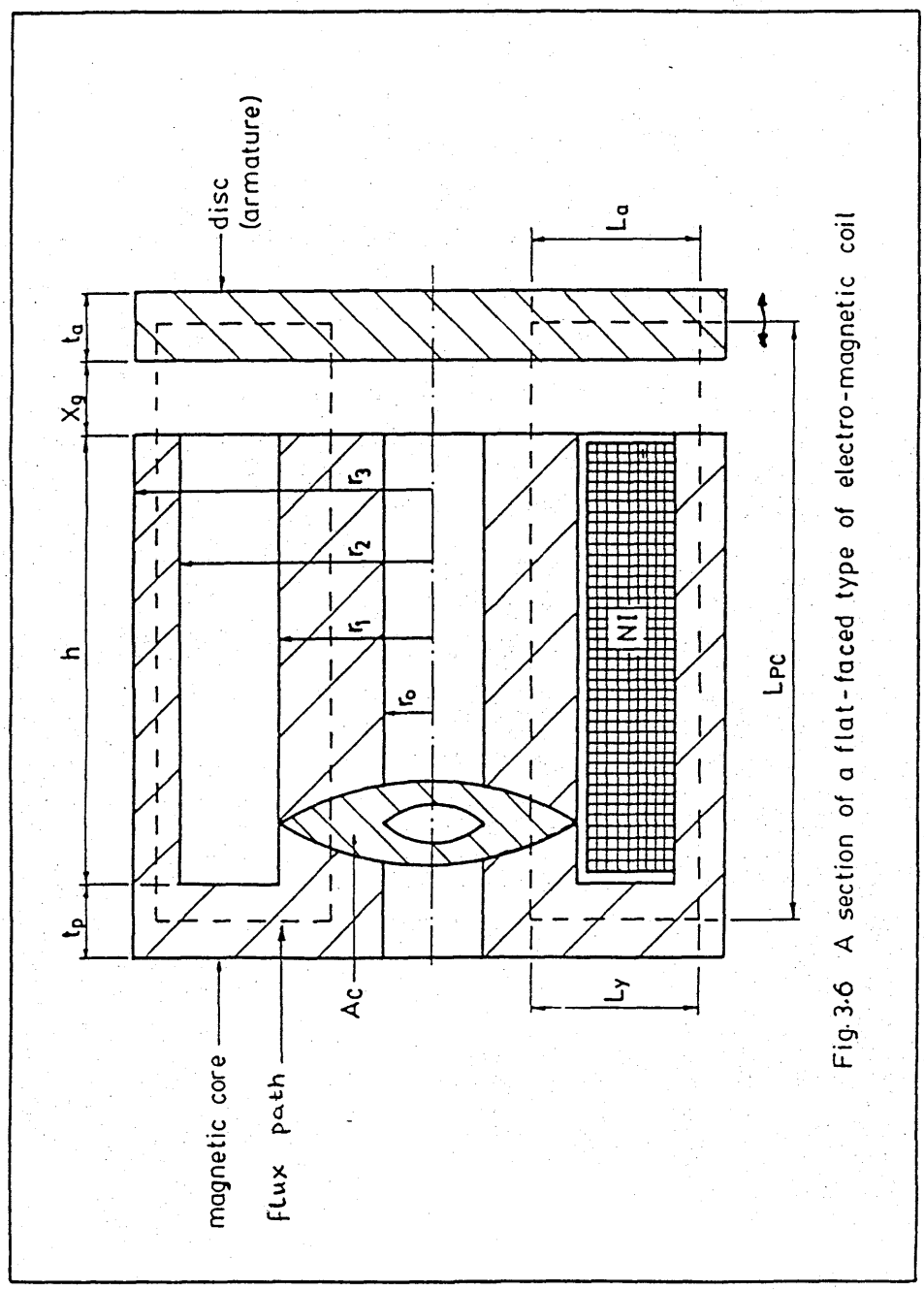

Fig. 3.6 A section of a flat-faced type of electro-magnetic coil

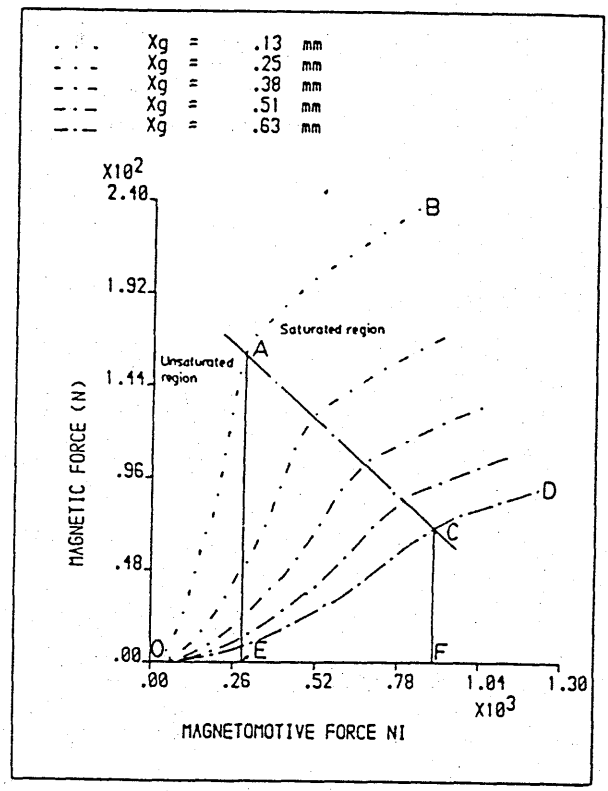

Fig. 3.7 Theoretical magnetic force versus magnetomotive force curves.

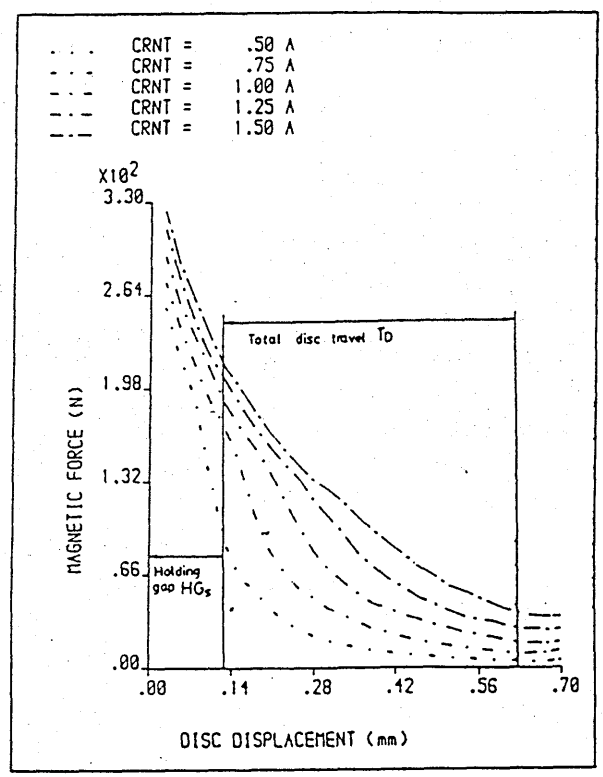

Fig. 3.8 Theoretical magnetic force - stroke curves.

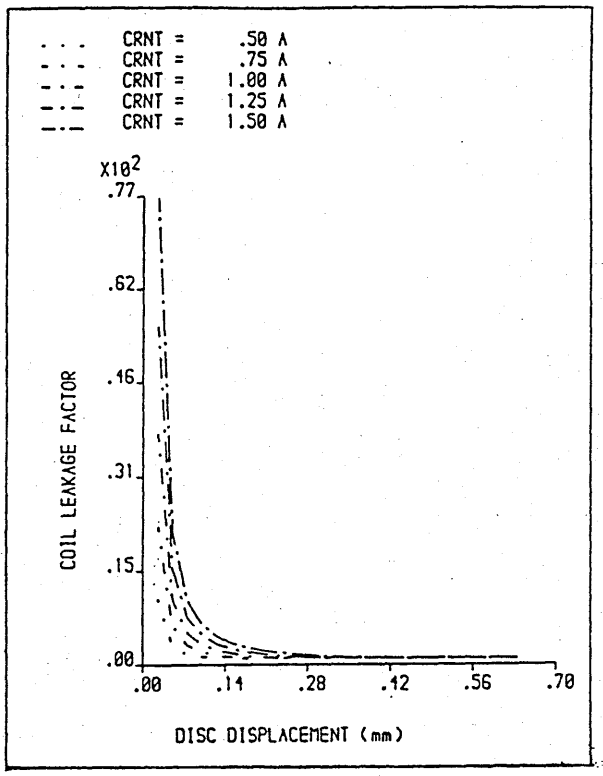

Fig. 3.9 Coil leakage factor.

CHAPTER 4

EXPERIMENTAL INVESTIGATION OF FLUID FORCES AND ELECTRO-MAGNETIC EFFECTS

4. Experimental investigation of fluid forces and electro-magnetic effects.

4.1 Introduction

A disc valve operation is controlled by the complex interaction between the fluid and electro-magnetic forces. To gain an insight into the valve performance, these forces must be clearly studied. It is the purpose of this chapter to discuss the tests carried out to determine both the fluid and electro-magnetic force characteristics of the valve. The description of the physical model of the disc valve (test valve) and the associated test rig are presented. The test valve has a single disc in a single chamber and is intended to simulate both single and double-disc valve flow patterns. The rig has the facility for allowing radial flow across the disc faces in both directions to simulate flow into and out of the load port and into the drain connection. The experimental data obtained will be used to compare with the theoretical results of Chapter 3.

4.2 Fluid mechanics of valve.

4.2.1 Description of fluid force test-rig

The fluid force test-rig has a hydraulic power pack unit, Hounsfield Tensometer, the test valve, air cooling fan and hydraulic pipe network that includes two turbine meters with overlapping flow ranges. The fluid force test-rig is schematically shown in Figure 4.1. The essential components of the test-rig are shown in Figures 4.2 and 4.3.

The hydraulic power pack has a pump (27) which is driven by 3 phase induction motor, relief valve/pressure regulator (26), pressure gauge (35) and oil temperature indicator. The electric motor is mounted on top of the unit and is connected to the pump via a shaft. The pump, relief valve and the pressure regulator are totally submerged in the oil reservoir. The

hydraulic power unit have one supply line and two return lines. When there is no demand, the relief valve circulates the oil in the reservoir. The pressure regulator (26) set the working pressure. The hydraulic power unit can supplying oil up to a pressure of 105 bar. An electric air cooling fan (28) driven by an induction motor cool the oil in the hydraulic power unit. With the aid of this air fan, the oil temperature was kept constant within $\pm 2^{o}C$. The oil from the hydraulic power unit is filtered before going to the test valve (1).

The exploded view of the test valve is shown in Figure 4.4. The valve has two major components:- (a) valve end-cover and (b) valve main body. The valve end-cover consists of an electro-magnetic coil, supply nozzle tube and oil supply fittings. The valve main body has a disc chamber, cross drilling for both drain and load ports and axial hole to incorporate a rod (10) and a linear bearing (11). The rod one end is screwed into the central hole of the disc while the other end is attached to a proof-ring type force transducer [64]. The force transducer measures the forces acting on the disc. The disc displacement is recorded by a dial gauge through a beam attached to a spindle linking the force transducer and the operating screws of the Hounsfield Tensometer. The beam is rigidly attached to the spindle with two nuts. Figure 4.5 shows the internal view of the disc chamber. The disc chamber houses the disc and it incorporates drain seats and radial slots to collect fluid to annular groove in the valve end cover. The assembled test valve is mounted on the Hounsfield tensometer as shown in Figure 4.3. Care is taken to ensure that the disc, rod, force transducer, and the operating screws are aligned to avoid unnecessary frictional forces.

Depending on the port connections, the test valve could be used to reproduce both single and double-disc valve configurations. For a single-

disc valve configuration, the disc chamber port acts as a drain port and for a double-disc valve configuration, the disc chamber port acts as load port and the other port in the test valve main body acts as drain port. In this work, only the double-disc valve configuration is considered. Hence the chamber port or load port is blocked and the drain port connected to the turbine flow meter hydraulic pipe network.

The flow meters pipe work incorporates a relief valve (29) to act as a safety valve against accidental closure of the two directional valves associated with the turbine type flow meters used. The output of the flowmeter pipe network is return to the hydraulic power unit. The relief valve is also connected to a spare return line in the unit (see Figure 4.2). The linear bearing in the valve reduces the frictional force associated with the movement of the rod. As a result there was a small oil leakage through the bearing and this is collected through a flexible tubing to a point upstream of the turbine meters. The turbine meters thus measure the total flow through the valve.

4.2.2 **Experiment 4.2.1 : Fluid characteristics of test valve**

The aim of this experiment was to determine the fluid forces and the pressure-flow characteristics in a floating disc chamber. The main physical dimensions of the test valve were as follows:

supply tube length = 19.05 mm, Supply nozzle diameter = 2.54 mm
Supply nozzle land diameter = 3.05 mm, Supply nozzle projection = 0.13 mm
Disc diameter = 25.27 mm, Disc thickness = 4.06 mm
Total disc travel = 0.51 mm, Rod diameter = 2.38 mm
Drain nozzle diameter = 3.81 mm, Drain nozzle land diameter = 5.66 mm
Drain nozzle projection = 0.38 mm, Drain tube length = 19.05 mm

After setting-up the test-rig as shown in Figures 4.1, 4.2 and 4.3, the

zero disc displacement which was the position where the disc touched the supply nozzle land was established. The zero position was established as follows:

(a) The operating handle (16) was adjusted clockwise or anti-clockwise until there was free movement of the disc (6) as indicated by the dial gauge (17).

(b) The force transducer amplifier (20) was zeroed.

(c) The operating handle was turned anti-clockwise until there was no more changes on the dial gauge reading but increased compressive force as read by the force transducer. This step ensured that the disc was flat on the supply nozzle land.

(d) The dial gauge pointer was set to zero.

(e) The operating handle was turned clockwise until the force reading was zero and the dial gauge reading was still zero.

The zero position of the disc could also be determined from the readings of the flow meter, the force transducer and the dial gauge. At zero position, the flow through the valve should be zero and there should be no changes in the dial gauge reading but a compressive force on the disc as a result of a static pressure force acting approximately across the supply nozzle area. The flow meter (31) is rated 1.5 to 15 GPM while (32) is rated 0.1 to 1.0 GPM. This shows that the turbine meters were not well suited for low flowrates and as such the actual zero disc position could not be accurately determined from the flowrate measurement alone. For small disc displacements from either the supply or drain nozzle, the turbine flowmeter (32) was used for its low flow rating. The other turbine meter (31) was used in the middle range of the disc travel as more flow passed through the valve in this region.

After zeroing the instruments and establishing the zero disc position, the

required supply pressure was set with the aid of the pressure regulator (26). The disc was given an incremental displacement step of 0.03 mm with the operating handle (16) of the Hounsfield tensometer. At each disc position, the fluid force acting on the disc, the various pressures, flowrate and the disc displacement were recorded. Throughout the test, care was taken to avoid reversal of disc displacement as the frictional forces associated with the test rig were not the same in both directions.

Figure 4.6 shows the comparison between computed and experimental fluid forces for a single disc moving in a chamber with a supply nozzle land diameter of 3.05 mm. This value of land diameter (about 1.2 times the supply nozzle diameter) gave a good compromise for fluid forces, flow pattern and pressure balance in the disc chamber. For a supply pressure greater than or equal to 56 bar, it was found that the disc and the rod assembly were pushed towards the drain seat as the disc approached its mid-stroke. A lock nut mechanism (see Figure 4.1) was incorporated in the test-rig to prevent this from happening but this may have increased the frictional force of the rig and thus caused the measured fluid forces to be more than that predicted.

For a larger land diameter, cavitation was prominent and this caused reduction in fluid forces, flowrate and pressure. In addition, negative fluid forces may be experienced when the distance between the disc and the nozzle tip was increased. Fig.4.7 shows a comparison between a cavitating and non-cavitating fluid forces acting on a single disc moving in a chamber with supply pressure of 100 bar. The supply nozzle diameter used with the non-cavitating valve was 3.05 mm while that of the cavitating valve was 3.56 mm. The two fluid force curves followed the same trend until the disc displacement was about 0.15 mm where cavitation was observed for the larger land diameter. From this point onward, it can be observed from the figure

that the cavitating fluid forces are much lower than the non-cavitating values. Negative fluid forces occurred for the cavitating valve for disc displacement between 0.25 mm and 0.40 mm from the supply nozzle tip. This negative fluid force is not desirable in a double-disc valve operation. Cavitation is a phenomena associated with a local pressure in a hydraulic system falling below the vapour pressure of the fluid used in the system. When cavitation occurred in the test valve, violent noise was generated as the vapour cavities collapsed on entering regions of higher pressure. The presence of cavitation can lead to erosion of the valve lands and it can be avoided by decreasing the upstream pressure or by increasing the back pressure. The cavitation might be caused by any of the following reasons: (1) flow restriction in the nozzle land region (i.e. if nozzle land diameter is too large), (2) presence of air in the system and (3) the local pressure in the valve chamber falling below the vapour pressure of the oil used. The third reasons could be minimised by either decreasing the supply pressure or increasing the back pressure. For best valve performance it is preferable if the cavitation phenomena can be eliminated through the valve design instead of altering the system pressure. Hence the flow restriction must be considered and the supply nozzle land diameter must not be greater than approximately 1.2 times the supply nozzle diameter.

From the measured supply pressure P_s, chamber pressure P_c and drain pressure P_D, the non-dimensional load pressure $(P_c - P_D)/(P_s - P_D)$, is computed. The disc displacement is non-dimensionalised with respect to total disc travel. The resulting load pressure curves are shown in Fig.4.8. The figure shows the blocked-load pressure sensitivity and there is a good agreement between the measured and the predicted pressures. Figure 4.9 shows the flowrate characteristics of the disc valve as the distance between the supply nozzle tip and the disc is increased. The leakage flow is a maximum at approximately the mid-position of the disc travel and

decreases rapidly with disc displacement away from this position because the discs modulated the valve orifices. These curves are a measure of the hydraulic loss. From the figure, it can be seen that the predicted and the measured flowrates agree reasonably well.

4.2.3 Disc valve discharge coefficients

In the literature little information could be obtained on discharge coefficients associated with a floating disc which is totally submerged in a fluid and also communicating with both inwards and outwards flows. Some of the published work deals with compressible air flow and, in many, compressibility effects mask other effects. In other papers some important parameters are not specified or one is not sure if the valve discharge is into air or is submerged.

Oki [29] was working mainly with a disc valve discharging water into air but he also quotes a few results for submerged flows. The ratio of the disc diameter to the supply nozzle used range between 1.2 to 1.55. Takenaka et el [28] investigated the flow and force characteristics of disc valves. The valves used had an infinite land and discs were 1.5, 2.5 and 3.0 times the valve nozzle diameter. He has observed that at small valve openings the flow may be considered laminar and C_d increases to a maximum and then as the gap is further increased it decreases, the rate of decrease reducing as the valve opening increases. Feng [65] shows relationship between C_d and Reynolds number, R_e, for a valve with large land but not all parameters were specified. It appears from his results that the valve land has not much effect, which is doubtful because of all other results and that obtained from this present work. Hagiwara [53] carried out both theoretical and experimental investigations into radial outwards and inwards flows with sharp and rounded entry corners.

From the measured supply pressure P_s, chamber pressure P_c and drain pressure P_D and the flowrate Q through the valve , the valve discharge coefficients can be calculated from an orifice type of flow equation. The supply nozzle side discharge coefficient C_{Dns} is given by

$$C_{Dns} = \frac{Q}{\pi D_{ns} X \sqrt{\frac{2(P_s - P_c)}{\rho}}} \tag{4.1}$$

Similarly the drain nozzle discharge coefficient C_{DnD} is given by

$$C_{DnD} = \frac{Q}{\pi D_{nD} (T_D - X) \sqrt{\frac{2(P_c - P_D)}{\rho}}} \tag{4.2}$$

The corresponding Reynolds number based on the nozzles geometry are given by the following equations:

for supply nozzle

$$R_{ens} = \frac{4\,Q}{\pi \nu D_{ns}} \tag{4.3}$$

and for drain nozzle

$$R_{enD} = \frac{4\,Q}{\pi \nu D_{nD}} \tag{4.4}$$

Figures 4.10 and 4.11 show the relationship between discharge coefficients and Reynolds number with respect to the supply nozzle and the drain nozzle respectively. From the Figures it can be seen that the discharge coefficients first increase with increase in Reynolds number and remain constant at a value close to 0.45 . The maximum Reynolds number encountered are 1500 and 1000 for the supply and drain nozzles respectively. Fig.4.12 shows a typical relationship between discharge coefficient C_d and Reynolds

number R_e for a constant system pressure. The discharge coefficient first increases until the Reynolds number is maximum which corresponds also to maximum flow through the valve. This occurs when the disc is in mid-position of its stroke. As the disc approaches the drain nozzle from the mid-position the valve flowrate decreases and consequently both the discharge coefficient and the Reynolds number decreases. The rate at which the discharge coefficients decrease with the Reynolds number in this region appears to be almost constant. For a small disc displacement, C_d increases with R_e to a maximum value (curve AB). As the disc displacement is further increased, C_d decreases to a constant value near the mid-stroke of the disc with increase in R_e (curve BC). Further increase in disc displacement (i.e. disc getting closer to drain nozzle) both C_d and R_e decreases rapidly at an approximate constant rate to zero (curve CA).

From Figure 4.12, it can be seen that C_d-R_e relationship is complex. To utilise the raw data, empirical formulae were developed to express the discharge coefficient as a function of both system pressure and disc displacement. A good agreement was obtained between the empirical formulae and the experimental data. It has been reported by J.F. Blackburn [according to the work of V.A. Khokhlov, "hydraulic loss and flow discharge coefficients through the orifices of a cylindrical spool-valve hydraulic performance mechanism" Avtomat i Telemekh, Vol 16, No. 1 ,pp.64-70, 1955] that discharge coefficients varies not only with Reynolds number but with system pressure. Since flowrates varies with disc displacement, it would be expected that discharge coefficient would also vary with disc displacement. The discharge coefficient obtained from experiment 4.2.1 was found to vary with nozzle geometry and supply pressure. A polynomial of the form

$$C_{Dns} = a_0 + a_1 Z + a_2 Z^2 \qquad (4.5)$$

was fitted to the supply nozzle discharge coefficients for a given supply

pressure, where $Z = x / T_D$, is the non-dimensional disc displacement with respect to the total disc travel. The resulting values of a_0, a_1 and a_2 are given in Table 4.1 for various supply pressures.

Table 4.1 Supply nozzle coefficients values

P_s (bar)	a_0	a_1	a_2
14.0	0.161	1.359	-1.592
28.0	0.156	1.212	-1.321
42.0	0.308	0.716	-0.931
56.0	0.372	0.539	-0.778
70.0	0.376	0.541	-0.788

From Table 4.1 it can be seen that the coefficients a_0, a_1 and a_2 vary with supply pressure. Assuming these coefficients have linear relationships with supply pressure, we can represent the supply nozzle discharge coefficients in the form,

$$C_{Dns} = (A_{00} + A_{01}P_s) + (A_{10} + A_{11}P_s)Z + (A_{20} + A_{21}P_s)Z^2 \qquad (4.6)$$

This equation applies for $Z \neq 0.0, 1.0$.

The unknown coefficients $A_{00} \ldots A_{21}$ were determined using a statistical matrix regression analysis routine. The values of the unknown coefficients are as follows

$A_{00} = 0.08080$ $A_{01} = 0.000323$ $r = 0.87$

$A_{10} = 1.56610$ $A_{11} = -1.1545E\text{-}03$ $r = 0.89$

$A_{20} = -1.7273$ $A_{21} = 1.0755E\text{-}03$ $r = 0.89$

Similarly, the drain nozzle discharge coefficient can be express in the form

$$C_{DnD} = b_0 + b_1 Z + b_2 Z^2 \qquad (4.7)$$

The resulting experimental values of b_0, b_1 and b_2 for the various supply pressures are shown in Table 4.2.

Table 4.2 Drain nozzle coefficient values

P_s (bar)	b_0	b_1	b_2
14.0	-0.031	1.916	-1.824
28.0	0.067	1.462	-1.161
42.0	0.131	1.185	-0.947
56.0	0.241	0.881	-0.871
70.0	0.243	0.888	-0.883

Again the coefficients b's are found to vary with supply pressure and the drain discharge coefficients can be expressed in a polynomial of the form

$$C_{DnD} = (B_{00} + B_{01}P_s) + (B_{10} + B_{11}P_s)Z + (B_{20} + B_{21}P_s)Z^2 \qquad (4.8)$$

This equation applies for $Z \neq 0.0, 1.0$.

The unknown coefficients $B_{00} \ldots B_{21}$ were determined using a statistical matrix regression analysis routine. The values of the unknown coefficients are shown below.

$B_{00} = -0.08640$ $B_{01} = 0.00036$ $r = 0.95$

$B_{10} = 2.05750$ $B_{11} = -0.00132$ $r = 0.92$

$B_{20} = -1.78880$ $B_{21} = 0.00109$ $r = 0.73$

The values of $A_{00} - A_{21}$ and $B_{00} - B_{21}$ as obtained in these forms were used in the steady-state theoretical model of the valve in Chapter 3. It should be worth noting that the discharge coefficients as obtained from experiment 4.2.1 used in this polynomial fittings did not include that obtained from

supply pressures greater than 70 bar because cavitation was encountered in the valve.

The discharge coefficients of the supply and drain nozzles are shown in Figures 4.13 and 4.14 respectively as a function of non-dimensional disc displacement. From Figures 4.10 and 4.11, the transition Reynolds number R_t is about 200. Orifice flow is laminar for Reynolds number $R_e < R_t$ with flowrates directly related to pressure drop. In the vicinity of R_t, both inertia and viscosity are important. For $R_e > R_t$, the flow can be treated as turbulent and described by the orifice equation (4.1) or (4.2). The orifice equation is used for all situations with a total disregard for the types of flow that can be encountered. Hence, the discrepancy between the measured discharge coefficient and that obtained from the derived empirical formulae as noted in Figs 4.13 and 4.14 near transition Reynolds number where disc displacement from both supply and drain nozzles is small.

The discharge coefficient results can only be compared qualitatively because the geometry of the free-floating disc valve is different from the existing flapper and disc valves in the literature. For example, the disc diameter to the supply nozzle ratio varies from one valve to another. That used by Takenaka et el [28] range from 2.5 to 3.5. In general, the flapper valve ratios are less than 5.0 compared to the disc valve investigated which has a minimum ratio of 10.0 . Clearly, the larger the diameter ratio, the smaller the discharge coefficient.

4.2.4 Experiment 4.2.2 : Repeatability of fluid force measurements.

The test procedure was the same as in experiment 4.2.1 except that the supply pressure was kept constant at 105 bar. The fluid force measurements were taken at two different periods and the results are shown in Figure 4.15. The two fluid force curves show that the fluid force measurements are

consistent with disc displacement. This reflect the repeatability of the fluid force measurements from the test-rig.

4.2.5 Experiment 4.2.3 : Effect of back pressure on fluid force characteristics.

The supply pressure was kept constant at 105 bar and the system back pressure was adjusted with the aid of a needle valve (34) {see Fig.4.1} situated downstream of the drain port (8). The disc zero position was determined as in previous experiments and the needle valve was fully-opened. The disc was given an incremental displacement in step of 0.03 mm from the supply nozzle land. The disc position was recorded by a dial gauge (17) and the corresponding fluid forces, pressures, and flowrates were registered by the appropriate instruments. The experimental procedure was repeated with the needle valve 87 and 67 per cent opened.

The results of varying the back pressure of the test valve on the fluid force curves are shown in Figure 4.16. From the Figure it can be seen that increasing the back pressure raises the fluid force in the region where the curve exhibits a minimum. The negative fluid force readings that occur within the region of cavitation in the valve disappear with increasing back pressure. This result suggests that a careful selection of the drain geometry will alter the fluid force characteristics of the valve. This will be discussed in Chapter 5 where the effect of the various parameters such as rod diameter, drain nozzle diameter, nozzle land diameter, etc are investigated based on the steady-state theoretical representation of the disc valve in Chapter 3.

4.3 Electro-magnetic force characteristics

In this section, the electro-magnetic characteristics of the electro-

magnetic coil used in the test valve were determined experimentally. Two different types of discs were used. They were: (1) a disc of 3.61 mm thickness with stops and (2) two flat discs of 2.54 mm and 4.06 mm thickness without stops. The stops were to prevent the disc from adhering to the coil surface otherwise the magnetic attraction force and the remanence would be too large. The discs are shown in Figure 4.17. The main dimensions of the electro-magnetic coil were as follows:

Effective coil outside diameter = 25.40 mm

Effective coil length = 15.88 mm

Total number of coil turns = 420 turns

Wire diameter = 0.22 mm

Coil Resistance = 11.2 ohm

4.3.1 **Experiment 4.3.1 : Electro-magnetic force characteristics of a coil using disc with stops.**

The apparatus used is shown in Figure 4.3 except that the hydraulic pipe network associated with the flow-force test rig were removed. The electro-magnetic force were determined with the disc in still air. The current level of the coil was provided by a special four-level switching amplifier (see Section 2.3.1 of Chapter 2 or appendix A2). The disc used had a diameter of 25.35 mm and therefore had a diametric clearance of 0.05 mm between the disc and the chamber diameter. The disc had stops of 3.61 mm thickness. The magnetic force acting on the disc was measured by the force transducer and the associated force transducer amplifier described in experiment 4.2.1. The electro-magnetic coil (5) used in the test valve (1) is shown in Figure 4.1. The wire leads were brought out to a BNC socket (2).

After setting up the apparatus, the zero position of the disc was established in the same manner as for the fluid characteristics

experiments. The required current level was selected after zeroing the force transducer and the dial gauge pointer. The disc was given an incremental displacement in steps of 0.03 mm with the aid of an operating handle (15). At each step, the disc displacement and the force acting on the disc were recorded. On reaching the maximum disc travel, the current was switched off and the disc was returned to its zero position before changing the current level of the coil. The frictional forces associated with the test rig for a positive disc displacement (i.e. disc moving away from the supply nozzle land) was greater than that of negative disc disc displacement and as such the tests were conducted without any reversal in disc displacement. The experiment was conducted for the coil current set at 500, 1000 and 1500 mA respectively and the results are shown in Fig.4.18. From this figure, it can be seen that the electro-magnetic force decreases almost inversely with an increase in disc displacement. The electro-magnetic force-stroke curves exhibit some local hump as the disc moves passed the mid-position of its stroke. This local hump is consistent as the coil current is increase from 500 to 1500 mA. The local hump which is more pronounced with large coil current, could be attributed to any of the following reasons: (a) the stops on the disc, (b) a possible jamming of the disc that might result from small clearance between the disc and its chamber and (c) the rod linking the disc to the force transducer might be bent and thus caused a frictional force between the rod and the linear bearing fitted into the valve body.

4.3.2 Experiment 4.3.2 : Examination of the local hump associated with the disc with stops.

To verify the causes of the local hump associated with the electro-magnetic force-stroke characteristics of a coil using a disc with stops, the diametric clearance between the disc and its chamber was increased to 0.13

mm. In addition, the rod was replaced with a newly fabricated one to eliminate any unevenness in the rod. Experiment 4.3.1 was repeated and the results were the same.

4.3.3 Experiment 4.3.3 : Electro-magnetic characteristics of coil using flat discs without stops.

In this section, two flat discs without stops were used to examine their magnetic characteristics. The discs were of thickness 2.54 and 4.06 mm respectively and the test procedure was the same as in experiment 4.3.2 except that flat discs without stops were used. The electro-magnetic forces were determined for coil currents from 500 to 1500 mA in steps of 250 mA and Figure 4.19 shows the results of the 2.54 mm disc thickness. The results of the 4.06 mm disc thickness are shown in Figure 4.20. From the two Figures it can be seen that the electro-magnetic force-stroke characteristics follow an inverse-square law for the flat discs without stops. The chained lines in the figures are the computed electro-magnetic characteristics of the coil based on the highly non-linear equations (3.60) through (3.82) of Chapter 3. The theory uses design data concerning the coil turns, cross-sectional areas of the core, magnetic lengths, coil permeances, flux densities and flux intensities of the various part of the magnetic circuit. The magnetic properties are obtained from the magnetisation curve for REMKO magnetic iron. For a given current the magnetic force associated with the thicker disc is greater than the thinner disc. As the disc displacement increases from the supply nozzle land, the magnetic force follows the inverse-square law to a point close to the mid-position of the disc total travel. For the next approximately 0.15 mm disc displacement, the magnetic force is constant. After which it drops sharply to follow the inverse-square law again. The position where the magnetic force becomes constant is seen to increase with current. Compared with the

disc with stops, the initial magnetic force or the sealing-in force of the flat discs are lower than the discs with stops. This is because the stops provide an additional flux path and thereby generate additional magnetic force to cause the observed local hump. A flat disc has no local hump. Owing to the complex nature of the equations governing the magnetic characteristics of the coil, simpler empirical formulae are sorted from the test data to assist the designer without resulting into tedious computations.

4.3.4 Empirical formulae

To make it possible for the designer to obtain for a specific electro-magnetic flat face coil the force - stroke characteristics for a given coil size, empirical formulae are developed from the series of test measurements carried out. From the experimental results, it was observed that the magnetic force -stroke characteristics for the flat discs without stops obeyed an exponential law. Expressing this relationship in a mathematical form we have

$$F_m = a\, e^{bX} \tag{4.9}$$

where F_m is the electro-magnetic force, X is the disc displacement from the supply nozzle land and a,b are coefficients that depend on current and disc thickness

To obtain coefficients 'a' and 'b', regression analysis are used. The resulting values of 'a' and 'b' and the determinating coefficient r for the 2.54 and 4.06 mm disc thickness are shown in Tables 4.3 and 4.4 respectively. The coefficient 'a' was also related to the current input to the coil in the form given by equation (4.10)

$$a = K\, I^C \tag{4.10}$$

Using regression analysis, the values of K and C for the different discs

used are shown in Table 4.5.

Table 4.3: Coefficients a and b for 2.54 mm disc thickness

Current (mA)	a	b	r
500	81.060	-4.527	0.998
750	117.790	-3.994	0.992
1000	166.690	-3.478	0.999
1250	182.770	-2.978	0.999
1500	211.98	-2.631	0.995

Table 4.4: Coefficients a and b for 4.06 mm disc thickness

Current (mA)	a	b	r
500	133.290	-7.6145	0.951
750	168.740	-5.2080	0.983
1000	202.740	-4.5633	0.982
1250	225.300	-3.6765	0.993
1500	237.840	-2.8528	1.000

Table 4.5: Coefficients K and C

Disc thickness T (mm)	K	C	r
2.54	0.3397	0.88470	0.984
4.06	4.6538	0.54213	0.990

The exponent b in equation (4.9) has a linear relationship with the coil input current and can be written as

$$b = D + E\,I \qquad (4.11)$$

The values of D and E are shown in Table 4.6.

Table 4.6: Coefficients D and E

Disc thickness T (mm)	D	E	r
2.54	-5.4448	1.9232E-03	0.994
4.06	-9.2050	4.42196E-03	0.930

From Tables 4.5 and 4.6, it can be seen that the coefficients K, C, D and E are functions of disc thickness used as an armature in a flat-faced electro-magnetic coil. The relationships between the disc thickness T and each of the coefficients K, C, D and E are expressed in equations (4.12) through (4.15) respectively using regression analysis.

$$K = 1.891 \times 10^{-3} T^{5.5688} \quad (4.12)$$

$$C = 2.3369 / T^{1.042} \quad (4.13)$$

$$D = 0.8222 - 2.46732\ T \quad (4.14)$$

$$E = 3.6887 \times 10^{-4} T^{1.77146} \quad (4.15)$$

From equations (4.9), (4.10) and (4.11) the electro-magnetic force - stroke characteristics of the flat face coil used in the disc valve can be expressed in the form

$$F_m = K\ I^C\ e^{(D + E\ I)X} \quad (4.16)$$

This empirical formula gives good agreement between the various series of tests for electro-magnetic coils of the flat-face magnet type (see Figs. 4.21 and 4.22) except for flat section of curves. With the aid of the Reynolds law of similarity, this relationship can be extended to cover other electro-magnetic coil sizes. It must be noted that these empirical formulae are not used in the theoretical model of the valve. They only serve as a quick method of calculating the electro-magnetic force-stroke characteristics of a flat face coil, given the coil current, disc thickness

and disc displacement.

With the aid of the empirical formulae, the effect of disc thickness on magnetic force-stroke curves for a given coil current and coil size were computed. Figure 4.23 shows for coil current of 500 mA the effect of varying the disc thickness from 2.5 to 5.0 mm on the force-stroke curves. From the Figure it can be seen that the force-stroke curves do not have significant change for disc thickness less than about 3.5 mm. For disc thickness greater than 3.5 mm, it can be seen that the initial force or the sealing-in force increases with disc thickness. However, this advantage must be offset against the low inertia of the thinner discs which improves the dynamic performance of the valve. For the disc thickness less than 3.5 mm it can be seen from the figure that the force levels fall off slowly as the distance between the coil surface and the disc face is increased. On the other hand, the force levels of disc thickness greater than 3.5 mm fall off quickly with disc displacement. This could be explained from the flux across the working gap of the thinner discs which is saturated while that of the thicker discs have negligible flux losses when they are operating close to the coil surface.

This chapter has validated both the theoretical fluid and electro-magnetic models of the disc valve presented in Chapter 3. The next chapter will be dealing with some design considerations for the double-disc valve based on the theoretical and experimental results of Chapters 3 and 4.

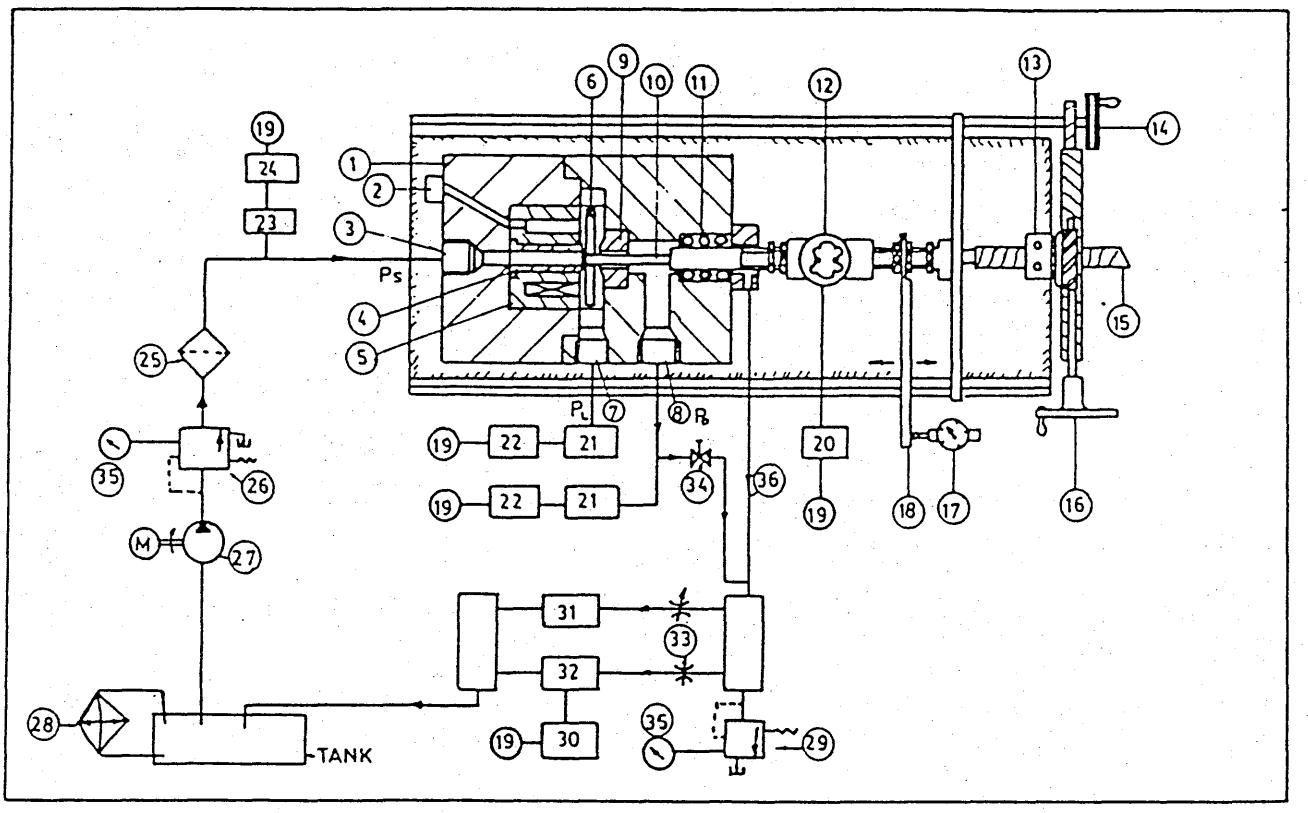

(1) Test valve
(2) Coil socket
(3) Supply port
(4) Supply nozzle
(5) Electro-magnetic coil
(6) Disc
(7) Load port
(8) Drain port
(9) Drain seat
(10) Push rod
(11) Linear bearing
(12) Force transducer
(13) Lock nut
(14) Quick return wheel
(15) Operating screws
(16) Operating handle
(17) Dial gauge
(18) Beam
(19) Digital voltimeters
(20) Force transducer amplifier
(21) Piezo-electric pressure transducer
(22) Amplifier for item No. 21
(23) Supply pressure transducer
(24) Amplifier for item No. 23
(25) Filter
(26) Pressure regulator/relief valve
(27) Pump
(28) Electric air fan
(29) Relief valve
(30) Flowmeter amplifier
(31) Turbine meter type B/$\frac{5}{8}$"/15 GPM
(32) Turbine meter type B/$\frac{1}{4}$"/1 GPM
(33) Directional valves
(34) Needle valve
(35) Pressure gauges
(36) Flexible tubing

Fig. 4.1 Schematic lay-out of fluid force test-rig.

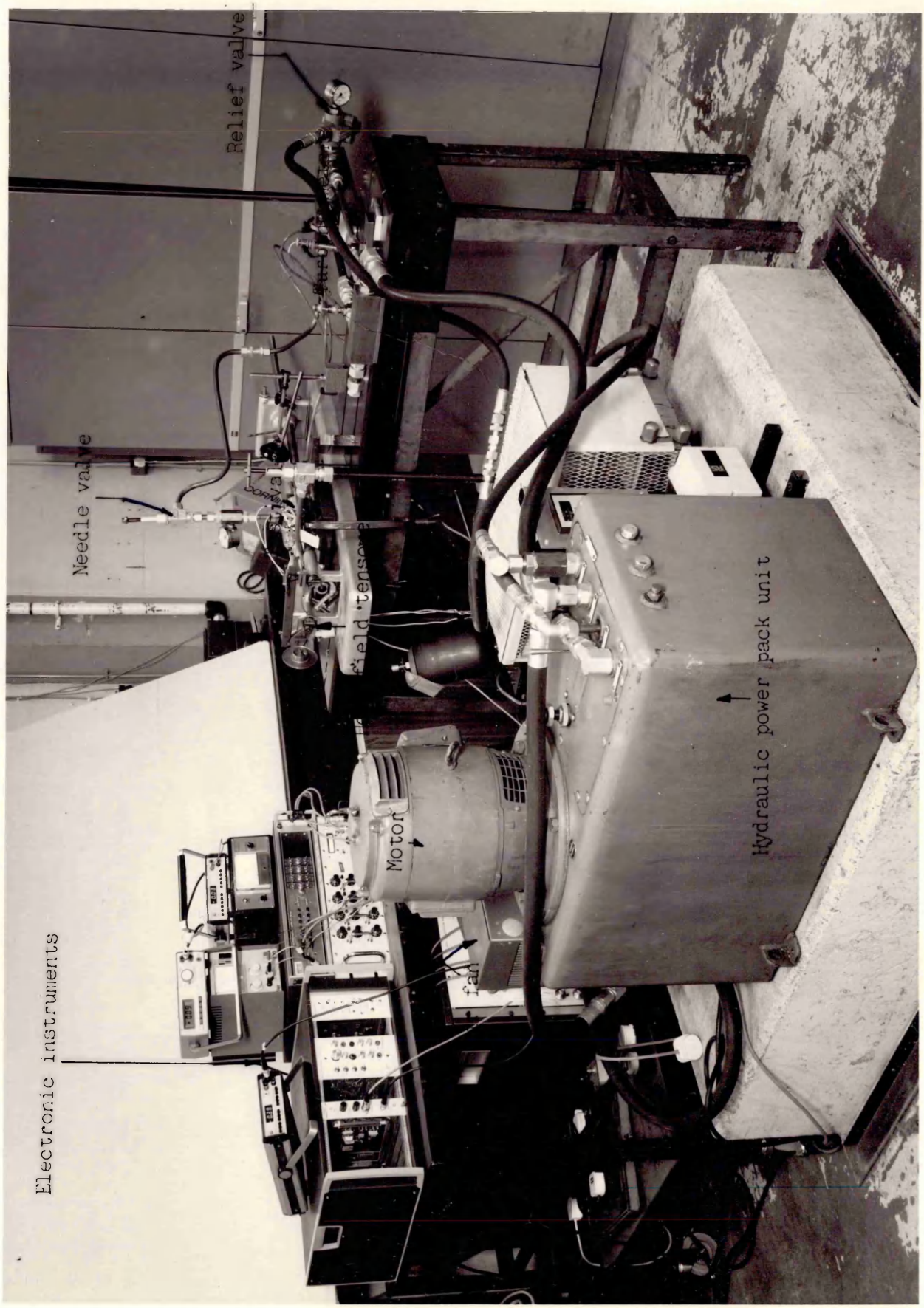

Fig. 4.2 Fluid force test-rig.

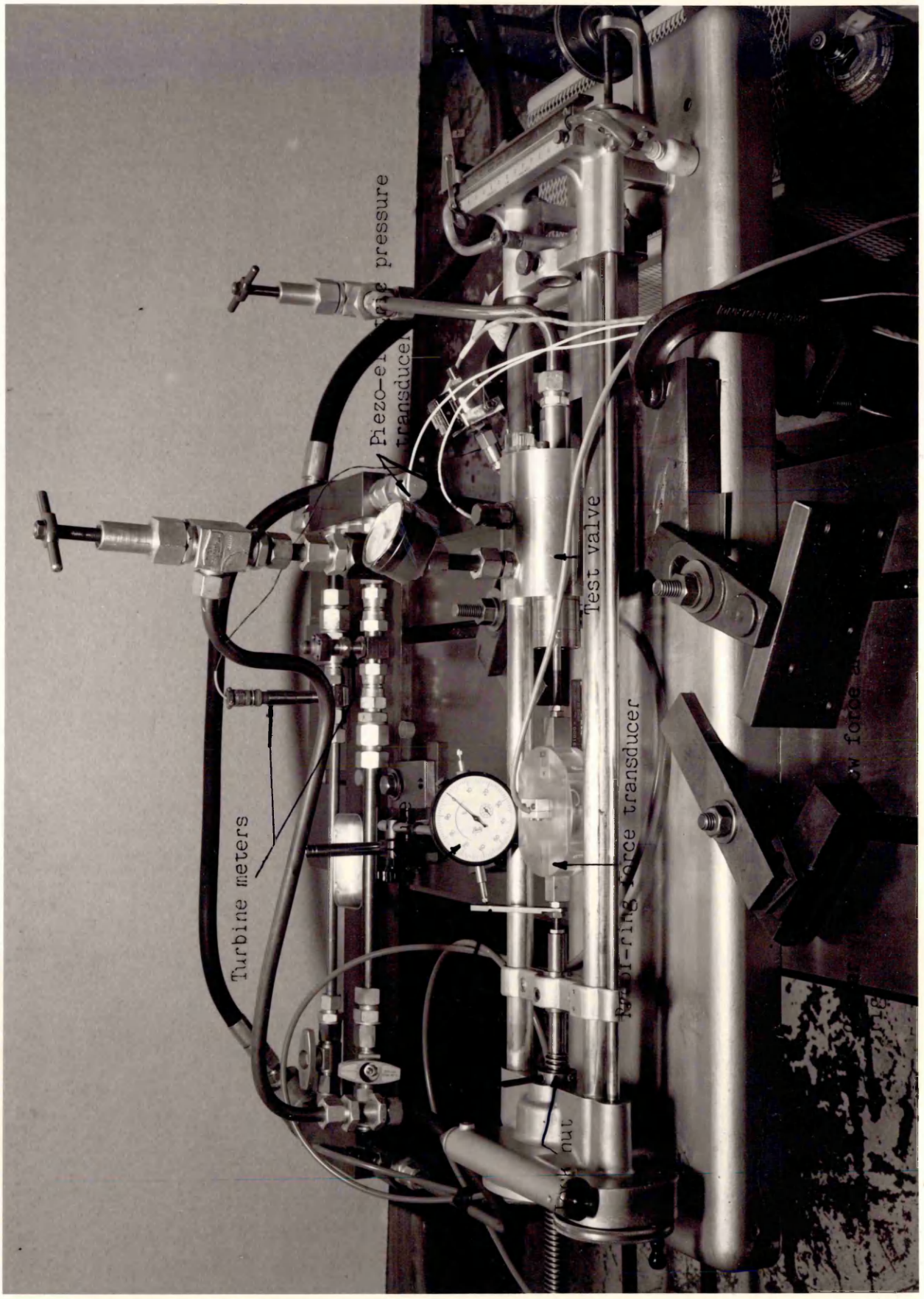
Turbine meters
Test valve

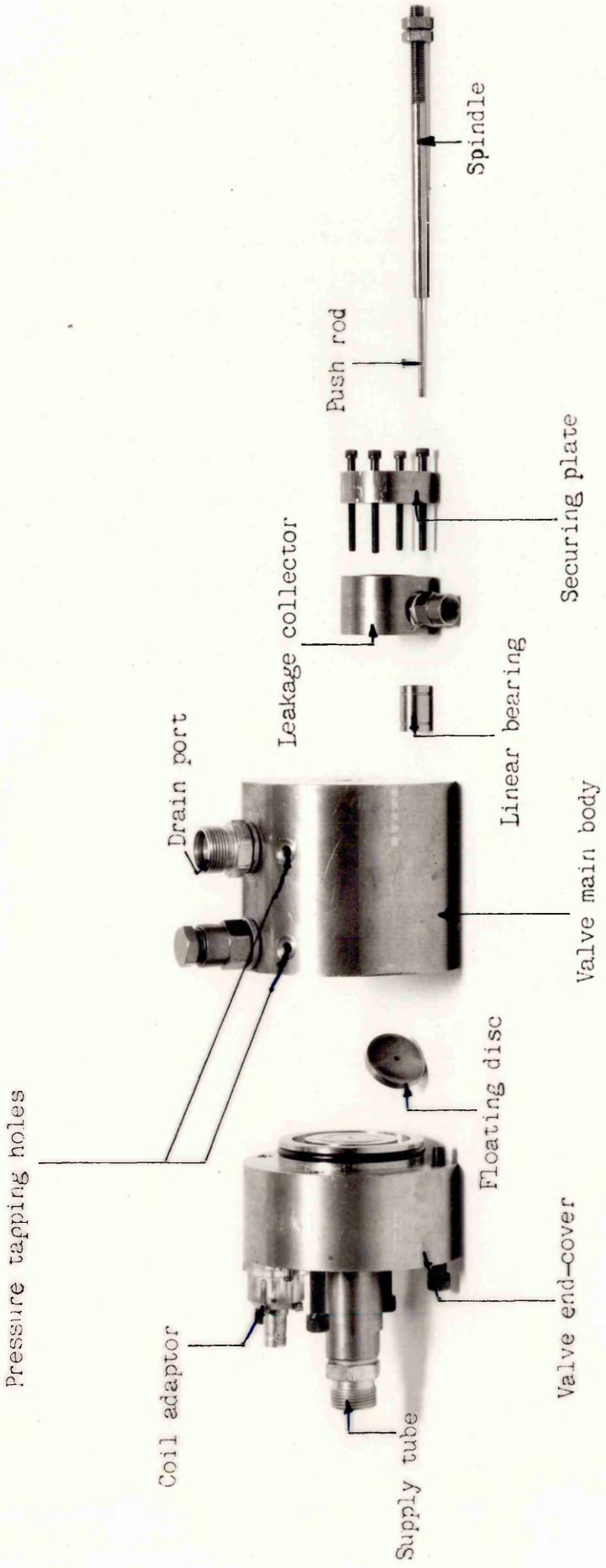

Fig. 4.4 Exploded view of the test valve.

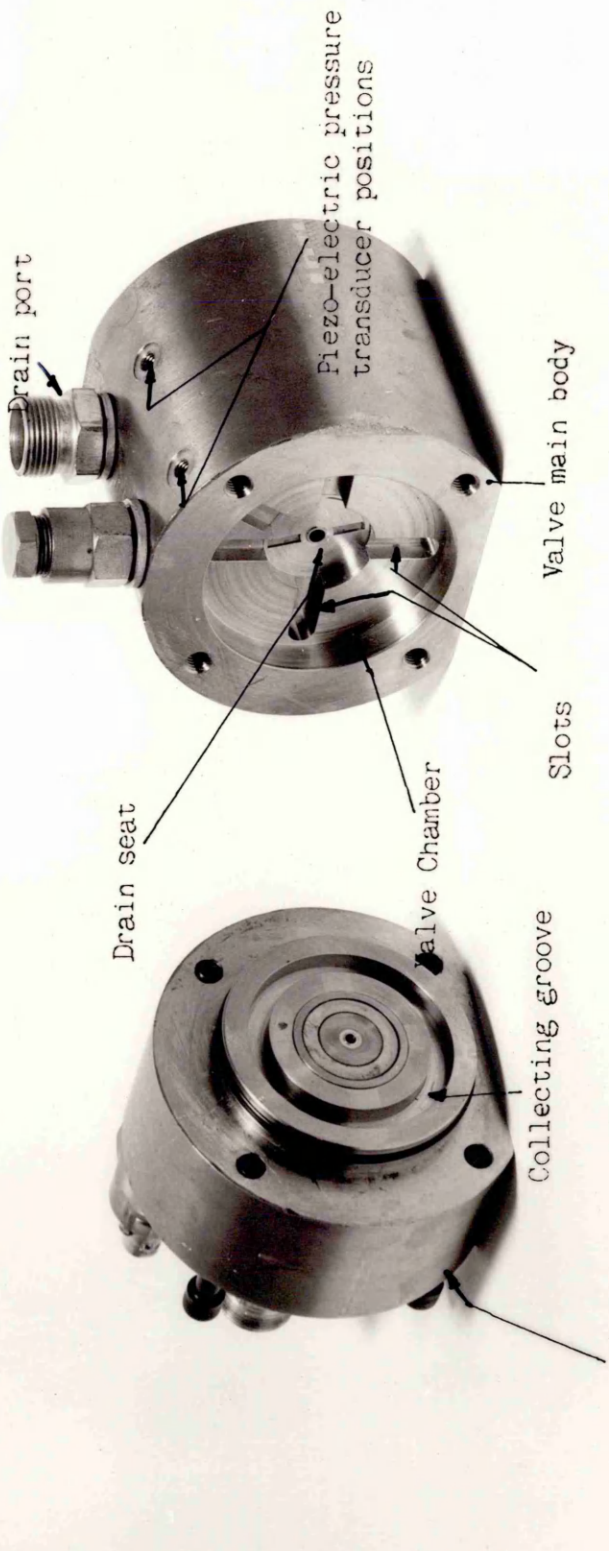

Fig. 4.5 Interior view of the test valve.

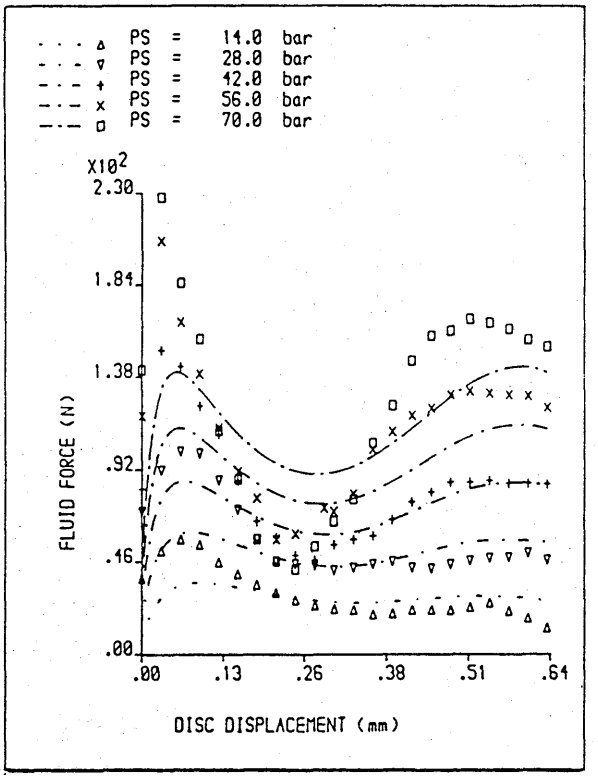

Fig. 4.6 Fluid force curves for 3.05 mm land diameter

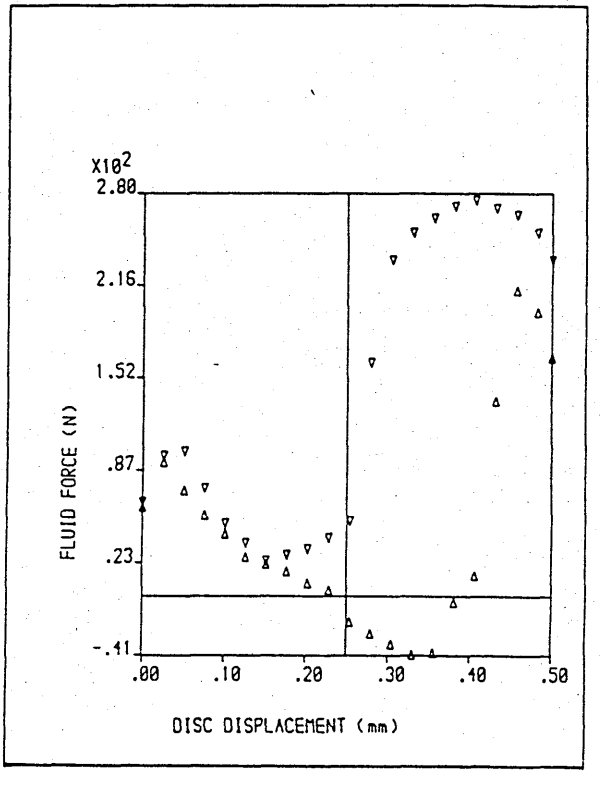

Fig.4.7 Effect of cavitation on fluid forces.

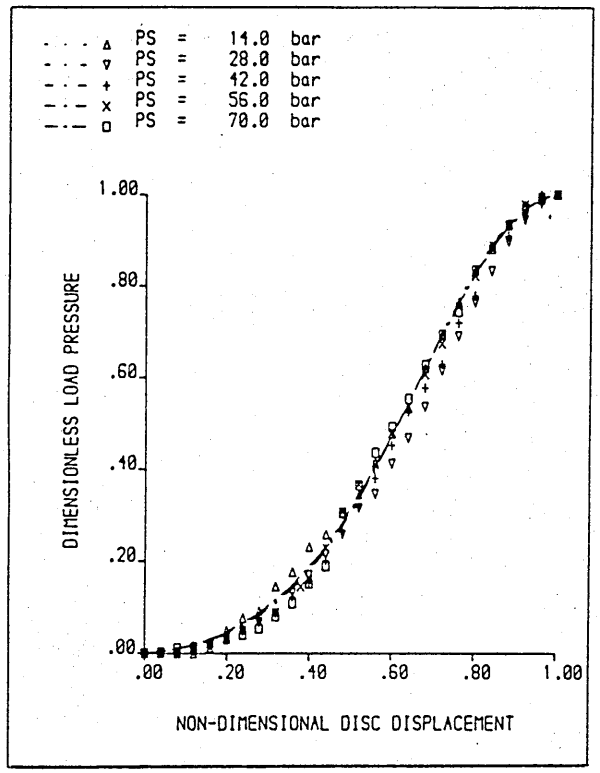

Fig. 4.8 Load pressure curves for 3.05 mm land diameter.

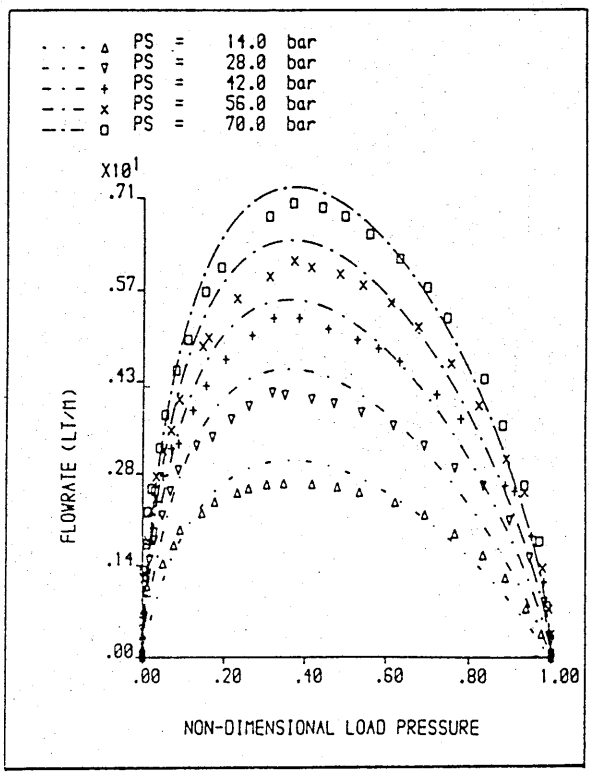

Fig. 4.9 Flowrate curves for 3.05 mm land diameter.

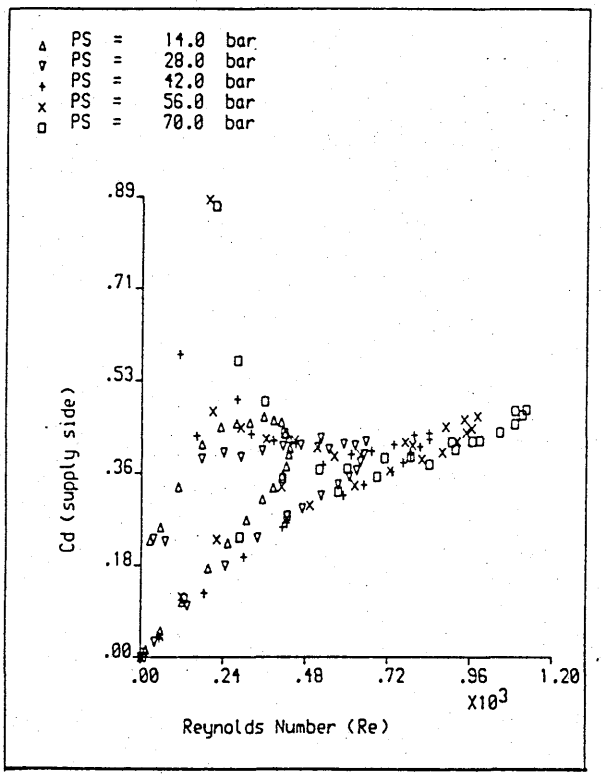

Fig. 4.10 Discharge coefficient as a function of Reynolds number (supply nozzle side).

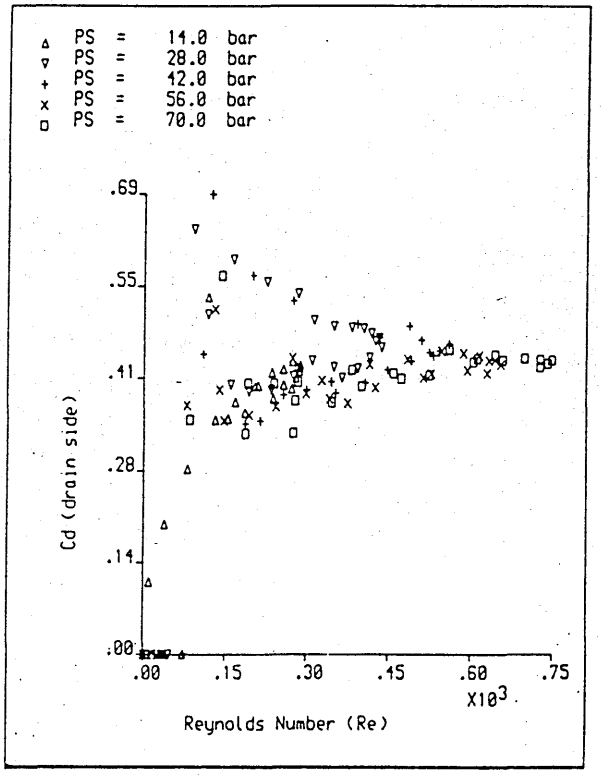

Fig. 4.11 Discharge coefficient as a function of Reynolds number (drain nozzle side).

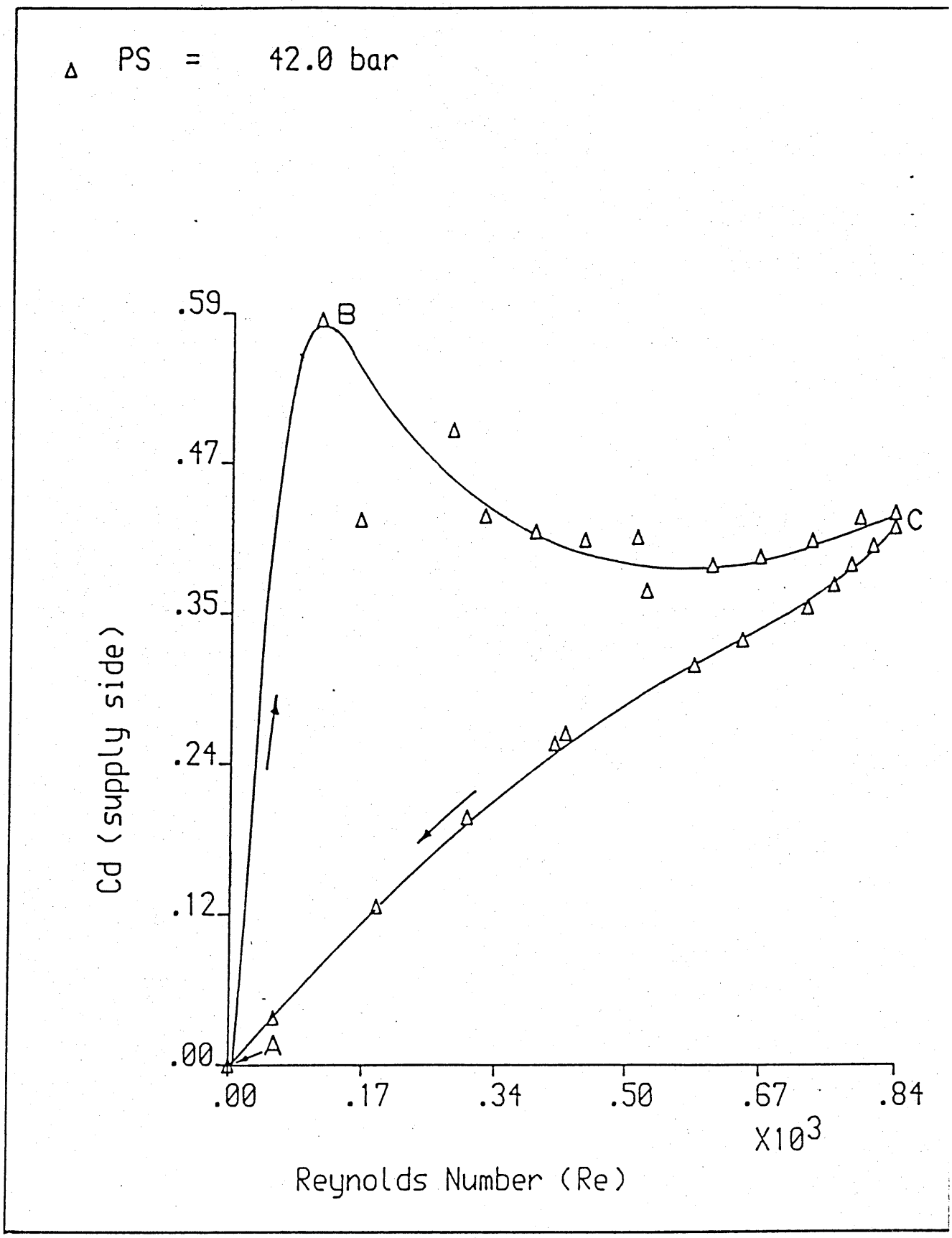

Fig. 4.12 Typical relationship between supply discharge coefficient and Reynolds number as a disc moves through the disc chamber.

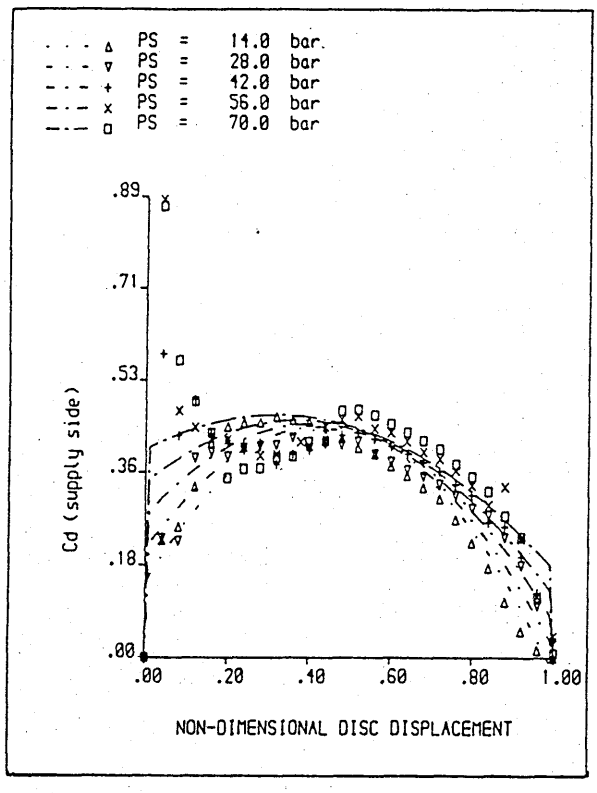

Fig. 4.13 Discharge coefficient as a function of disc displacement (supply nozzle side).

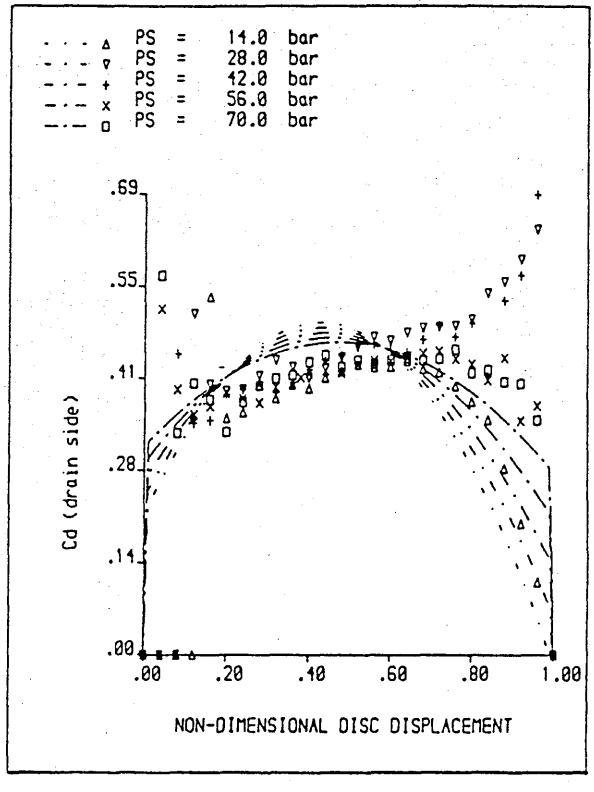

Fig. 4.14 Discharge coefficient as a function of disc displacement (drain nozzle side).

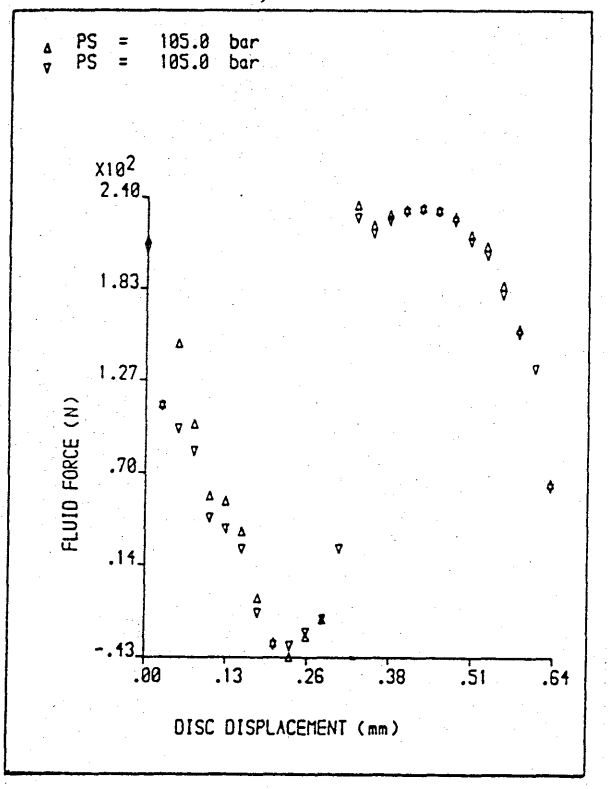

Fig. 4.15 Consistency of fluid force measurements.

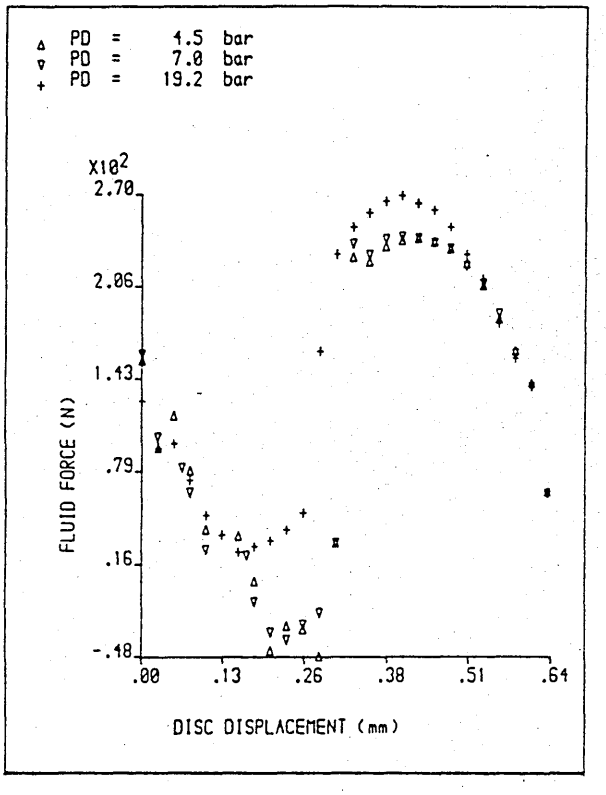

Fig. 4.16 Effect of back pressure on fluid forces.

Disc thickness	2.54 mm	3.61 mm	4.06 mm
Type	No stops	With stops	No stops

Fig.4.17 Different discs used with the test valve

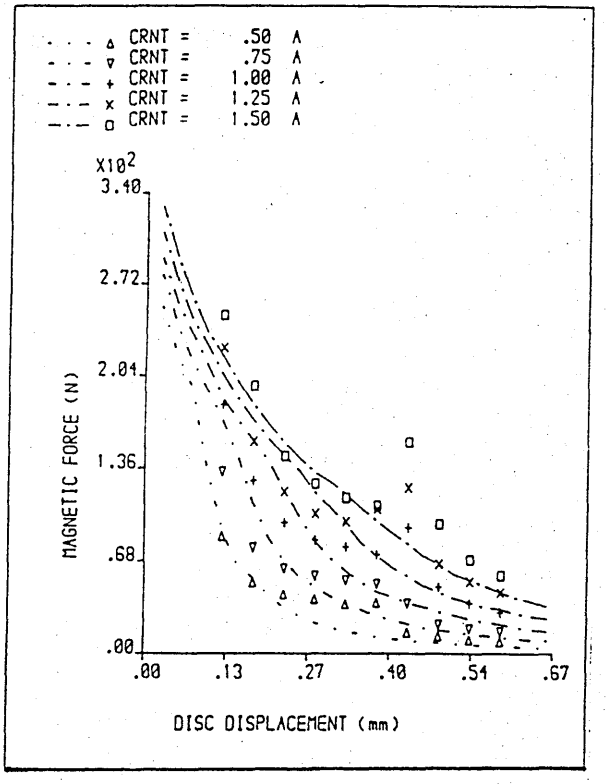

Fig. 4.18 Electro-magnetic force-stroke curves (3.61 mm disc thickness with stops).

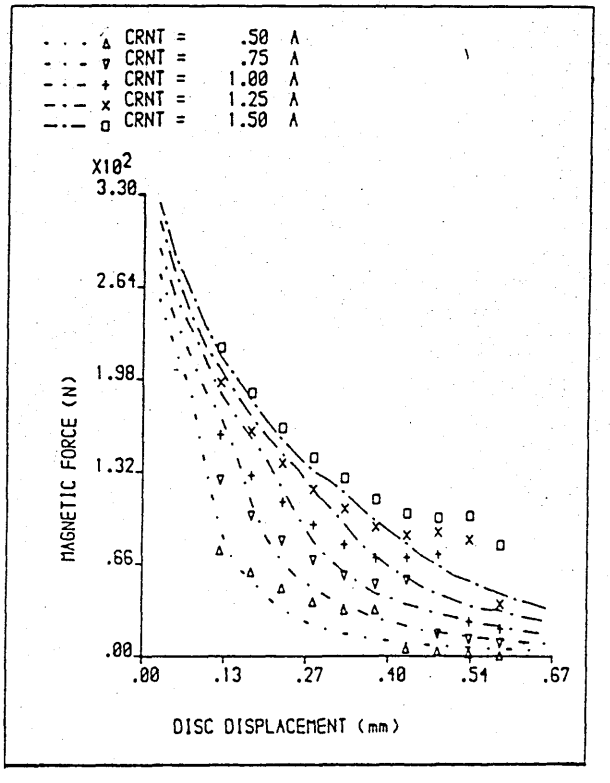

Fig. 4.19 Showing the comparison of experimental and theoretical magnetic force (2.54 mm disc thickness without stops).

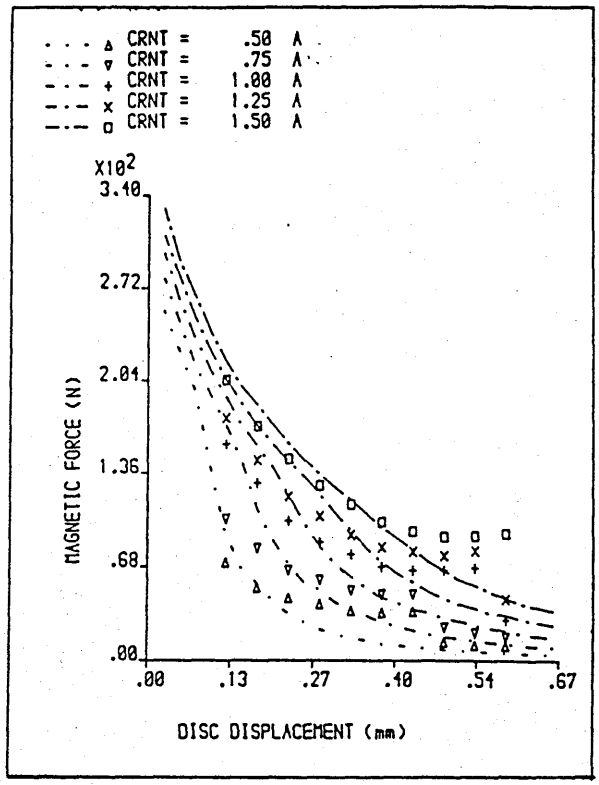

Fig. 4.20 Comparison of experimental and theoretical magnetic force-stroke curves for disc without stops of 4.06 mm thickness.

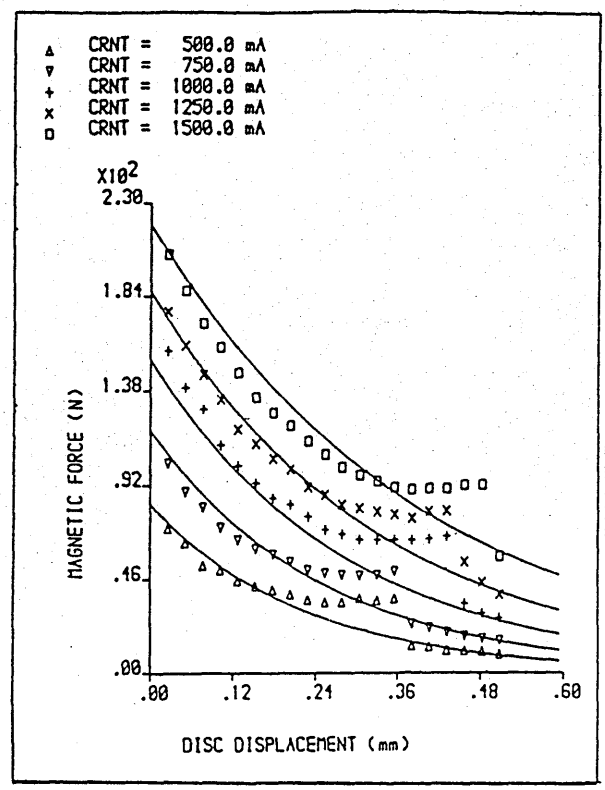

Fig. 4.21 Empirical Magnetic force - stroke curves for disc without stops of 2.54 mm thickness.

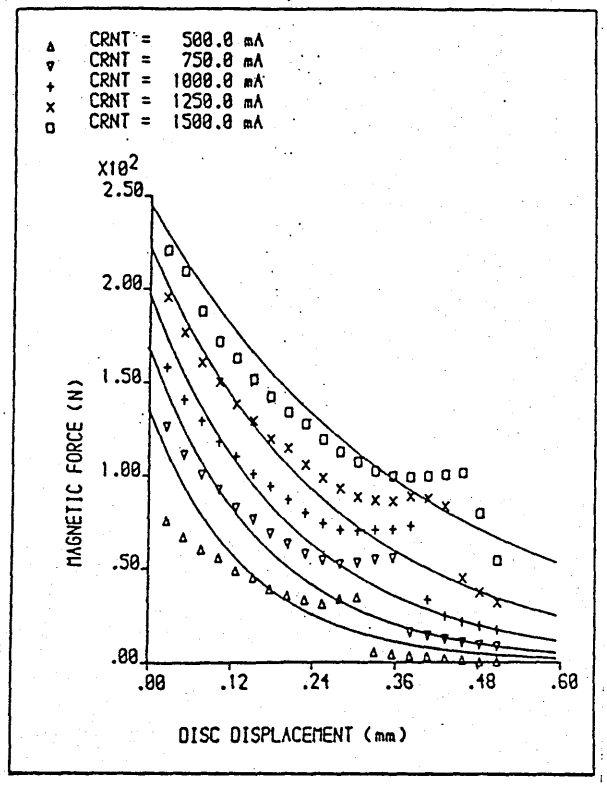

Fig. 4.22 Empirical Magnetic force - stroke curves for disc without stops of 4.06 mm thickness.

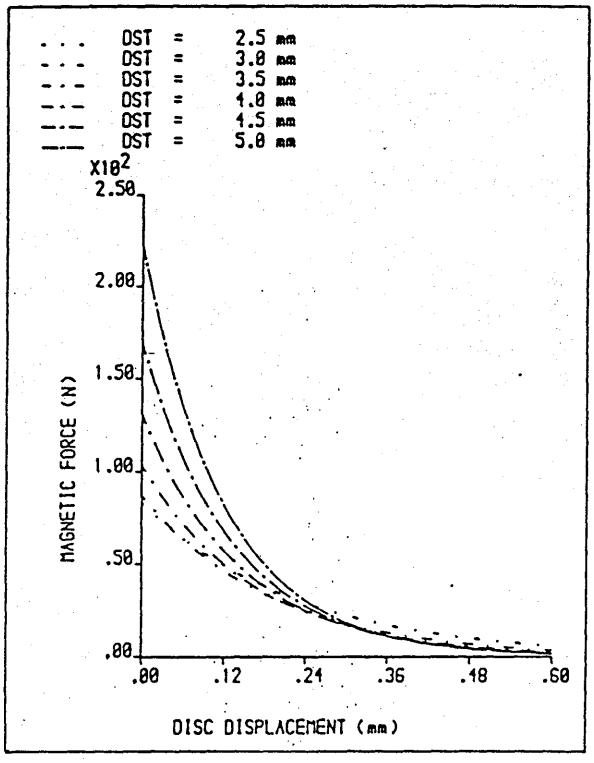

Fig. 4.23 Effect of disc thickness DST on magnetic force-stroke curves for coil current of 500 mA.

CHAPTER 5

DESIGN CONSIDERATIONS FOR THE DOUBLE-DISC VALVE

5. Design considerations for the double-disc valve

5.1 Introduction

In Chapter 4, the fluid mechanics of the disc valve was established from a special flow-force rig constructed to determine the complex fluid forces acting on a single disc. The rig had the facility for allowing radial flow across the disc faces in both directions to simulate flow into and out of the load port into the drain connection. The fluid forces obtained from the experiment agreed well with that of theoretical prediction in Chapter 3.

Two different supply nozzle land diameters were used. They were in ratios of 1.2 and 1.4 to the supply nozzle diameter respectively. Cavitation was prominent with the larger land diameter and occurred for disc displacements from the supply nozzle tip of less than about 30 per cent of the total disc travel. The presence of the cavitation caused a reduction in fluid force, flowrate and load pressure. The cavitation was due to the flow restriction in the nozzle land region as decreasing the supply nozzle land diameter to nozzle diameter ratio to a value less than 1.2, reduced the occurrence of cavitation. Increasing the back pressure or decreasing the system pressure tended to reduce the onset of cavitation. However, altering the system pressure is not the best compromise and in good valve design the flow saturation or restriction should be considered in selecting the valve variable geometries and this is the subject of this chapter.

With the smaller supply nozzle land diameter, negative flow-forces were measured for disc displacements in the region of 25 to 45 per cent of total disc travel for a supply pressure of 105 bar. This could be owing to the large pressure drop across the drain side of the disc. The flow restriction may be eliminated by increasing the drain holding gap as noted in the geometrical equations derived in this chapter.

Tests, using the same rig as for the flow-force experiments, were made to measure the electro-magnetic force induced in the disc for various current levels in the coil and also for the force variation with distance of the disc from the coil face. This is particularly important for determining the correct holding gap between the coil face and the nozzle abutment for the disc. Theoretical predictions agree well with electro-magnetic force data for a single disc thus allowing the theoretical model to be used with some confidence for determining suitable values for the main geometric variables of the double-disc valve.

In this chapter some geometrical design considerations for the double-disc valve will be present together with their effect on the double-disc valve characteristics. The theoretical model of Chapter 3 conveniently allows any of the main geometric parameters to be varied independently.

5.2 Some geometrical design considerations

5.2.1 Geometrical relationship between a disc and its chamber

In selecting the clearance between a disc diameter and its chamber diameter, the following points were considered: (i) Thermal expansion of the disc material and (ii) Possible jamming or tilting of the disc inside its chamber.

(a) **Thermal expansion**

For a given temperature rise, $d\theta$, the expansion, dD, on the disc diameter is given by:

$$dD = \theta_c . D . d\theta \qquad (5.1)$$

where θ_c is the coefficient of linear expansion of the disc material, D is the disc diameter and $d\theta$ is the rise in temperature.

To avoid any jamming of the disc in its chamber, dD must be less than the

diametric clearance between the disc and its chamber. For REMKO magnetic iron used for the disc, $\theta_c = 17 \times 10^{-6}/^{o}K$ and assuming a temperature rise of $35^{o}K$ and disc diameter of 31.75 mm approx., the maximum expansion on the disc diameter would be 0.02 mm and is therefore acceptible in comparison with the diametric clearance of approximately 0.1 mm.

(b) **Disc tilting in its chamber**

Figure 5.1 shows a disc PQRS jammed in its chamber KLMN. The aim of this section is to establish a necessary condition to avoid this effect.

From triangle PQR or PRS, it can be seen that if PR > CD, there will be no disc jamming in its chamber. In mathematical form we have

$$D^2 + t_a^2 > CD^2 \tag{5.2}$$

where t_a is the disc thickness, D is the disc diameter and CD is the chamber diameter.

For a flat and uniform disc, the distance SP must be equal to RQ and PQ parallel to RS. From triangle RPQ,

$$\tan\theta_t = RQ/PQ = t_a/D \tag{5.3}$$

where θ_t = angle of tilt.

Also from triangle PLQ,

$$\sin\theta_t = PL/PQ \tag{5.4}$$

From triangle PKS we have,

$$\cos\theta_t = KP/SP \tag{5.5}$$

The chamber width is given by

$$KL = PQ\sin\theta_t + SP\cos\theta_t = D\sin\theta_t + t_a\cos\theta_t \tag{5.6}$$

From equation (5.3), $D\sin\theta_t = t_a\cos\theta_t$ which can be substituted in equation (5.6) to give

$$KL = 2t_a\cos\theta_t \tag{5.7}$$

For normal valve operation, the disc chamber is given by

$$KL = T_D + t_a \tag{5.8}$$

where T_D is the total disc travel.

Equating equations (5.7) and (5.8) to get

$$T_D = t_a(2\cos\theta_t - 1) \tag{5.9}$$

The disc chamber diameter is given by

$$CD = D + dD \tag{5.10}$$

where dD is the diametric clearance between disc and its chamber.

From equations (5.2) and (5.3) we have

$$\tan\theta_t = t_a/(CD^2 - t_a^2)^{1/2} \tag{5.11}$$

Equation (5.11) gives the relationship between the disc thickness and maximum angle of tilt, for a given disc chamber diameter.

Using equation (5.10) in (5.2) gives

$$dD = CD - (CD^2 - t_a^2)^{1/2} \tag{5.12}$$

Equation (5.12) gives the maximum theoretical diametric clearance between the disc and its chamber for which tilting is likely to occur. From a practical point of view, the author recommends that a clearance of less than 40 per cent of that given in equation (5.12) should be used.

From equation (5.9), if there is no disc tilting, (that is $\theta_t = 0$), we have

$$T_{Dmax} = t_a \tag{5.13}$$

In the valve design, T_D is less than $t_a/10$ owing to the limitation of magnetic force available over a long stroke. From the electro-magnetic properties of the disc, it is found that the magnetic force increases with disc thickness for a given displacement. From this discussion, it follows that the disc thickness controls both the magnetic force required and the tilting action of the disc. The thinner the disc, the smaller the diametric

clearance becomes. This will consequently increase the contamination sensitivity of the valve. The thicker the disc, the greater the disc inertia and the speed of response decreases. In selecting the disc thickness, therefore, there should be a compromise between the magnetic properties, the dynamic performance and the jamming possibilities of the disc in its chamber. For this valve design, the diametric clearance, dD, is about 0.3 per cent of chamber diameter of 31.75 mm and the disc thickness is about 7.5 times the total disc travel of 0.51 mm.

5.2.2 Effect of disc chamber geometry on valve leakage flow

Leakage flow for proportional action of the valve is defined as the flow through the valve, owing to underlap only, with the valve in its neutral or null position and under no load conditions. This flow is of the orifice resistance type, i.e., it is proportional to the port area and the square root of the pressure drop and is largely independent of temperature. Total leakage flow does, of course, include viscous losses which are a function of the design of the valve, diametral clearances and temperature. Figure 5.2 shows the disc valve chamber in which the disc is in its null position. The aim of this section is to derive expressions for the geometry of the disc chamber with a view to limiting the valve null leakage flow.

In the neutral position, the leakage flow is governed by the supply nozzle curtain area, the drain nozzle curtain area and the annular space formed by the push rod and the drain nozzle diameters. The supply nozzle area must be greater than or equal to the maximum supply curtain area for the supply nozzle to act as an orifice. That is

$$D_{ns} \geq 4\ T_D \qquad (5.14)$$

To limit the null leakage flow it is desirable that the supply curtain area

is greater than that of the drain. In mathematical form we have

$$D_{ns}\, X_{f1} \geq D_{nD}\, X_{f2} \tag{5.15}$$

To further limit the leakage flow, the push rod diameter can be used to restrict the flow through the drain port. That is

$$\left[\, 4\, D_{nD}\, X_{f2} \,\right] \geq \left[\, D_{nD}^2 - D_R^2 \,\right] \tag{5.16}$$

For effective valve design equations (5.14) through (5.16) should be satisfied. From Fig.5.2 it can be seen that the total disc travel T_D is given by

$$T_D = X_{f1} + X_{f2} \tag{5.17}$$

where X_{f1} and X_{f2} are the respective supply and drain neutral gap between the disc surfaces.

The rod clearance C_R is given by

$$C_R = X_{f1} - X_{f2} \tag{5.18}$$

The values of D_R and X_{f2} are governed by the maximum allowable leakage flow through the valve. The total null leakage flow is given by

$$Q_c = 2\, C_{DnD} \pi D_{nD}\, X_{f2} \sqrt{\frac{P_s}{\rho}} \tag{5.19}$$

The total centre flow through the valve is useful because it gives the power loss at the null operating point. The valve total disc travel T_D should be as small as possible to achieve largest pressure sensitivity and smallest null leakage. However, it must be large enough to permit passage of dirt particle sizes expected in the fluid. It may be of interest to tabulate some compatible values of the quantities involved in equations (5.14) through (5.19). Selecting five T_D values, the results are given in Table 5.1. The null leakage flow is computed from (5.19) with P_s=70 bar, C_D=0.5 and tabulated to show the large increase in this flow with increasing total disc travel. It should be emphasized that Table 5.1

contains recommended design values based on the use of equations (5.14) through (5.18) with an equality sign assumed.

Table 5.1 Typical design values of T_D, D_{ns}, D_{nD}, D_R, C_R, X_{f1}, X_{f2} and Q_c

T_D (mm)	D_{ns} (mm)	X_{f1} (mm)	X_{f2} (mm)	C_R (mm)	D_{nD} (mm)	D_R (mm)	Q_c (Lt/min)
0.25	1.02	0.15	0.10	0.05	1.52	1.27	2.70
0.38	1.52	0.20	0.18	0.02	1.75	1.35	5.43
0.51	2.03	0.30	0.20	0.10	2.03	1.59	7.20
0.64	2.54	0.40	0.24	0.16	2.54	2.00	10.70
0.76	3.00	0.46	0.30	0.16	3.00	2.38	16.20

5.2.3 Effect of disc chamber geometry on valve flow saturation

It is possible to obtain a design relation between T_D and HG_D from a consideration of flow saturation. The disc chamber passage volumes (see Fig. 5.3) should be at least four times the maximum orifice volumes to prevent flow saturation and to ensure that the orifices are the controlling restrictions [55]. This implies that the drain side of disc chamber volume must be greater than that of the supply nozzle tube,

$$\left[(D^2 - D_{nLD}^2) HG_D \right] > \left[4 D_{ns}^2 (L_{snt} + T_D) \right] \tag{5.20}$$

and the supply side of disc chamber volume must be greater than that of the supply nozzle tube

$$\left[(D^2 - D_{snL}^2)(HG_s + T_D) \right] > \left[4 D_{ns}^2 (L_{snt} + T_D) \right] \tag{5.21}$$

From equations (5.20) and (5.21) it implies that

$$HG_D > \left[\frac{1 - (D_{nsL} / D)^2}{1 - (D_{nLD} / D)^2} \right] (HG_s + T_D) \tag{5.22}$$

If $D_{nsL} / D \ll 1$ and $D_{nLD} / D \ll 1$ then equation (5.22) can be rewritten as

$$HG_D > (HG_s + T_D) \tag{5.23}$$

Equation (5.23) suggests that the total disc travel T_D should be less than the drain holding gap HG_D to avoid flow saturation in the valve. Experience has shown that cavitation are likely to occur in the valve if there is flow restriction within the valve. Dividing equation (5.20) by D^2 and assuming that $D_{nLD}/D \ll 1$ and $T_D \ll L_{snt}$ we have

$$\left[HG_D / L_{snt} \right] > \left[4 \left(D_{ns} / D \right)^2 \right] \qquad (5.24)$$

Equation (5.24) shows the geometrical relationship between the drain holding gap HG_D and the supply tube length L_{snt}.

5.3 Effect of parameter changes on valve theoretical steady-state model

In Section 3.1 of Chapter 3, a theoretical steady-state fluid characteristics model of the disc valve was developed. In Section 4.2 of Chapter 4, the complex fluid forces acting on a single disc were determined under blocked-load conditions and the force data agreed well with theoretical predictions. This allows the theoretical model to be used with some confidence for determining suitable values for the main geometric variables of the double-disc valve. In this section, the effect of changing different parameters in the model will be presented with one parameter varied at a time. Table 3.1 shows the assumed values for the parameters.

Using these values for the valve parameters, the theoretical model shows that the level of rise in the fluid forces when the disc approaches the drain nozzle, noted in Chapters 3 and 4, can be controlled by the correct choice of drain nozzle geometry and drain holding gap. The theoretical steady-state fluid model for the valve shows that the ratio of the drain nozzle area to that of the supply nozzle influences the fluid forces acting on a single-disc in its chamber. The net fluid forces acting on a double-disc valve configuration under blocked load conditions are shown in Fig.5.4

for various drain-to-supply nozzle area ratios. From the figure it can be seen that when the area ratio is increased from 1.08 to 1.85, the gradient at null position falls off quickly and a point of inflection is observed for area ratio of 1.85. For best stable characteristics of the valve near null position, figure 5.4 suggests equal areas for the drain and supply nozzles. Where the net fluid force curve crosses the displacement axis it corresponds to the position of zero net fluid force and the discs and the rod assembly is stationary at that point if the curve gradient is negative. The theoretical model has shown that increasing the drain holding gap lowers the fluid force rise that occurs after the disc displacement passes its mid-position. The effect of drain holding gap will be fully discussed later. Using equal areas for the drain and supply nozzles, the new assumed values for the parameters used in the model are shown in Table 5.2.

Table 5.2 Physical constants of the valve main parameters

DSD = 31.65 mm	PS = 70 bar
TD = 0.51 mm	CR = 0.00 mm
HGS = 0.13 mm	RODD = 2.38 mm
HGD = 0.51 mm	DND = 3.18 mm
SND = 3.18 mm	DNTL = 3.81 mm
SNLD = 3.81 mm	VSCO = at 35 °C
DNLD = 3.81 mm	VSCF = 1.00
SNTL = 15.88 mm	CRNT = 0.00 A

The valve disc diameter DSD is varied in the theoretical model between 12.7 and 38.1 mm (which corresponds to disc-to-supply nozzle diameter ratio of 4.0 to 12.0). Figure 5.5 shows the effect of disc-to-supply nozzle diameter ratio on net fluid forces acting on a double-disc valve. From the figure it can be seen that when the diameter ratio is increased from 4.0 to 12.0, the

gradient at null position increases quickly. The figure suggests that for proportional valve operation, a high diameter ratio (possibly greater than 10) should be used and a small diameter ratio for a switching action as the net fluid force decreases with decrease in diameter ratio. This is because small net fluid force will demand a small electrical power. Increasing the disc diameter DSD has no effect on the load pressure but the null leakage flowrate decreases slightly with increase in disc-to-supply nozzle diameter ratio.

To see how the total disc travel TD influences the valve fluid characteristics, five different values of TD ranging from 0.25 to 0.76 mm ($\pm$ 50 per cent of the value shown in Table 5.2) are used in the valve model. Figure 5.6 shows the net fluid forces acting on a double-disc valve for various total disc travel. From the figure, it can be seen that the null fluid force gradient decreases with increase in total disc travel and a point of inflexion near the null position is possible for total disc travels greater than 0.76 mm. From Fig.5.6, it can be observed that the maximum fluid force that occurs as the discs and rod assembly moves away from left to right remains constant for TD greater than 0.38 mm. For this valve configuration, the best compromise between the null gradient and force level is achieved for total disc travel equal to 0.51 mm. Total disc travel TD has no significant effect on load pressure but the null leakage flowrate increases with TD.

Fig.5.7 shows the effect of varying supply nozzle holding gap HGS, from 0.03 to 0.25 mm on net fluid forces acting on a double-disc valve. From the figure it can be seen that the net fluid force first increases with positive gradient to a maximum and then decreases with negative gradient. Increasing the supply holding gap is seen to reduce the level of the first maximum fluid force. This can be attributed to flow restriction on the

supply side of disc for small HGS. This implies that HGS and rod clearance must be carefully chosen to match the maximum fluid force for switching action of valve. The null fluid force gradient decreases with increase in HGS. Hence for proportional valve operation select a small value of HGS (say HGS < 0.13 mm) and for a switching action select a large value of HGS (say HGS > 0.13 mm). For both switching and proportional operations of valve, the best compromising HGS is 0.13 mm. Supply holding gap HGS, has no significant effect on load pressure but the flowrate increases slightly with increase in HGS. The most important effect here seems to be that with a suitable choice of HGS the fluid forces are almost reduced to zero although this has to be balanced against the rapid reductions in electromagnetic force available with increasing HGS.

Fig. 5.8 shows the effect of varying the drain holding gap HGD, between 0.13 and 1.02 mm, on the net fluid force acting on a double-disc valve. The null gradient is seen to increase with increase in HGD but the rate of increase, decreases for HGD>0.25 mm and there is no significant effect for HGD>0.51 mm. This confirms the geometrical relationships derived in section 5.5.4 in which HGD is required to be greater than the sum of the total disc travel TD (0.51 mm used in the model) and the supply nozzle holding gap HGS (0.13 mm used in the model). There is a large decrease in net fluid force level with decrease in HGD below 0.51 mm which could be attributed to flow restriction on the drain side of the disc chamber. A point of inflexion near valve null position occurs for HGD = 0.13 mm which suggests that for proportional valve operation, HGD must be at least equal to 0.51 mm and HGD less than 0.25 mm for switching operation. Drain holding gap HGD, has no significant effect on both load pressure and flowrate but null leakage flow increases slightly with increase in HGD.

The supply nozzle diameter SND, is varied between 1.90 and 4.44 mm (which

corresponds to a disc-to-supply nozzle diameter ratio of 16.7 to 7.2 and also to a drain-to-supply area ratio of 2.8 to 0.51) and the resulting net fluid force acting on a double-disc valve is shown in Figure 5.9. The figure shows that the null fluid force gradient decreases with decrease in SND (with decrease in both disc-to-supply nozzle diameter ratio and drain-to-supply area ratio) and at null conditions, the net fluid force is negative for SND<3.18 mm. For a switching valve operation this will simply introduce a time delay as the disc will not lift off its supply seat. This can be overcome by using a shorter rod. A point of inflexion is observed for SND=1.90 mm (area ratio of 2.8). The theoretical steady-state model has shown that a negative fluid force occurs for a drain-to-supply area ratio less than 0.7 and disc-to-supply diameter ratio less than 8.0. This implies that the disc will not close off its drain nozzle seat and this will not be a good configuration for a switching valve. For a switching valve, therefore, the area ratio should not be less than 1. For proportional operation, Fig.5.9 suggests an area ratio not greater than 1 is required to obtain the best null valve stability. The best compromising area ratio for both switching and proportional valve operations is seen to be one.

Fig. 5.10 shows the effect of SND on non-dimensional leakage flow under blocked-load conditions. From the figure it can be seen that the percentage of leakage flow increases with decrease in SND. The supply nozzle diameter has a slight effect on valve load pressure with the best null pressure gradient occurring for a drain-to-supply nozzle area ratio of one.

Varying both the supply nozzle diameter SNLD and drain nozzle land diameter DNLD over the range $\pm$ 13 per cent of their nominal values has no significant effect on fluid force, pressure and flowrate. From practical experience, an increase in SNLD or DNLD will increase the chance of oil cavitation in the valve which will consequently cause a reduction in

flowrate, pressure and fluid forces. This is because of flow restriction in the valve land regions. From the experimental results of Chapter 4, both the drain and nozzle land diameters should not be greater than 1.2 times the respective nozzle diameters.

Varying both the supply nozzle tube length SNTL and the drain nozzle tube length DNTL over the range ± 33 per cent of their nominal values has no significant effect on fluid forces, flowrate and load pressure.

Figure 5.11 shows the effect of varying the supply pressure PS between 17.5 and 140.0 bar on the fluid forces acting on a double-disc disc. The figure shows that the valve is stable around the null region over the supply pressure range used in the model. It also shows that for a given valve there is a maximum pressure above which the valve destabilises. For drain-to-supply nozzle area ratio of one, the maximum pressure is 140 bar as the valve flowrate saturates for pressures greater than this value. However, for an area ratio greater than unity, this maximum pressure is reduced. For example, when the area ratio is 2.25, the maximum pressure is 70 bar. Increasing PS is seen in Fig. 5.12 to cause a large increase in flowrate. The non-dimensional load pressure is independent of supply pressure over the range used in the computer model.

From the fluid force characteristics shown in Fig.4.6 and the magnetic force characteristics shown in Fig.4.20 in Chapter 4, it can be seen that when x=0, the magnetic force might be greater than the fluid forces acting on a single-disc of the valve. In a double-disc valve operation, the net fluid and magnetic forces will be negative for x=0 and the disc will not lift from its supply nozzle seat. For proportional operation of the valve, the discs and rod assembly are not to be operated within the small region where the net fluid and magnetic forces are negative. For this reason, a rod length is used with a clearance which is equal to twice the distance

between the supply nozzle tip and the position where the net fluid and magnetic forces cease to be negative.

The effect of varying the rod clearance CR between 0.00 and 0.20 mm on the net fluid forces acting on a double-disc valve is shown in Fig. 5.13. From the Figure it can be seen that CR significantly influences the shape of the fluid forces. The null gradient reduces with increase in rod-clearance. From the figure, it can be seen that when x=0, the net fluid force is zero for CR=0 and is about 1.2 times the product of supply pressure and supply nozzle area for CR>0. For CR=0, the gradient of the net fluid force is first negative for disc displacement of about 12.5 per cent of T_D and the maximum fluid force occurs here. For switching valve operation, the point where the disc takes up the rod-clearance should be the place where the maximum fluid force occurs. For this reason, the best rod-clearance is seen to be about 12.5 per cent of total disc travel (which is about 2 per cent of supply nozzle diameter). For proportional valve operation, the fluid force gradient should be negative and this implies that the discs and the rod assembly moving together as a solid body should operate within the region of negative fluid force gradient which is about 75 per cent of total disc travel. Hence the best rod-clearance should be 25 per cent of total disc travel (about 4 per cent of supply nozzle diameter) which is twice that for switching action. For a rod clearance greater than 25 per cent of total disc travel, the valve requires a powerful electro-magnetic coil to be able to pull the disc towards its adjacent nozzle for switching action.

Fig.5.14 shows the effect of rod clearance CR on the total drain flow through the valve under blocked-load conditions. The flowrate is seen to decrease with increase in CR. This is because the discs are close to the drain nozzles for a large CR and thereby reducing the curtain areas through which flow can pass. The rod clearance has no significant effect on null

pressure gradient (see Fig.5.15). However, increasing the rod-clearance from 0.00 to 0.20 mm (about 0 to 20 per cent of total disc travel), the range of load pressure drops from 100 to 56 per cent of supply pressure. For CR>0, the pressure at each load port is greater than 50 per cent of supply pressure and this result in increase in hydraulic stiffness.

The theoretical model has shown that the push rod diameter has no significant effect on fluid force, flowrate and load pressure when the rod diameter is less than or equal to 80 per cent of drain nozzle diameter. For rod diameters greater than this value, the flowrate, fluid force and null load pressure drop dramatically as the flow passing through the drain annular passage is highly restricted. From Table 5.1, it can be seen that the best compatible rod diameter should lie between 77 and 80 per cent of drain nozzle diameter. For a given rod diameter, there is a correct choice of rod length to avoid buckling in the annular space formed by the rod and the drain diameter. The influence of rod geometry on the likelihood of buckling is given in appendix A10. Fig. 5.16 shows the effect of rod length on buckling load. The critical load gives an idea of the maximum force that a given double-disc valve size can withstand without any failure and is well in excess of any possible fluid and electro-magnetic forces likely to be encountered.

When the valve is operated in proportional mode, the electro-magnetic coils receive a differential current from the PWM amplifier. The discs and rod assembly then adopt a position where the net fluid forces balance that of the magnetic forces acting on the discs. Fig.5.17 shows the combined fluid and magnetic forces acting on a 31 mm diameter double-disc valve under blocked load conditions. The maximum current that can be generated by the PWM amplifier is 1500 mA and the currents in coil 1 and 2 are given a differential coil current, ΔI, ranging from 0 to 1500 mA. The total disc

travel T_D for zero rod-clearance is shown in Fig. 5.17 as AB and the mid-position is denoted as 0. With rod-clearance, the disc travel is limited to A'B' with mid-stroke of discs and rod assembly now at position 0'. The rod-clearance here is given by distance AA' + BB'. The distance 00' is equal to one-quarter of the rod-clearance. In the figure, when the differential coil current, ΔI=1500mA, the net forces acting on the discs and the rod assembly are positive throughout the disc displacement. This shows that the valve acts as a switching device at a differential coil current of 1500 mA as the right-hand disc closes the right-hand supply nozzle at the same time that the left-hand disc closes off the left-hand drain nozzle. When ΔI=900 mA, the net force crosses the displacement axis at point c which corresponds to the position where the net fluid forces balance the net magnetic forces. Position d, e and 0' correspond to the balance points for ΔI= 600, 300 and 0 mA respectively.

The resulting position of the discs and rod assembly for a range of differential coil currents is shown in Fig.5.18. The figure shows that the position of the discs and rod assembly is proportional to the differential current applied to the valve electro-magnetic coils over most of the disc displacement range. The solid line in Fig.5.18 is merely a straight line drawn through the data to show the very good linearity. From Fig.5.17, it can be seen that the disc displacement should not be greater than 0'B' to be within the proportional region of the valve and the corresponding maximum differential current to operate the valve for a supply pressure of 70 bar is 1200 mA (from linear regression analysis) for the valve configuration used.

Shell Tellus oil R37 was used throughout the experiments conducted with both the prototype and pre-production versions of the double-disc valve. Typical viscosity-temperature characteristics of Shell Tellus oils R are

shown in appendix A11. The normal working temperature range for most commercial valves is 20° through 60°C and the corresponding viscosities, as extracted from appendix A11, are shown in Table 5.3.

Table 5.3 Shell Tellus R37 oil viscosity at different oil temperatures.

Temperature °C	Kinematic viscosity cs (in^2/sec)	Absolute viscosity lb-sec/in^2
20	95.0 (0.15)	1.21
30	58.3 (0.09)	0.74
40	36.2 (0.06)	0.46
50	24.6 (0.04)	0.31
60	17.5 (0.03)	0.22

The viscosity is seen to decrease markedly with temperature. The values of the absolute viscosities as shown in Table 5.3 are used to calculate the effect of oil viscosity on the fluid forces acting on the double-disc valve. Fig. 5.19 shows the effect of oil temperature (TEMP) or viscosity on fluid forces acting on a double-disc valve. Both the fluid force level and null fluid force gradient are seen from the figure to decrease with oil temperature (or with decrease in oil viscosity). When the valve is operated in a proportional mode, the electro-magnetic coils receive a differential current from a PWM amplifier. The discs and rod assembly then adopt a position where the net fluid forces balance that of the magnetic forces acting on the discs. For a given differential current, the magnetic forces acting on the discs remain constant with oil temperature while the fluid forces vary. This must mean that the valve is always viscosity-temperatue dependent which is a major disadvantage. Figure 5.20 shows the resulting position of the discs and rod assembly for a range of differential coil currents with oil temperatures of 20 °C, 35 °C and 50 °C. The figure shows

that the position of the discs and rod assembly is proportional to the differential current applied to the valve electro-magnetic coils over most of the disc displacement range. The slope of differential coil current versus discs and rod assembly position reduces with increase in oil temperature. This implies that the valve must always be designed for the worst case i.e maximum operating temperature. Oil viscosity has little effect on load pressure while flowrate increases with decrease in viscosity as the oil becomes thinner.

All the valve geometrical parameters shown in Table 5.2 are scaled linearly between 0.5 and 4.0. Fig.5.21 shows the effect of scaling, VSCF, on net fluid forces acting on a double-disc valve for equal drain-to-supply nozzle area. From the figure, it can be seen that the gradient at null position falls off quickly and a point of inflection is observed for linear scaling greater than or equal to 3.0. For best stable characteristics of the valve near null position, Fig.5.21 suggests that the valve must not be scaled-up more than 3.0. For a valve with drain-to-supply nozzle area greater than unity, the valve becomes unstable for geometrical scaling greater than 1.5. It can be concluded that linear scaling or geometrical scaling should be done with care as the valve general performance depend on many parameters which may be inter-related. The nozzle land diameter, for example, must be less than 1.2 times the nozzle diameter to avoid cavitation. In scaling the valve, the various geometrical relationships derived in section 5.2 must be considered to effect a good valve performance. Flowrate increases with valve scaling as shown in Fig. 5.22 for unity drain-to-supply nozzle area ratio. However, the flowrate flattens out near the valve mid-stroke when VSCF > 1.5 for valves whose drain-to-supply nozzle area ratio greater than unity. This can be attributed to valve flow saturation. Pressure gain is unaffected by linear scaling.

The geometric design considerations for the double-disc valve have been presented in this chapter. The next chapter will be looking at dynamic characteristics of the valve based on an approximately lumped parameter model.

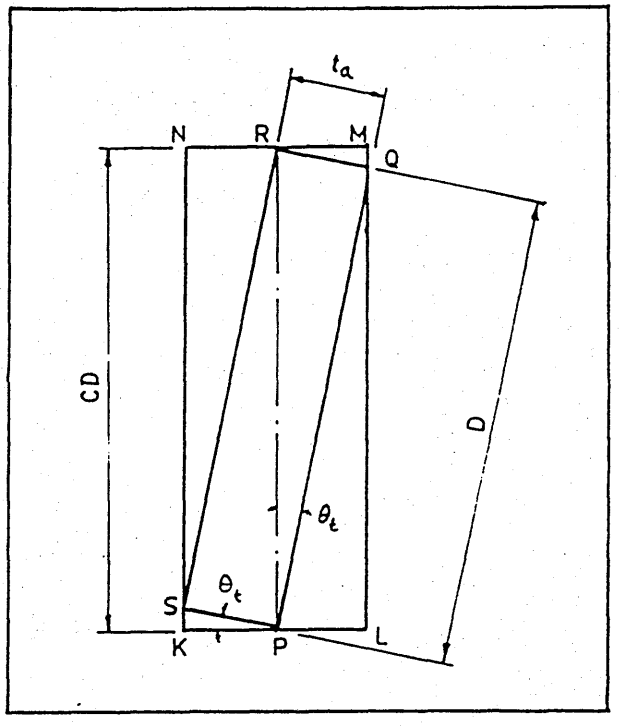

Fig. 5.1 Jamming conditions of a disc in its chamber.

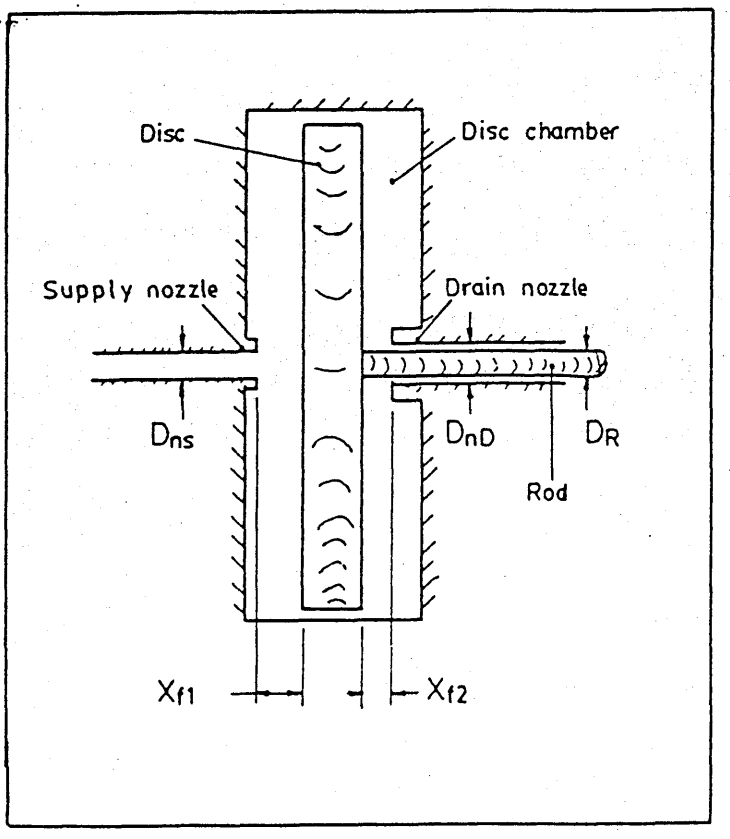

Fig. 5.2 Effect of disc chamber geometry on valve null flow.

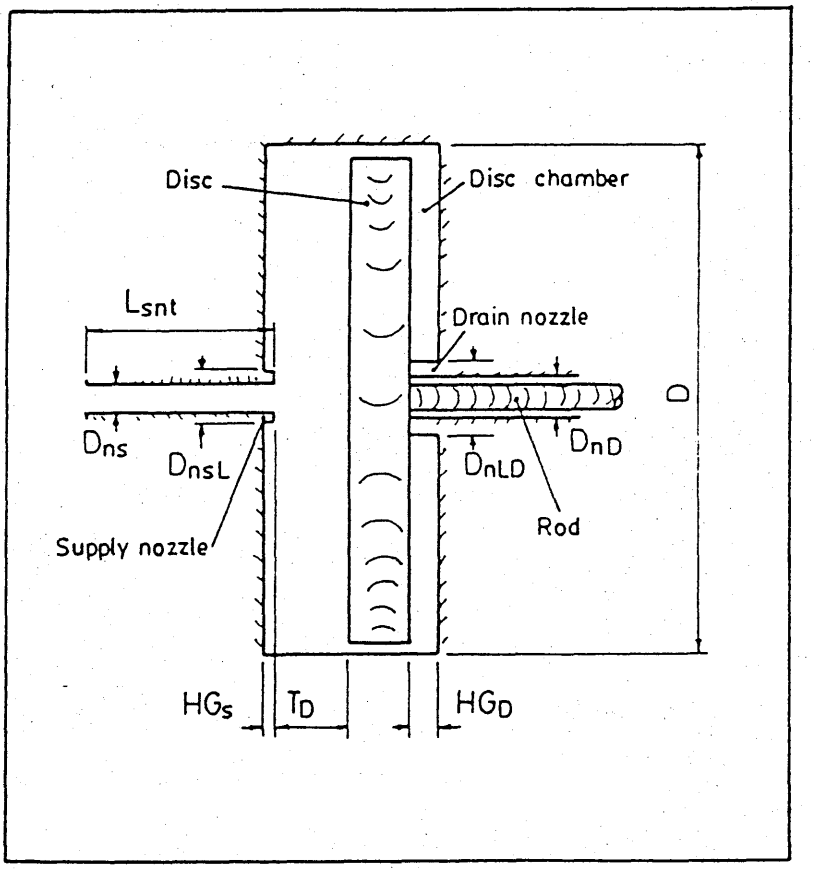

Fig. 5.3 Typical disc chamber passage.

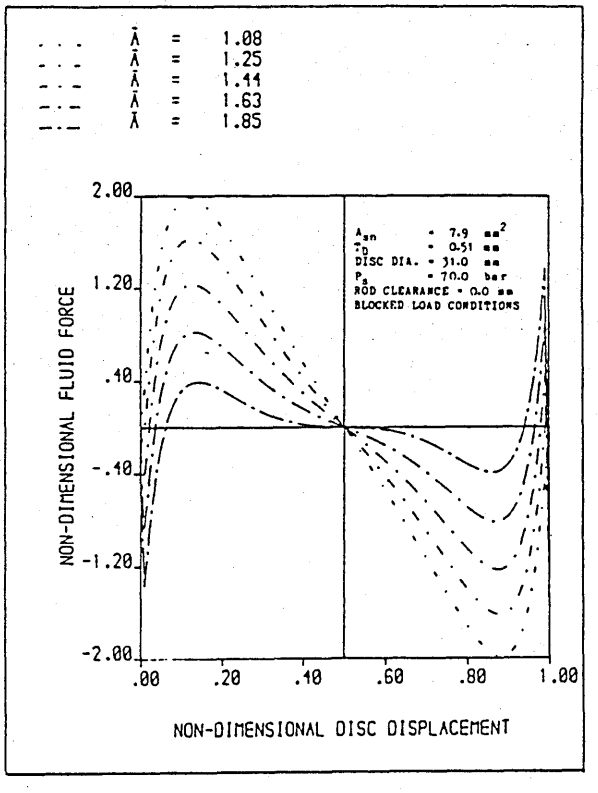

Fig 5.4 Effect of drain-to-supply nozzle area ratio on double-disc valve.

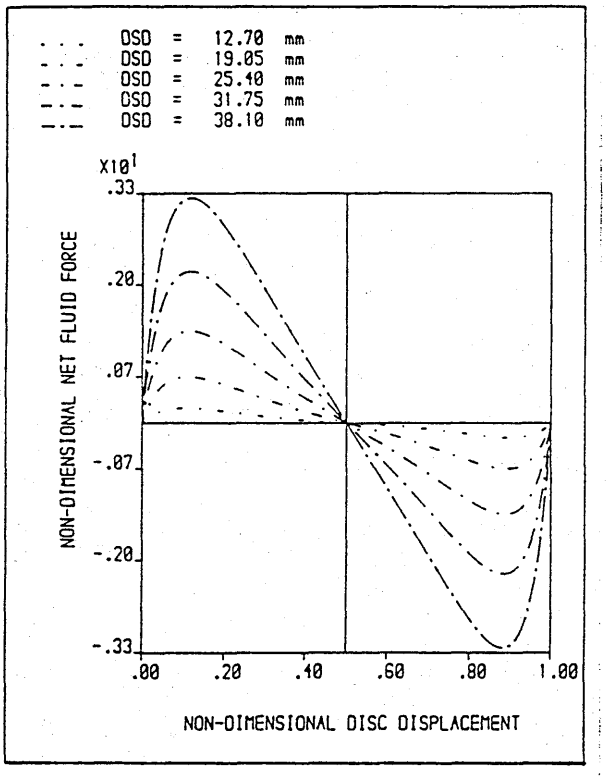

Fig. 5.5 Effect of DSD on net fluid forces acting on a double-disc valve.

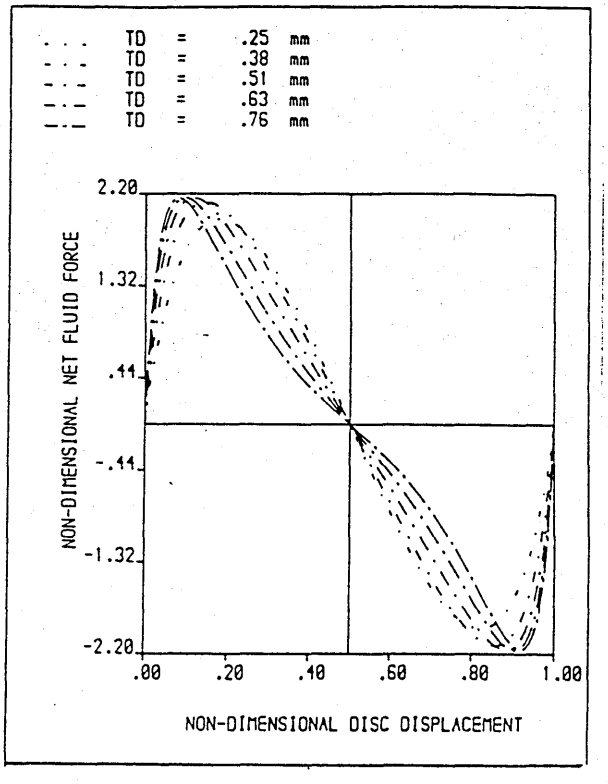

Fig. 5.6 Effect of TD on net fluid forces acting on a double-disc valve.

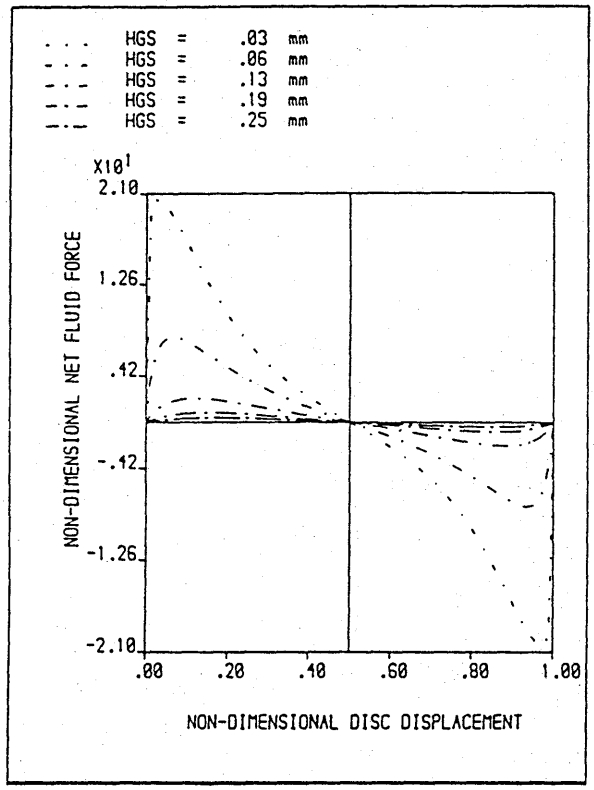

Fig. 5.7 Effect of HGS on net fluid forces acting on a double-disc valve.

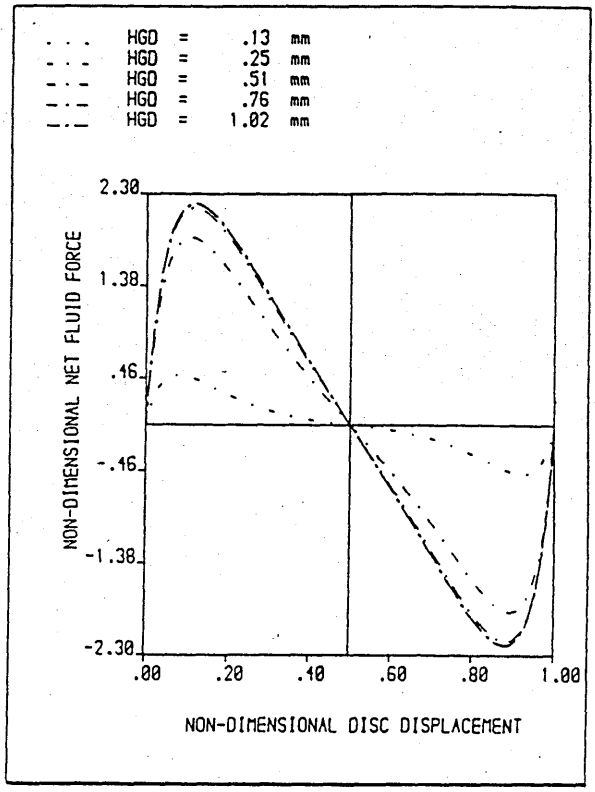

Fig. 5.8 Effect of HGD on net fluid forces acting on a double-disc valve.

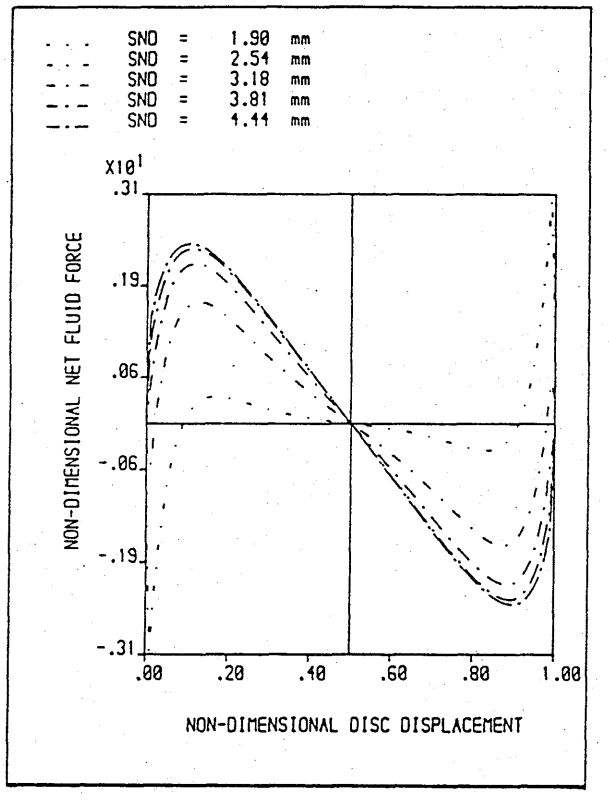

Fig. 5.9 Effect of SND on net fluid forces acting on a double-disc valve.

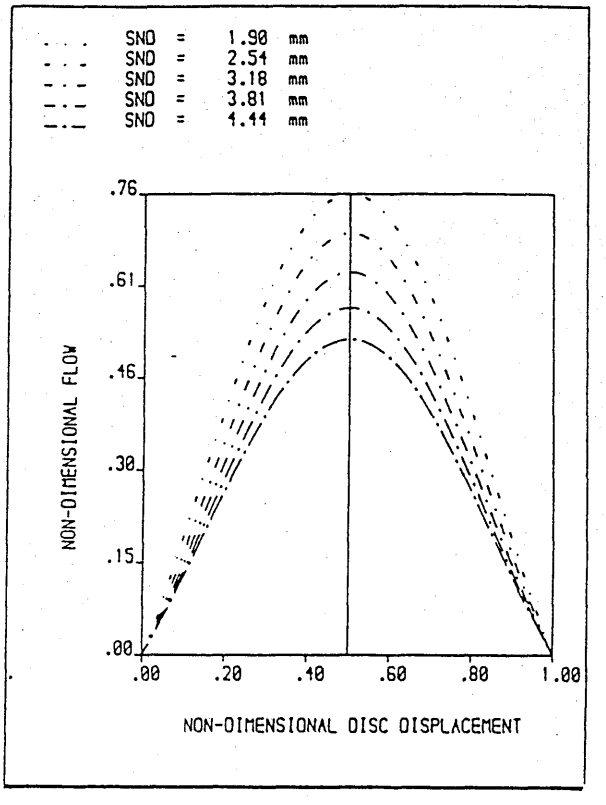

Fig. 5.10 Effect of SND on total drain flow.

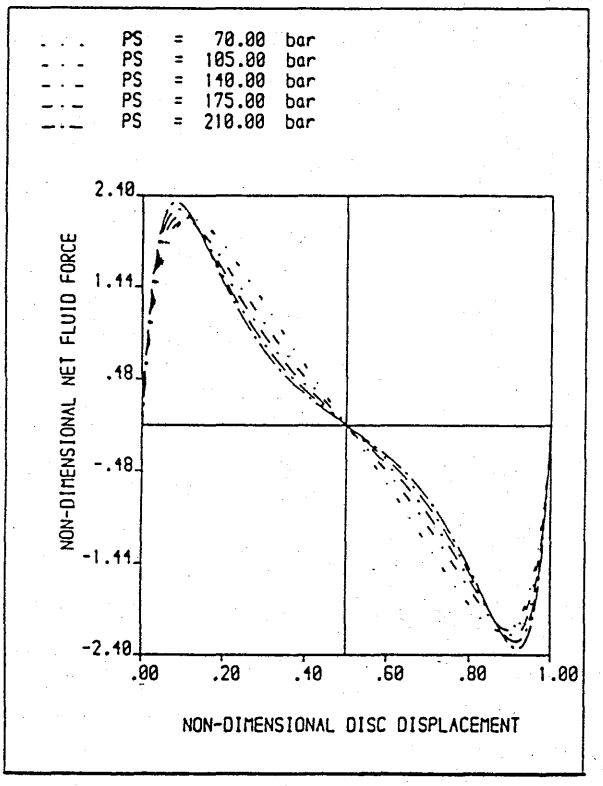

Fig. 5.11 Effect of PS on net fluid forces acting on a double-disc valve.

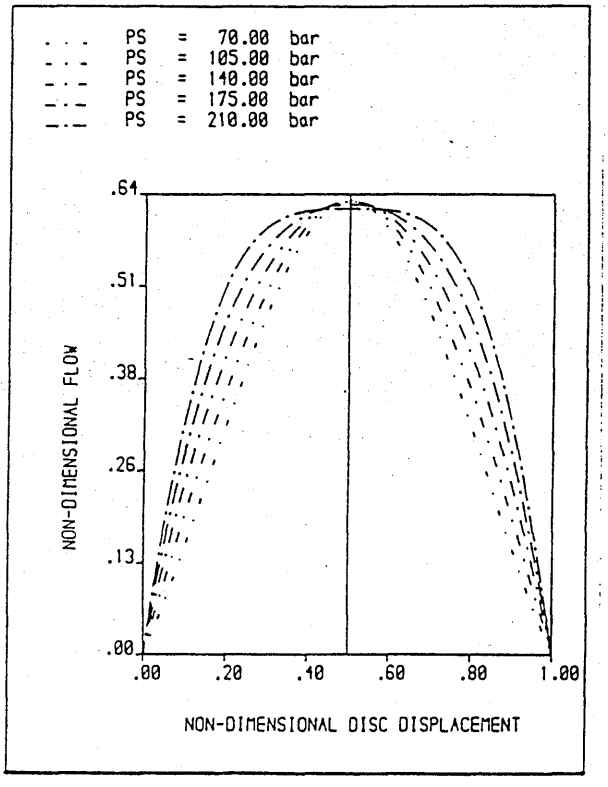

Fig. 5.12 Effect of PS on total drain flow.

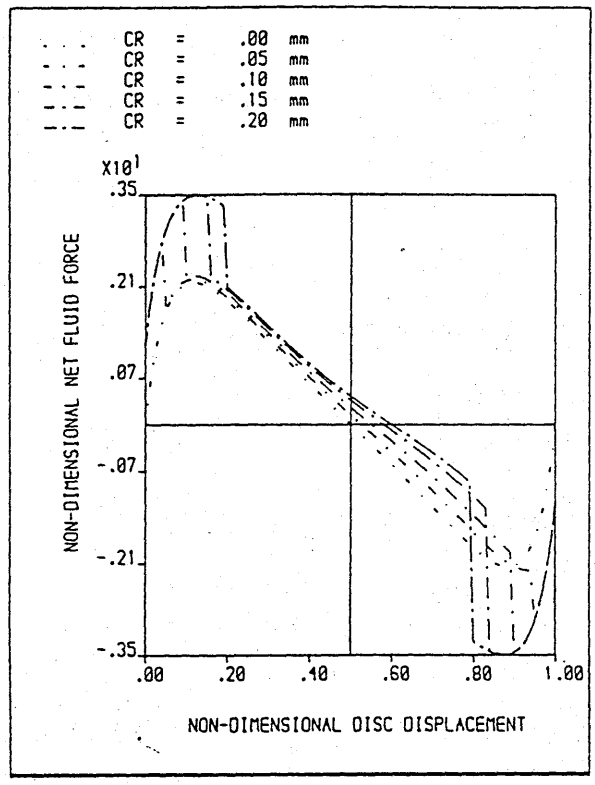

Fig. 5.13 Effect of CR on net fluid forces acting on a double-disc valve.

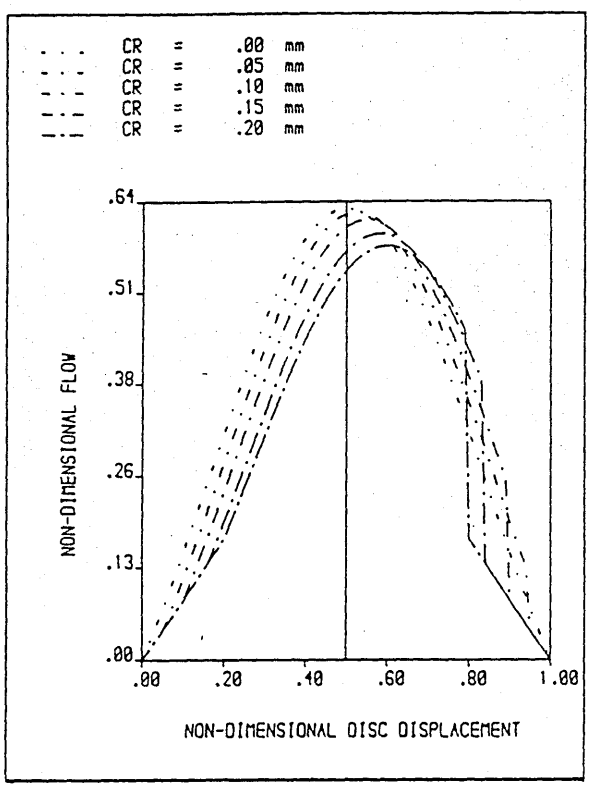

Fig. 5.14 Effect of CR on total drain flow.

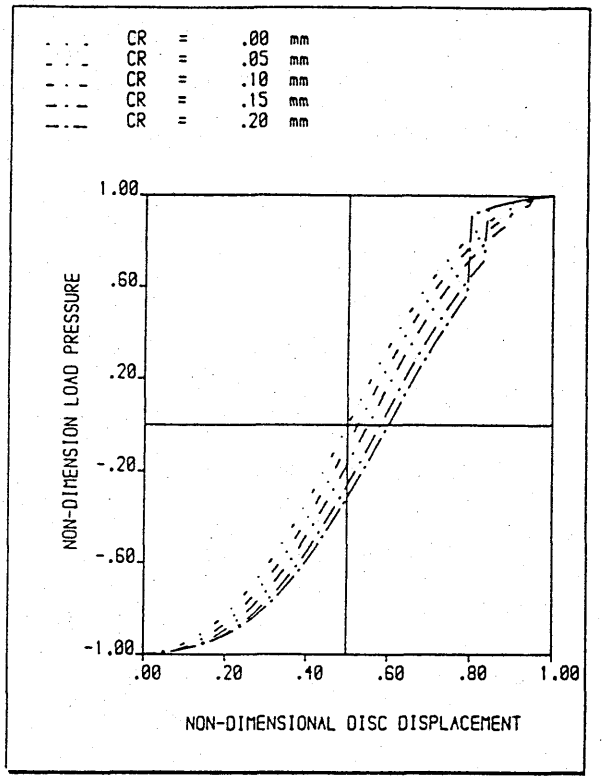

Fig. 5.15 Effect of CR on load pressure curves.

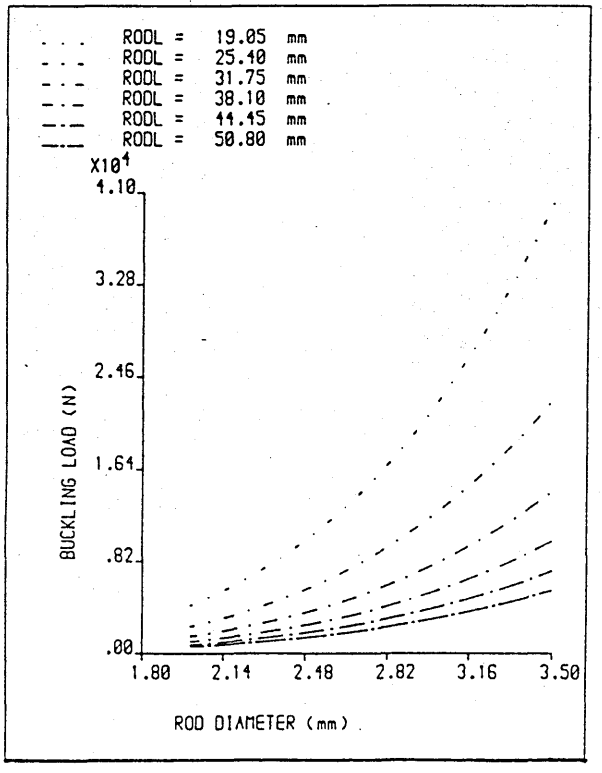

Fig. 5.16 Effect of rod length RODL on buckling load.

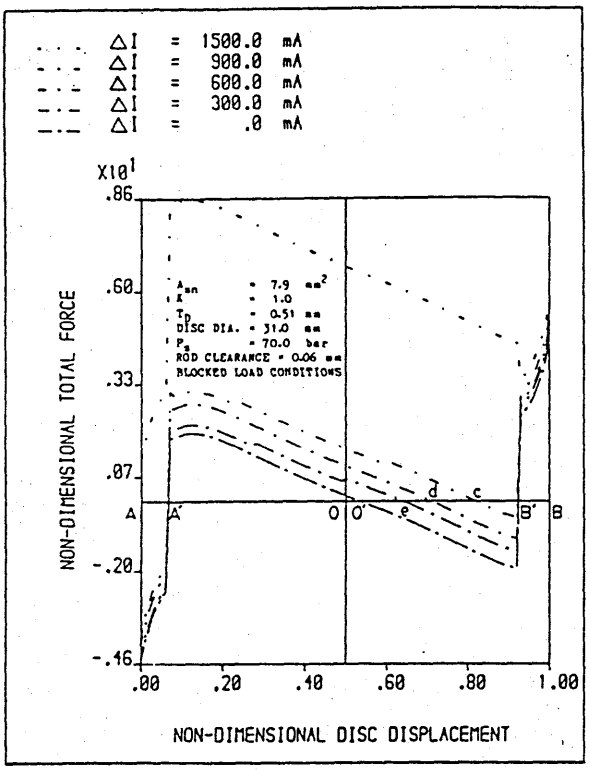

Fig.5.17 Combined fluid and electro-magnetic forces acting on a double-disc valve for proportional control.

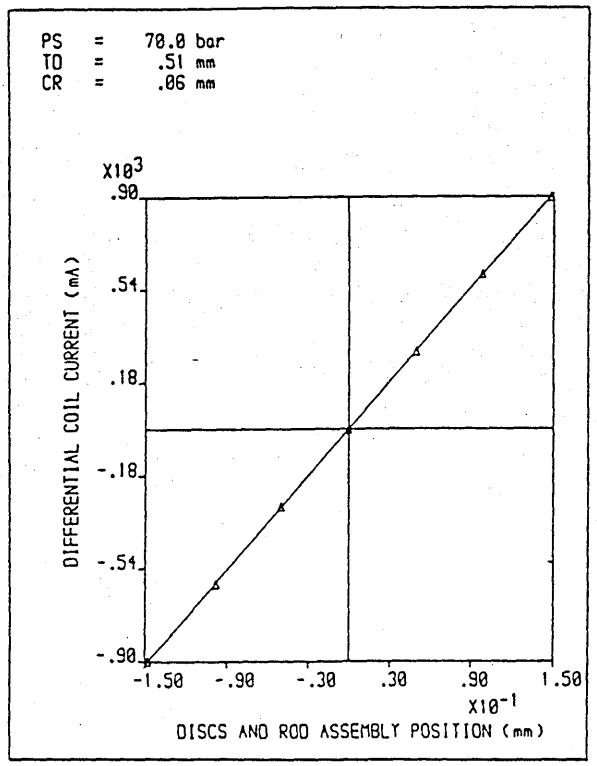

Fig.5.18 Proportional relationship between differential coil current and disc displacement from Fig.5.17.

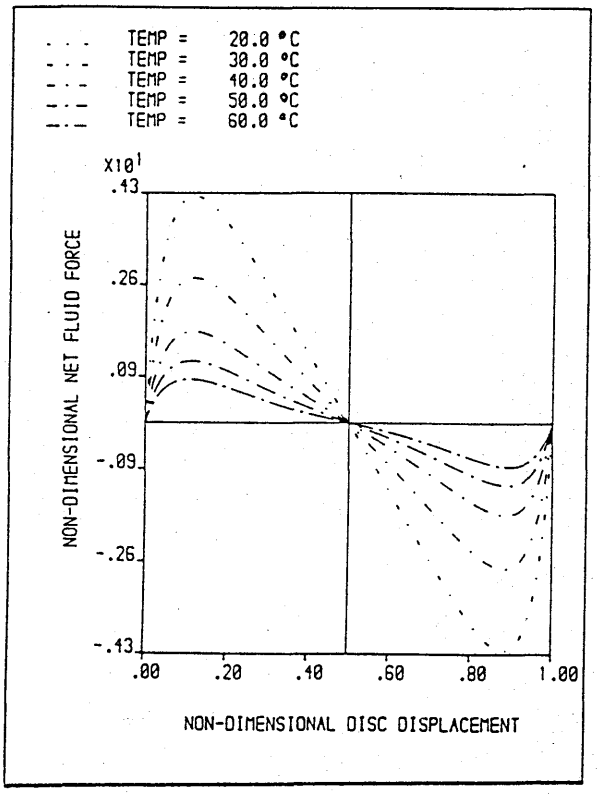

Fig. 5.19 Effect of oil temperature TEMP on net fluid forces acting on a double-disc valve.

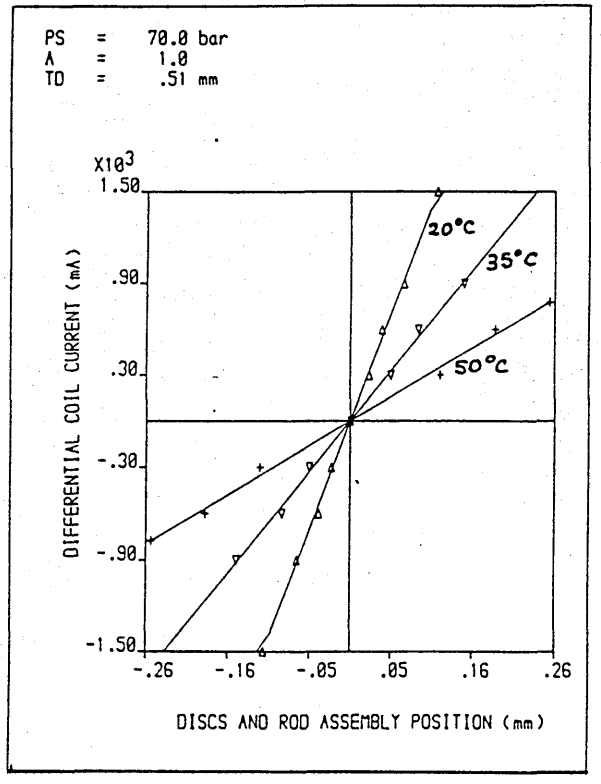

Fig.5.20 Effect of oil viscosity-temperature on valve for proportional control.

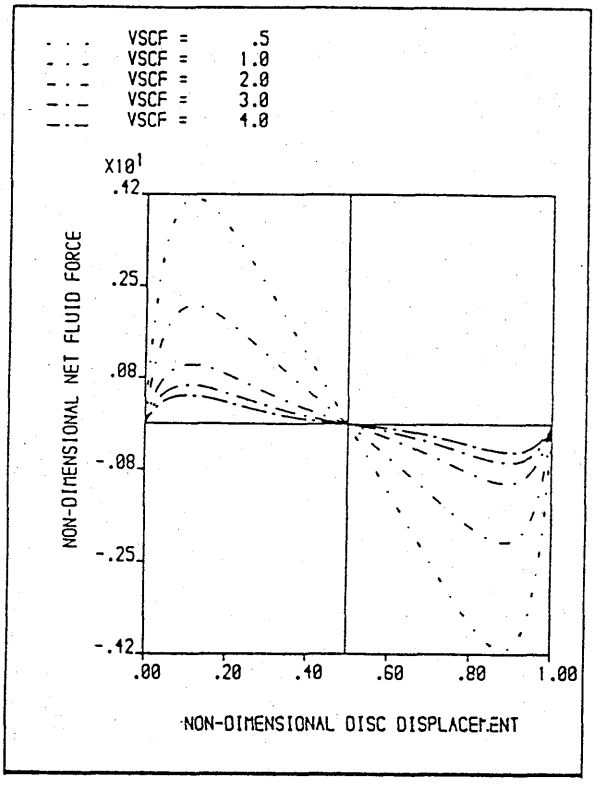

Fig. 5.21 Effect of linear scaling VSCF on net fluid forces acting on a double-disc valve.

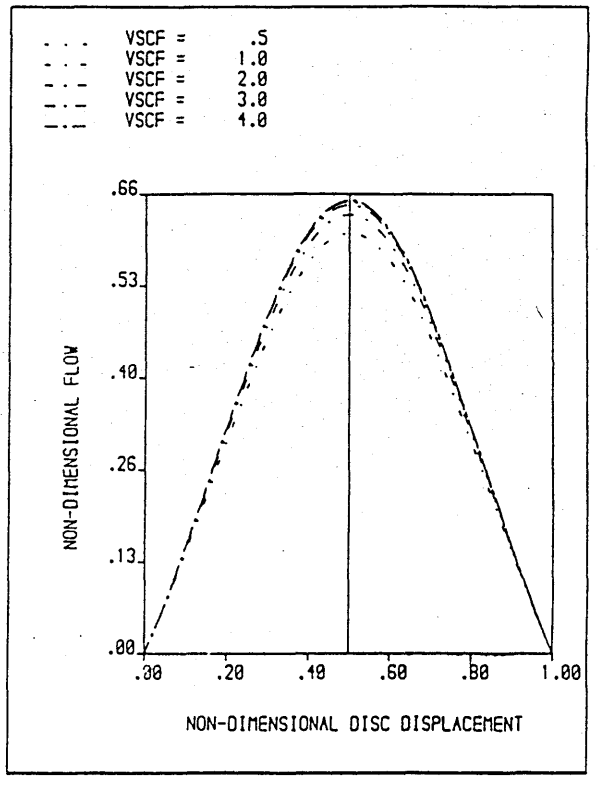

Fig. 5.22 Effect of linear scaling VSCF on total drain flow.

CHAPTER 6

APPROXIMATE LUMPED PARAMETER DYNAMIC MODEL FOR PROPORTIONAL CONTROL

6. Approximate lumped parameter dynamic model for proportional control

6.1 Introduction

The double-disc valve is a device that uses mechanical motion to control a source of fluid power. Because the valve is the mechanical/electrical-to-fluid interface in a hydraulic system, its performance is crucial in the overall control system design. Therefore a dynamic model of the valve performance characteristics is useful to the system designer.

In analysing the fluid forces of the valve under steady-state conditions, it is possible to use a spatial distributed parameter approach. This was because the flow is assumed to be radial, laminar and fully developed within the valve chamber. Even with all these assumptions, the accurate theoretical evaluation of the fluid forces is complex owing to the difficulty in precise assessment of the flow patterns in the nozzle land regions. Evidently under dynamic flow conditions, the determination of the fluid forces becomes even more complicated because of acceleration and deceleration of the flow and the movement of the discs.

The purpose of this chapter is to establish an approximate lumped parameter dynamic model of the valve under investigation. The relationship between pressure and flow are non-linear and a linearized approach is therefore used throughout the analysis. The dynamic characteristics of the electro-magnetic solenoid used in the valve are also included.

6.2 Flow equations

Consider the four-way double-disc valve shown in Fig. 6.1. The orifices are completely analogous to the four arms of a Wheatstone bridge, and this analogy is helpful in visualizing valve operation. Arrows at the ports indicate the assumed directions of flows, and the numbers at ports refer to

the subscripts of the flow and the area at the ports. The two floating discs are assumed to be moving as a solid body. Let the valve be given a positive displacement from the null or neutral position, that is, the position z = 0, which is chosen to be the symmetrical position of the discs in the chambers.

Flow through the valve restrictions are described by the orifice type of equation:

$$Q = C_D A \sqrt{\frac{2\Delta P}{\rho}}$$

where Q is the flow rate, p is the pressure difference across the orifice, is the density, A is the annular curtain area and C_D is the discharge coefficient.

Therefore

$$Q_1 = C_{Dns} A_1 \sqrt{\frac{2(P_s - P_1)}{\rho}} \qquad (6.1)$$

$$Q_2 = C_{DnD} A_2 \sqrt{\frac{2(P_1 - P_D)}{\rho}} \qquad (6.2)$$

$$Q_3 = C_{DnD} A_3 \sqrt{\frac{2(P_2 - P_D)}{\rho}} \qquad (6.3)$$

$$Q_4 = C_{Dns} A_4 \sqrt{\frac{2(P_s - P_2)}{\rho}} \qquad (6.4)$$

The return line pressure P_D will be neglected because it is usually much smaller than the other pressures involved. If the return pressure is appreciable, then P_s can be interpreted as the pressure difference, that is, supply pressure minus return pressure, across the valve. The orifice areas depend on valve geometry and four equations are required to define the areas A_1, A_2, A_3, and A_4 as a function of valve displacement.

Therefore,

$$A_1 = \pi D_{ns} (z_{f1} + z) \tag{6.5}$$

$$A_2 = \pi D_{nD} (z_{f2} - z) \tag{6.6}$$

$$A_3 = \pi D_{nD} (z_{f2} + z) \tag{6.7}$$

$$A_4 = \pi D_{ns} (z_{f1} - z) \tag{6.8}$$

Considering only the steady-state characteristics, the compressibility flows are zero and the continuity equations for the two valve chambers are

$$Q_L = Q_1 - Q_2 \tag{6.9}$$

$$Q_L = Q_3 - Q_4 \tag{6.10}$$

A dynamic analysis would require inclusion of the compressibility flows which depend on the valve chamber volumes. However, this is best achieved by considering the combination of valve and actuator, because the actuator and lines contribute appreciable volumes. Now, by definition,

$$P_L = P_1 - P_2 \tag{6.11}$$

Q_L is the flow through the load and P_L is the pressure drop across the load.

Equations (6.1) through (6.11) are required to define the pressure-flow behaviour of a four-way valve. These 11 equations can be solved simultaneously to yield load flow as a function of valve position and load pressure; that is

$$Q_L = f(z, P_L) \tag{6.12}$$

The plot of equation (6.12) is known as the pressure-flow curves for the valve and is a complete description of steady-state valve performance. All the performance parameters, such as valve coefficients, can be obtained from these curves. For example, selecting a value for z will numerically determine all the orifice areas. Then choose a series of values for Q_L and solve (6.9) and (6.10) for P_1 and P_2, respectively, for each Q_L value. Thus it is possible to tabulate z, Q_L, P_1, P_2, and also P_L.

Assuming P_D is very small compared to the other quantities and using equations (6.1), (6.2), (6.5) and (6.6) in (6.9) gives

$$Q_L = C_{Dns}\pi D_{ns}\,(z_{f1} + z)\sqrt{\frac{2(P_s - P_1)}{\rho}} - C_{DnD}\pi D_{nD}\,(z_{f2} - z)\sqrt{\frac{2P_1}{\rho}} \qquad (6.13)$$

Similarly using equations (6.3), (6.4), (6.7) and (6.8) in (6.10) gives

$$Q_L = C_{DnD}\pi D_{nD}\,(z_{f2} + z)\sqrt{\frac{2P_2}{\rho}} - C_{Dns}\pi D_{ns}\,(z_{f1} - z)\sqrt{\frac{2(P_s - P_2)}{\rho}} \qquad (6.14)$$

The total leakage flow through the valve is given by

$$Q_c = Q_2 + Q_3 \qquad (6.15)$$

The total centre flow or leakage through the valve is useful because it gives the power loss at the null operating point. At this point, $z = P_L = 0$ and $P_1 = P_2 = P_s/2$ so that $A_2 = A_3$, and equation (6.15) gives the total leakage flow as

$$Q_c = 2\,C_{DnD}\pi D_{nD}\,z_{f2}\sqrt{\frac{P_s}{\rho}} \qquad (6.16)$$

6.2.1 Linearized analysis of valve

Using linearized analysis, the valve coefficients at null, that is, at the point where $z = Q_L = P_L = 0$ and $P_1 = P_2 = P_s/2$ can be determined. The values of the valve coefficients vary with the operating point. The most important operating point is the origin of the pressure-flow curves (that is, where $Q_L = P_L = z = 0$) because system operation usually occurs near this region, the valve flow gain is largest, giving high system gain, and the flow-pressure coefficient is smallest, giving a low damping ratio. Hence this operating point is the most critical from a stability viewpoint, and a system stable at this point is usually stable at all operating points. The linearized form of equation (6.13) is

$$\triangle Q_L = \left.\frac{\partial Q_L}{\partial z}\right|_o \triangle z + \left.\frac{\partial Q_L}{\partial P_1}\right|_o \triangle P_1 \qquad (6.17)$$

The null valve coefficients can be obtained by differentiating equation (6.13) and evaluating the derivatives at null. Therefore

$$\left.\frac{\partial Q_L}{\partial z}\right|_o = \pi\left[C_{Dns}\, D_{ns} + C_{DnD}\, D_{nD}\right]\sqrt{\frac{P_s}{\rho}} \tag{6.18}$$

$$\left.\frac{Q_L}{P_1}\right|_o = -\frac{\pi\left[C_{Dns}\, D_{ns}\, z_{f1} + C_{DnD}\, D_{nD}\, z_{f2}\right]}{\sqrt{\rho P_s}} \tag{6.19}$$

In a similar fashion equation (6.14) may be linearized about null to obtain

$$\Delta Q_L = \left.\frac{\partial Q_L}{\partial z}\right|_o \Delta z + \left.\frac{\partial Q_L}{\partial P_2}\right|_o \Delta P_2 \tag{6.20}$$

where

$$\left.\frac{\partial Q_L}{\partial z}\right|_o = \pi\left[C_{Dns}\, D_{ns} + C_{DnD}\, D_{nD}\right]\sqrt{\frac{P_s}{\rho}} \tag{6.21}$$

$$\left.\frac{Q_L}{P_2}\right|_o = \frac{\pi\left[C_{Dns}\, D_{ns}\, z_{f1} + C_{DnD}\, D_{nD}\, z_{f2}\right]}{\sqrt{\rho P_s}} \tag{6.22}$$

Addition of equation (6.17) and (6.18) and combining with (6.11) yields

$$\Delta Q_L = K_{qo}\Delta z - K_{co}\Delta P_L \tag{6.23}$$

This is the linearized form of the pressure-flow equation of the double-disc valve for operation at null. The null coefficients are obtained directly from this equation.

$$K_{qo} \equiv \left.\frac{\Delta Q_L}{\Delta z}\right|_{\Delta P_L = 0} = \pi\left[C_{Dns}\, D_{ns} + C_{DnD}\, D_{nD}\right]\sqrt{\frac{P_s}{\rho}} \tag{6.24}$$

$$K_{po} \equiv \left.\frac{\Delta P_L}{\Delta z}\right|_{\Delta Q_L = 0} = \frac{\left[1 + \dfrac{C_{DnD}\, D_{nD}}{C_{Dns}\, D_{ns}}\right] P_s}{z_{f1} + \dfrac{C_{DnD}\, D_{nD}}{C_{Dns}\, D_{ns}}\, z_{f2}} \tag{6.25}$$

$$K_{co} = \frac{\Delta Q_L}{\Delta P_L}\bigg|_{\Delta z=0} = \frac{\pi \left[C_{Dns}\, D_{ns}\, z_{f1} + C_{DnD}\, D_{nD}\, z_{f2}\right]}{2\sqrt{\rho P_s}} \qquad (6.26)$$

6.3 Fluid forces

The significant fluid forces acting on the valve are:-

(a) that resulting from the static pressure acting on the nozzle area projected onto the disc,

(b) the velocity or dynamic pressure,

(c) that due to both the radial outward and inward flow and

(d) transient fluid force.

6.3.1 Steady-state fluid forces

Consider the double-disc valve configuration in Fig. 6.2 in which the two discs and the rod are moving as a rigid body to the right. It has been assumed that the current in coil 2 is greater than that of coil 1.

Considering disc 1, the fluid forces acting on it are the static pressure P_s acting on the nozzle area projected onto the disc, the velocity or dynamic pressure and that resulting from both the radial outward and inward flows. Using Bernoulli's equation, the static and dynamic pressure force F_{sd} on the disc is given by

$$F_{sd} = \left[P_s + \frac{u_1^2}{2}\right] A_{sn} \qquad (6.27)$$

where u_1 is the fluid velocity at the plane of the nozzle diameter and is given by

$$u_1 = Q_1/A_{sn} \qquad (6.28)$$

The radial outward fluid force F_{1ro} acting on disc 1 (from chapter 3) is given by

$$F_{1ro} = 2\pi \int_{r_{a1}}^{R_L} P_{1L}(r)\, r\, dr \tag{6.29}$$

where

$$P_{1L}(r) = P_1 + \frac{6\mu Q_1}{\pi h_{1L}^3} \ln\left(\frac{R_L}{r}\right) + \frac{0.193\rho Q_1^2}{\pi^2 h_{1L}^2}\left[\frac{1}{R_L^2} - \frac{1}{r^2}\right] \tag{6.30}$$

Combining equations (6.27), (6.28), (6.29) and (6.30) gives

$$F_{1L} = A_{sn} P_s + C_{1L} P_1 + C_{2L} Q_1 + C_{3L} Q_1^2 \tag{6.31}$$

where

$$A_{sn} = \frac{\pi D_{ns}^2}{4} \tag{6.32}$$

$$C_{1L} = \pi(R_L^2 - r_{a1}^2) \tag{6.33}$$

$$C_{2L} = \frac{3\mu}{h_{1L}^3}\left[R_L^2 - r_{a1}^2\left\{2 \ln\left(\frac{R_L}{r_{a1}}\right) + 1\right\}\right] \tag{6.34}$$

$$C_{3L} = \frac{\rho}{2A_{sn}} + \frac{0.193\rho}{\pi^2 h_{1L}^2}\left[1 - \left(\frac{r_{a1}}{R_L}\right)^2 - 2 \ln\left(\frac{R_L}{r_{a1}}\right)\right] \tag{6.35}$$

From chapter 3, the radial inward fluid force is given by

$$F_{1R} = 2\pi \int_{r_{dG}}^{R_L} P_{1R}(r)\, r\, dr \tag{6.36}$$

where

$$P_{1R}(r) = P_1 + \frac{6\mu Q_2}{\pi h_{1R}^3} \ln\left(\frac{r}{R_L}\right) + \frac{0.193\rho Q_2^2}{\pi^2 h_{1R}^2}\left[\frac{1}{r^2} - \frac{1}{R_L^2}\right] \tag{6.37}$$

Using equation (6.37) in (6.36) and integrating gives

$$F_{1R} = C_{1R} P_1 + C_{2R} Q_2 + C_{3R} Q_2^2 \tag{6.38}$$

where

$$C_{1R} = \pi(R_L^2 - r_{dG}^2) \tag{6.39}$$

$$C_{2R} = \frac{-3\mu}{h_{1R}^3}\left[R_L^2 - r_{dG}^2\left\{2\ln\left(\frac{R_L}{r_{dG}}\right) + 1\right\}\right] \tag{6.40}$$

$$C_{3R} = \frac{0.193\rho}{\pi^2 h_{1R}^2}\left[-1 + \left(\frac{r_{dG}}{R_L}\right)^2 + 2\ln\left(\frac{R_L}{r_{dG}}\right)\right] \tag{6.41}$$

$$h_{1L} = HG_s + z_{f1} + z \tag{6.42}$$

$$h_{1R} = HG_D + z_{f2} - z \tag{6.43}$$

Similar reasoning leads to the equations for the fluid forces acting on disc 2. The fluid force acting on the supply side of disc 2 is given by

$$F_{2R} = A_{sn} P_s + B_{1R} P_2 + B_{2R} Q_4 + B_{3R} Q_4^2 \tag{6.44}$$

where coefficients B_{1R} to B_{3R} are the same with that of C_{1L} to C_{3L} with suffix R instead of L, a2 instead of a1 , 2R instead of 1L, and z replaced by -z.

The fluid force acting on the drain side of disc 2 is given by

$$F_{2L} = B_{1L} P_2 + B_{2L} Q_3 + B_{3L} Q_3^2 \tag{6.45}$$

where coefficients B_{1L} to B_{3L} are the same with that of C_{1R} to C_{3R} with suffix R instead of L , 2L instead of 1R and z replaced by -z.

Now the resulting fluid force F_f acting on the two discs and the push rod moving together as a rigid body is the difference of the net fluid forces F_1 and F_2 acting on the discs. Thus

$$F_f = F_2 - F_1 = (F_{2R} - F_{2L}) - (F_{1L} - F_{1R}) \tag{6.46}$$

A linearized analysis would be used as the equations are highly nonlinear and the following assumptions would be made:

(a) the valve operations are close to null so that $P_1 \simeq P_2 \simeq P_s/2$

(b) the absolute viscosity of the fluid is constant

(c) the fluid density is constant

(d) the valve displacement z is small so that h_{1L}, h_{1R}, h_{2R} and h_{2L} can be approximated by the following equations:

$$h_{1L} = z_{f1} + HG_s \tag{6.47}$$

$$h_{1R} = z_{f2} + HG_D \tag{6.48}$$

$$h_{2L} = z_{f2} + HG_D \tag{6.49}$$

$$h_{2R} = z_{f1} + HG_s \tag{6.50}$$

(e) the two disc chambers are identical so that $R_L = R_R$ and $r_{a1} = r_{a2}$.

From conditions (d) and (e), the coefficients C's and B's are related as follows:

$$C_{1L} = B_{1R},\ C_{2L} = B_{2R},\ C_{3L} = B_{3R},\ C_{1R} = B_{1L},\ C_{2R} = B_{2L} \text{ and } C_{3R} = B_{3L} \tag{6.51}$$

Under these assumptions, equation (6.46) can be approximated by

$$F_f = - K_f z \tag{6.52}$$

where

$$K_f = 2\pi \left[C_{2L}\, C_{Dns}\, D_{ns} + C_{2R}\, C_{DnD}\, D_{nD}\right] \sqrt{\frac{P_s}{\rho}} + 4\pi^2 \left[C_{3L}\, C_{Dns}^2\, D_{ns}^2\, z_{f1} + C_{3R}\, C_{DnD}^2\, D_{nD}^2\, z_{f2}\right] \frac{P_s}{\rho} \tag{6.53}$$

Equation (6.52) is the steady-state fluid force on a double-disc valve. Because this force depends on valve displacement, it is completely analogous to a centering spring on the valve.

6.3.2 Transient fluid forces

The forces so far discussed are static and their value can be calculated for a given static disc displacement and flow rate. However, during unsteady or transient conditions the flow rate is not steady and the fluid

accelerations involved cause additional fluid forces. Consider the fluid slug, of length L_{snt1}, and cross-sectional area A_{ns1}, in the valve left-hand supply nozzle tube in Fig. 6.3.

The magnitude of the transient fluid force is given by Newton's second law as

Force F = mass x acceleration

i.e

$$F = \rho L_{nst1} A_{ns1} \frac{d}{dt}\left(\frac{Q_1}{A_{ns1}}\right) = \rho L_{nst1} \frac{dQ_1}{dt} \qquad (6.54)$$

Here the fluid is assumed to be incompressible so that the volumetric flow rate through the valve supply nozzle tube equals that through the orifice. In addition the slug is assumed to move at velocity Q_1/A_{ns1}. F is the force required to produce the rate of change of momentum; the reaction F_r on the left hand disc is equal and opposite to F. For example, if the flow Q_1 is increasing, the accelerating force must be in the positive z direction, but the reaction F_r on the disc is opposite and tends to close the drain nozzle. F_r is thus stabilising. If, however, the same analysis is applied to the right-hand supply nozzle tube flow Q_4, it is seen that as Q_4 increases, F_r is destabilising and tends to open the left-hand drain nozzle curtain area further. The transient force on the left hand disc in Fig. 6.3 is

$$F_{rt1} = \rho L_{nst1} \frac{dQ_1}{dt} \qquad (6.55)$$

Similarly, the transient force on the right hand disc is given by

$$F_{rt2} = \rho L_{nst2} \frac{dQ_4}{dt} \qquad (6.56)$$

The resultant transient fluid force is given by

$$T_{rff} = F_{rt2} - F_{rt1} \qquad (6.57)$$

Differentiating the flow rates in equations (6.1) and (6.4) with respect to

time t and neglecting the drain pressure P_D, the respective transient fluid forces are

$$\rho L_{snt1} \frac{dQ_1}{dt} = L_{snt1} C_{Dns} \pi D_{ns} \left[\sqrt{2\rho(P_s-P_1)} \frac{dz}{dt} - \frac{(z_{f1} + z)\frac{dP_1}{dt}}{\sqrt{\frac{2(P_s-P_1)}{\rho}}} \right] \tag{6.58}$$

$$\rho L_{snt2} \frac{dQ_4}{dt} = L_{snt2} C_{Dns} \pi D_{ns} \left[\sqrt{2\rho(P_s-P_2)} \frac{dz}{dt} - \frac{(z_{f1} - z)\frac{dP_2}{dt}}{\sqrt{\frac{2(P_s-P_2)}{\rho}}} \right] \tag{6.59}$$

Thus we note that the transient fluid forces are proportional to the disc velocity and pressure changes. The velocity term is the more significant because it represents a damping force. There is little direct evidence to indicate that the pressure rate term contributes substantially to valve dynamics, and therefore it is usually neglected [66]. In most dynamic analysis it is sufficient to consider $P_L = 0$. That is $P_1 \simeq P_2 \simeq P_s/2$ for valve operation near null position. This value also gives the largest fluid forces.

Neglecting the pressure derivative terms, the final expression for the transient fluid force becomes

$$T_{rff} = - B_f \frac{dz}{dt} \tag{6.60}$$

where

$$B_f = \pi \left[C_{Dns} D_{ns} L_{snt1} + C_{Dns} D_{ns} L_{snt2} \right] \sqrt{\rho P_s} \tag{6.61}$$

6.4 Electro-magnetic subsystem

The double-disc valve have two coils. Each of the coils has an inductance L in series with resistance R. In general, L varies with z (disc displacement) but its variation is small compared to other factors and has been ignored in the analysis.

The resulting equation for coil current is

$$I = \frac{V}{R_c}(1 + T_c\, s) \tag{6.62}$$

where $T_c = L/R_c$ the coil time constant and 's' is the Laplace operator.

The magnetic force F_m exerted on the disc is a nonlinear function of I and Z (disc displacement). That is $F_m = f(I,Z)$ and using the normal linearization techniques

$$\delta F_m = \frac{\partial F_m}{\partial I}\delta I + \frac{\partial F_m}{\partial Z}\delta Z \quad \text{or} \quad f_m = C_{FI}\, i + C_{FX}\, z \tag{6.63}$$

where lower case letters represent small pertubations of the parameters represented by the higher case symbols and $C_{FI} = \partial F_m/\partial I$, $C_{FX} = \partial F_m/\partial Z$ both measured at reference condition. Equation (6.62) is transposed to small pertubations by replacing I and V by i and v.

Referring to Fig. 6.4, the two coils on an electro-magnetic solenoid are generally supply from a push-pull source. A voltage V_{cc} in the amplifier driving the solenoids establishes a quiescent current I_0 in each coil but there is no net force on the two discs and the push rod solid body because the currents oppose each other and the fluid force acts against the motion of the discs. An increase in the input to the amplifier causes the current in one coil to increase as the current in the other coil decreases simultaneously by the same amount. Hence the current in the two coils may

be written

$$i_1 = I_o - i \tag{6.64}$$

$$i_2 = I_o + i \tag{6.65}$$

where i_1, i_2 = current in each coil, respectively,

I_o = constant quiescent current in each coil, amp

i = signal current in each coil, amp

The quiescent current I_o is usually about one half the maximum signal input to the amplifier, the current in one electro-magnetic coil will be zero so that the maximum differential current will occur in the coil. With such a quiescent current level, which is required because of the amplifier characteristics, the efficiency is only 50 per cent. This is a minor point, however, because the electrical power involved is small compared with hydraulic losses.

Figure 6.5 is a sketch of the coils configuration employed in the double-disc valve. The electro-magnetic force exerted on each of the discs is given by

$$f_{m1} = C_{FI}\, i_1 + C_{FX}\, z_1 \tag{6.66}$$

$$f_{m2} = C_{FI}\, i_2 + C_{FX}\, z_2 \tag{6.67}$$

The value of z_1 and z_2 are the same and equal to $HG_s + z_{f1}$ when the discs are centred. When the discs are displaced z from the centre or neutral position,

$$z_1 = HG_s + z_{f1} + z \tag{6.68}$$

$$z_2 = HG_s + z_{f1} - z \tag{6.69}$$

The resultant electro-magnetic force f_m in the positive z direction is given by

$$f_m = f_{m2} - f_{m1} \tag{6.70}$$

Using equations (6.64) through (6.69) in equation (6.70) gives

$$f_m = 2\, C_{FI}\, i - 2\, C_{FX}\, z \tag{6.71}$$

The coefficients C_{FI} and C_{FX} would be obtained from the definition of electro-magnetic force of a flat-face magnet used in the valve.

The electro-magnetic force F_m is given by [61]

$$F_m = \frac{\mu_g A_c (NI)^2}{4 g^2} \tag{6.72}$$

where μ_g is the permeability of the oil gap, I is the current in the coil, N is the number of coil turns, g is the distance between the disc and the magnetic surface and A_c is the cross-sectional area of the iron core

Now

$$C_{FI} = \left.\frac{\partial F_m}{\partial I}\right|_o = \frac{\mu_g A_c N^2 I_o}{2 g_o^2} \tag{6.73}$$

$$C_{FX} = \left.\frac{\partial F_m}{\partial g}\right|_o = -\frac{\mu_g A_c (NI_o)^2}{2 g_o^3} \tag{6.74}$$

$$g = HG_s + z_{f1} \pm z \tag{6.75}$$

where I_o is the constant quiescent current in each coil, g_o is the value of g when discs are centred i.e. $z = 0$, HG_s is the supply nozzle holding gap and z_{f1} is the neutral position of the disc from the supply nozzle tip.

6.5 Mechanical characteristics of a double-disc valve

An approximation to the dynamic performance of the double-disc valve can be found by summing the forces acting on such a system. Therefore, by combining the fluid forces and the electro-magnetic force with the discs

inertia force, the force balance becomes

$$f_m + f_{ft} = M_v \frac{d^2z}{dt^2} \tag{6.76}$$

where f_m is the resultant electro-magnetic force, f_{ft} is the sum of transient and steady state fluid forces and M_v is the mass of moving parts of the valve.

Equations (6.52), (6.60), (6.71) and (6.76) are the four basic equations and may be solved simultaneously to obtain

$$\frac{z}{i} = \frac{2\,C_{FI}/M_v}{s^2 + (B_f/M_v)\,s + (K_f + 2\,C_{FX})/M_v} \tag{6.77}$$

Using equation (6.62) in (6.77), the valve transfer function can be rewritten in terms of coil voltage V as

$$\frac{z}{v} = \frac{K_v}{(1 + T_c\,s)\,[s^2 + (2\,\zeta_v\,w_v)\,s + w_v^2]} \tag{6.78}$$

where

$$w_v = \sqrt{\frac{K_f + 2\,C_{FX}}{M_v}}\,, \quad \zeta_v = \frac{B_f}{2\,M_v\,w_v} \text{ and } K_v = \frac{2\,C_{FX}}{R_c\,M_v}$$

The transfer function of a servovalve alone can be defined as [66]

$$\frac{\triangle x_v}{\triangle v} = \frac{r\,K_o\,w_o^2}{(1 + s/w_r)\,[s^2 + (2\,\zeta_o\,w_o)\,s + w_o^2]} \tag{6.79}$$

where the coefficients in equation (6.79) are define in appendix A12. However, usual practice is to use no load (i.e., P_L=0) flow $\triangle Q_L = K_q \triangle x_v$ as an output parameter rather than spool position. Comparing equations (6.78) and (6.79), it can be seen that the transfer function of a double-disc

valve has the same form as that of a servovalve. Except that the numerical values for the damping ratios, natural frequencies, time constants of the coils and the static gain constants are different. Although, the two transfer functions have the same form, the double-disc valve can be described as a highly underlap servovalve. The hydraulic stiffness of the valve is low compared with conventional servovalve.

The transfer function of a valve-equal area piston combination can be shown to be [66]

$$\frac{x_p}{z} = \frac{(K_q/A_p)\, w_h^2}{s\,[s^2 + (2\,\zeta_h\, w_h)\, s + w_h^2]} \tag{6.70}$$

where

$$w_h = \sqrt{\frac{4\beta_e\, A_p^2}{V_t\, M_t}} = \text{hydraulic natural frequency} \tag{6.71}$$

$$\zeta_h = \frac{K_{ce}}{A_p}\sqrt{\frac{\beta_e M_t}{V_t}} + \frac{B}{4A_p}\sqrt{\frac{V_t}{\beta_e M_t}} = \text{damping ratio} \tag{6.72}$$

This transfer function assumes spring loads are absent, no load disturbance, all pressures are uniform, no line losses, negligible minor losses, no pressure saturation, constant fluid density and temperature and that the piston is centred as the natural frequency is lowest in this position. Variations in the gain constant K_q/A_p, the hydraulic natural frequency w_h, and especially in the damping ratio ζ_h occur and cause considerable shifting in the frequency response with different operating positions of the piston.

This chapter has presented the transfer function of a double-disc valve based on approximate lumped parameter concepts. It shows that the double-disc valve can be looked at as an underlap servovalve. The next chapter will describe the results of experiment conducted with the double-disc

valves in position control configuration with two different cylinders. Some possible area of applications of valve will be outlined.

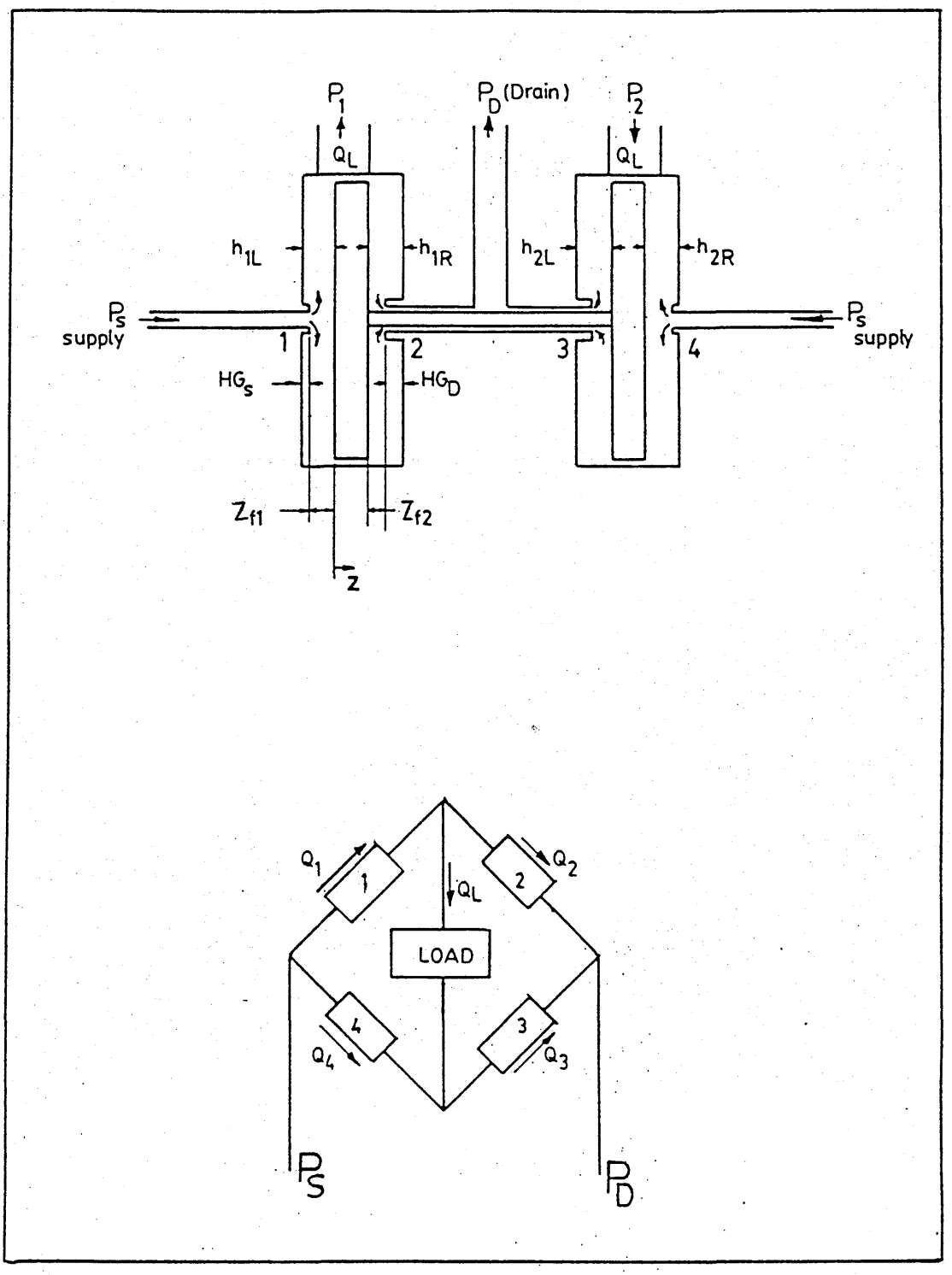

Fig. 6.1 Four-way double-disc valve operating about the mid-position.

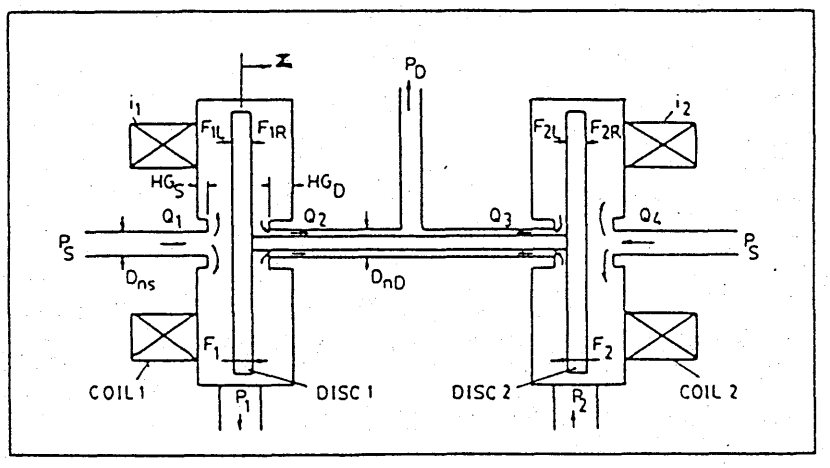

Fig. 6.2 Fluid forces on a double-disc valve.

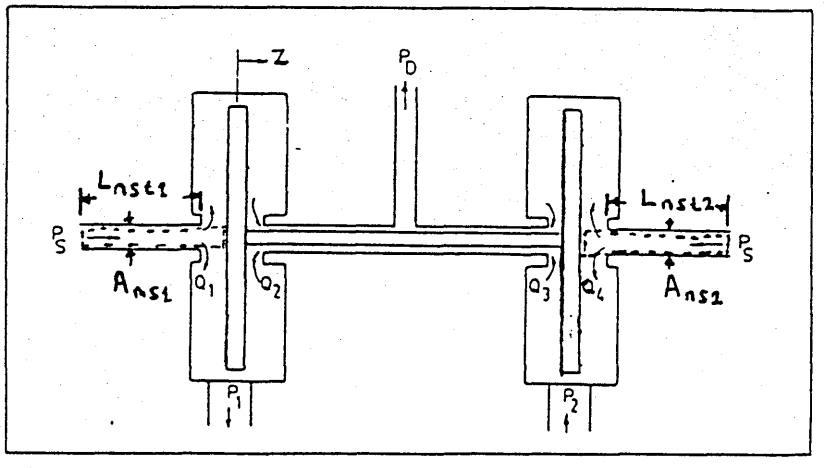

Fig. 6.3 Transient fluid forces.

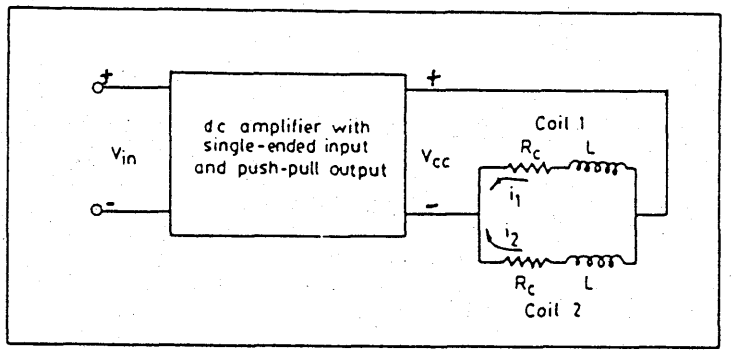

Fig. 6.4 Schematic of electro-magnetic coils being driven from an amplifier.

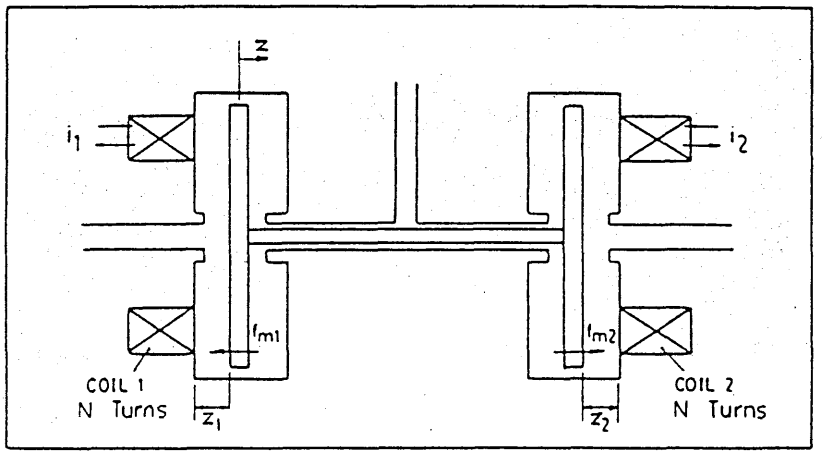

Fig. 6.5 Electro-magnetic forces.

CHAPTER 7

APPLICATIONS OF DOUBLE-DISC VALVE

7 Applications of double-disc valve

This chapter deals with experiments carried out with the prototype and pre-production valves. The tests were conducted with a long-stroke unequal area cylinder for flow calibration purposes and also with a short-stroke equal area cylinder. In the latter tests the cylinder was connected for closed-loop position control under conditions of constant load. Proportional control of the valve was achieved using pulse-width-modulation. Some possible areas of application of the valve are also presented.

7.1 Prototype valve - unequal area cylinder combination

To gain insight into the performance of the floating double - disc valve in working conditions, an experimental rig was set up. The experimental rig incorporated the prototype valve, high pressure hydraulic rig (see appendix A13), long stroke cylinder, feedback potentiometer and valve mounting block.

A block diagram of the experimental set-up with the valve providing a position control system in open-loop is shown in Fig.7.1. The pressures in both disc chambers were measured with the aid of piezo-electric transducers. Pressure transducers were installed at the supply line and return line to record the supply and drain pressures. Cavitation is likely to occur in any hydraulic system. To check this, a needle valve was fitted just downstream of the valve so that the back pressure could be adjusted to any desired value. The piston or jack position was recorded by monitoring the feedback potentiometer. The various pressure time-histories of the system were also recorded. These recordings were accomplished with the aid of the RSP programme [67] used in conjunction with an Interdata 7/16 Minicomputer and Micro-Consultants analogue data acquisition system. A permanent record of results were made with the aid of the associated X-Y

plotter.

Fig.7.2 shows a typical jack output position time-history for the case when the valve was fully switched and the jack was extending. The speed of the jack remained constant at 6.7 in/s (170 mm/s) until it completed its stroke. The jack speed is given by the gradient of the jack output position time-history and the product of speed and effective piston area gives the average load flowrate. The flowrate in this case was 11.8 lt/min. Fig.7.3 shows the corresponding pressure time-history associated with the jack output position time-history shown in Fig.7.2. From the figure it can be seen that the two chamber pressures on either side of the piston remained constant during the jack moving period. The pressure, P_1, in chamber 1 remained constant at 240 Psi (17 bar) when jack was still moving and dropped to about 50 Psi (3.5 bar), the drain pressure, on completion of its motion. On the other hand, the pressure P_2, in chamber 2 rose from 160 Psi (11 bar) to 950 Psi (67 bar), the supply pressure.

Figs. 7.4 and 7.5 show the typical pressures and jack output position time-histories under retracting conditions. Under the retracting conditions, the pressure P_2, dropped from 350 Psi (24.5 bar) to drain pressure and chamber pressure P_1, rose from 750 Psi (52.5 bar) to 950 Psi (67 bar). The jack speed was 5.0 in/s (127 mm/s) and the corresponding flowrate was 8.8 lt/min.

7.1.1 Effect of carrier frequency on the prototype valve - sinusoidal test

For a given supply pressure, the range of carrier frequencies that the valve is controllable was determined with the aid of an analogue pulse-width-modulator and a switching amplifier. The pulse-width-modulator amplifier has a summing operational amplifier and a comparator. The comparator was used to compared the d.c. voltage level of the carrier

signal (sawtooth) with that of an input signal (sinusoidal).

The ratio of the carrier frequency to the input frequency was carefully chosen to be as high as possible. This was to ensure that the input signal did not make any contribution to the output position of the system. According to Ikebe et el [41], this ratio must be greater than 7. The main principle behind this approach was as follows: for a high ratio of carrier frequency to input frequency, the trigger level of the comparator was gradually varied and the mark/space ratio of the modulator output thus changed accordingly. The valve responded with the pulse-width-modulator output.

The speed control of the valve was varied sinusoidally by using a sine wave input to trigger the comparator of the analogue Pulse-width-modulator. In so doing, the mark/space ratio of the output waveform varied with the sine wave input. The experimental set up was the same as for the flow capacity estimation. The jack output position was recorded using the RSP programme for various carrier frequencies. The speed of the jack at any point on the position time-history shown in Fig.7.6 is given by the slope at that point. Clearly, it can be seen that the jack speed is not symmetrical for both extending and retracting situations. This could be attributed to the cylinder which is not symmetrical and the two valve chambers might not be identical. A typical speed versus carrier frequency curve for the four-way arrangement of the valve is as shown in Fig.7.7. The figure shows that the full jack speeds in extending and retracting conditions were 6.7 in/s (170 mm/s) and 8.1 in/s (206 mm/s) respectively. For carrier frequency of 100 Hz, the speed control ranges of the valve in extending and retracting conditions were 0 to 4.4 in/s (112 mm/s) and 0 to 0.76 in/s (19 mm/s) respectively. When the carrier frequency was increased to 200 Hz, the speed control ranges were increased to 5.7 in/s (145 mm/s) in extending

situations and 0.95 in/s (24 mm/s) in retracting conditions.

Generally, valves using pulse-width-modulation techniques often generate large hydraulic noise downstream of the valve which may adversely affect the accuracy of a positioning system. This hydraulic noise was found to be controllable by selecting the correct choice of carrier frequency and the hydraulic pipe network. For a quiet valve operation, the carrier frequency must be greater than the natural frequency of the complete hydraulic system and the structural modes of the equipment or environment. For the prototype valve under investigation, it was found that the valve was quiet for carrier frequencies greater than 200 Hz. When a PWM signal was applied to the valve, the discs couldnot completely respond to the high frequency switching because of the disc and fluid inertia forces. Instead, the discs tended to follow the average value of the modulated signal as the PWM carrier frequency was approximately 2 KHz, which was well above the natural frequencies of the valve components. Each coil, in a sense, acted as a demodulator and each disc position was proportional to the amplifier input signal.

7.1.2 Prototype valve as a three-way valve

To have approximately symmetrical velocity characteristics for the long stroke cylinder, the valve was re-piped as a three-way valve. In this arrangement, side 1 load port was blanked-off and as a result the disc chamber 1 acted as a control chamber. Figure 7.8 shows the pipe connections. The supply oil was taken from the high pressure rig. In this configuration the piston end of the cylinder always communicated with the supply pressure while the blank end side communicated with load port 2. With this arrangement, when the jack was extending, there was a possibility of reverse supply flow from the piston end of the cylinder. To prevent this reverse flow, an in-line check valve was installed upstream of the valve.

The full speed tests to estimate the valve flow capacity were repeated. Fig. 7.9 shows the typical jack output position and pressure time-histories of an extending jack under 3-way valve arrangement. The speed of the jack remained constant at 6.2 in/s (157 mm/s) until it completed its stroke. The corresponding valve flowrate was 11 lt/min. From the figure it can be seen that the two chamber pressures on either side of the piston remained constant during the jack moving period. The pressure, P_2, in chamber 2 remained constant at 860 Psi (60 bar) when jack was still moving and rose to 1500 Psi (105 bar), the supply pressure, on completion of its motion. On the other hand, the pressure P_1, in chamber 1 remained constant at drain pressure as disc 1 chamber acted as a control chamber.

Fig. 7.10 shows the typical pressure and jack output position time-histories of a retracting jack under 3-way valve arrangement. Under the retracting conditions, the pressure P_2, dropped from 687 Psi (48 bar) to drain pressure and chamber pressure P_1, remained constant at supply pressure of 1500 Psi (105 bar). The drain pressure remained constant at 204 Psi (14 bar) during the jack motion and dropped to 86 Psi (6 bar) on jack's completion of motion. The jack speed was 8.0 in/s (203 mm/s) and the corresponding flowrate was 14.1 lt/min.

All the experiments conducted so far with the valve employed discs with thickness of 3.73 mm and total disc travel of about 0.23 mm. In order to increase the flow capacity of the valve, the disc thickness was reduced to 3.56 mm and this modification increased the total disc travel from 0.23 mm to 0.41 mm. The full speed test was repeated and a flowrate of 18.3 lt/min was observed for 1000 Psi (70 bar) pressure drop across the valve.

The pressure-flow characteristic from these results is shown in Fig.7.11. From the figure it can be seen that flowrate increases with total disc

travel and supply pressure. Positive flowrates are defined for jack extending and negative for jack retracting. The linearity of the flow-pressure curves shows the laminar nature of flow.

7.2 Prototype valve on an equal area ram rig

The equal area ram rig consisted of the prototype valve, feedback potentiometer, a carriage, and a mounting block. One end of the piston was connected to the carriage which moved freely on a flat test bench with the aid of ball races. The output position of the piston was measured through the potentiometer connected to the carriage and mounted alongside the ram. The prototype valve - equal area cylinder rig is shown in Figure 7.12.

7.2.1 Initial problems with prototype valve - equal area ram combination

After calibrating the feedback potentiometer and the instruments, the prototype valve was used in a closed-loop to control an equal area ram. It was found that the valve could only perform switching functions and that it could only stop the actuator in one or two positions between the fully extended and retracted positions of the ram. In addition, a high error signal voltage was required to actuate the valve. This initial problems could be attributed to the following: (a) long disc travel, (b) the magnetic forces are more than the fluid forces and as such the valve only performed switching actions, (c) the saw tooth waveform amplitude is far greater than that of the error signal and this might have caused the input dead-band. The ways in which these effects might influence the valve performance will now be discussed.

(a) **Effect of error signal gain on input dead-band**

The valve was used in a closed-loop as shown in Figure 7.13. The closed-loop position system consists of the prototype valve, the single output feedback potentiometer, disc valve amplifier, equal area ram and a carriage

(see Fig.7.12). The supply pressure was set to 28 bar. The hydraulic pipe connection is shown in Figure 7.14. The error signal gain was set to 1 and the valve was given an incremental displacement by increasing the amplifier input voltage until the output position of the actuator changed. The error signal amplitude that resulted in change of the piston output position was recorded as the input dead-band. The error signal gain was increased in steps of 0.5 from 1 to 10 and the corresponding input dead-band were recorded. The result is shown in Figure 7.15. From the figure it can be seen that the input dead-band decreases as the error signal gain is increased. Using this technique, the input dead-band could only be reduced from 4.5 V to 0.5 V. The result shows the switching properties of the valve.

(b) **Effect of carrier frequency on input dead-band**

The test procedure and apparatus are the same as in the previous experiment. In this experiment, the input dead-band and error signal gain relationships were investigated at two distinct carrier frequencies of 250 and 1250 Hz. The results are as shown in Figure 7.16. From the figure it can be seen that increasing the carrier frequency has no effect on the input dead-band.

(c) **Effect of sawtooth amplitude on input dead-band**

The pulse-width-modulation action of the disc valve amplifier was obtained from a comparator. This comparator compares the sawtooth waveform with the error signal. Consequently the amplitude of the sawtooth waveform must have a significant effect on the input dead-band. The amplitude of the sawtooth waveform was made adjustable with the aid of an output buffer used between the sawtooth waveform generator circuit and the comparator (see appendix A10). The test procedure and apparatus remained the same as in the previous experiments. The input dead-band and error signal gain relationships were investigated with the sawtooth amplitude set to 5 V and 2 V pk-pk. The

results are as shown in Figure 7.17. From the figure it can be seen that reducing the sawtooth amplitude reduced the input dead-band significantly. Using the amplitude of the sawtooth waveform to reduce the input dead-band, limit cycle oscillation was possible for a large error signal gain. Ideally, the error signal gain must be within that of the sawtooth waveform.

For a gain of 5 and sawtooth amplitude of 2 V pk-pk, the maximum input dead-band was 0.2 V. This represented $\pm$ 0.1 V input hysteresis. The maximum current available from the disc valve amplifier was 1450 mA. When there was zero error signal, the current level of each of the two electro-magnetic coils of the valve was one-half of the maximum current. Therefore the dead-band region in terms of current was 540 - 910 mA for a sawtooth amplitude of 2 V pk-pk. The corresponding dead-band region for a sawtooth amplitude of 5 V pk-pk with an error signal gain of 5 was 420 - 1030 mA. Clearly decreasing the sawtooth amplitude reduced the input dead-band. For correct operation of the valve, the sawtooth amplitude should be less than 2 V pk-pk, error gain set below 5 and carrier frequency greater than 1KHz should be employed.

7.2.2 Static characteristics of prototype valve - equal area ram combination

The apparatus consisted of the high pressure hydraulic rig, the equal area ram and the prototype valve. Figure 7.18 shows the layout of the apparatus in a closed-loop position control. After setting up the equipment, the high pressure hydraulic rig was switched on and the required supply pressure was selected. The input voltage was varied in small steps so that the piston could be moved from its fully retracted position to its fully extended position and then brought back to its fully retracted position. For the range of the demand input voltages, the output positions (as measured with

an electronic displacement transducer) were measured. This procedure ensured that both linearity and hysteresis were checked. The results are shown in Figure 7.19. From the figure it can be seen that the overall valve-cylinder linearity was good. However the proportional action of the valve was not smooth. This can be attributed to the input dead-band associated with the valve as discussed earlier in this chapter which caused the valve to perform a stepping action.

7.2.3 Stiffness characteristics of prototype valve and equal area ram

The schematic layout of apparatus used to determined the static stiffness of the valve is shown in Figure 7.20. The pulley arrangement in Fig. 7.20 was used to apply a constant axial load to the equal area ram. The effect of such load on the positioning action of the valve was determine from this experiment.

The valve was operated in a closed-loop configuration and the following procedure was carried out: (a) The piston of the equal area ram was fully retracted and an axial load was applied through the pulley arrangement. (b) The input voltage was varied in small steps so that the piston could be moved from its fully retracted position to its fully extended position and then brought back to its fully retracted position. For the range of the demand input voltages, the output position (as measured with an electronic displacement transducer) were measured. This procedure ensured that both linearity and hysteresis were checked. To determine the maximum load that the valve-cylinder could carry, the piston was positioned at a convenient position and a load (weight) applied through the pulley arrangement was increased until the output position of the actuator shifted. The load so obtained was recorded as the static stiffness of the valve-cylinder combination.

The static characteristic of the control system subjected to a constant axial load of 55 N is shown in Figure 7.21. The result shows that the valve characteristic is quite linear with little hysteresis. The maximum axial load that the prototype valve could withstand was 90 N for a supply pressure of 28 bar. The valve was found to exhibit limit cycle oscillations when a load greater than 90 N was applied. The valve was operated in a closed-loop position control and the feedback signal corresponding to the output position of the actuator changed as the system was not stiff enough to withstand the load. The shift in the output position resulted in an error signal which in turn acted on the valve to cause a shift in the disc position and thereby created a limit cycle oscillation. Increasing the error signal gain also resulted in limit cycle oscillation.

7.3 Experimental investigation of pre-production valve

In this section, the experiments carried out with the pre-production valve are presented. The tests were carried out with a short-stroke equal area cylinder connected for closed-loop position control under conditions of constant load. The pre-production valve ports are of the CETOP standards and the valve is sub-base mounted. Fig. 7.22 shows the pre-production valve -equal area cylinder rig.

7.3.1 Static characteristics of pre-production valve-equal area cylinder

Fig. 7.23 shows typical results of output position (as measured with an electronic displacement transducer) over a range of demand input voltages. Fig. 7.24 shows a typical relationship between the demand input voltage and the differential current across the electro-magnetic coils of the pre-production valve. The result shows a remarkable linearity. The results shown in Fig. 7.23 were obtained under the following conditions:

Supply pressure, PS = 37.1 bar, Drain pressure, PD = 10.8 bar

Oil temperature, TEMP = 36.0°C, disc thickness, DST = 3.81 mm

Rod length, RODL = 24.68 mm, Rod clearance, CR = 0.25 mm

Rod diameter, RODD = 3.18 mm, Total disc travel, TDT = 0.50 mm

Static weights, LOAD = 564.0 N, Carrier frequency, CF = 2.20 KHz

Loop gain, GAIN = 2, Actuator stroke, AST = 93.2 mm.

From Fig. 7.23 it can be seen that good linearity with low loop gains together with insignificant hysteresis were achieved. The pre-production valve has been operated with the equal area cylinder over a range of operating temperatures (25°C-40°C), system pressures (28 - 105 bar), loop gains (1 - 10), carrier frequencies (0.25 - 2.20 KHz) and load conditions. Different disc chamber geometries have been investigated by altering any of the following parameters: rod dimensions, disc thickness, rod clearance and total disc travel. Table 7.1 shows the summary of the different rod dimensions and discs used in the investigation.

Table 7.1 Summary of the different push rods and discs used with the pre-production valve.

Disc thickness (mm)	Rod diameter (mm)	Rod length (mm)	Total disc travel (mm)	Rod clearance (mm)
4.08	2.54	24.64	0.23	0.05
		24.59	0.18	0.10
3.81	2.54	24.89	0.50	0.05
	3.17	24.89	0.50	0.05
		24.69	0.25	0.25

The positioning action of the valve-actuator combination is achieved by the complex interactions between the fluid forces, F_f and the electro-magnetic

forces, F_m acting on the valve discs. Three different modes of valve control can be established which depend on the magnitudes of F_f and F_m. They are:

(a) $F_m > F_f$: If the magnetic forces are much greater than the fluid forces in the valve neutral position, the two discs are pulled towards the supply nozzles and thereby cutting-off supply to load ports. The stiffness of the valve-cylinder system is reduced as the load ports are now coupled to the drain. To increase the stiffness, two check valves can be installed in the load lines. This is advantageous in low pressure applications when the valve is being used as a pilot device. Provision have been made in the disc valve amplifier to energise the two coils at the same time to pull the two discs to shut-off the supply flow. In this mode, there is zero quiescent power loss. Positioning accuracy depends on the electrical gain. The valve exhibits some hysteresis as a result of the non-linear electro-magnetic forces which can be controlled by increasing the amplifier gain.

(b) $F_m < F_f$: If the magnetic forces are less than the fluid forces in valve neutral position, very good proportional control can be obtained with little or no hysteresis. However, the range of available magnetic forces must balance the fluid forces otherwise a large differential coil current is required to operate the valve.

(c) F_m slightly less than F_f in the neutral disc position but greater than F_f at some position within the discs and rod assembly travel. Linearity might be acceptable but limit cycle oscillation can occur.

For a large rod clearance, the null load pressures are greater than half the supply pressure. Under this condition, the magnetic force, F_m is less than the fluid force, F_f so that the discs are not pulled to close-off the supply nozzles. This increases the hydraulic stiffness of the valve-cylinder actuator at the expense of system dynamic response. For a given

oil supply pressure, F_f is fixed but F_m can be controlled by the amount of coil current input. The coil current is controlled by the electrical power supply to the disc valve amplifier. For a supply pressure less than 35 bar (for example, for pilot valve applications) the electrical power supply required is 0-18 V ($\pm$9 V). For a direct acting single stage valve with a supply pressure of 70 bar, a 0-24 V ($\pm$12V) power supply is required.

7.3.2 Valve-switching characteristics

Selection of the valve parameters for steady-state operations has been shown in Chapters 3 and 5 to be a compromise between fluid and electromagnetic force considerations. It must also take into account whether the valve is to be used in both switching and proportional modes. Factors such as discs masses, rod inertia, disc travel, fluid inertia in the valve, coil dynamics, and so on become important when valve switching characteristics are being considered.

To determine the switching speed of the valve, the switching amplifier described in Chapter 2 was used to energise the coils of the valve controlling an equal area cylinder in open-loop position control. The load pressures and coil currents time-histories were collected using a Bryans/Physical Data Recorder. The Data Recorder has four channels and a total of 4096 samples of input signal were recorded. The Data Recorder has a pre-trigger delay feature which allowed some desired number of samples to be allocated to the period immediately preceding the event to be recorded.

Using a mechanical switch and operational amplifier, the Data Recorder was externally triggered to record the pressures and currents time-histories of the valve and at the same time the valve coils were triggered. Fig.7.25 shows typical switching characteristics for a 31mm dia. double-disc valve operating at a supply pressure of 1000 Psi (70 bar) with coil 1 on and coil

2 off. Completion of disc switching is signalled by a detectable local minima in the transient current in the attracting coil, caused by the rapid change in flux through the disc when it stops, and this was used for estimating switching times with oil flowing in the valve. The coil 1 current minima can be seen in curve I_1 of Fig.7.25 as point b. The valve coil 1 was switched on at point a on the figure. The decaying current of coil 2 is shown in the figure as I_2. The pressures time-histories acting on the sides 1 and 2 of the cylinder are shown as curves P_1 and P_2 respectively. From the figure, it can be seen that there is a pure time delay before P_2 starts to increase. This time delay is due to the time constant of the electromagnetic coil. The load pressure P_2 increases to almost supply pressure before dropping to a constant value during which the piston of the cylinder was moving. On the other hand, the load pressure P_1 dropped from supply pressure to a constant value below that of P_2 when the piston was moving. The rod clearance was taken-up at position c of curve P_1 and disc 1 completed its travel at point d. The switching time for this set-up of rod-clearance of 0.15 mm is 12 ms and the time delay is 5 ms. Fig.7.26 shows the effect of varying the rod-clearance on switching time for various supply pressures. The solid lines in the figure are merely straight lines drawn through the experimental data. Variation of rod-clearance and supply pressure between 400 and 1200 Psi caused variations in switching time between 5 and 20 ms.

7.3.3 Frequency response

The frequency response of the control system is the amplitude ratio and phase shift of the output relative to the input as a function of frequency. The procedure used to measure the frequency response is to apply a sinusoidal input and record the output of the system in response to the sinusoidal input. The input amplitude used is large enough to minimise the

non-linearity distortions of threshold and hysteresis on the output and small enough to avoid saturation of the control system elements within the frequency of interest. The ratio of the output amplitude to the input amplitude and the output angle relative to the input is plotted as a function of the input frequency.

Fig. 7.27 is a frequency response plot for the control system in closed-loop with an input command of ±10% of the full scale input. The response shows a phase lag of 90 degrees at 25 rad/sec (4.0 Hz). The solid lines in the figure are the theoretical curve fittings of the experimental frequency response data. The theoretical transfer function of the contol system is treated in Section 6.5 of Chapter 6. The theoretical curves were obtained from a computer program developed by Usman [68] for the calculations of empirical formulae generated by Zaman and Griffin [69] for determining the frequency response from transfer function data of any order. Zaman and Griffin developed the empirical formulae using Levy [70] and Sanathanan et el [71] methods.

7.3.4 **Transient response**

Fig. 7.28 shows the transient response of the pre-production valve-equal area cylinder combination in closed-loop position control with system pressure of 35 bar and amplifier gain of 2. The results are summarised in Table 7.2.

Table 7.2 Results of transient response

	Extending jack	Retracting jack
Settling time (sec)	0.96	0.73
Rise time (sec)	0.40	0.40
Damping ratio	0.40	0.53
Natural frequency (rad/s)	10.40	10.30

From Table 7.2 it can be seen that the damping ratio in extending conditions was smaller than that obtained from the retracting situations. The difference in the transient responses for both the retracting and extending jack conditions of the system could be due to the unequal volumes on both sides of the actuator used. This arose from the unequal load pipelines length. The two supply nozzle land diameters were not identical but of diameters 3.20 mm and 3.52 mm respectively. This difference in supply nozzle land diameter may also have contributed to the discrepancies in the transient response results. However, the characteristics of the actuator dominated the dynamic response of the overall system.

7.4 Possible areas of valve applications

Double-disc valves can be used directly as single-stage proportional devices in closed loop control systems. However, as their performance is not as good as electro-hydraulic servo-valves owing to lower valve stiffness and significant load flow losses, they will probably find most application in low-cost systems where these deficiencies are minimised. Two such applications are now briefly presented:

(a) Swashplate angle control

The force requirements for actuating the swashplate of a variable delivery pump are fairly modest so that the stiffness characteristics of a double-disc valve make it suitable for this type of application.

Figure 7.29 shows a schematic of an electro-hydraulic double-disc valve operated swashplate linkage. From the figure, the input signal to the disc amplifier is the desired or demand swashplate angle. When the demand angle is changed, the valve receives an electrical signal from the amplifier, which is proportional to the error between the input signal to the system

and the voltage from the angular feedback transducer representing the swashplate position. This error signal shifts the valve discs and thereby porting fluid to the stroking pistons which rotates the pump swashplate. The swashplate provides an electrical feedback through an angular transducer that monitors the rotation of the connecting link B about point A which is linked to the swashplate via a drag link. This motion corrects the valve disc displacement, blocks the flow of control fluid to the control pistons and stops the swashplate at the position commanded by the input signal. The system remains in this position until the input signals is given a new command.

(b) **Double-disc valve as a pilot device**

When large fluid flow rates are required it is usually necessary to use two stages in the control valve arrangement. This is necessary to maintain a satisfactory response at high flow rates. Loss of response in single stage valves at large flow rates, is due to high disc or spool inertia and large flow forces, resulting in the need for a large electro-magnetic coil. Feedback loop are often provided at each stage, making them more flexible.

A proposed arrangement with an equal area ram is sketched in Figure 7.30. It has a pilot double-disc valve, having an electrical feedback path to a disc valve amplifier (PWM). The output from the amplifier actuates the electro-magnetic coils of the pilot valve. The electro-magnetic coils control the positions of the discs in the pilot valve chambers. The movement of the pilot valve discs varies the differential pressure acting on the ends of the spool valve. This is clearly more effective for dealing with large forces. The output flowrate from the spool valve drives the piston, which is also provided with a feedback loop.

7.4.1 Double-disc valve as a 3-way valve

The double-disc valve may be used as a 3-way valve with only one load port active. That is, with supply S, drain D, and one load port, L1. It also has two electrical coils which can be designated C1 and C2. The valve can be drawn schematically as shown in the sketch. However, the two discs do not necessarily have the same diameter and flow characteristics.

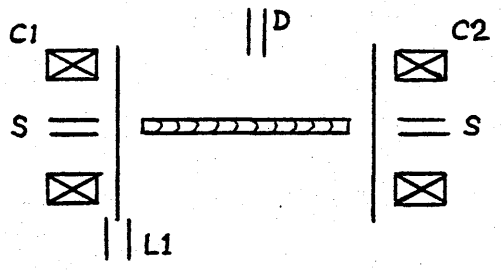

Representing a coil switched on by 1 and switched off by 0 the various combinations of coil activation can be shown in a table

C1	C2	L1	
0	0	S/D	
1	0	D	
0	1	S	
1	1	-	possible but does not provide any extra function.
PWM	PWM	PROP	

where PWM represents pulse-width-modulation to provide proportional (PROP) action. This valve can be used as a simple on-off switch in a hydraulic line or can provide proportional flow control. However, in general, to control a cylinder two load ports are required so that two 3-way valves are required for this purpose.

For convenience the two valves can be drawn as follows

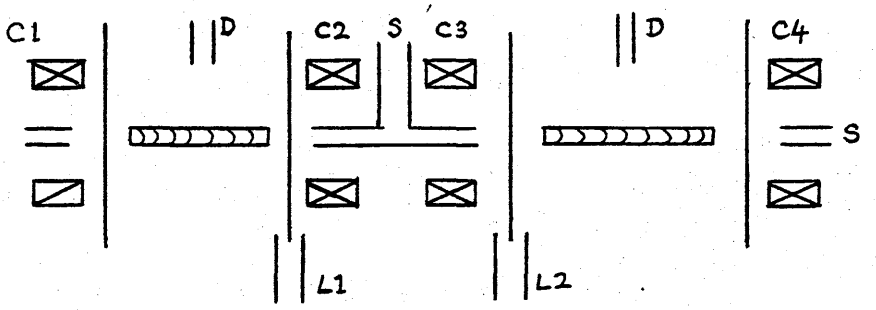

and the configuration table is now much larger causing more valve connection possibilities.

	C1	C2	C3	C4	L1	L2
1	0	0	0	0	S/D	S/D
2	1	0	1	0	S	D
3	0	1	0	1	D	S
4	1	0	0	1	S	S
5	0	1	1	0	D	D
6	1	0	0	0	S	S/D
7	0	1	0	0	D	S/D
8	0	0	0	1	S/D	S
9	0	0	1	0	S/D	D
10	PWM	PWM	PWM	PWM	PROP	PROP

All combinations involving 3 or 4 coils are probably impossible to operate. Of the combinations listed 6-9 are not useful thus leaving the following useful valves **all which can be remotely electrically selected.**

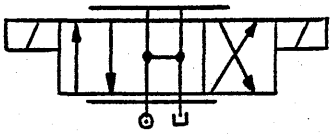

Combination

1, 2 and 3

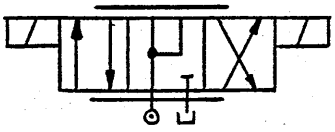

2, 3 and 4

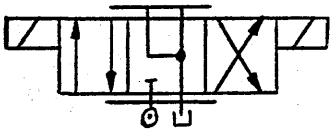

2, 3 and 5

By a suitable choice of coil activation a power cylinder may be controlled by two 3-way valves to give :-

(a) Rapid or proportional control in either direction

(b) open centre in mid-position

(c) pressurised load ports in mid-position

(d) vented load ports in mid-position.

This Chapter has described the results of experiments conducted with the double-disc valves in position control configuration with two different cylinders. Some possible areas of application have been outlined. The next Chapter will present the main conclusions reached in this study and recommendations for future work are also given.

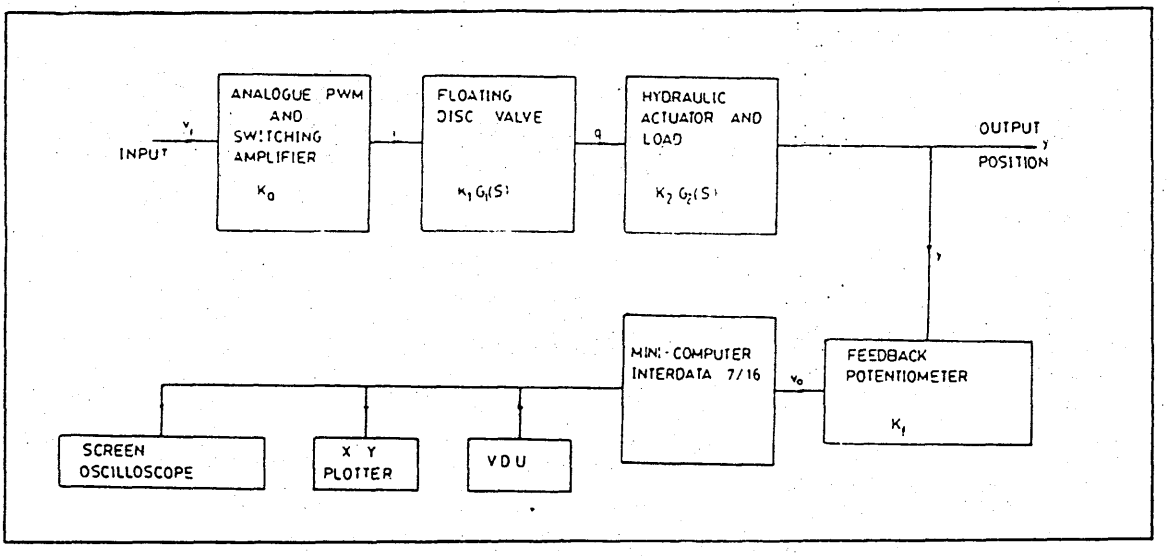

Fig. 7.1 Experimental set-up of an open-loop position control system.

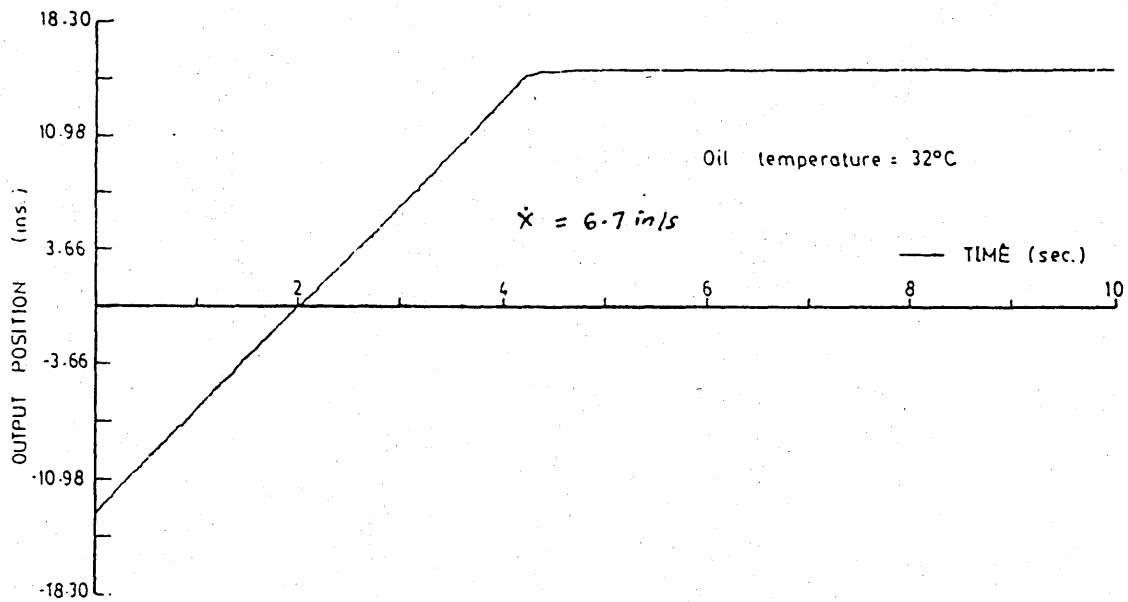

Fig. 7.2 Typical output position time-history of an extending jack under 4-way valve arrangement.

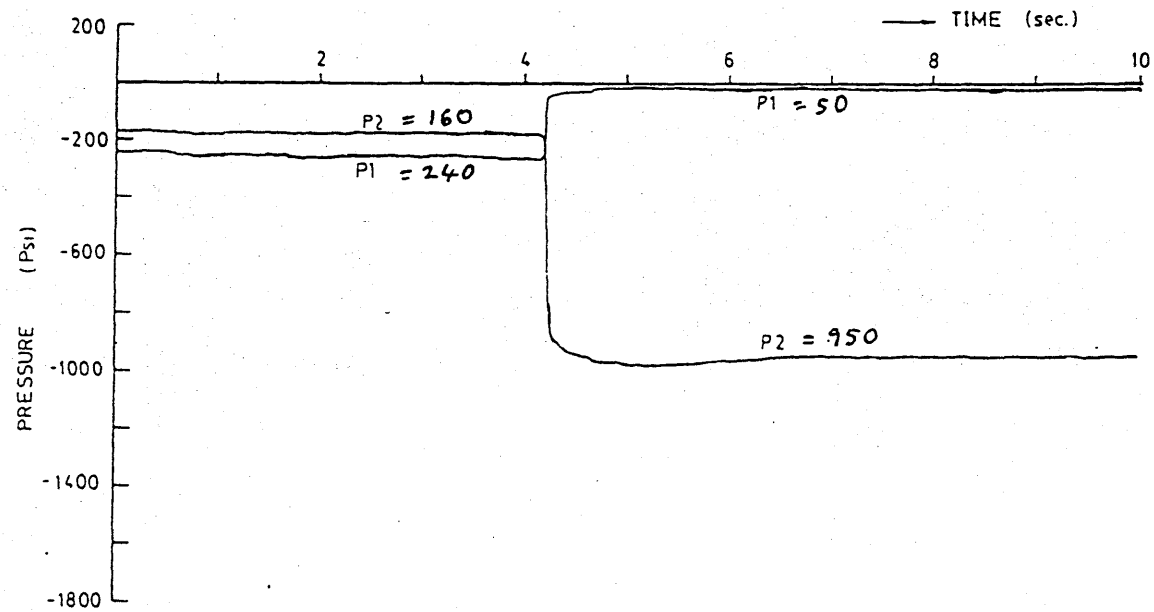

Fig. 7.3 Typical pressure time-history of an extending jack under 4-way valve arrangement.

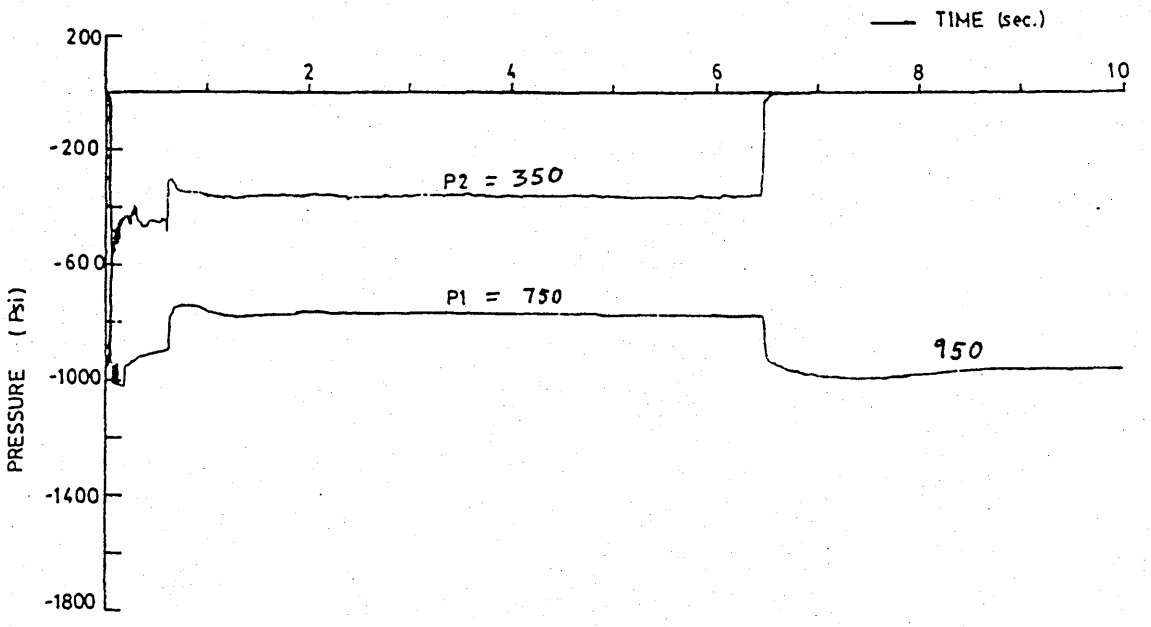

Fig. 7.4 Typical pressure time-history of a retracting jack under 4-way valve arrangement.

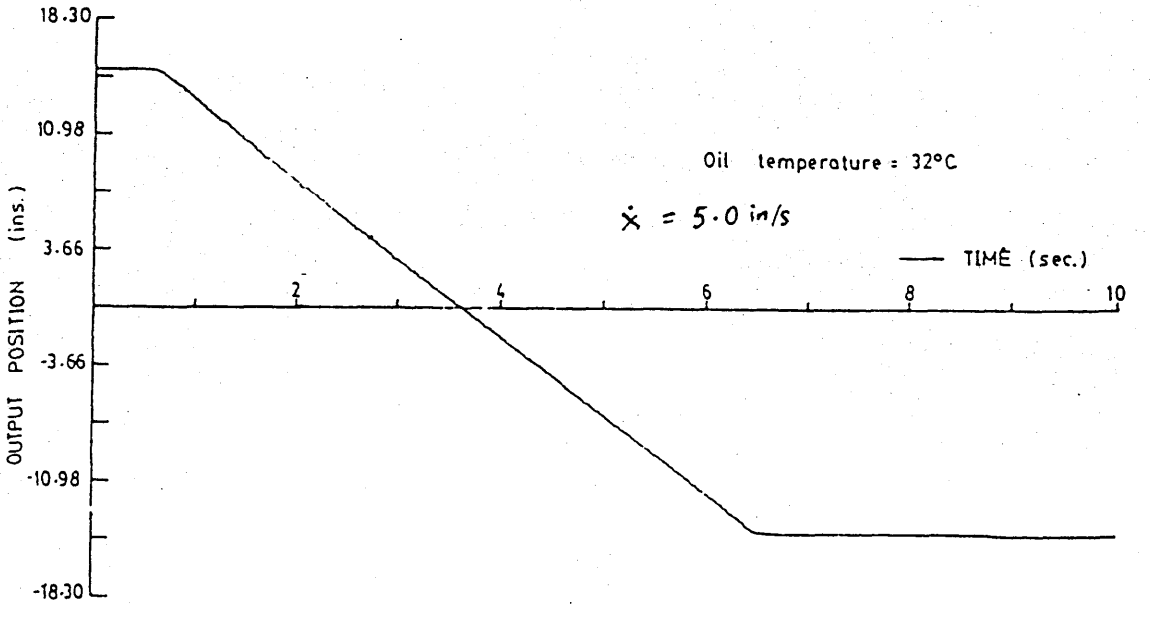

Fig. 7.5 Typical output position time-history of a retracting jack under 4-way valve arrangement.

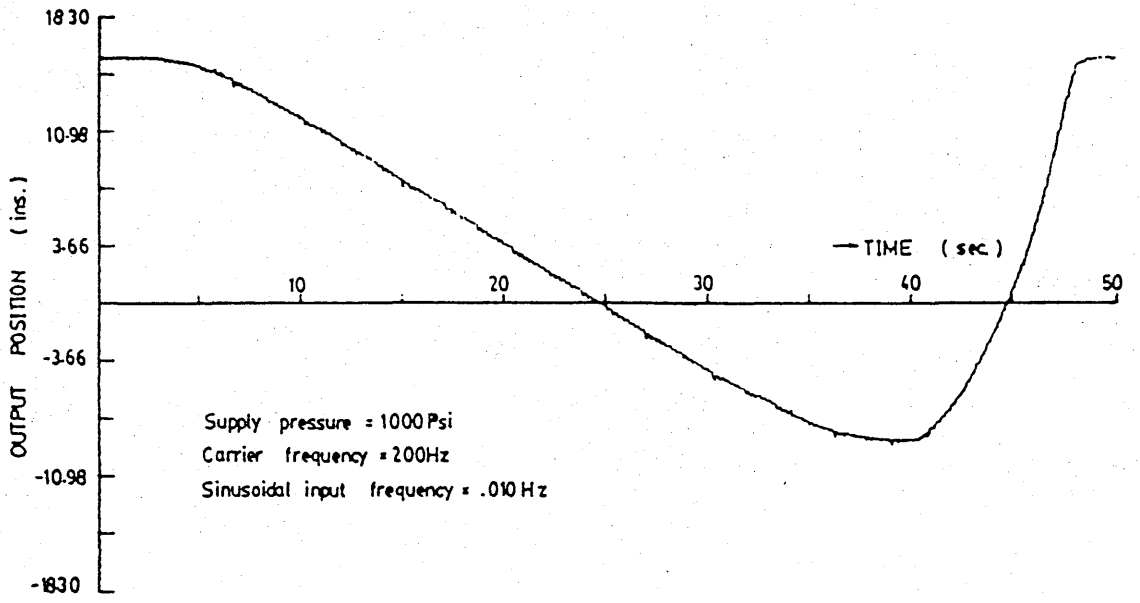

Fig. 7.6 Typical system response to sinusoidal input (4-way valve arrangement).

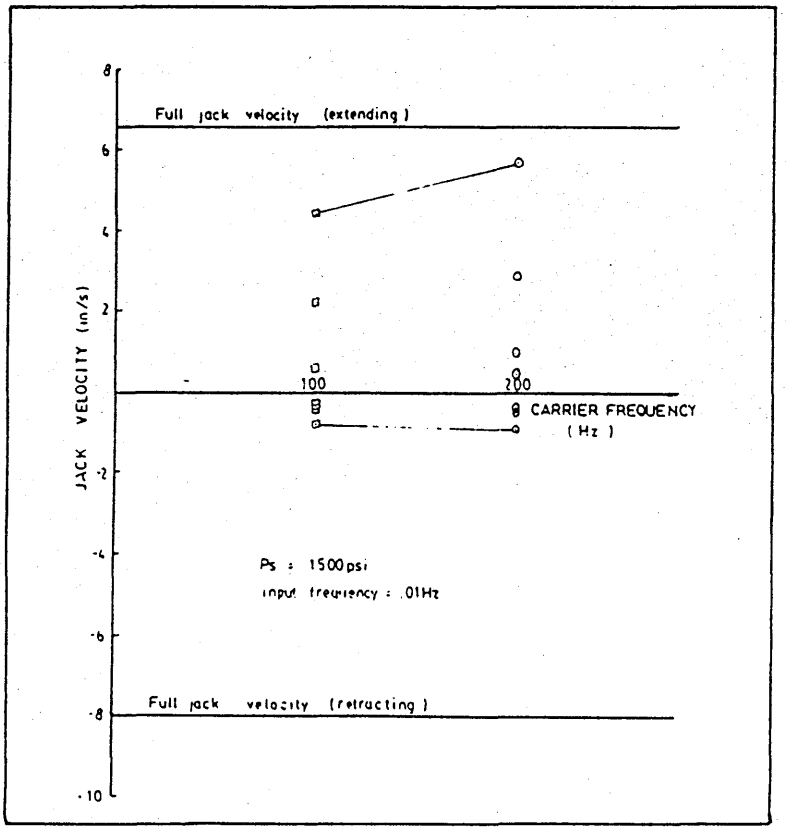

Fig. 7.7 Effect of carrier frequency on speed control (4-way valve arrangement).

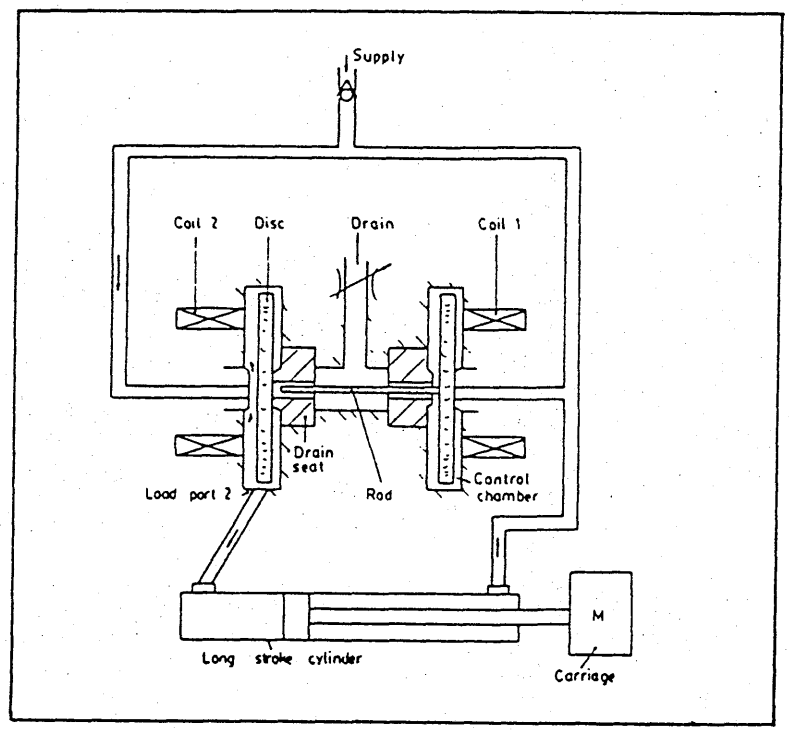

Fig. 7.8 Hydraulic pipe connections of a 3-way valve configuration.

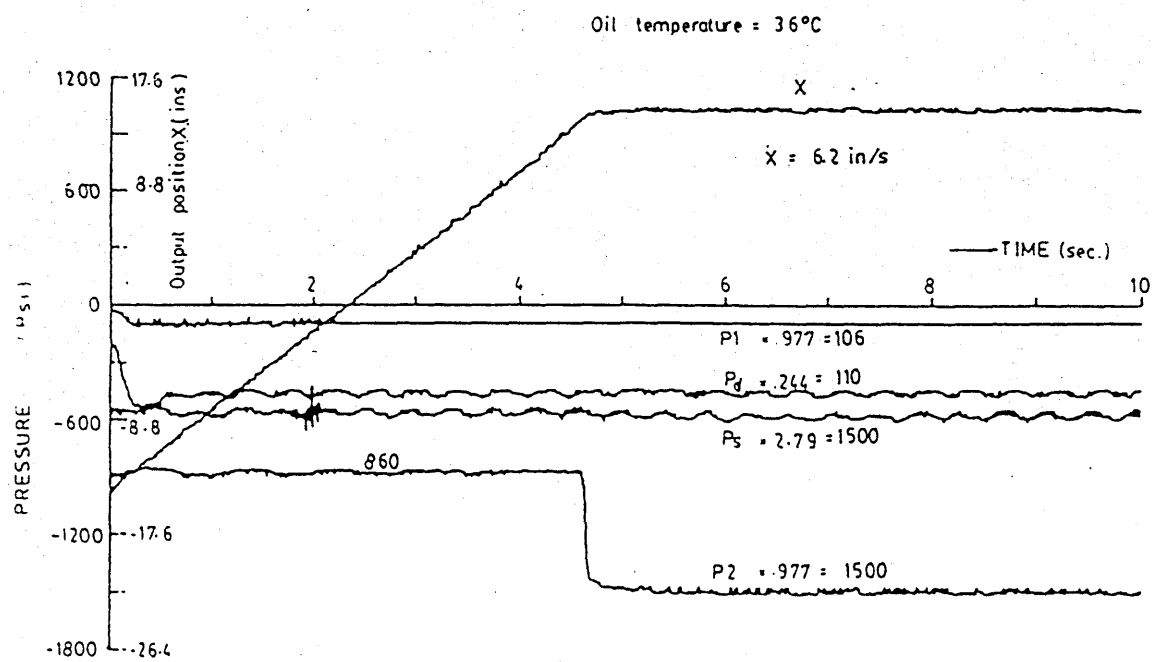

Fig. 7.9 Typical output position and pressure time-histories of an extending jack under 3-way valve arrangement.

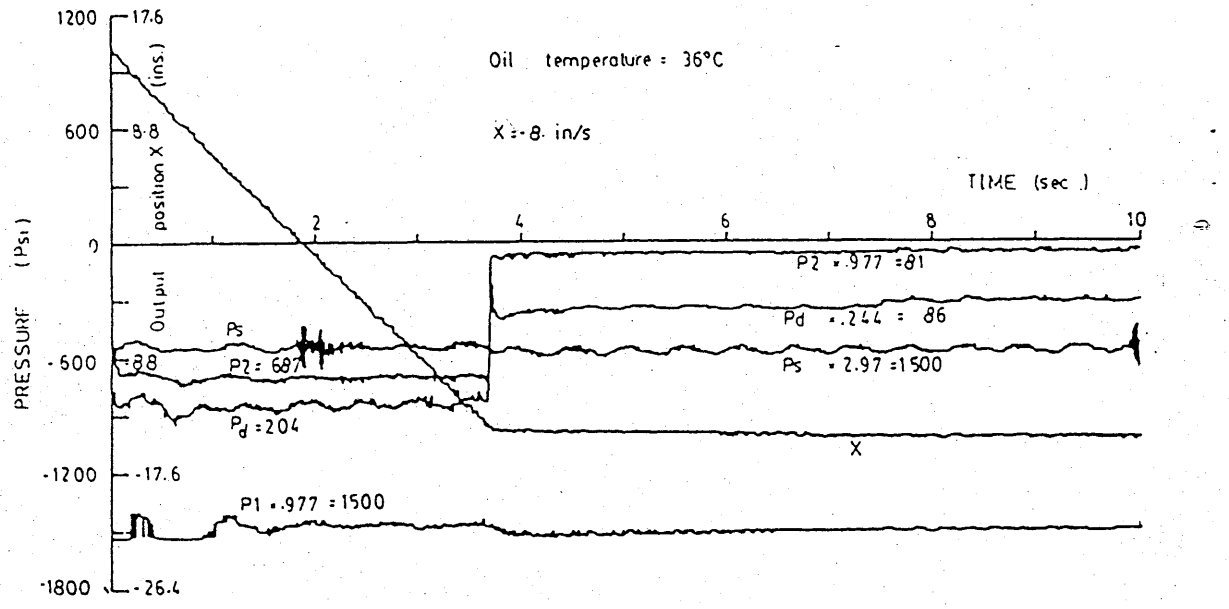

Fig. 7.10 Typical output position and pressure time-histories of a retracting jack under 3-way valve arrangement.

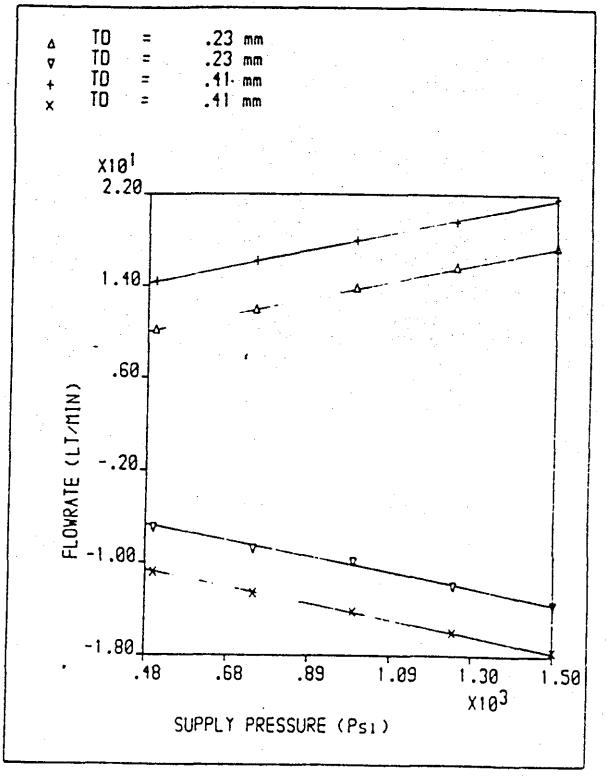

Fig. 7.11 Pressure-flow characteristics of a prototype double-disc valve.

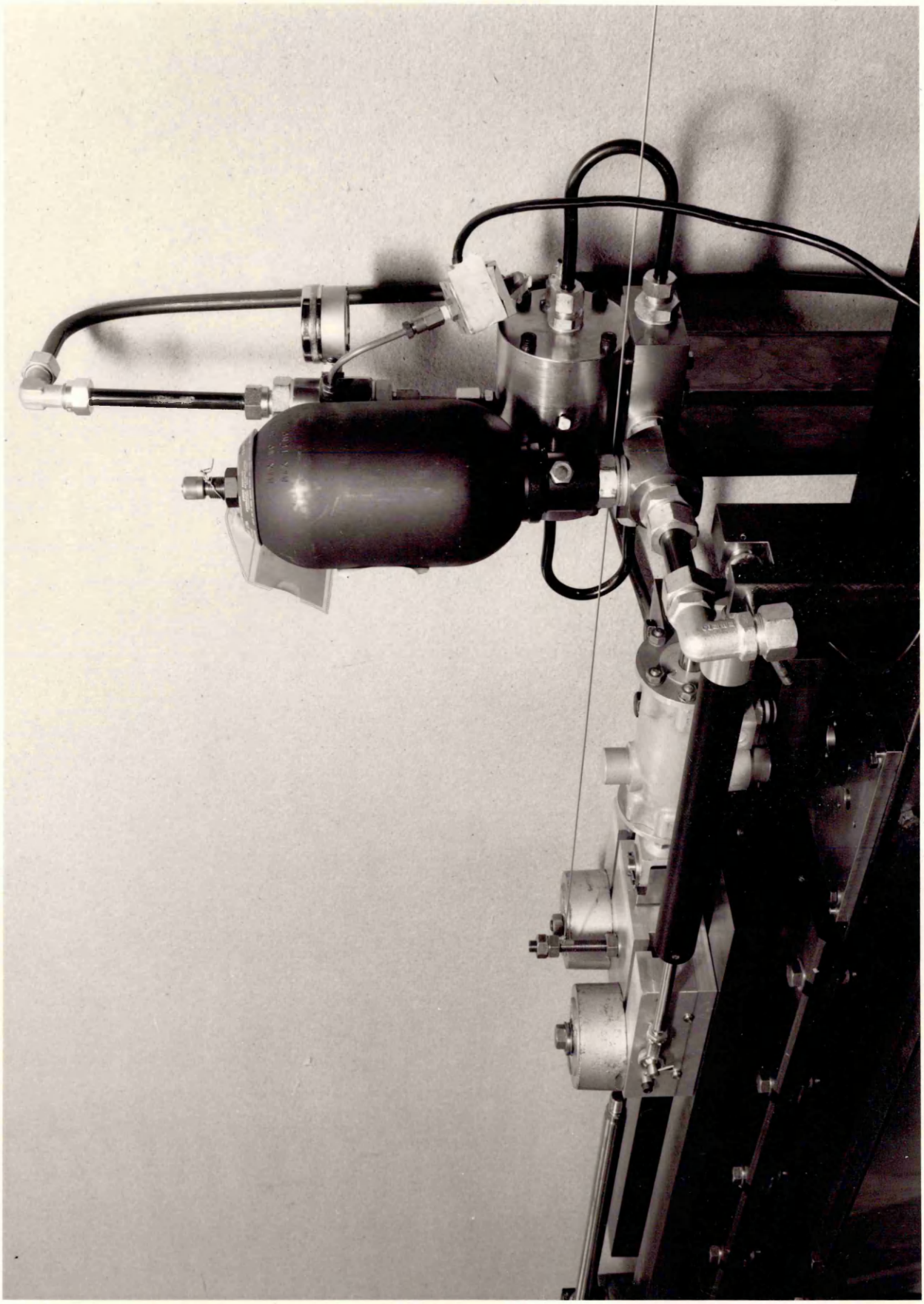

Fig. 7.12 Prototype double-disc valve-equal area cylinder rig.

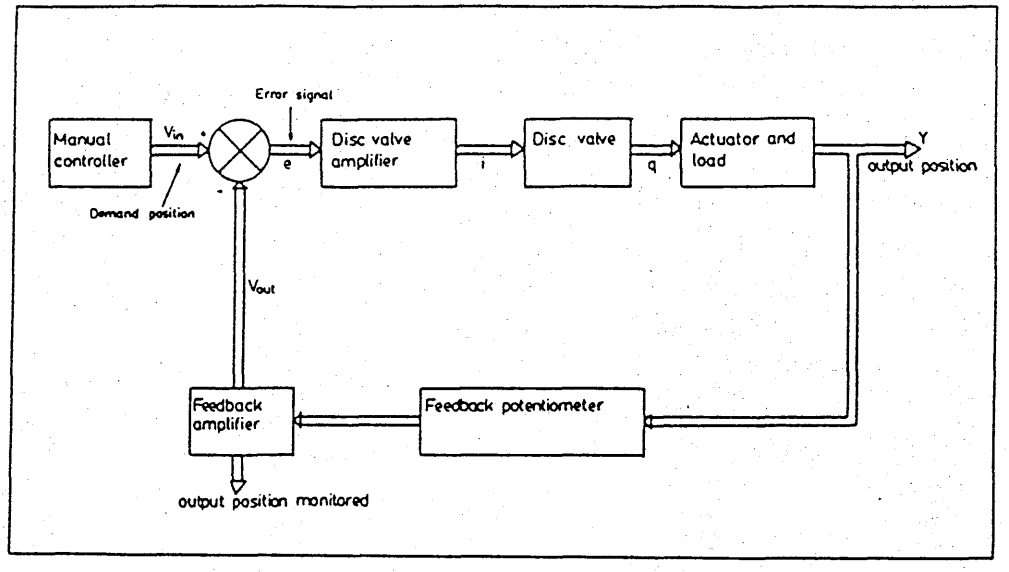

Fig. 7.13 Experimental set-up of a closed-loop position control system.

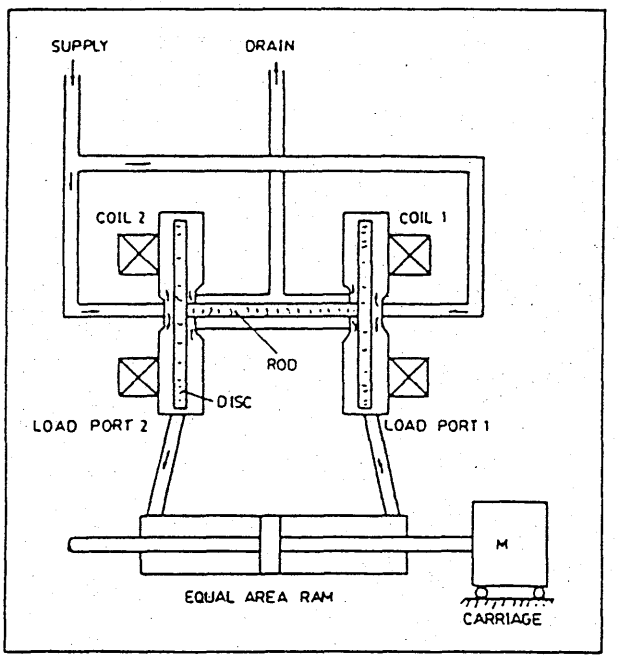

Fig. 7.14 Hydraulic pipe connections of a 4-way prototype double-disc valve and equal area ram combination.

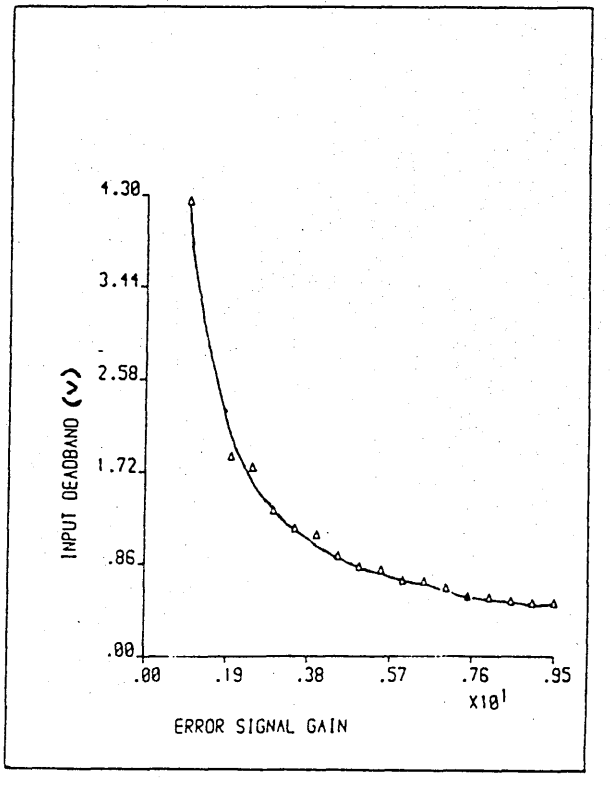

Fig. 7.15 Effect of error signal gain on input dead-band.

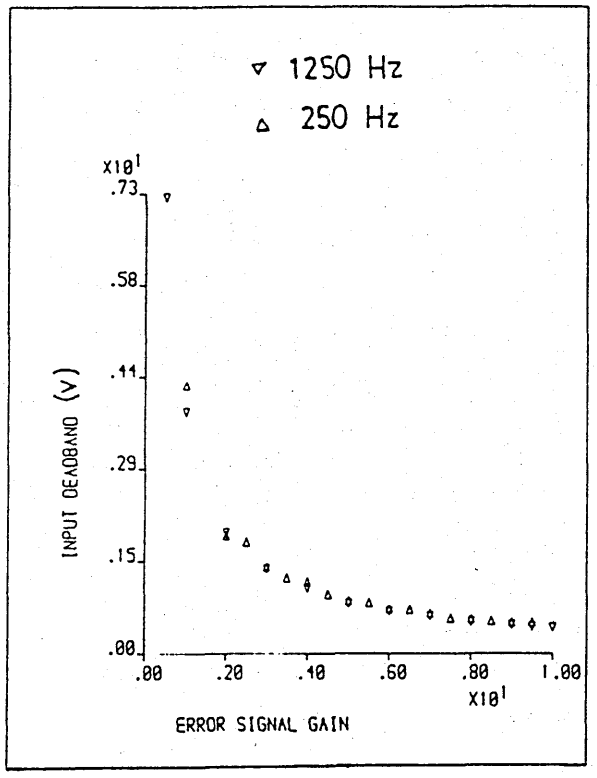

Fig. 7.16 Effect of carrier frequency on input dead-band.

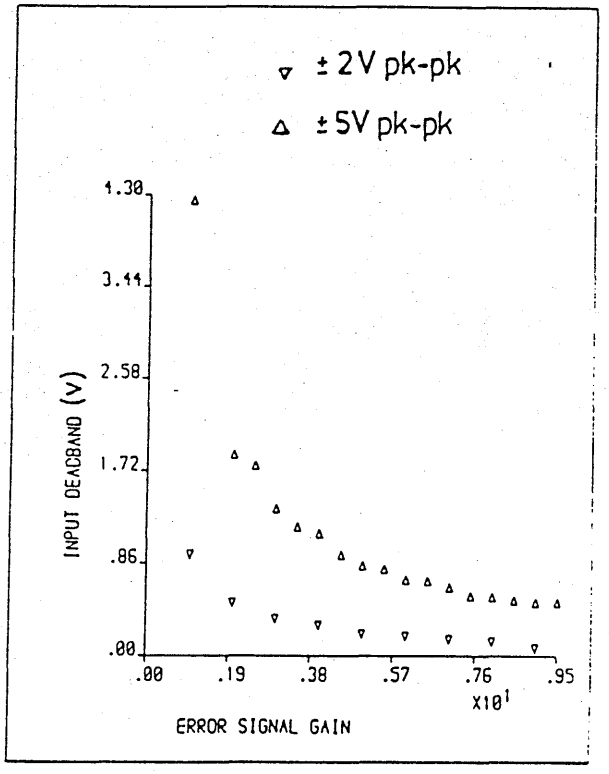

Fig. 7.17 Effect of sawtooth amplitude on input dead-band.

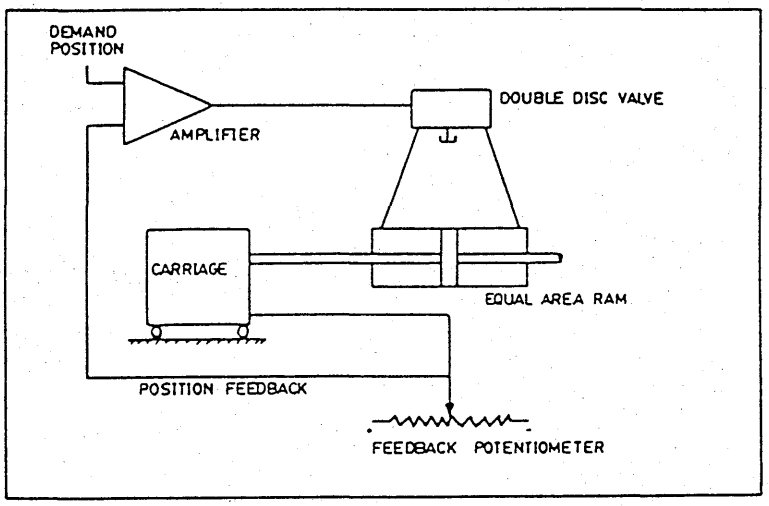

Fig. 7.18 Schematic layout of static characteristics measurement rig.

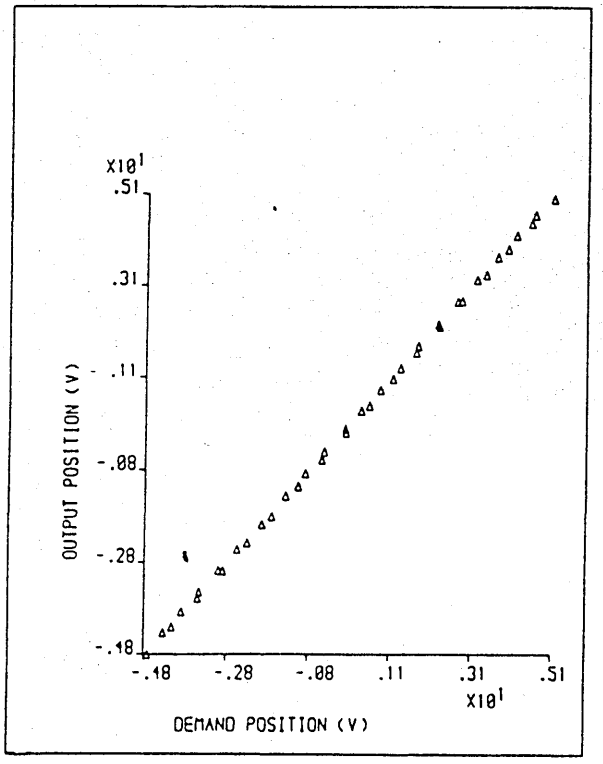

Fig. 7.19 Static characteristics of prototype valve-cylinder closed-loop position control.

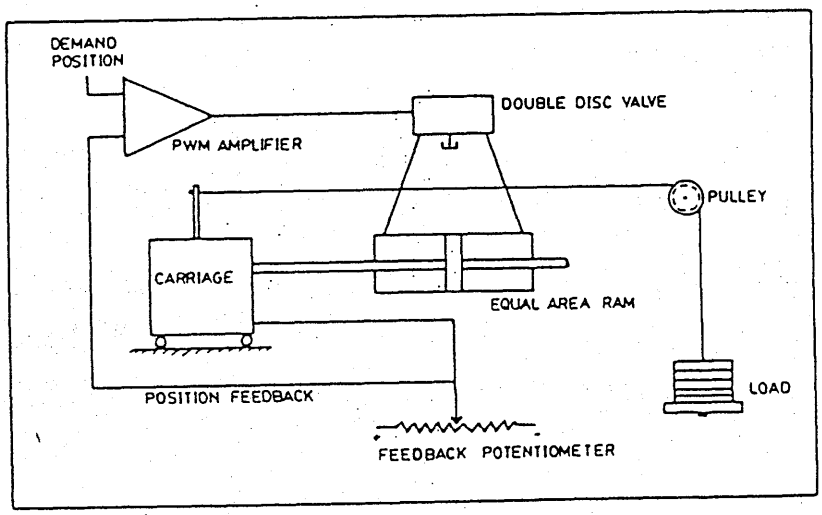

Fig. 7.20 Schematic layout of static stiffness measurement rig.

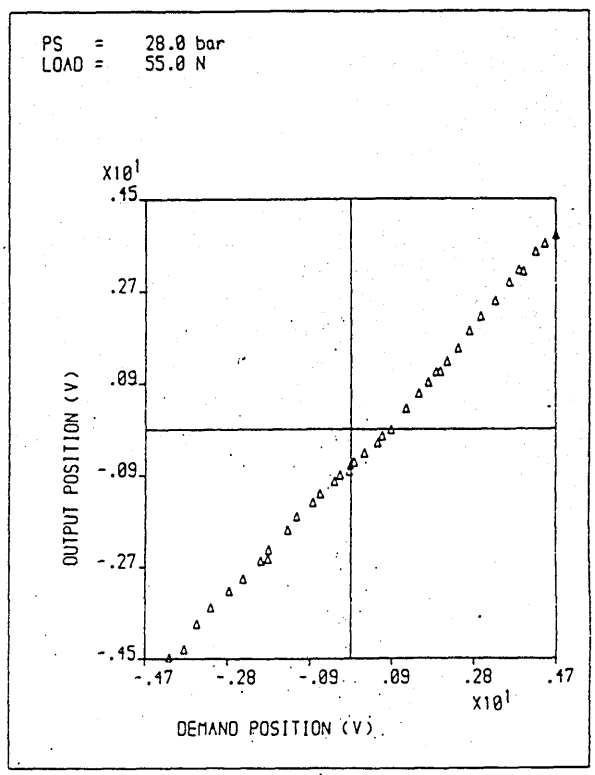

Fig. 7.21 Static stiffness of prototype valve-cylinder closed-loop position control.

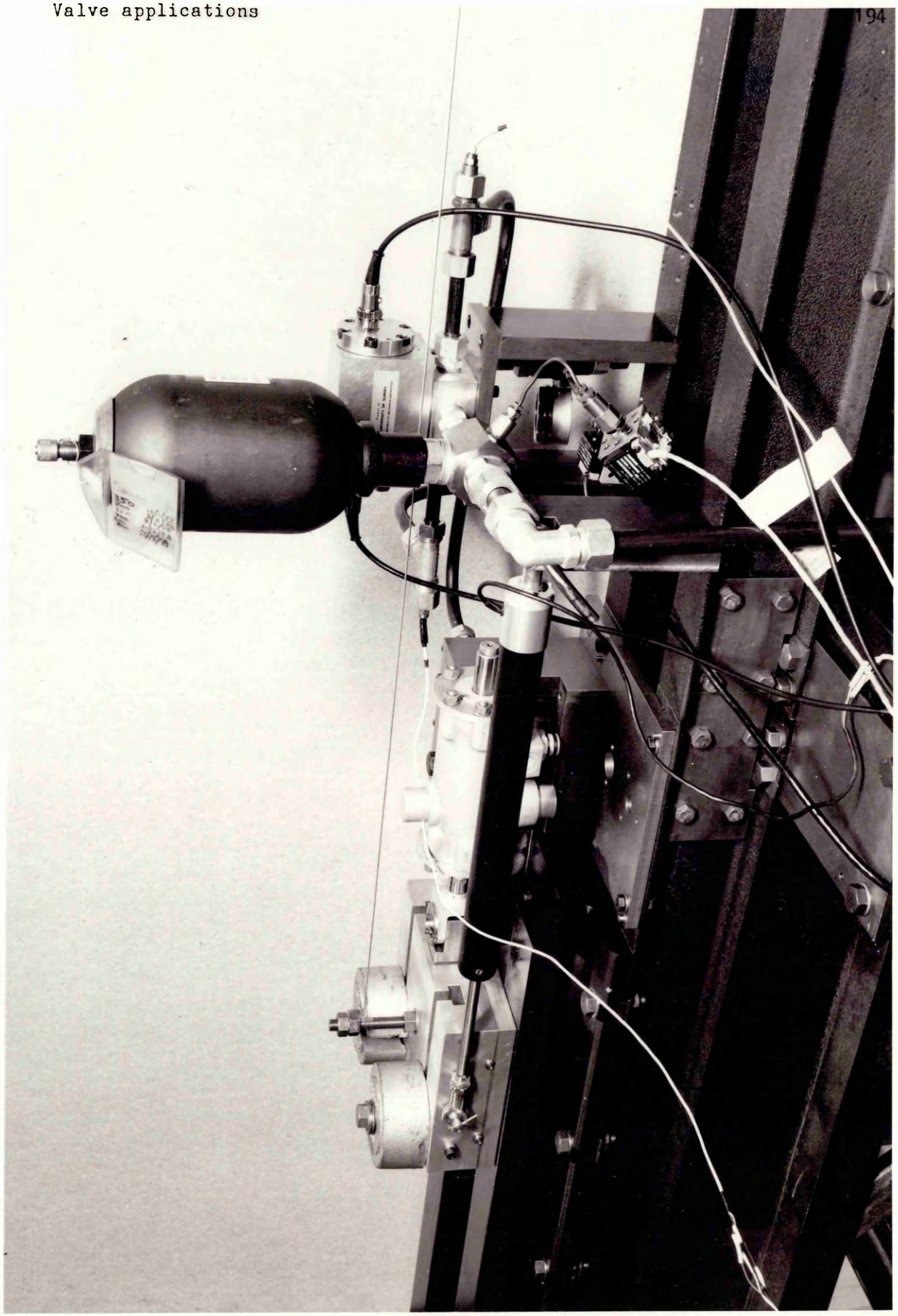

Fig. 7.22 Pre-production valve-equal area cylinder rig.

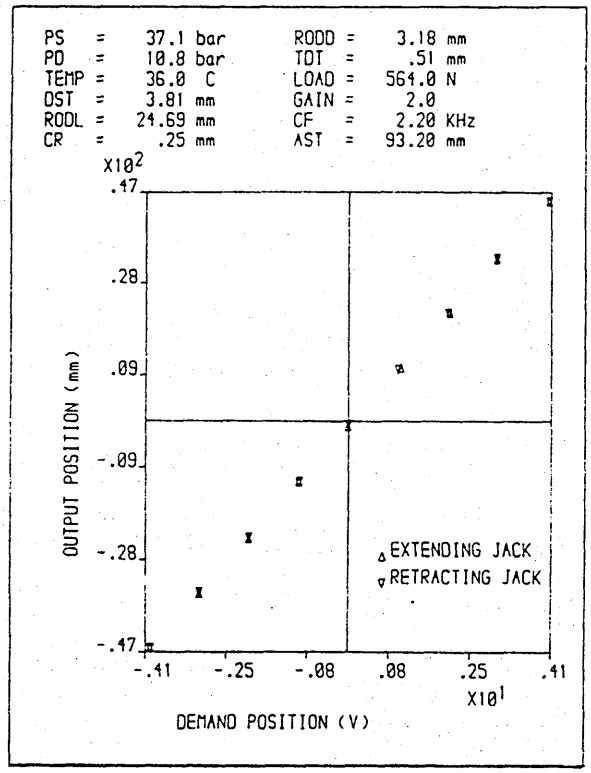

Fig. 7.23 Pre-production valve-cylinder closed-loop position control linearity.

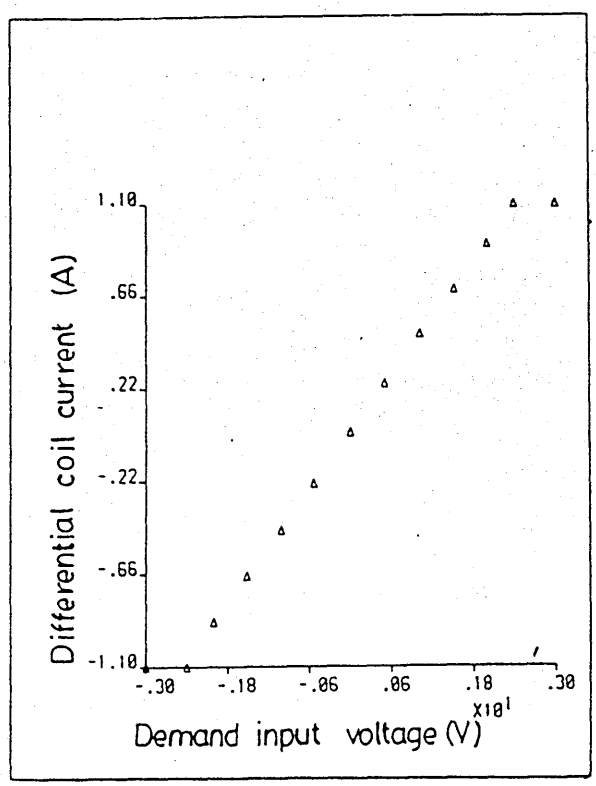

Fig. 7.24 Typical relationship between the demand input voltage and the differential current across the electro-magnetic coils of a pre-production valve.

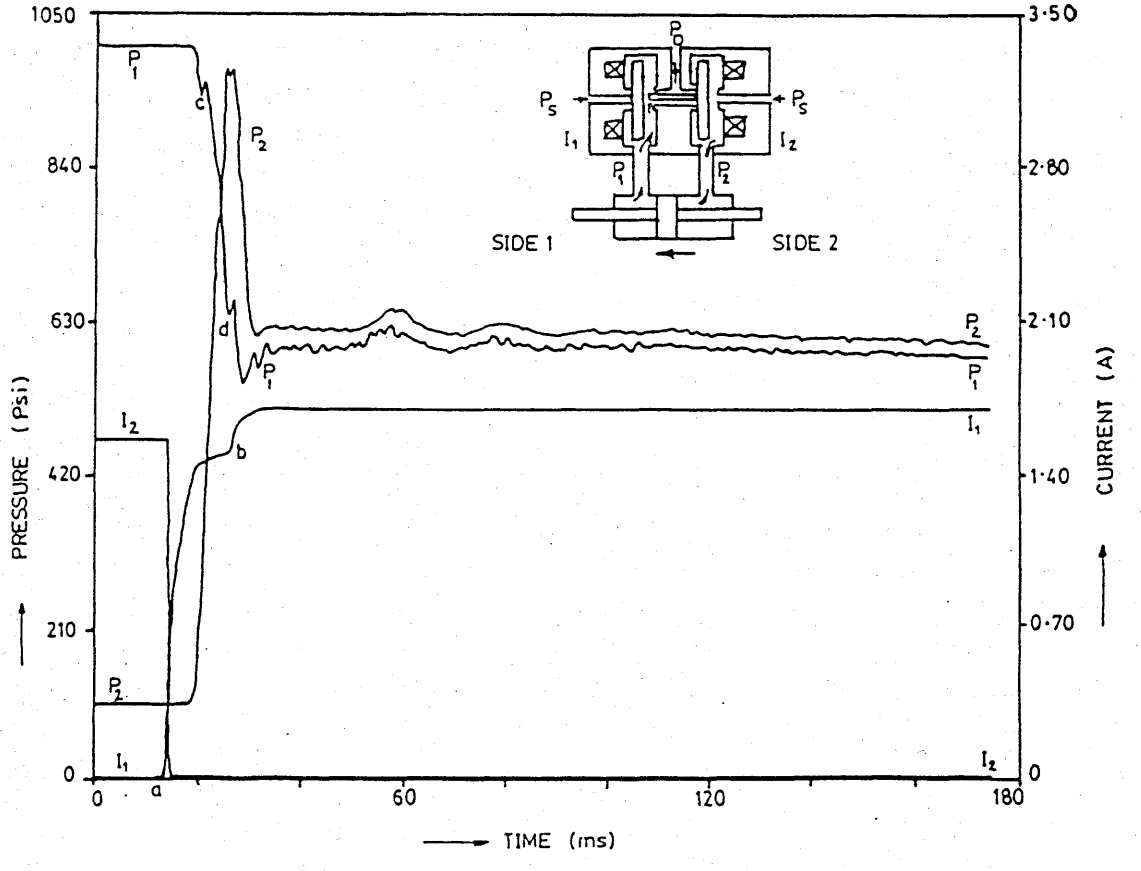

Fig. 7.25 Typical switching characteristics of pre-production valve-cylinder open-loop position control.

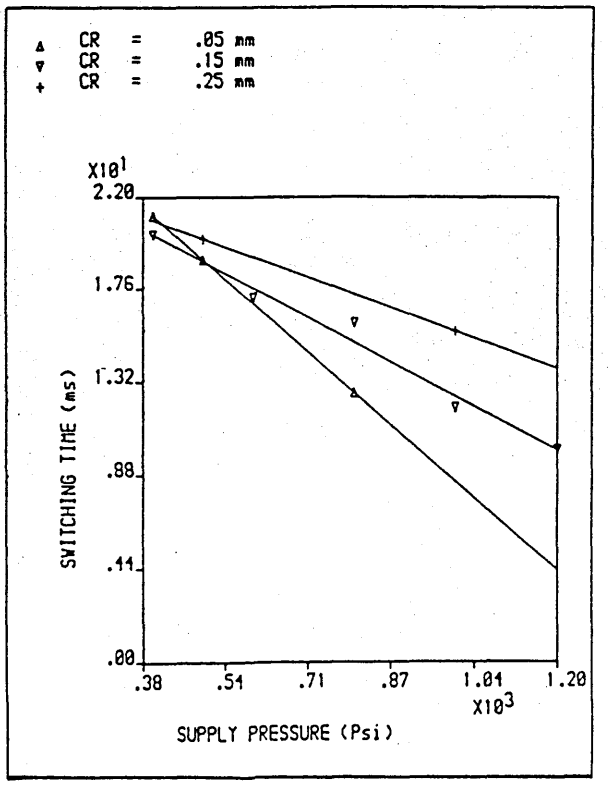

Fig. 7.26 Effect of rod-clearance on valve switching time.

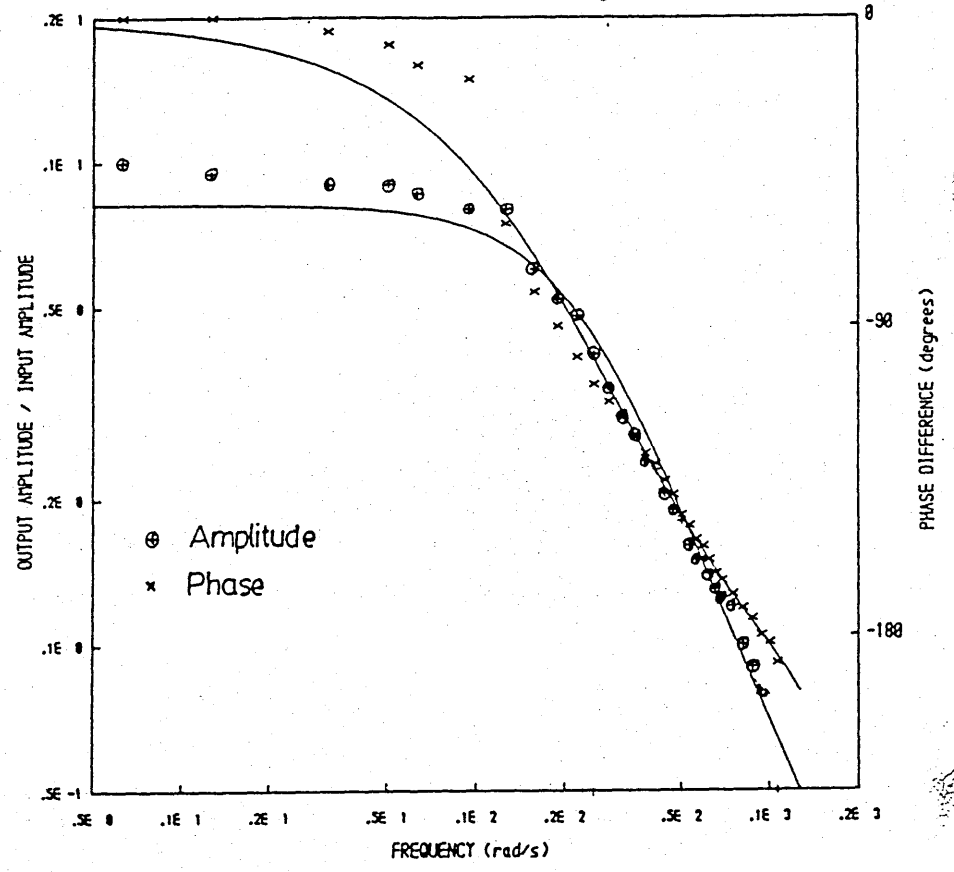

Fig. 7.27 Typical frequency response of pre-production valve-cylinder closed-loop position control at 70 bar system pressure.

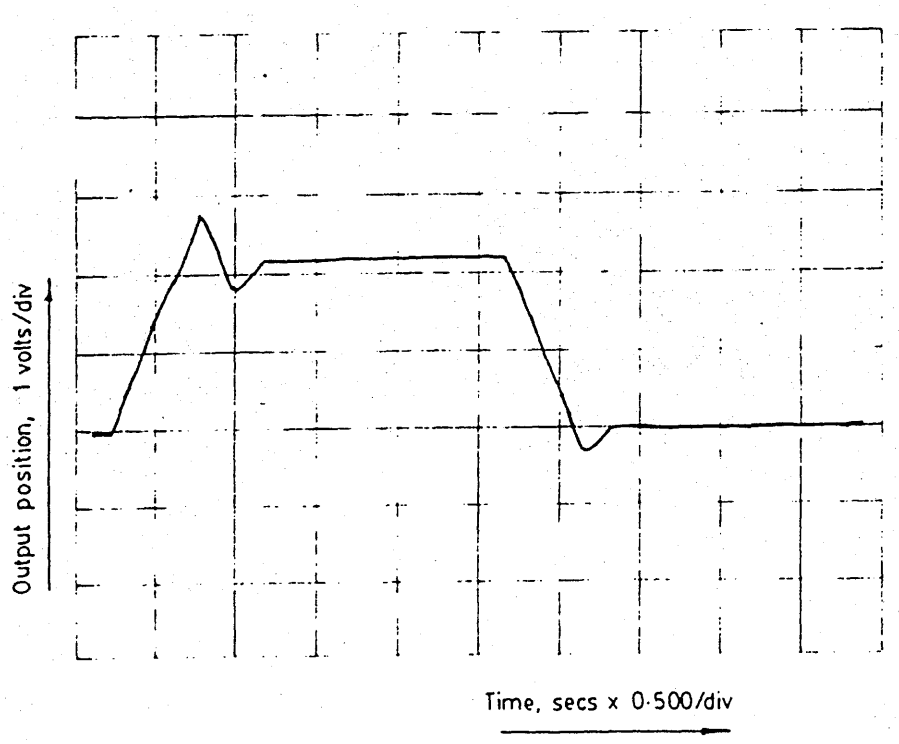

Fig. 7.28 Transient response of pre-production valve-cylinder closed-loop position control.

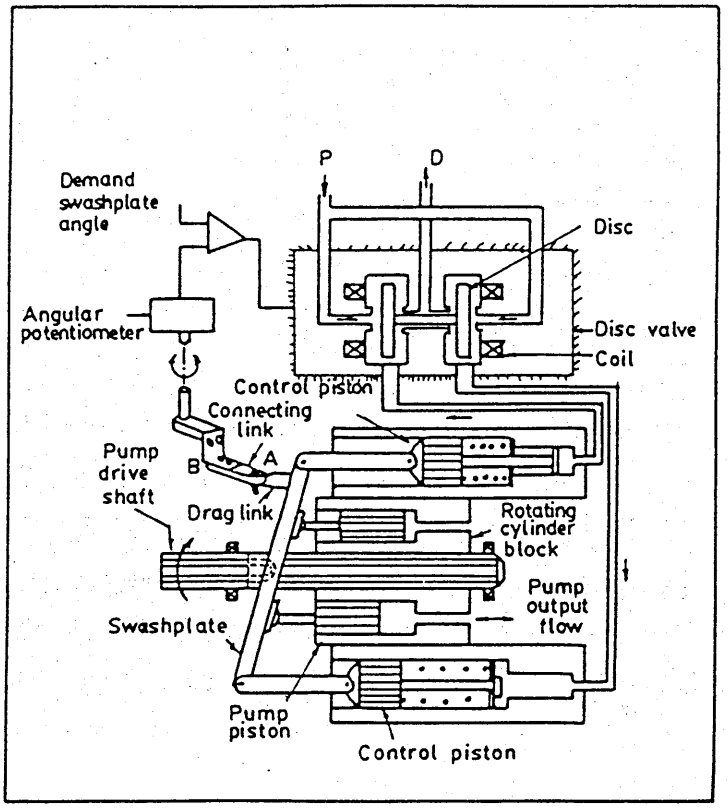

Fig. 7.29 Schematic of an electro-hydraulic double-disc valve operated stroker.

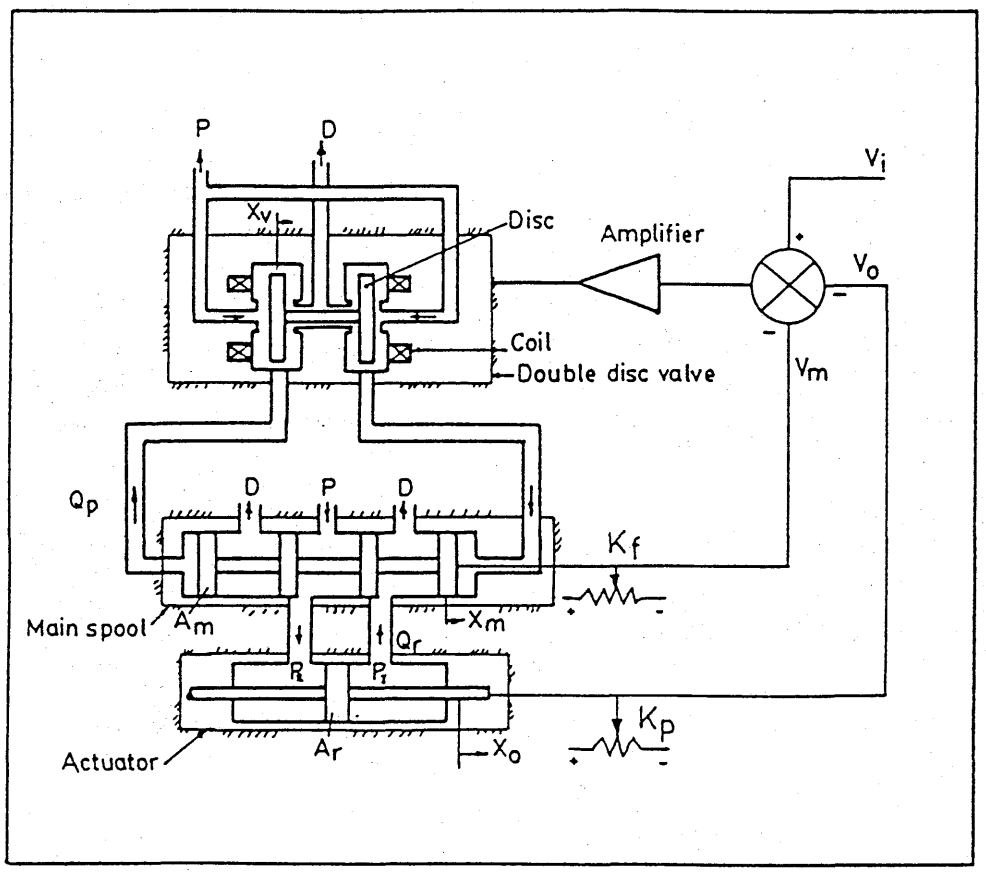

Fig. 7.30 Two-stage double-disc valve and actuator with feedback.

CHAPTER 8

CONCLUSIONS AND RECOMMENDATIONS

8 Conclusions and Recommendations

8.1 Conclusions

The increasing demand for cheap, simply constructed and reliable electro-hydraulic valves in the hydraulic industry has led to this work. Available in the market at present are servo-valves and both switching and proportional solenoid operated directional valves. Servo-valves are highly developed and sophisticated but they are very expensive because of the precision machining of components and are highly sensitive to contamination as a result of close tolerances. The directional valves do not meet the dynamic specifications of industry because of high inertia, hysteresis, stiction, and the relative high power required to operate these valves. The present work is aimed at eliminating many of these disadvantages and the concept of a floating disc valve with no sliding surfaces has evolved. The concept of floating disc devices were originally used in pneumatic valves in a different context and its use in hydraulic valves is a novel idea. A magnetic circuit with a better flux density than a conventional solenoid operated valve is seen as an advantage if correctly designed into a fluid valve.

One of the main objectives of the present research is to develop two versions of a novel disc type electro-hydraulic valve to the stage where they can be used to control hydraulic cylinders. Such valve-cylinder combinations can be used for low-cost manipulators in the robotics and programmable automation fields. The valve can also be geared towards mobile plant and remote control applications. As a result of its simplicity in construction, the disc type valve is aimed to fill the gap between the highly sophisticated servo-valve and the normal digital on/off or directional valve.

There are two versions of the valve that have been investigated in this thesis based on single- and double-disc configurations. The single-disc valve has no inherent facility for closing off supply flow in the switched state with a corresponding loss of power. To limit the quiescent power loss it has small supply port restrictors thereby giving potential problem with contamination. However, the two disc arrangement does not have these limitations and the present research has been concentrated on this arrangement. Cavitation was experienced with initial tests carried out with the test valve model but was found to be minimised by either increasing the back pressure of the system or decreasing the supply pressure. Decreasing the supply nozzle land diameter to supply nozzle diameter ratio to a value less than 1.2 also reduces the incipient of cavitation.

A flow-force rig has been constructed to determine the complex fluid forces acting on a single disc. The rig has the facility for allowing radial flow across the disc faces in both directions to simulate flow into and out of the load port into the drain connections. Theoretical predictions agree with fluid force data for a single disc thus allowing the theoretical model to be used with some confidence for determining suitable values for the main geometric variables of the double-disc valve. Empirical discharge coefficients were obtained from the tests carried out with a single disc in a floating disc chamber and were found to vary with the system pressure, Reynolds number and disc displacement. The empirical discharge coefficients were used in the theoretical steady-state fluid characteristics of the valve.

A computer-aided steady-state theoretical design package has been developed using several subroutines to display the data graphically and also make the package interactive with a graphic terminal. The package also allows any of the main parameters governing the valve performance to be varied

independently.

The theoretical steady-state fluid model for the valve has shown that the ratio of the drain nozzle area to that of the supply nozzle influences the fluid forces acting on a single-disc in its chamber. For best stable characteristics of the valve near null position, the model suggests equal areas for the drain and supply nozzles. A disc-to-supply nozzle diameter ratio greater than 10 should be used for proportional valve operation, and a diameter ratio less than 10 for a switching action as the net fluid force gradient increases with diameter ratio. The best compromise between the null gradient and force level is achieved for total disc travel equal to 20 per cent of supply nozzle diameter.

For both switching and proportional operations of 31 mm dia. valve, the best compromise value of supply holding gap is 0.13 mm. With a suitable choice of supply holding gap the fluid forces can almost be reduced to zero. The model requires the drain holding gap to be greater than the sum of the total disc travel and the supply nozzle holding gap. The result suggests that for proportional valve operation, the drain nozzle holding gap must be at least equal to 0.51 mm and less than 0.25 mm for switching operation to achieve best results.

In a double-disc valve with zero rod-clearance, the net fluid and magnetic forces are negative for zero disc displacement and the disc will not lift from its supply nozzle seat. For proportional operation of the valve, the discs and rod assembly are not to be operated within the small region where the net fluid and magnetic forces is negative. For this reason, a rod length is used with a clearance which is equal to twice the distance between the supply nozzle tip and the position where the net fluid and magnetic forces cease to be negative. For the particular valve under

discussion, the best rod clearance is about 25 per cent of the total disc travel.

When the valve is operated in proportional mode, the electro-magnetic coils receive a differential current from the PWM amplifier. The discs and rod assembly then adopt a position where the net fluid forces balance that of the magnetic forces acting on the discs. For a given differential current, the magnetic forces acting on the discs remain constant with oil temperature while the fluid forces vary. This must mean that the valve is always viscosity-temperature dependent which is a major disadvantage. The slope of differential coil current versus discs and rod assembly position reduces with increase in oil temperature. This implies that the valve must always be designed for the worst case (i.e maximum operating temperature).

For best stable characteristics of the valve near null position, the model suggests that the valve must not be scaled-up more than 3.0 and that linear scaling or geometrical scaling should be done with care as the valve general performance depends on many parameters which may be inter-related. The model has also shown that the valve flowrate may be increased by increasing any one of the following valve parameters: total disc travel, supply nozzle diameter, supply pressure, and valve scaling.

Tests, using the same flow-force rig, has been made regarding the electro-magnetic force induced in the disc for various current levels in the coil and also for the force variation with distance of the disc from the coil face. Theoretical predictions agree well with the electro-magnetic force data. Two types of discs were used in the experiments. They were discs with and without stops on them. The experimental results show that disc with stops exhibit more non-linearity than the corresponding disc without stops. Discs without stops are cheaper and easier to fabricate and are preferred for the better electro-magnetic characteristics. The effect of varying the

floating disc (armature) thickness on the electro-magnetic force-stroke characteristics was investigated experimentally, and an empirical formulae were developed which would be useful for rapid valve design calculations. These empirical formulae agree very well with the experimental data and show that reasonable magnetic force could be obtained with a disc thickness as low as 2.5 mm. The low inertia of thin discs improves the dynamic performance of the valve.

A pre-production version of the double-disc valve incorporating ideas for manufacturing cost reduction has been designed in cartridge form to ISO and CETOP standards. From an economic point of view, ease of manufacture is an important factor in the design, because cost inevitably plays an important role in the acceptance of a new valve for general use. Most of the parts are made with wide tolerances which enhances the inter-changeability of the cartridge components. A major advantage is the potential high reliability of operation due to the small number of moving parts without sliding surfaces. The valve is suitable for manufacture by CNC machining as it involves only grinding and turning operations.

The pre-production valve may be scaled up to provide larger flows than the present flow capacity of 18 litre/min as a single stage valve. The disadvantage is the high quiescent hydraulic power losses when operated with pulse-width-modulation to provide proportional control. In switching applications of the valve, there is no quiescent flow losses. For pilot operation, the valve may be scaled down to limit the flow capacity and quiescent flow losses and this may be a more attractive possibility. In the valve design, standard 'O' seals are necessary to prevent both internal and external oil leakages at moderate cost. In view of this, the limit of the valve size as a pilot device is dictated by the availability of the 'O' seals sizes. Another limiting factor is the size of the electro-magnetic

coil. The coil consists of the magnetic iron core, brass or plastic bobbin and the central hole to take up the supply nozzle tube. For a given working pressure, there is a corresponding cross-sectional area of the magnetic iron core and the ampere-turns of the electro-magnetic coil that will give a satisfactory valve performance. With the present state of coil technology, the coil size could be reduced from the present 27 mm outside diameter to 13.5 mm without too much difficulty.

A four-level switching amplifier consisting of operational amplifiers, timers and power transistor output has been constructed to control the valve in the switching mode of operation. The amplifier incorporates the established technique of overdriving the coil with a large amplitude pulse at the commencement of switching. The holding voltage provides enough electro-magnetic force to hold the disc on the supply nozzle seat after switching is completed. Using this amplifier without overdriving the electromagnetic coils, a switching time of 10 ms has been achieved for a pressure drop of 70 bar across the pre-production valve. Variation of the supply pressure between 40 and 100 bar with suitable adjusted to the rod-clearance causes variations in switching time between 5 and 20 ms. Switching times can be further reduced by using thinner discs and shorter disc travel.

Both analogue and digital pulse-width-modulation (PWM) amplifiers have been constructed for use with the valve in proportional control mode with no overdriving of the coil. Using the digital PWM, the valve can be controlled by a microprocessor for remote control applications. A computer program has been written in INTEL 8080 language on the University of Surrey Prime computer system to control the digital PWM amplifier and a CP/M based computer has been used to drive the digital PWM amplifier. Under PWM mode with a carrier frequency of 2.2 KHz, it has been shown that dimensions are

not critical and wear problem can be reduced dramatically as the discs are not switched fully from nozzle to nozzle. This consequently improves the contamination insensitivity of the valve.

Intensive tests have been conducted with the prototype double-disc valve controlling a long stroke unequal area cylinder similar to types used in robot arms. Both switching and proportional modes of operation have been demonstrated in open and closed loop position control modes. An attempt has been made to use the prototype valve with an equal area cylinder but the positioning is not very good as the valve requires a large differential current to operate the valve discs. This could be due to the unsymmetrical nature of the disc chambers.

The pre-production valve has been tested with a short-stroke equal area cylinder in closed-loop position control under conditions of constant low load using pulse-width-modulation. Experimental results show that good linearity and low drift may be achieved over a range of operating temperatures, pressures and load conditions using moderate loop gains. From the intensive tests with the system, it has been established that the rod dimensions play an important role in the valve characteristics, for a given disc chamber geometry. Two different thickness of discs have been used in the tests and it has been found that the thinner one gave a better control resolution. This is because the thinner discs are operated farther away from their respective electro-magnetic coil surfaces in a region where both the magnetic and fluid forces are fairly linear. From this data, applications such as a remotely operated directional valve, a variable delivery pump control and a cheap robot position control can be designed. The valve also has potential applications in (1) mobile earth moving equipment, (2) machine tool industry, (3) aircraft industry, (4) power steering in automotive industry, (5) pressure control devices, (6) flow

control devices, (7) Vibrators and (8) the programmable automation field.

It has been established that there are significantly fewer critical dimensions within the valve than for a comparable electro-hydraulic servo-valve so that manufacturing costs should be low. Also design criteria has been formulated to provide a valve with acceptable performance for either switching or proportional mode operation using the same overall body configuration. This can be achieved by a suitable selection of disc thickness and centre rod dimensions at minimal cost.

The double-disc valve is deficient in the following ways: (a) too much leakage when used in the proportional mode, (b) low hydraulic stiffness, (c) for proportional control it requires careful matching of electro-magnetic and fluid forces to get disc balancing at different displacements, and (d) fluid forces seem to be very dependent on oil temperature.

Some possible advantages of the double-disc valve over the conventional electro-hydraulic valve are: (a) fast switching action, (b) relatively contamination insensitive, (c) potential used with non-lubricating liquids, (d) complex valve actions can be obtained with remote electrical operation, (e) cheapness, and (f) may be easily configured to operate as a switching or proportional valve.

8.2 Recommendations for future work

1. Future work should explore the possibility of a low-cost integrated valve-cylinder-position feedback assembly for robotic systems given that there is a need for very inexpensive units.

2. The main disadvantage of the present valve is its high leakage flow under pulse-width-modulation proportional mode. This can be improved by redesigning the valve-centre-section. At present, the two drain orifices

are active any time the valve is operated proportionally with the leakage flow being highest in the neutral position. This can be modified by changing the push-rod design to a spool-type having a land at either end of the spool which ensure that only one drain orifice is active at any time. At the neutral position there will be no leakage flow as the two drain orifices are shut by the spool lands. The flow characteristics of the proposed modified valve will compare more favourably with the servo-valve. Also the valve speed of response will be increased and the rod clearance of the present design will no longer be a critical dimension.

3. The present electro-magnetic coil design could be modified to be used in directly operating commercial spool type valves. The relative high force obtainable from this type of coil makes it more attractive than the present proportional solenoid in the market provided a larger diameter spool with shorter stroke is used to achieve the same flow capacity.

4. The double-disc valve may be used as a 3-way valve with only one load port active. That is, with supply S, drain D, and one load port L1. It also has two electrical coils which can be designated C1 and C2. However, the two discs do not necessarily have to have the same diameter and flow characteristics. This valve could be used on a simple on-off switch in a hydraulic line or could provide proportional flow control. However, in general, to control a cylinder two load ports are required so that two 3-way valves are required for this purpose. By a suitable choice of coil activation a power cylinder could be controlled by two 3-way disc valves to give:- (a) rapid or proportional control in either direction; (b) open centre in mid-position; (c) pressurised load ports in mid-position; (d) vented load ports in mid-position. The valve coils could be remotely electrically selected and thus open the way for microprocessor control applications.

BIBLIOGRAPHY

Bibliography

[1] Maskrey,R.H. and Thayer,W.J. : A brief history of electro-hydraulic servomechanism. Trans. ASME, Vol. 100, pp.110-116, June 1978.

[2] Bolting,L.R., Eynon,G.T., and Foster,K. : The response of a high-pressure pneumatic servomechanism to step and sine wave inputs, Proc. Inst. Mech. Engrs., London, 184(Pt.1),54, 1969-70.

[3] Nightingale,J.M. : Hydraulic servo. Fundamentals Machine Design, 1956.

[4] McCloy,D and Martin,H.R. : Control of Fluid power - Analysis and Design, 2nd Edition, Ellis Horwood ltd, 1980.

[5] Boulden,L.L. : Valves that take orders from computer. Machine design, pp.70-74, June 27, 1974.

[6] Günter,D.: Digital electrohydraulic control mechanisms. Feinmechanische Werke Mainz Gm bH Mainz, W-Germany. Proc. of the National Fluid Power supply system and control conference. 1973

[7] Gizeski,T.: Digital Actuators, Instrument & Control systems, Vol.32, Nov. 1959, pp.1686-1687.

[8] Gizeski,T.: Digital positioning, Instrument & Control systems, Vol.34, March 1961, pp872.

[9] EI-Ibiary,Y.M.; Ukrainetz,P.R.; Nikiforuk,P.N.: Design and assessment of a new solenoid-operated ball valve for digital applications. Proc. 34th Nat. Conf. on Fluid Power, Chicago, Vol.32, 1978, pp.31-34.

[10] Seidel,D.S.: Research and demonstration of a digital flight control system electro-hydraulic servo control valve actuator experimental model. Hydraulic research and manufacturing company. Technical documentry report RTD-TRD-63-4240, WPAFB, Ohio,1964.

[11] Anderson,R.L.: Evaluation of a high response electrohydraulic digital control valve. Final Progress Report. Feb.1972-Feb.1973, (NASA-CR-124176) Bentea Corp. Invine, Califonia.

[12] Jenney,G.D.: An investigation of a digital electro-hydraulic servovalve. Dynamic controls Inc., Dayton, Ohio, Final Report 4/79-4/80.

[13] Mansfeld,G.: A gaurd short course on ' Advance Flight Control Actuation Systems', DFVLR, Braunschweig, 22.9.1981.

[14] Tsai,S.C.; Ukrainetz,P.R.: Response characteristic of a Pulse-Width-Modulated electrohydraulic servo. Trans. ASME, Vol.92, pp.204-214, June 1970.

[15] Delmege,A.: Acceleration switching Servovalves. Sixth Servo Conf., 27-31. Jan. 1964, Vickers Inc. Detroit Michigan.

[16] Delmege,A.: Acceleration switching transfer valve. Firmenschrift Vickers Inc. Detroit Michigan, 1964.

[17] Tourtellotte,F.: The role of the Pulse Length Modulation in an accelerated switching valve system. Firmenschrift Vickers Inc., Detroit Michigan, 1971, Q:N74-16138.

[18] Murtaugh,S.A.: an introduction to the time-modulated accelerated switching electro-hydraulic servomechanism. ASME Journal of the Basic Eng. Vol.81, pp.263-273, June 1959.

[19] Levine, G.A.: Discussion of reference [18].

[20] Gordon.R.A.: The application of Pulse-Width-Modulation to a relatively high flow, electrohydraulic flow control valve. Ph.D. Thesis at the Univ. of Saskat chewan, Saskatoon, Oct. 1963.

[21] Bahr, J.: 'The Foil element, a new fluid logic element' I.B.M. Zurich Research Lab., Report No. RZ-181, 1965.

[22] Post, K.H.: A new hydraulic ball valve element, 2nd Fluid Power symposia, 4-7 Jan. 1971, Guildford. GB. pp.E1-1/E1-12.

[23] Parker, G.A.;Yüksel, I.: A novel electro-hydraulic switching valve. 6th Fluid Power Symposium 8.-10. April 1981, Paper G1, pp.305-320.

[24] Post, K.H.: Electro-hydraulic valves with fluidic ball elements, Proc. of the National fluid power supply system and control conference (1973).

[25] Mansfeld, G.: Fast switching ball valves as digital control elements for an electro-hydraulic servo actuator. 6th International Fluid Power Symposium Cambridge, England, 8-10 April 1981, paper G3, pp.335-348.

[26] Schrenk, E.: Disc valves, flow patterns, resistance and loading., Forschungsabeiten auf dem Ingen., 272, (1925) (In German) Also: BHRA T.547, 17pp incl. 27 figs. (Jan.,1957).

[27] Goldstein, S.R. and Richardson, H.H.: A differential pulse-length modulated pneumatic servo utilizer floating - flapper disc switching valves. Transactions of the ASME series D, 90/1968/Nr.2, pp.143-151.

[28] Takenaka, T.; Yamane, R.; Iwamizu, T.: Thrust of the disc valves. Bull. JSME, 7, 27, pp.558-66 (1964).

[29] Oki, I.: Experimental research on disc valves. Bull. JSME, 4,13, pp.87-9 (1961).

[30] Horsnell, R.: Flow through a plate valve. University of Nottingham, B.Sc. Thesis (1960).

[31] Streeter, V.L.: Fluid Mechanics, McGraw-Hill (1966).

[32] Takenaka,T; Urata,E: Static and dynamic characteristics of oil-hydraulic control valves. Proc. of the 1968 Fluid Power International Conf. 10.-12. Sept. 1968, pp.67-74.

[33] Lichtarowicz, A.; Duggins,R.K.;Markland,E.: Discharge Coefficients for incompressible non-cavitating flow through long orifices, Journal Mech. Eng. Sci. London, 1965, Vol.7, No.2.

[34] Lichtarowicz, A: Flow and force characteristics of flapper valves. Proc. 3rd International Fluid Power Symposium, Paper B1 pp.B1-1/B1-24, 9.-11. May, 1973.

[35] Yüksel, I.: An investigation of an electro-hydraulic free floating switching valves. Ph.D. thesis, University of Surrey, 1981.

[36] Mansfeld,G.; Tersteegen,J.: 'Electro-hydraulic positioning drive with fast-acting solenoid valves and pulse-modulated control'. (Elektrohydraulisher positionierantrieb mit schnellschaltenden Magnetventilen und pulsmodulierter Ansteurung). Zeitschrift olhydraulik und pneumatik 22, (1978), No.11, pp.647-652. (In German).

[37] Sawamura,T.; Hanafusa,H.; Inui,T.: Fundamental analysis of an electrohydraulic servomechanisms operated by PWM mode. JSME Bulletin 1960, pp.1-12.

[38] Sawamura,T.; Hanafusa.H.; Inui,T.: Frequency characteristics of PWM mode electrohydraulic servos. JSME Bulletin 1960, pp.123-135.

[39] Boddy,D.E.: Analysis and design of Pulse-Width-Modulation hydraulic control systems. Ph.D. Thesis, Purdue University, 1966.

[40] Decker,R.L.: Pulse width modulation of solenoid valvves for low cost analog control. Basic Fluid Power Research Centre, Stillwater, USA, Oklahoma state Univ. Annual Report Nr.10, Oct. 1976, pp.48.1-48.3.

[41] Ikebe,Y.; Nakada,T.: On a Piezoelectric Flapper type servo-valve operated by a Pulse-width-modulated signal. Trans. of the ASME, Journal of Dynamic Systems, Measurement & Control magazine, 1974, pp.88-94.

[42] Taft,C.K.; Harned,T.J.: Electro-fluid Pulse-width Modulated valve. ASME paper Nr.78-WA/DSC-8, Dec. 1978,12pp.

[43] Davidson,A.R.: Puse rate modulated linearizes hydraulic actuator controls. Control Eng., Dec. 1974, pp.48-51.

[44] Armstrong,P.J.; McCloy,D.: Sub-optimal solution for time optimal control of a hydraulic servomechanism. JACC, Paper 6B2, Atlanta (1970).

[45] Armstrong,P.J; McCloy,D.: Optimisation of hydraulic servo using On/Off controllers. 2nd Fluid Power Symposium, 4.-7. Jan. 1971, Guildford, GB. pp.B3-49/B3-67.

[46] Wang,P.K.C.: Analytical design of electro-hydraulic servo mechanisms with near time-optimal responses. IEEE Trans. Aut. Control, Vol.8, No.1, pp.15-26, 1963.

[47] Devies,R.M.: Analytical design of time optimal transient response of hydraulic servomechanisms. Journal Mech. Eng. Sci., Vol.7, No.1, 1965.

[48] Martin,H.A.; McCloy,D.: Some aspects of the response of bistable hydraulic servos. 2nd Fluid Power Syposium, 4.-7. Jan. 1971, Guildford, GB. pp.B3-49/B3-67.

[49] Baeck,H.A.: Hydraulic on-off servo: Simple,rugged positioner. Control Eng. Dec. 1967, pp.79-82.

[50] - Parallel screw threads of Whitworth form. British standards Institution, BS84, 1956.

[51] - Static strength of screwed fasteners. Engineering Sciences Data Item No. 67019, January 1967.

[52] - Tension in steel Bolts resulting from tightening torque (Tentative) Engineering Sciences Data Item No. 72022, 1972.

[53] Hagiwara,T.: Studies of the characteristics of radial-flow nozzles. Bull. JSME, Vol.5, 20, pp.656-683, 1962.

[54] Moller,P.S.: Radial flow without swirl between parallel discs. Aerospace Quarterly, Vol.14, pp.163-186, 1963.

[55] Blackburn,J.F.;Rleethof,G. and Shearer,J.L.: Fluid Power Control. M.I.T. Press, 1960.

[56] Barwell,F.T.: Bearing systems: Principles and Practice. Oxford University Press, 1979.

[57] Livesey,J.L.: Inertia effects in viscous flows. International Journal of Mechanical Science, Vol.1, p.84, 1960.

[58] Savage,S.B.: Laminar radial flow between parallel plates. ASME Journal of Applied Mechanics, Vol.31, No.2, pp.594-596, 1964.

[59] Jackson,J.D.; Symmons,G.R.: The pressure distribution in a hydrostatic thrust bearing. International Journal of Mechanical Science, Vol.7, pp.239-242, April, 1965.

[60] McCandlish,D.: Design methods for hydrostatic thrust bearing. 2nd Fluid Power Symposium, 4th-7th Jan. 1971, Guildford, Paper G1.

[61] Roters, H.C. : Electro-magnetic devices, John Wiley,1941.

[62] Hazeltine,L.A. : Electrical Engineering, Macmillan Co. New York, 1924.

[63] E02 : Curve and surface fitting, Subroutine E02AEF NAGLIB: 1350/0: MK 5, May 1977.

[64] Rayner,A.R. : Load cell weighing. B.Sc., dissertation, Dept. of Mech. Eng., Univ. of Surrey, England, July 1970.

[65] Feng, T.Y. : Static and dynamic control characteristics of a flapper nozzle valves. Trans. ASME, 1959, Vol. 81, series D, pp. 275-84.

[66] Merritt, H.E. : Hydraulic control systems. John Wiley, 1967.

[67] Moore,E.L.: The RSP programme for an Interdata 7/16 Minicomputer, Dept. of Mech. Eng., University of Surrey, June 1976.

[68] Usman, A.: Transfer function of an electro-hydraulic servo system, B.Sc. Final year project, Dept. of Mech. Eng., University of Surrey, May 1980.

[69] Zaman, M., and Griffin, A.W.J.: Transfer function from sampled impulse responses, Measurement and control, Vol.3,June 1970, T101-T108.

[70] Levy, E.C.: Complex curve fitting, IRE Transaction on Automatic Control, May 1959, AC-4, 37,44.

[71] Sanathanan, C.K., and Koerner,J.: Complex function systhesis as a ratio of two complex polynomials, IEEE Transactions on Automatic Control, January 1963, AC-8, 56-58.

[72] Martson, R.M.: Waveform generator projects for the home constructor, Newnes Technical Books, 1978.

[73] Vassilios, J.G.: Microprocessor controlled digital PWM, Computer Design Journal, January 1981.

[74] The TTL DATA BOOK for Design Engineers, 2nd ed., Texas instrument Inc.

[75] Quarndon Electronics Catalogue for 74 series TTL digital integrated circuits.

APPENDICES

APPENDIX A1

Design procedure for a flat-faced armature type of electro-magnetic coil

A1: Design equations for a flat-faced electro-magnetic coil

For illustrating the symbols used in this appendix and a practical mechanical form of construction, a typical flat-faced armature type electro-magnetic coil is shown in Fig. A1.1. The following equations are required to determine the size of the coil:

(a) Force equation

The force equation is given by

$$F_m = \frac{B_g^2 A_c}{\mu_g} \qquad (A1.1)$$

where B_g is the flux density in the working gap and A_c is the area of the working gap.

(b) Magnetic force equation

The exciting magnetomotive force NI, which provide flux required for the given force-stroke, is determined by the magnetic circuit equation for the electro-magnetic coil. This equation is given by

$$NI = \frac{2 B_g x_g}{\mu_g} + \Sigma H_i L_i \qquad (A1.2)$$

where the first term represents the magnetomotive force necessary to establish the flux at a density of B_g across a working gap of length X_g, and the second term represents the magnetomotive force necessary to establish the flux in the iron parts of the circuit.

(c) Coil resistance

The coil resistance R_c is given by

$$R_c = 4 \rho_c (r_{1b} + r_{2b}) N / d_c^2 \qquad (A1.3)$$

where $r_{1b} + r_{2b}$ is the mean diameter of a turn on the coil winding, d_c the bare wire diameter, and ρ_c the volume resistivity of the copper wire.

(d) **Voltage equation**

The assigned coil voltage, E is given by

$$E = IR_c \tag{A1.4}$$

(e) **Coil space factor**

The coil space factor f_s is given by

$$f_s = \pi d_c^2 N/(4h_{1b}(r_{2b}-r_{1b})) \tag{A1.5}$$

The space factor of bobbin-wound coils are governed by the following inequality:

$$0.4 < f_s < 0.6$$

(f) **Heating equation**

To keep the temperature rise within a given limit, the coil must have a sectional area and heat conducting surface. The energy dissipation as heat in the electro-magnetic coil is given by

$$\theta_f = \frac{\rho_c}{2kf_s(r_{2b}-r_{1b})}\left[\frac{NI}{h_{1b}}\right]^2 \tag{A1.6}$$

where θ_f is the final temperature rise of the coil, k the heat-dissipation coefficient, f_s the space factor, $r_{2b} - r_{1b}$ the gross coil wall thickness, and h_{1b} the gross coil depth.

For weight economy the following inequality holds:

$$3 < \frac{h_p}{r_{2p} - r_{1p}} < 4 \tag{A1.7}$$

For a safe design, the cross-sectional areas of the yoke, the armature, the inner pole core and the outer pore core must be equal to effect uniform flux throughout the magnetic path. That is

$$r_{3p}^2 - r_{2p}^2 = r_{1p}^2 - r_{op}^2 = (r_{2p} + r_{1p})t_a = (r_{2p} + r_{1p})t_p \tag{A1.8}$$

For a given flux density of the magnetic material and the required magnetic force, the cross-sectional area of each of the working faces or gaps may be estimated from equation (A1.1). Knowing the area, r_{1p} can be estimated as r_{op} is equal to the outside radius of the supply nozzle used in the disc

valve to allow oil flow through the valve. The following constants can be substituted in equation (A1.6):

ρ_c = 2.1971 X 10^{-8} ohm-metre at 90°C for copper wire

k = 11.78 watt/m^2 °C for a temperature rise of 70°C

f_s = 0.5, assumed

Dimensional constraints

The pre-production valve had a coil leakage problem as with the prototype valve. About drawing no. CDL3-1/1 in Chapter 2, it can be seen that the coil leakage can occur at five different positions. These positions are:

(1) Through the supply line and is checked with '0' seal no. 17001.

(2) Through the outside diameter of the supply nozzle tube.

(3) Through the interface between the coil spool and the magnetic inner pole core.

(4) Through the interface between the coil spool and the magnetic outer pole core.

(5) Through the outside of the magnetic outer pole core and is checked by an '0' seal no. 17030.

To prevent coil leakage, enough radial clearance must be provided between the coil spool and the magnetic core to have enough space to accommodate alradite for sealing purposes. The pre-production valve and the prototype valve have coils with only about 0.03 mm radial clearance between coil spool and the magnetic inner pole core. Clearly this clearance is small and there is no alradite in the market now that have a low viscosity to effect sealing. The minimum clearance that any of the available commercial alradite can be used to seal is 0.5 mm.

The gross winding depth $r_{2p} - r_{1p}$ will include besides the thickness of the winding itself:

(1) the thickness of the bobbin tube = $r_{1b}-r_{ob} > 0.51$ mm;

(2) the insulation between bobbin and the coil, consisting of two or more layers of alradite, according to the voltage, $r_{ob}-r_{1p} > 0.38$ mm;

(3) the insulation outside of the coil, consisting of two or more layer of alradite and a protecting layer of tape $r_{2p}-r_{2b} > 0.76$ mm;

(4) an allowance of about 0.25 mm between the insulated coil and the outside iron for irregularities in winding.

Total allowance = 1.91 mm = $r_{2b} - r_{ob}$. The number of coil layers is given by

$$N_L = (r_{2b}-r_{1b}-2d_c)/d_c \qquad (A1.9)$$

Two layers are left in equation (A1.9) to enable the coil winding to be bound with any thin sticky tape of thickness less than d_c. It also provide space for coil sealing against leakage. The number of layers N_L should be a whole number and so, if small, r_{2b} may slightly be changed to get whole number of layers. The number of layers must be an even number so that the beginning and ending of the winding will be at the same end of the coil, as this facilitates the mechanical problem of bringing the leads to the coil through the surrounding magnetic iron case.

Besides the insulated wire, the axial length h_{1p} includes:

(1) the thickness of two flanges of the bobbin, each having about the same thickness as the brass tube = $h_{2b}-h_{1b} > 1.52$ mm;

(2) three or more thickness of alradite = $h_p-h_{2b} > 0.38$ mm;

(3) an allowance of about 0.25 mm total for imperfect fit of bobbin in the iron shell.

Total allowances = 2.15 mm = $h_{1p}-h_{1b}$. The number of turns per layer is given by

$$N_{PL} = (h_{1b}-d_c)/d_c \qquad (A1.10)$$

An allowance of 1 turn per layer is provided in equation (A1.10) for space

lost at the ends. The total number of coil turns N is given by $N_L N_{PL}$.

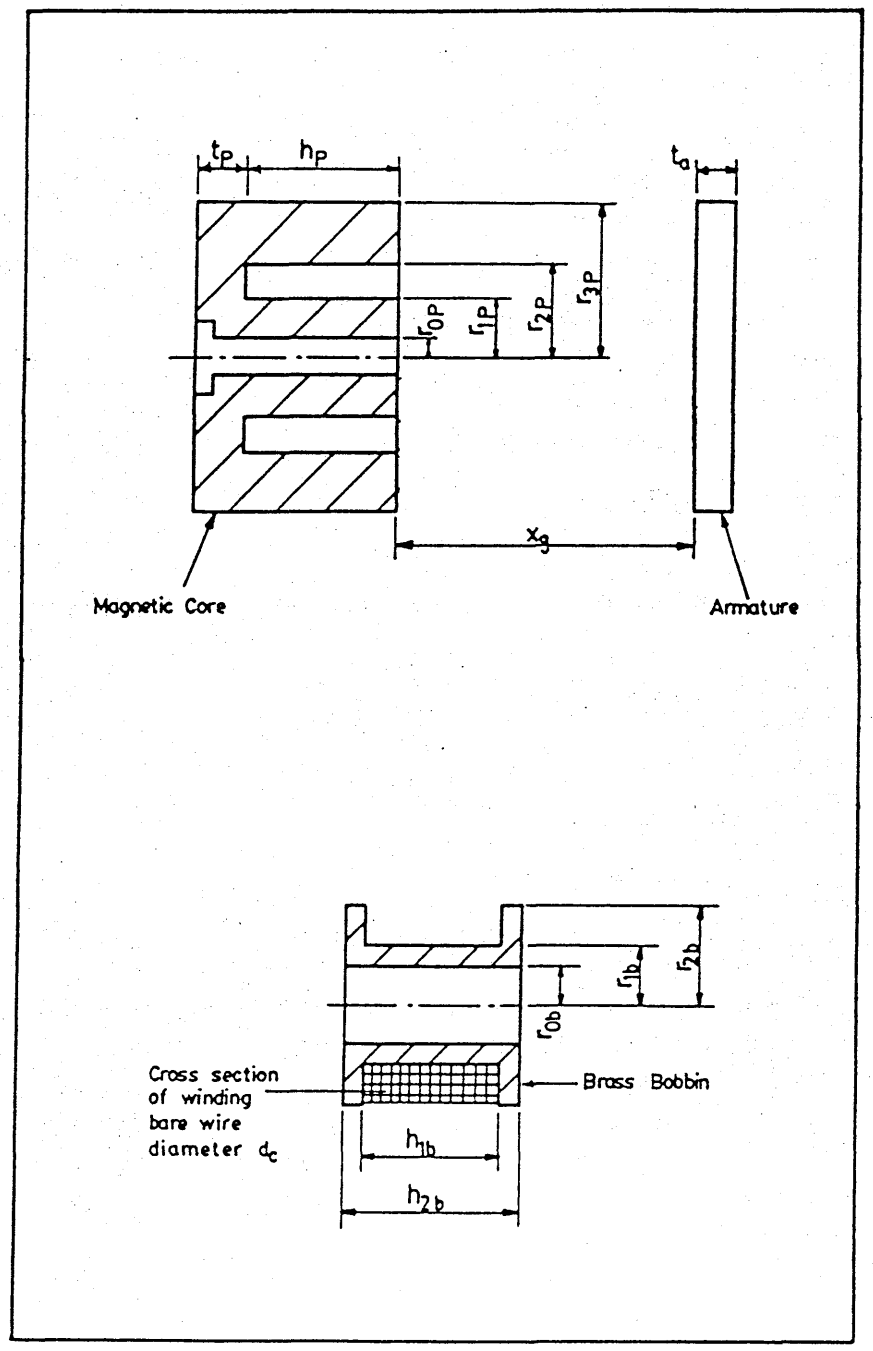

Fig. A1.1 Cross-section through a flat-faced armature type electro-magnetic coil.

APPENDIX A2

Four-level switching amplifier

A2: FOUR-LEVEL SWITCHING AMPLIFIER

In electro-mechanical solenoid systems, two current levels are required to operate the system efficiently. First, when the armature of the solenoid system is moved, it requires high power to obtain fast response. Secondary, in a stationary position, the armature can be held against static forces with low power.

A unidirectional solenoid (single coil) system can be operated by a two-level switching amplifier, whereas a bidirectional (dual coil) system requires a four-level switching amplifier. The four-level are maximum positive current level, minimum positive current level and two corresponding levels that are delayed by half the input signal period.

The switching amplifier to be described here has a monostable pulse generator, bistable and power amplifier circuits. The block diagram and voltage waveforms of the switching amplifier is shown in figure A2.1. A bipolar square wave input operate the amplifier. The amplifier is constructed so that half the circuit admit the positive going input signal when the other half admit the negative going signal.

A2-1 Monostable circuit

This circuit has two '555 timer' ICS. The '555 timer' is designed to give a monostable timing action, and acts as a pulse generator. The timer can generate pulses with periods ranging from 5 microseconds to several hundred seconds, and can be triggered at frequencies up to 100KHz [72].

The pulse timing periods are independent of supply-rail voltage and thermal variations. The electronic circuit for the monostable pulse-generator is shown in Fig. A2.2. The IC1 in Fig. A2.2 is used as a Schmitt trigger, which converts any input waveform into a rectangular output waveform. This

waveform is converted into a form suitable for triggering the IC2 monostable via C2 and R2. The peak-to-peak amplitude of the initial input waveform must be greater than 1/2Vcc. The pulse periods of the circuit are fully variable via C1 and R1 and the output pulse amplitude is fully variable via R3.

A2-2 Bistable signal generator

A diode and an operational amplifier are used to generate a bistable signal which is compatible with the square wave input signal. Fig. A2.3 shows two types of bistable signal generators. In Fig. A2.3a, the diode prevents the output voltage from going negative and this signal is inverted through an operational amplifier to obtain the negative bistable signal. In a similar manner, Fig. A2.3b generates a positive bistable signal. With this arrangement, half the period of the input square wave switches one monostable to produce a positive going output signal. The other half period of the square wave generates a similar negative going output signal.

A2-3 Power stage amplifier

The power stage incorporates two operational amplifier and two NPN transistors (Q1,Q2). they are arranged in push-pull mode (see Fig. A2.4). This arrangement allows the use of two separate coils in the circuit. Because no even harmonics are present in the output of a push-pull amplifier, this circuit will give more output per active for a given amount of distortion. For the same reason, a push-pull arrangement obtain less distortion for a given power output per transistor.

With the arrangement of the preceding circuits, the positive going input signal drives one transistor when the negative going signal drives the other transistor. The Zener diodes, ZD1 and ZD2, are placed across the coils to protect the transistors from the coils stored energy effects.

Excessive current will flow through the Zener diodes whenever the coil induced voltage level exceeds the Zener breakdown voltage.

For analysis purpose, one side of the power amplifier shown in Fig. A2.5 would be considered. From this figure the following equations can be derived:

$$I_b = I_s - I_f \qquad \text{(A2-1)}$$

$$I_c = I_e \qquad \text{(A2-2)}$$

The reverse transmission factor B is defined by:

$$B = I_f/I_e = I_f/I_c \qquad \text{(A2-3)}$$

$$I_b = V_b/R_b \qquad \text{(A2-4)}$$

The transfer gain A is defined by:

$$A = I_c/I_b = h_{fe} \qquad \text{(A2-5)}$$

The feedback gain is given by:

$$A_f = I_c/I_s = A/(1+BA) \qquad \text{(A2-6)}$$

Equation (A2-4) shows that the operational amplifier, 741, output voltage V_b results in a proportional transistor base current I_b. With the common-emitter configuration of Fig. A2.4 or Fig. A2.5, its output function acts as a current amplifier. For a purely resistive collector load, a step change in base current I_b will result in a step change in collector current I_c.

The effects of the feedback are:

(a) To improve the stability of the amplifier. (b) If the feedback network does not contain reactive elements, the complete gain is not a function of frequency. Under these circumstances a large reduction in frequency and phase distortion is obtained. (c) Non-linear distortion is reduced. (d) Noise is reduced. (e) System bandwidth increases. (f) To improve characteristics of current amplifier.

These electronic circuits are combined as a four-level switching amplifier

shown in Fig. A2.6.

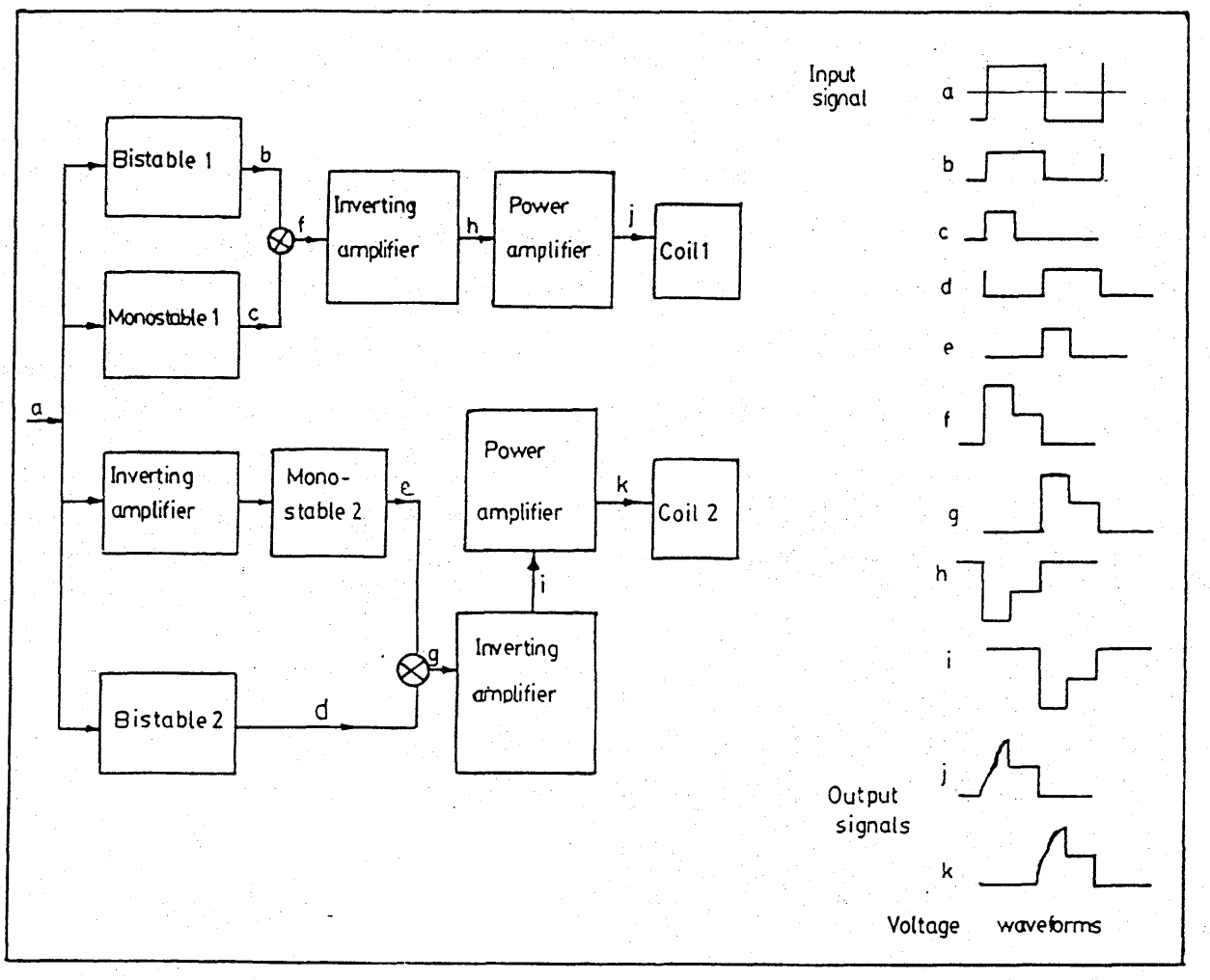

Fig. A2.1 Block diagram and voltage waveform of a switching amplifier.

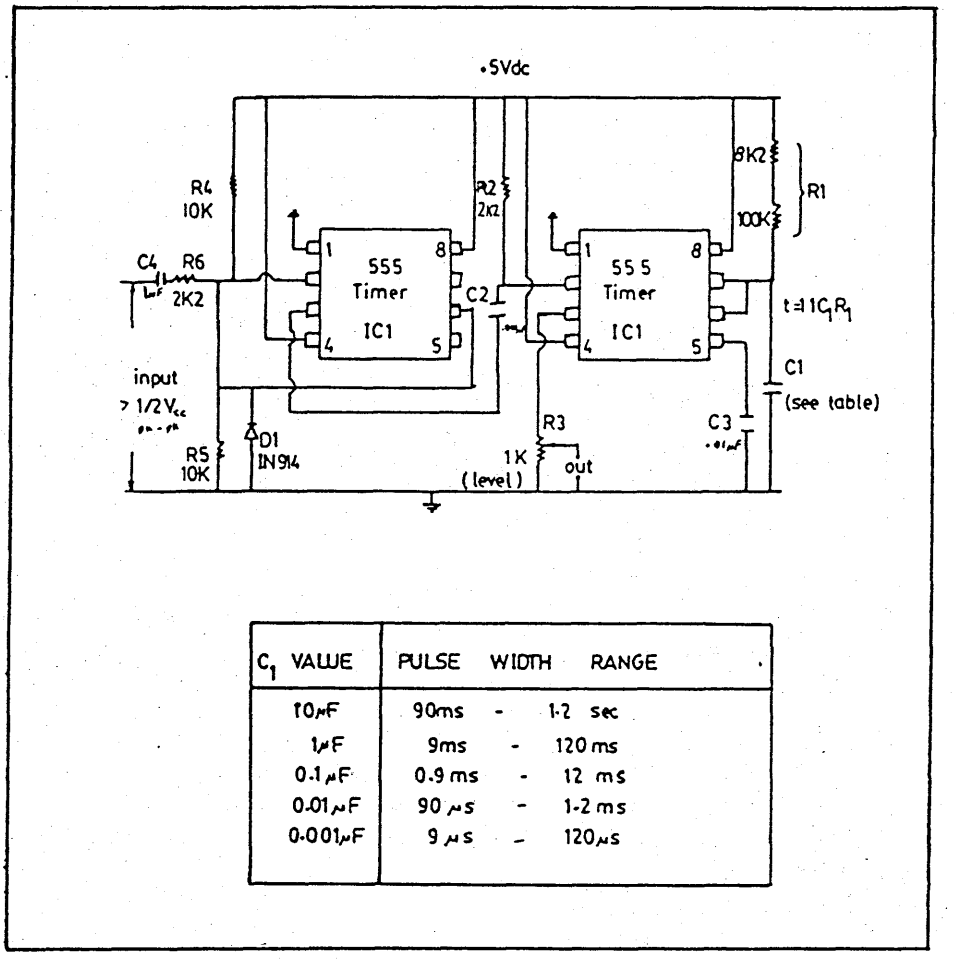

C_1 VALUE	PULSE WIDTH RANGE
10μF	90ms - 1·2 sec
1μF	9ms - 120 ms
0·1μF	0·9 ms - 12 ms
0·01μF	90 μs - 1·2 ms
0·001μF	9 μs - 120μs

Fig. A2.2 An electronic circuit diagram of a monostable pulse generator.

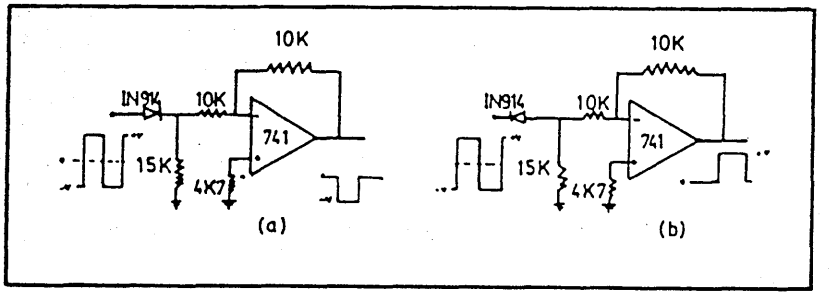

Fig. A2.3 An electronic circuit diagram of two types of bistable signal generator

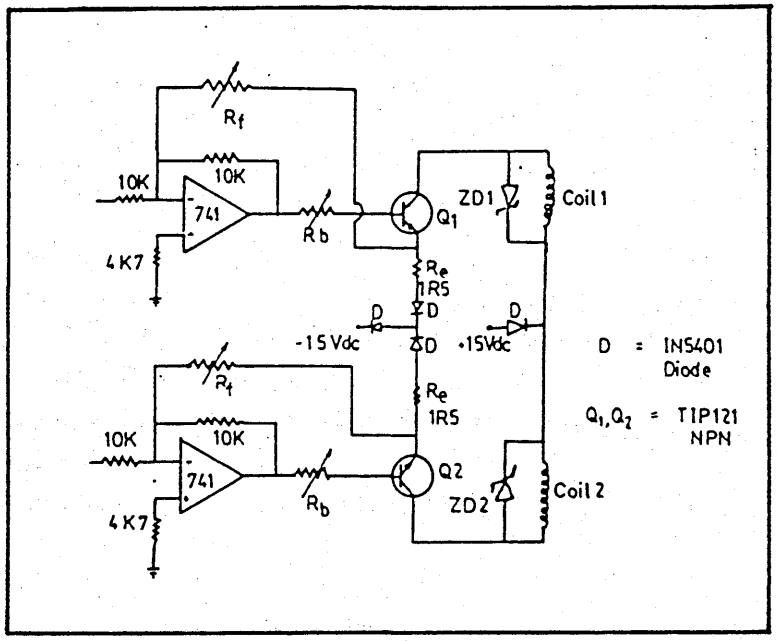

Fig. A2.4 Current power amplifier arranged in push-pull mode

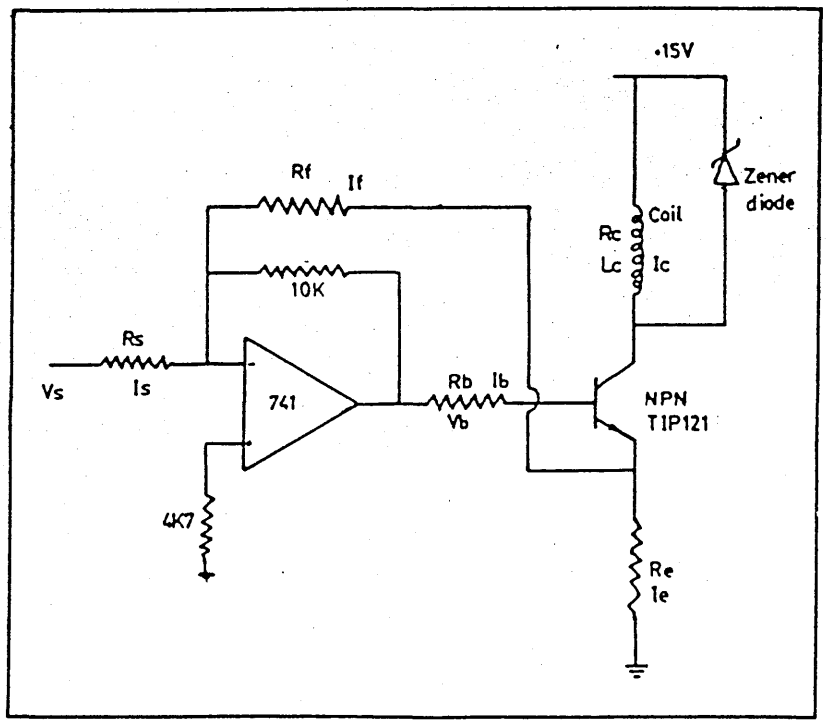

Fig. A2.5 Schematic diagram of a power amplifier.

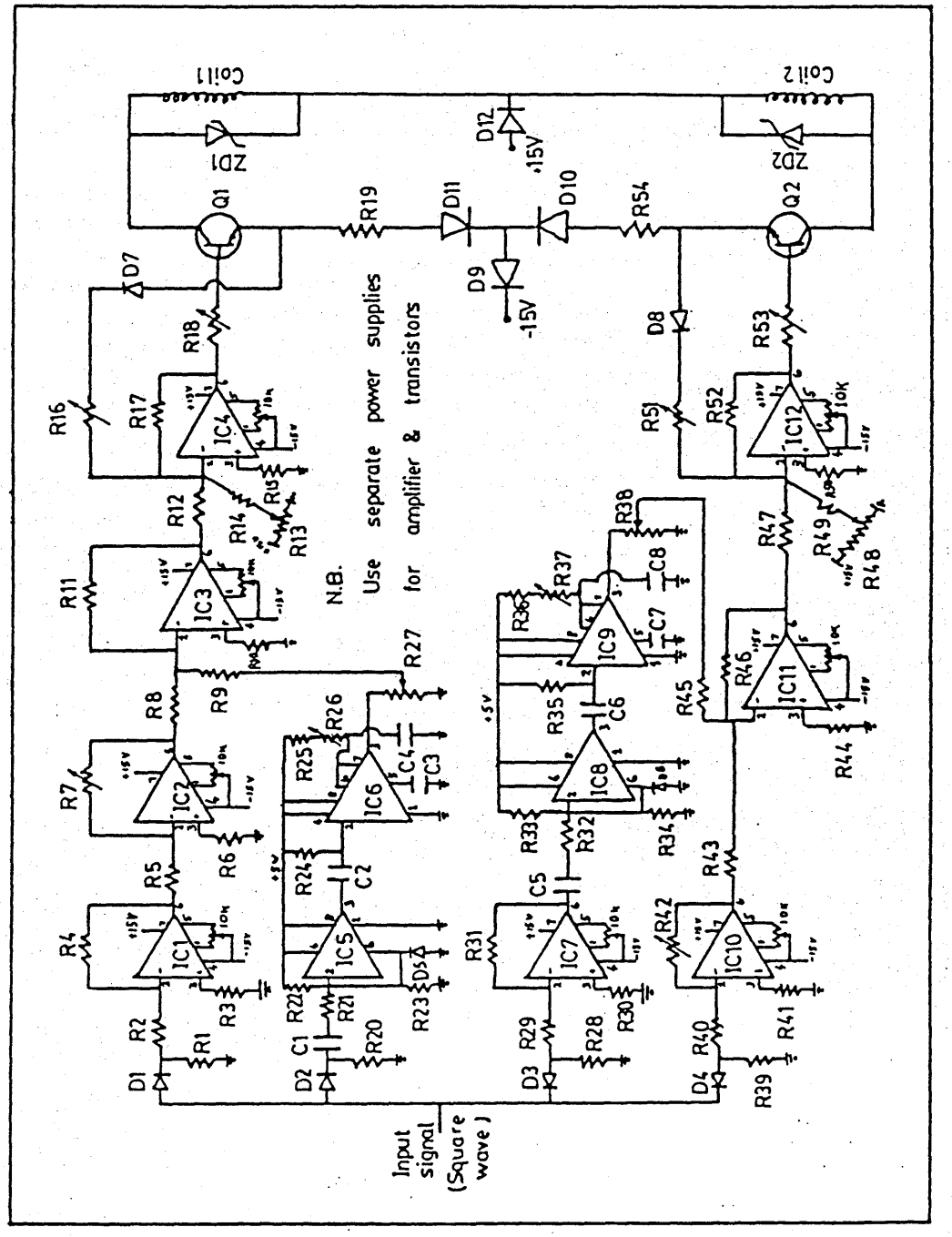

Fig. A2.6 An electronic circuit diagram of a four-level switching amplifier

APPENDIX A3

Analogue pulse-width-modulator

A3: ANALOGUE PULSE-WIDTH-MODULATOR

A3-1 Design approach

The analogue Pulse-Width-Modulator (PWM) in Fig. A3.1 is made up of three sections, these being an inverting operational amplifier (IC1), a summing operational amplifier (IC2) and a differential voltage comparator switch (IC3).

The inverting operational amplifier network, which is built round IC1, comprises R4-R5 and is driven from a variable potential divider R1-R2-R3, that is wired between the positive and negative voltage supply lines.

The summing operational amplifier, (IC2), sum the output of IC1 and the feedback from the system under investigation (i.e. position servo system whose output is converted to voltage via a potentiometer arrangement). The output of IC2 is an error signal. In other words, IC1 and IC2 form a summing junction of a control system whose output is an error signal.

The IC3 is wired as a simple voltage comparator, and has one input applied from the output of IC2 via resistor R11. The operational amplifier IC3 switches into positive or negative saturation each time the triangle waveform amplitude goes more than a few millivolts below or above the reference voltage set via R2 and the feedback voltage.

By adjusting the reference voltage, therefore, the operational amplifier (IC3) can be made to change state at any point on the triangle waveform and a variable mark/space ratio rectangular wave is thus available at the output of the operational amplifier (IC3). The amplitude of the output is adjusted via R13. The frequency of the output waveform is that of the triangular frequency.

This analogue PWM provides useful rectangular waveforms up to a maximum

frequency of about 10 KHz. Operation beyond this range is poor, because of the slew rate limitations of the 741 operational amplifier.

A3-2 Parts list

Table A3.1 shows the components value.

Table A3.1

Component Function	Circuit Reference	Value
Mark/space ratio	R2	10K
	R1	10K
	R3	10K
Input resistors	R4	10K
	R7	10K
	R8	10K
	R11	10K
	R12	10K
	R14	10K
Feedback resistors	R5	10K
	R10	10K
Output resistor	R13	10K
Earthing resistors	R6	4K7
	R9	4k7
operational amplifiers	IC1	741
	IC2	741
	IC3	741

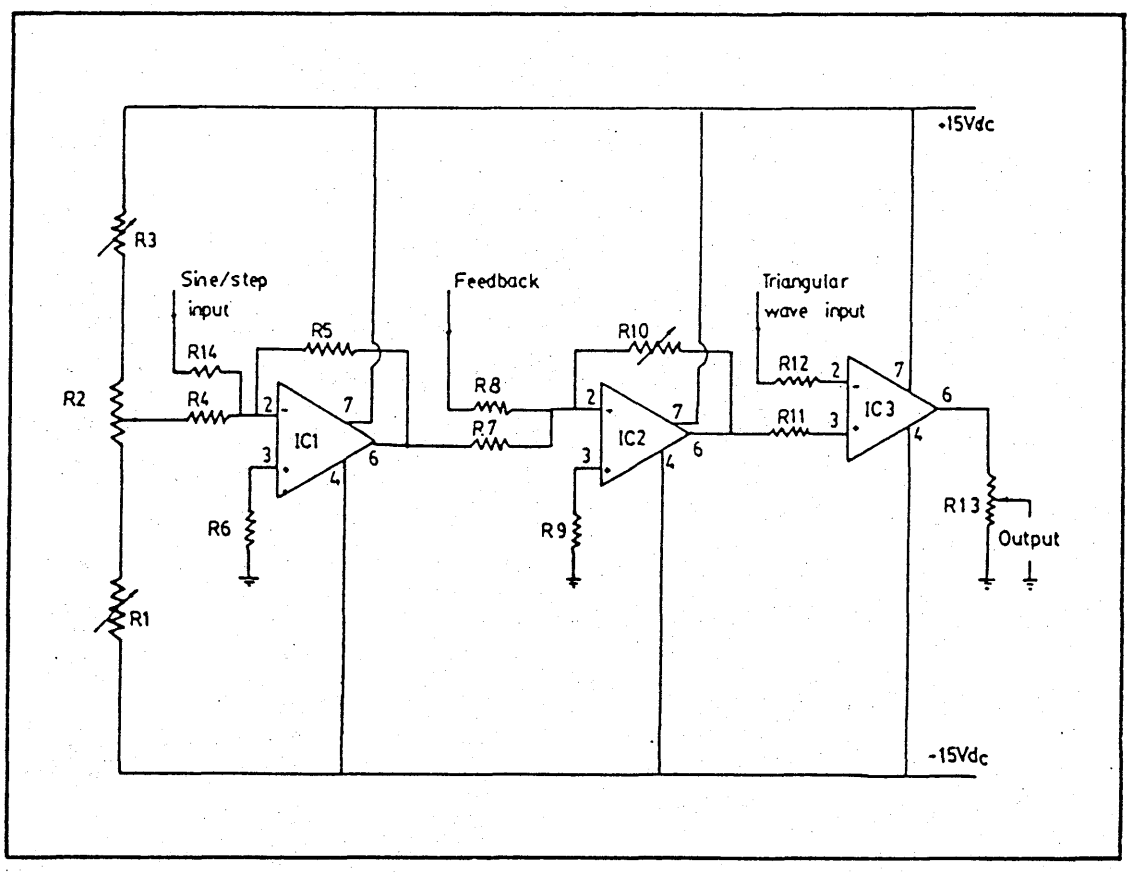

Fig. A3.1 An electronic circuit diagram of an analogue pulse-width-modulator amplifier.

APPENDIX A4

Principle of pulse-width-modulation (PWM) technique

A4: PRINCIPLE OF PULSE-WIDTH-MODULATION TECHNIQUE

Figure A4.1 shows a method by which a regular signal e(t) shown in Figure A4.2a is transformed to a pulse train. The pulse train M(t) having a given magnitude (amplitude) V_p is shown in Figure A4.2b. In Figure A4.1, a triangular wave (sawtooth waveform) $r_s(t)$ with amplitude V_s and period T_s is generated. The comparator compared the triangular wave with the input signal. Its output is V_p or $-V_p$ according to whether the input is positive or negative. The amplitude of the triangular wave V_s should at any time be at least as large as the magnitude $|e(t)|$ of the input signal e(t). Otherwise the output of the comparator is not a pulse train. On the other hand, the periods T_s of the triangular wave should be short enough so that the signal M(t) is nearly a constant during each period and can be approximated by a staircase function. The width of each step of this function is the period T_s of the triangular wave. It appears from the block diagram of the signal modulator, shown in Figure A4.1, that a regular signal e(t) is modulated to obtain a pulse train M(t) with amplitude V_p.

The following relations could be obtained for $|e(t)| \leq V_s$.

$$e(nT_s + t_{n1}) = r_s(nT_s + t_{n1}) = (-V_s + 2V_s t_{n1}/T_s) \tag{A4.1}$$

$$t_{n1} + t_{n2} = T_s \tag{A4.2}$$

$$nT_s < t < nT_s + t_{n1}; \qquad M(t) = -V_p \tag{A4.3}$$

$$nT_s + t_{n1} < t < (n+1)T_s; \qquad M(t) = V_p \tag{A4.4}$$

where n is non-negative integer.

The time average A_m of the modulated signal M(t) for the period from $t = nT_s$ to $t = (n+1)T_s$ is

$$A_m = \frac{1}{T_s}\int_{nT_s}^{(n+1)T_s} M(t)\,dt = \frac{V_p}{T_s}(t_{n2} - t_{n1}) \qquad (A4.5)$$

If $0 \leq t \leq T_s$, we have

$$e(nT_s + t) \simeq e(nT_s + t_{n1}) \simeq$$

$$A_i = \frac{1}{T_s}\int_{nT_s}^{(n+1)T_s} e(t)\,dt \qquad (A4.6)$$

where A_i is the time average of e(t) for the period from $t = nT_s$ to $t = (n+1)T_s$.

From equations (A4.1), (A4.2) and (A4.6) we have

$$t_{n1} - t_{n2} \simeq \frac{T_s}{V_s} A_i \qquad (A4.7)$$

From equation (A4.7), it can be seen that when $A_i = 0$, we have

$$t_{n1} = t_{n2}$$

The following equation could be obtained by substituting equation (A4.7) into (A4.5)

$$A_m \simeq \frac{V_p}{V_s} A_i \qquad (A4.8)$$

Hence the time average A_m of the modulated signal for a period T_s is proportional to the magnitude of the original signal in the corresponding period.

This method of signal modulation is called pulse-width-modulation (PWM). This approach is generally used in communication to improve the "signal to noise ratio". In this present work, the PWM technique is used to convert a switching double disc valve into a proportional device.

Although the period T_s of this wave is short enough, the choice of the amplitude of the triangular wave is defined to be improper when $V_s < |e(t)| \simeq |A_i|$.

From Figure A4.2, when $e(t) \simeq A_i > V_s$;

$$t_{n1} = T_s,\ t_{n2} = 0,\quad M(t) = -V_p \tag{A4.9}$$

and when $e(t) \simeq A_i < -V_s$;

$$t_{n1} = 0,\ t_{n2} = T_s,\ M(t) = V_p \tag{A4.10}$$

When this technique is applied, it must be borne in mind that the method has a saturation limits at $A_i = \pm V_s$.

The major assumptions made in applying the PWM technique are: (a) the non-linearity is not a function of time, (b) the input pulse signal is not distorted in its width in the time domain and (c) the magnitude of the pulse is constant and is not distorted in magnitude by passing through the time independent non-linearity of the system.

When applying PWM technique to a closed-loop system, attention should be paid not only to the time rate of change of the input but to the bandwidth of the linear element in choosing the period T_s and the magnitude V_s of the triangular wave. Thus the amplitude at any time be at least as large as the absolute value of the signal coming into the non-linear element. The period T_s of the triangular wave should be short enough so that the signal coming into the non-linear element is nearly a constant during each period of the triangular wave.

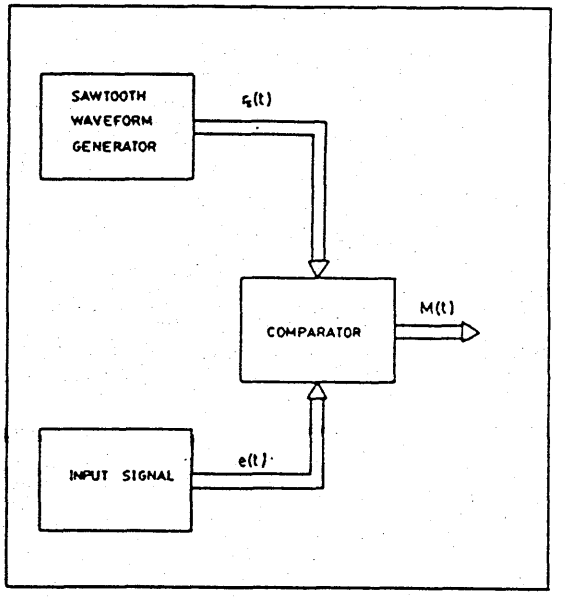

Fig. A4.1 Formation of pulse train.

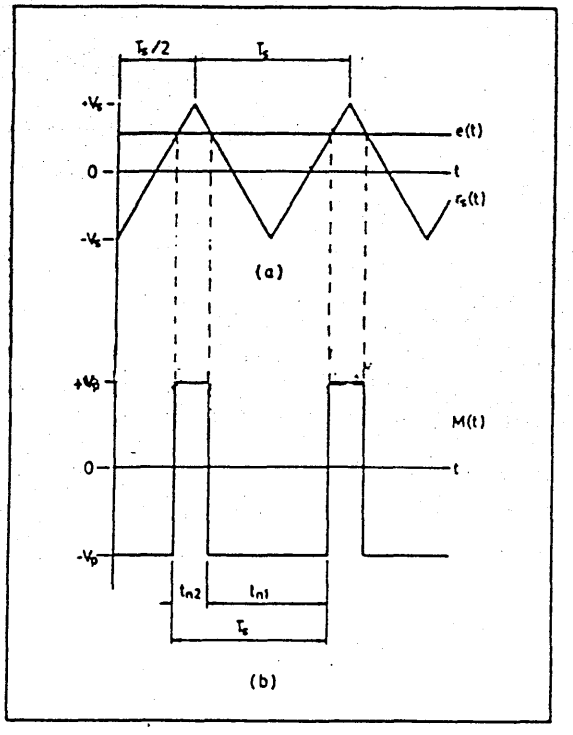

Fig. A4.2 (a) Sawtooth waveform and error signal.
(b) Modulated signal.

APPENDIX A5

Disc valve amplifier

A5: DISC VALVE AMPLIFIER

A5-1 Introduction

The electronic control of a double-disc valve requires a switching amplifier and a simple pulse-width-modulator (PWM) to effect both switching and proportional control. The PWM generates pulses that drive the switching amplifier. The ouput transistor power stage of the switching amplifier provides the necessary current to the electro-magnetic coils of the valve. Initially, the Four-level switching amplifier described in Appendix A2 was used with the analogue PWM described in Appendix A3. This arrangement had the following disadvantages:

(a) Two power supplies were required to drive the electronic amplifiers because of current limitation.

(b) As a result of (a) there was earth problem and cross-over distortions.

(c) The add-on pulses or the overdrive principle associated with the Four-level switching amplifier has an adverse effect on the proportionality of the valve.

(d) External waveform generator was required to provide the necessary sawtooth waveform required for the pulse-width-modulation action.

The aim of the disc valve amplifier is to eliminate the above disadvantages. The disc valve amplifier incorporates both the analogue PWM and the switching amplifier. It uses only one power supply and has a built-in sawtooth waveform generator. The add-on pulses of the Four-level switching amplifier had been removed in this disc valve amplifier.

The disc valve amplifier has a manual controller, auto controller, feedback amplifier, waveform generator, comparator and a switching amplifier. Fig. A5.1 shows the major components of the disc valve amplifier.

A5-2 Manual controller

The manual controller has a Joystick controller and potentiometer controller as shown in Fig. A5.2. The switch S1 in the figure selects either a Joystick controller or potentiometer controller.

The Joystick controller has a dual axis Joystick potentiometer supplied with two 10K linear carbon track potentiometers. The Joystick has integral centre return springs which may, if desired, be removed allowing the control stick to stay in any position. In this application only one of the potentiometers was used. The control voltage from the Joystick was small in amplitude owing to the small sweep angle. For this reason an operational amplifier was incorporated to permit gain adjustment.

The potentiometer controller has a 10K linear potentiometer and two resistors with values 5K2 and 10K (variable). These two resistors were used to balance the voltage swing of the linear potentiometer.

The manual control unit is housed in a moulded plastic box and linked to the disc valve amplifier via a 4 core screen flexible cable with 5 pins DIN type connectors. The DIN pin assignments are:
Pin 1 + 15 V; Pin 2 Not connected; Pin 3 Earth; Pin 4 Control voltage; and Pin 5 -15 V.

A5-3 Auto controller

The auto controller can accept any signal from an external source.

A5-4 Summing amplifier

The summing amplifier circuit is shown in Fig. A5.3. It has an operational amplifier used to sum the output of the manual controller, auto controller and a feedback signal as required in a closed - loop control operation of

the disc valve amplifier to provide a variable amplitude error signal. The output of the summing amplifier is called an error signal and its amplitude can be varied via a 100 K variable resistor shown in Fig. A5.3. The error signal gain is important in the disc valve control. The higher the error signal gain, the better the control as the input dead-band of the valve decreases.

A5-5 Feedback amplifier

Often in a closed-loop position control, the electrical stroke of a feedback transducer might not be equal to the stroke of an actuator or the feedback signal amplitude might not match that of the command signal. Considering these facts, a feedback amplifier whose electronic circuit is shown in Fig. A5.4 was incorporated in the disc valve amplifier.

The feedback amplifier has three operational amplifiers, two of which were wired as voltage followers and the third one was wired as a summing junction. The voltage follower A was incorporated to prevent current being drawn from the feedback potentiometer. The voltage follower C was used to monitor the corrected feedback signal without drawing any current. The operational amplifier B was used to sum the uncorrected feedback signal and an adjustable offset signal used to correct any discrepancy in the mid-positions of the feedback potentiometer stroke and that of the actuator. Feedback signal amplitude adjustment is made possible via 100 K potentiometer on the front panel of the disc valve amplifier.

A5-6 Waveform generator

The waveform generator has a monolithic integrated circuit (type 8038CC) that gives simultaneous sine, square and triangular outputs and an output buffer amplifier (see Fig. A5.5). The triangular output waveform is

selected without any adjustment of the duty cycle being made and terminals 4 and 5 are shorted together as shown in Fig. A5.5. The frequency f of the signal generator is controlled by the timing resistor R and the capacitor C and is given by $f = 0.15 / RC$.

Pins 7 and 8 are shorted together, and the magnitude of the charging current I due to R is given by $I = V_{cc} / 5R$. For best performance, this charging current should be within 10 microamp and 1 mA according to the manufacturer specifications. For best stability capacitor C should be a low temperature coefficient type, e.g. silvered mica, polystyrene type, etc. Electrolytic capacitors are not good for timing action.

To prevent overload and to provide maximum amplitude the waveform output is passed through an **output buffer amplifier**. The output buffer amplifier has an operational amplifier 741 and resistors wired as shown in Fig. A5.5. The circuit allows amplitude adjustment which means that the generator output signal level which is fixed at one-third of the power supply can be altered at will.

A5-7 Comparator

Fig. A5.6 shows the circuit that generates the pulse-width-modulation (PWM) signal used to trigger the switching section of the disc valve amplifier. The circuit has two operational amplifiers A and B. The operational amplifier A compares the error signal with that of the sawtooth amplitude and its output level is controlled via operational amplifier B. The output of the comparator is a series of time width varying rectangular waveforms which can be switched on or off via switch S3 in the figure.

A5-8 Switching amplifier

The switching amplifier section of the disc valve amplifier is an improved

version of the Four-level switching amplifier. In the present design, the monostable circuit of the Four-level switching amplifier has been removed and the output transistor power stage has been made more efficient. The transistor stages and the operational amplifiers now share the same power supply. The number of integrated circuits have been reduced from 12 to 1. Four operational amplifiers (741 type) are now combined as one integrated circuit (348 type). Fig. A5.7 shows the electronic circuits of the switching amplifier.

The switching amplifier has diode wave clippers, operational amplifiers and the power stage amplifier circuits. The diode wave clipper performs the same function as the bistable circuit described in Appendix A2-2. The transistor power output stage is described below.

A5-8.1 Transistor power output stage

Each of the output transistor power stages of the disc valve amplifier has four resistors connected as a self-biasing circuit. The bias circuit is shown in Fig. A5.8(a) and it has four resistors which provide improved stability of the quiescent operating point. The input resistors R_1 and R_2 are used to give fixed bias, while the emitter resistor R_E provides a bias voltage that varies with I_c. This compensates somewhat for changes in h_{FE} or temperature on the quiescent operating point. Its operation is based on the fact that the critical variable to be stablised is the collector current rather than the base current. The combination of R_1 and R_2 constitutes a voltage divider to bring the base to the proper potential to forward bias the emitter junction. If I_c tends to increase, because of an increasing in h_{FE} due to a rise in temperature, the current $I_c + I_B$ in R_E increases, raising the potential of the emitter with respect to negative supply level. This, in turn, reduces V_{BE}, the forward bias on the base-emitter junction, reduces the base current and, therefore, limits the

increase in I_c. In other words, any increase in collector current is fed back to the base circuit and modifies the bias in such a way as to oppose a further increase in I_c.

A5-8.2 Analysis of the self-biasing circuit

Quantitative analysis of the circuit is simplified if the voltage divider (Fig. A5.8(b)) is replaced by its Thèvenin equivalent (Fig. A5.8(c)) where

$$V_B = R_1 V_{cc}/(R_1 + R_2) \text{ and } R_B = R_1R_2/(R_1 + R_2) \qquad (A5.1)$$

Writing a voltage equation around the input as redrawn in Fig. A5.8(d), gives

$$V_B - I_BR_B - V_{BE} - (I_c + I_B)R_E = 0 \qquad (A5.2)$$

I_c in equation (A5.2) can be replaced with I_Bh_{FE} and solving for the base current to get

$$I_B = \frac{V_B - V_{BE}}{R_B}\left[\frac{1}{1 + (1 + h_{FE})\, R_E/R_B}\right] \qquad (A5.3)$$

For a fixed-bias circuit

$$I_c = h_{FE}I_B \qquad (A5.4)$$

and for the four-resistor bias circuit, I_c is h_{FE} times the I_B value in equation (A5.3), leading to

$$I_c = \frac{V_B - V_{BE}}{R_B}\left[\frac{h_{FE}}{1 + (1 + h_{FE})\, R_E/R_B}\right]$$

I_c can be made less affected by temperature-induced changes of V_{BE} by making V_B larger. V_{BE} is about 0.7 V, although V_B may be made 4 V.
We may also neglect unity with respect to h_{FE} and then have

$$I_c \simeq \frac{V_B}{R_B}\left[\frac{h_{FE}}{1 + h_{FE}\,(R_E/R_B)}\right] \qquad (A5.5)$$

With the fixed-bias circuit, I_c was given by equation (A5.4), and was directly affected by changes in h_{FE}, with the bias current held constant. With equation (A5.5) for the four-resistor circuit, however, we have h_{FE} appearing both in the numerator and the denominator. It may be seen that the sensitivity of I_c to changes in h_{FE} can be reduced if we choose R_E/R_B correctly.

If we make $R_E = 0$, however, then equation (A5.5) reduces to

$$I_c = (V_B/R_B)\, h_{FE} \qquad (A5.6)$$

and I_c will vary directly as h_{FE}, which is the undesirable situation in the fixed-bias circuit.

If we make $R_E/R_B \tilde{=} 1$, then the $h_{FE}(R_E/R_B)$ term in the denominator would be the influencing factor. The h_{FE} terms in the numerator and denominator would about cancel and I_c would be independent of h_{FE} which is the result desired. R_E must be small in magnitude or we lose signal gain and dc power, however, and R_B must be larger with respect to h_{IE} of the transistor with which it is in parallel or we lose gain again. Hence some compromise between ideal bias stability and gain performance must be made.

Experience has shown that a satisfactory four-resistor bias circuit can be designed by selecting V_B in the region of 3 to 4 V and R_E/R_B in the region of 0.05 to 0.1. The R_E/R_B is called the stabilising ratio. This ratio serves as an index of stability, which increases as I_c is made more stable by the circuit design.

A5-9 Complete circuit

All the electronic circuits described so far are combined as one amplifier called the disc valve amplifier and Fig. A5-9 shows the block diagram of the essential components of the amplifier. Corresponding waveforms of the

various sections of the amplifier are shown in Fig. A5-10.

In Fig. A5-9, switch S1 selects between a Joystick controller and a potentiometer controller. The amplifier can be used for both open and closed - loop control and this is achieved through switch S2. The output of the comparator is a series of time width varying rectangular waveforms which can be switched on or off via switch S3. The wave clipper I admits only the positive going section of the rectangular waveforms. These pulses are inverted by an inverting amplifier as the power amplifier I requires a negative going signal. The wave clipper II admits the negative going signal which is compatible to power amplifier II. The current output of the power amplifiers are used to drive the coils of the disc valve.

The two coils can be switched on at the same time via a coil activator. The coil activator simply set-up a dc voltage to enable the transistors to be switched on or off. When switch S4 is on, the disc valve amplifier is in a pulse-width-modulation mode. Otherwise the two coils are fully switched on. The switch arrangement is shown in Fig. A5-7 as S4a and S4b. This arrangement allows the two discs of the double-disc valve to be pulled does shutting off the valve oil supply. With $\pm$ 15 V power supply, the amplifier can provide a maximum current of 1.55 A.

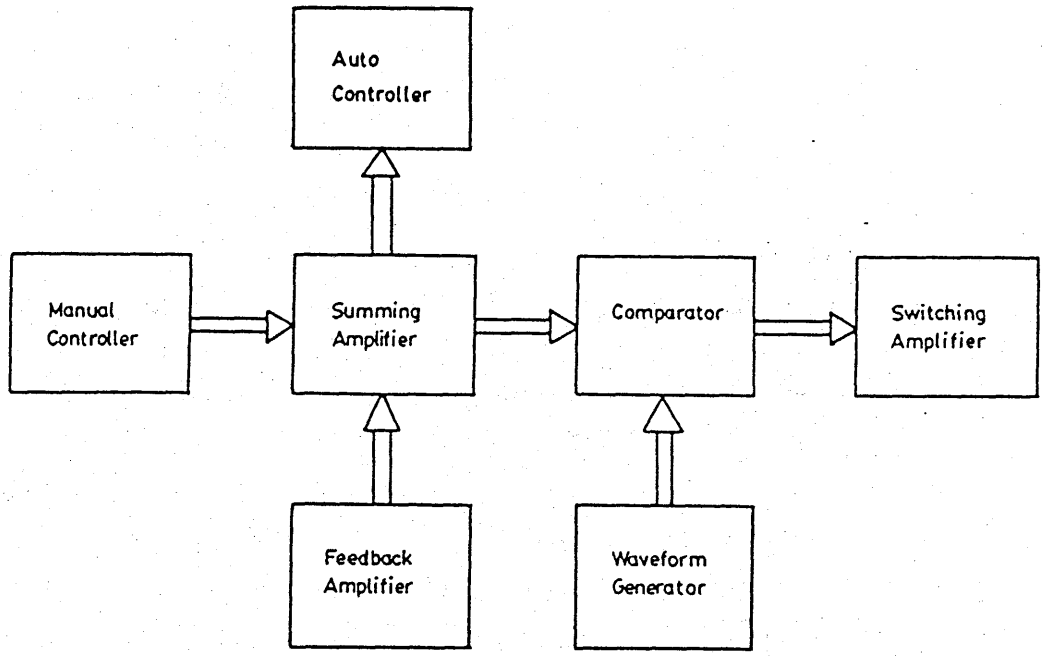

Fig. A 5.1 Basic components of a disc valve amplifier

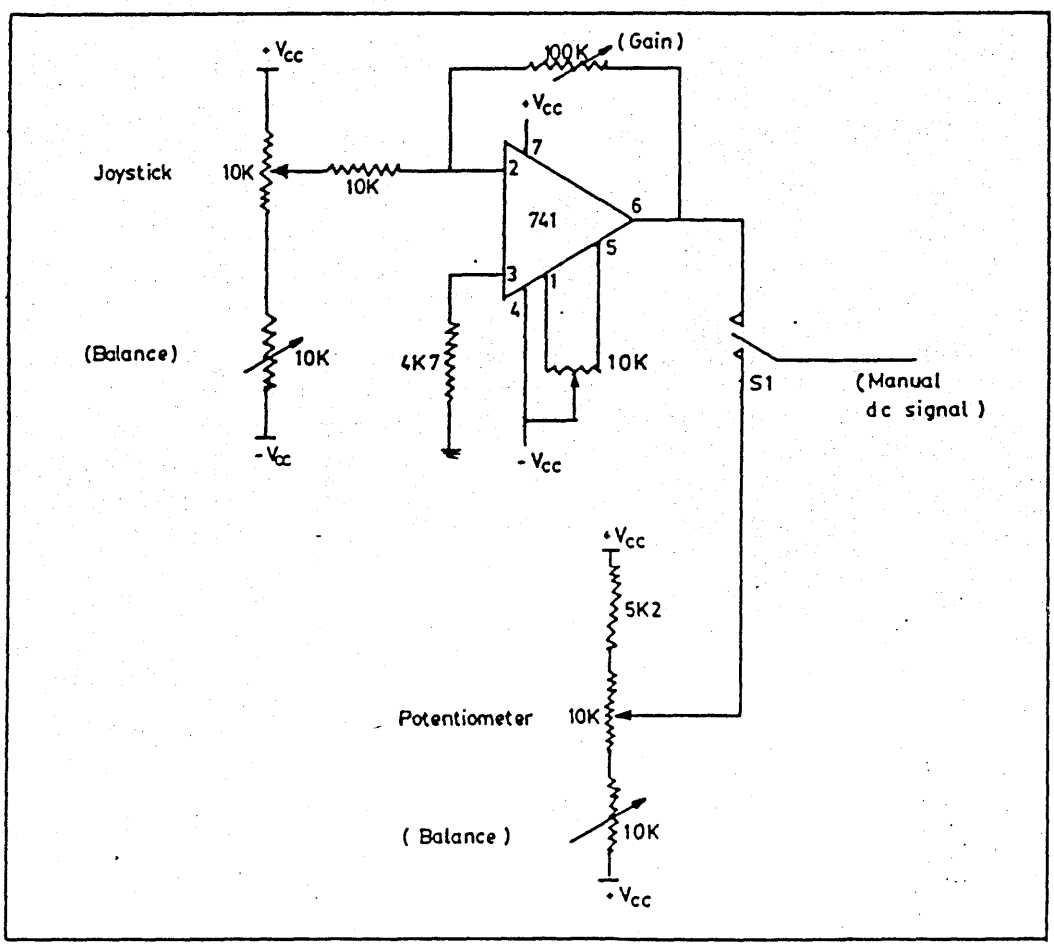

Fig. A 5.2 An electronic circuit diagram of a manual controller

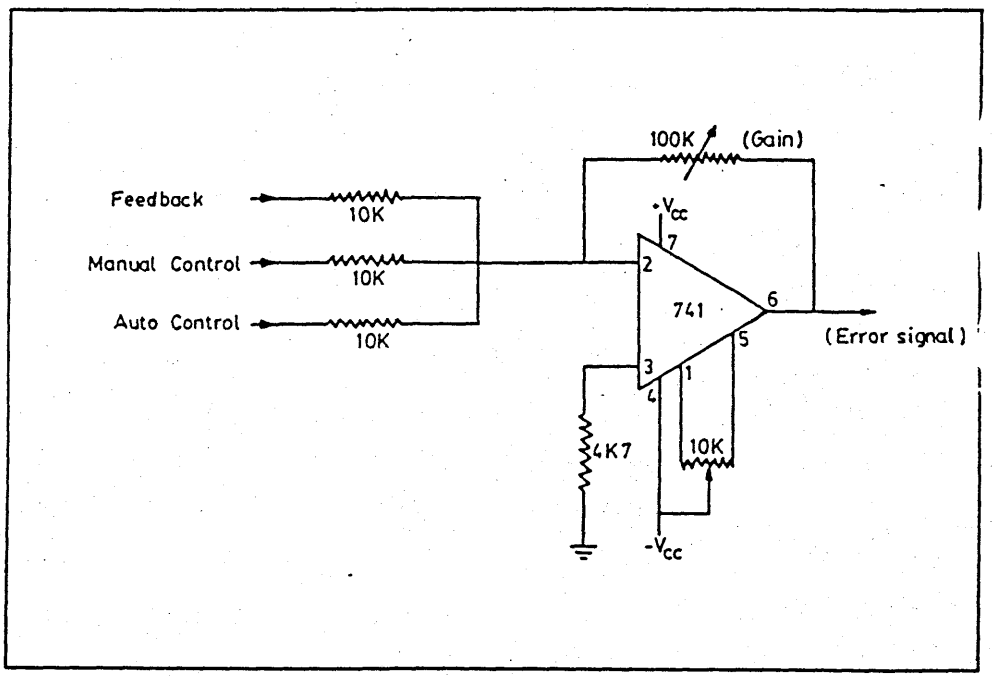

Fig. A5.3 An electronic circuit diagram of a summing amplifier

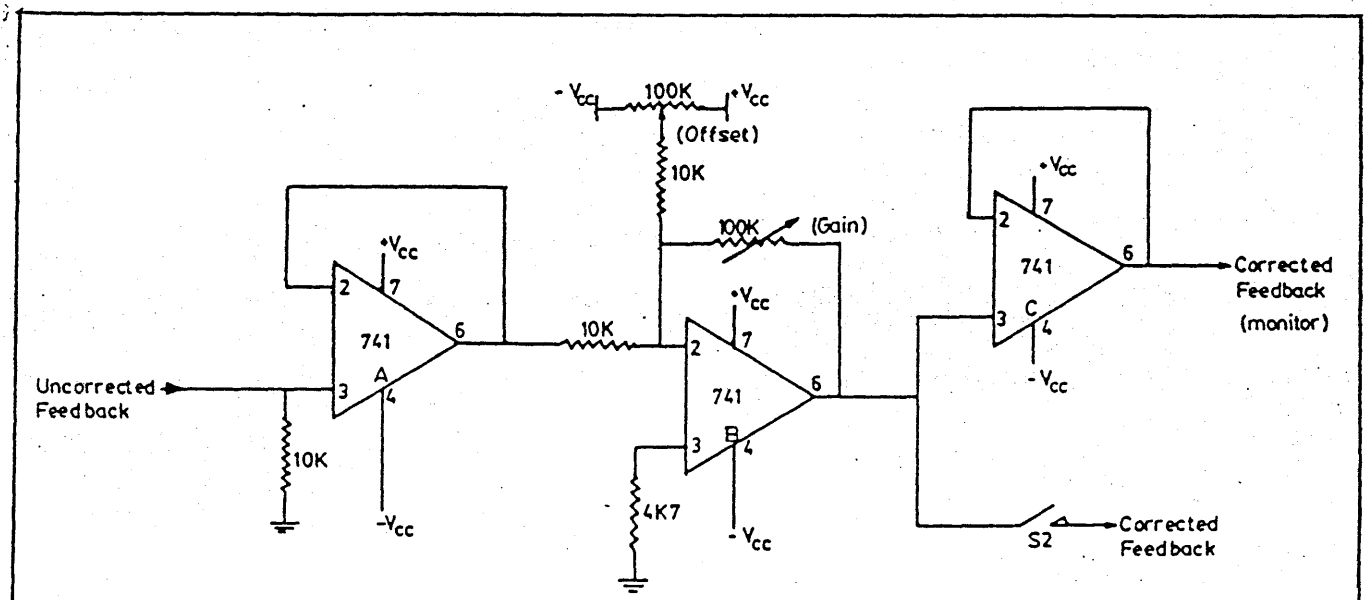

Fig. A5.4 An electronic circuit diagram of a feedback amplifier

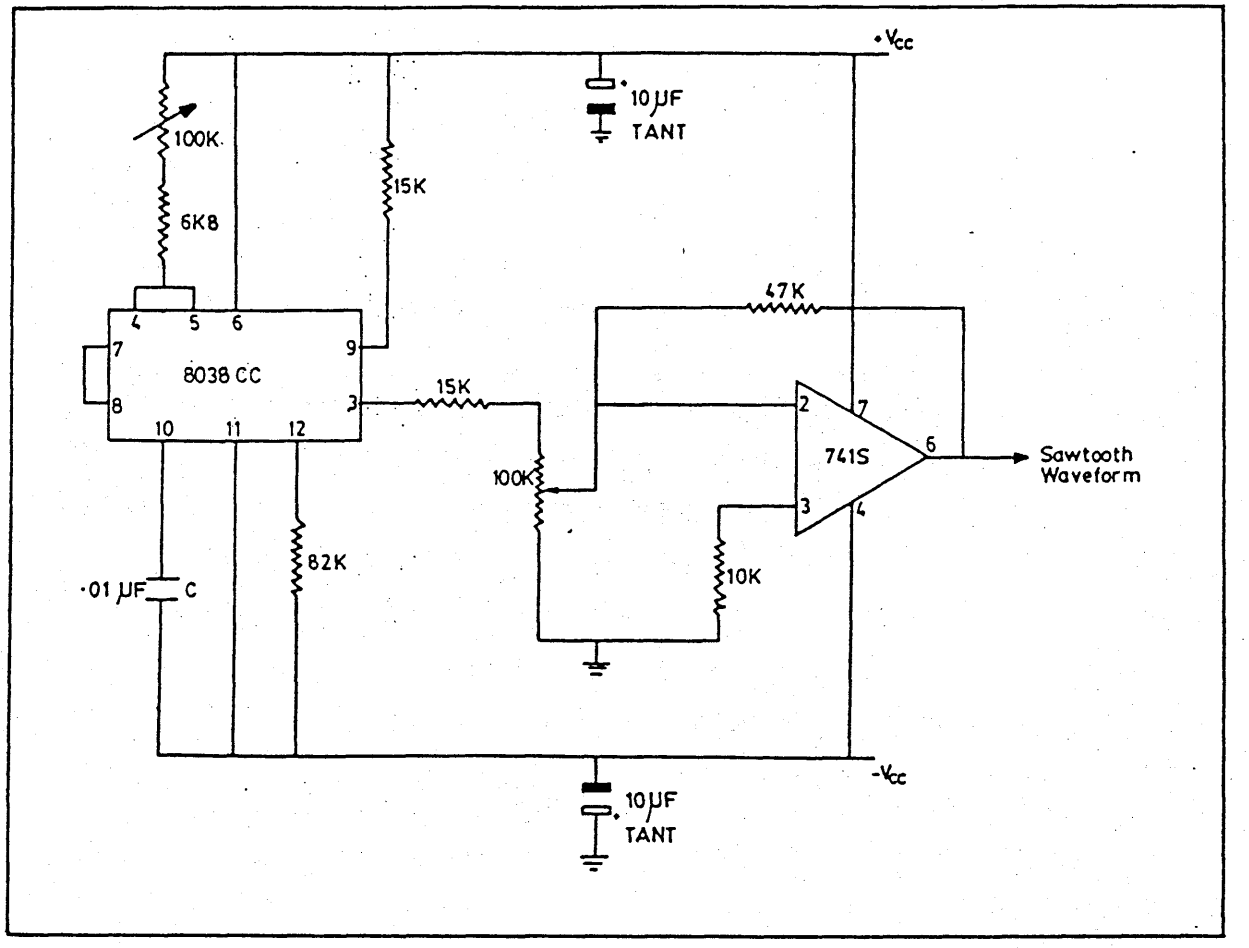

Fig. A5.5 An electronic circuit diagram of a waveform generator

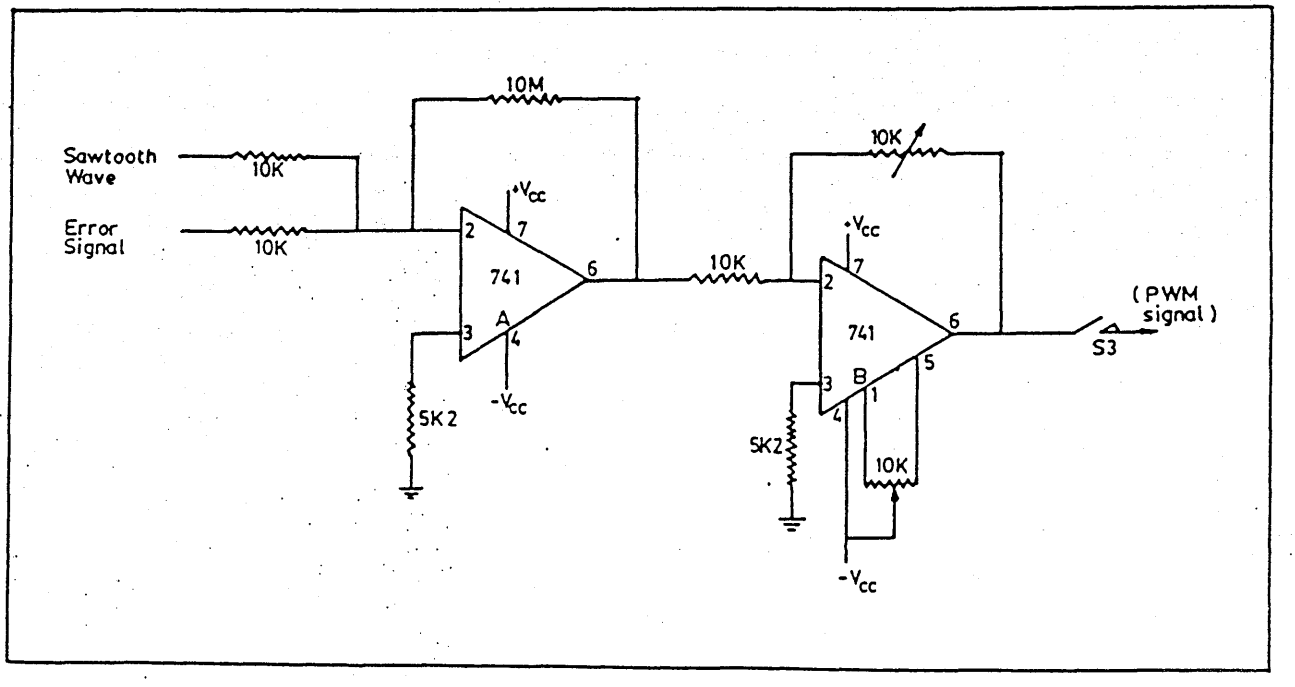

Fig. A5.6 An electronic circuit diagram of a comparator

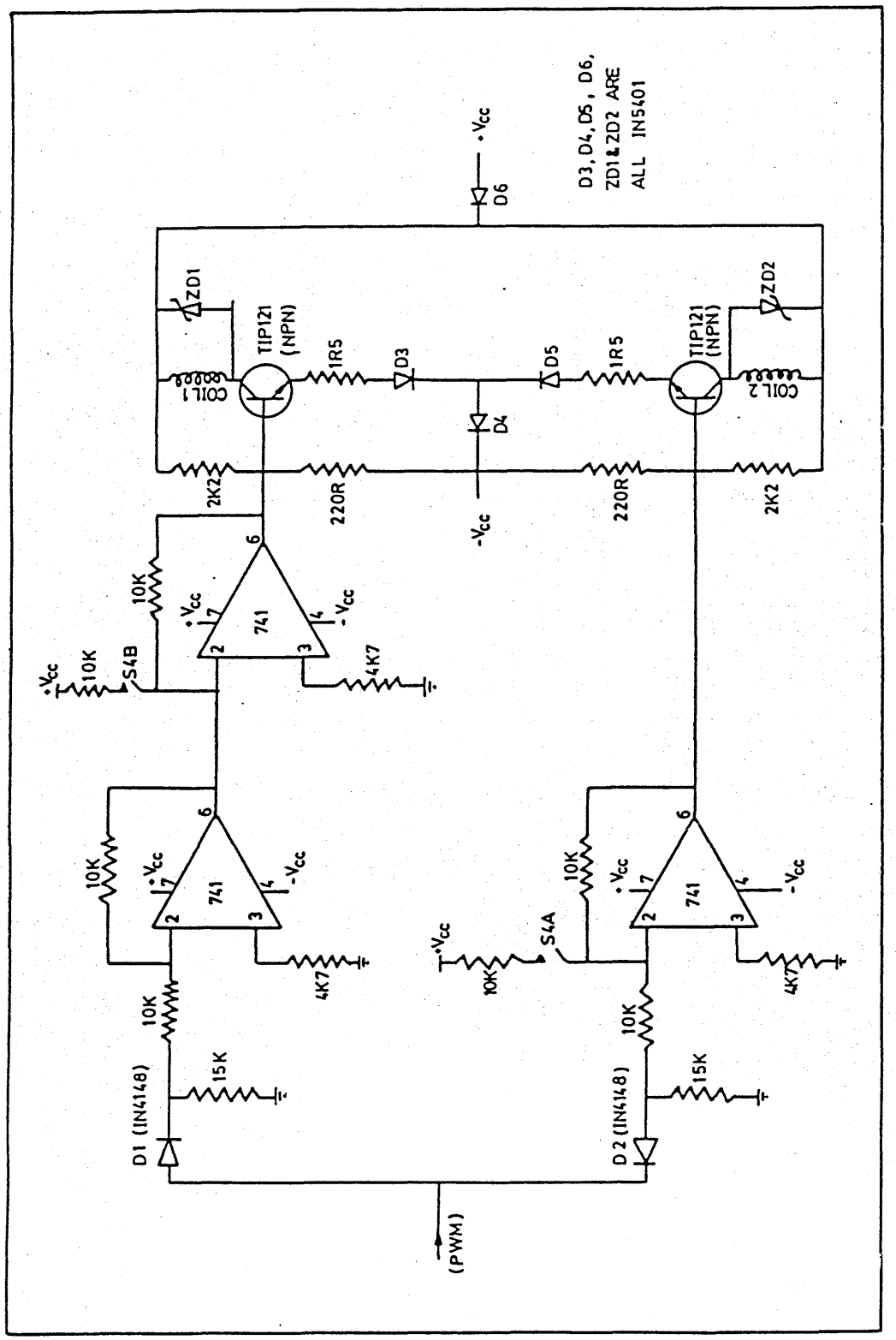

Fig. A 5.7 An electronic circuit diagram of a switching amplifier

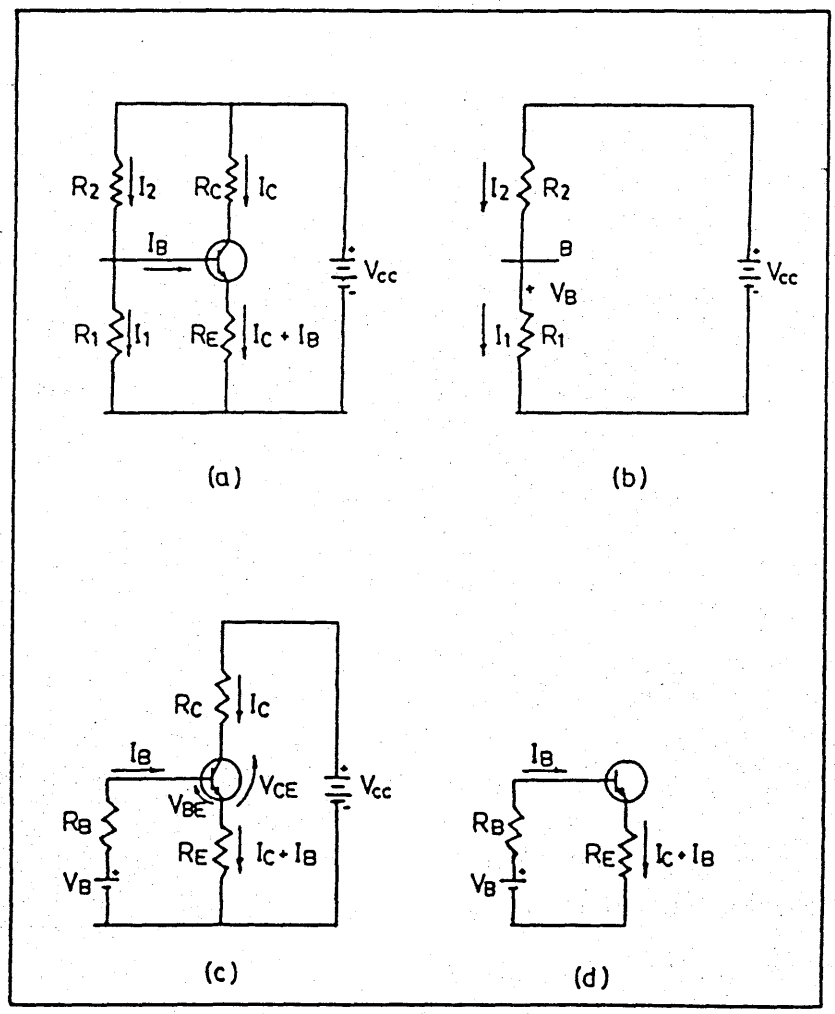

Fig. A5.8 (a) The four-resistor bias circuit; (b), (c), and (d) reduced circuits.

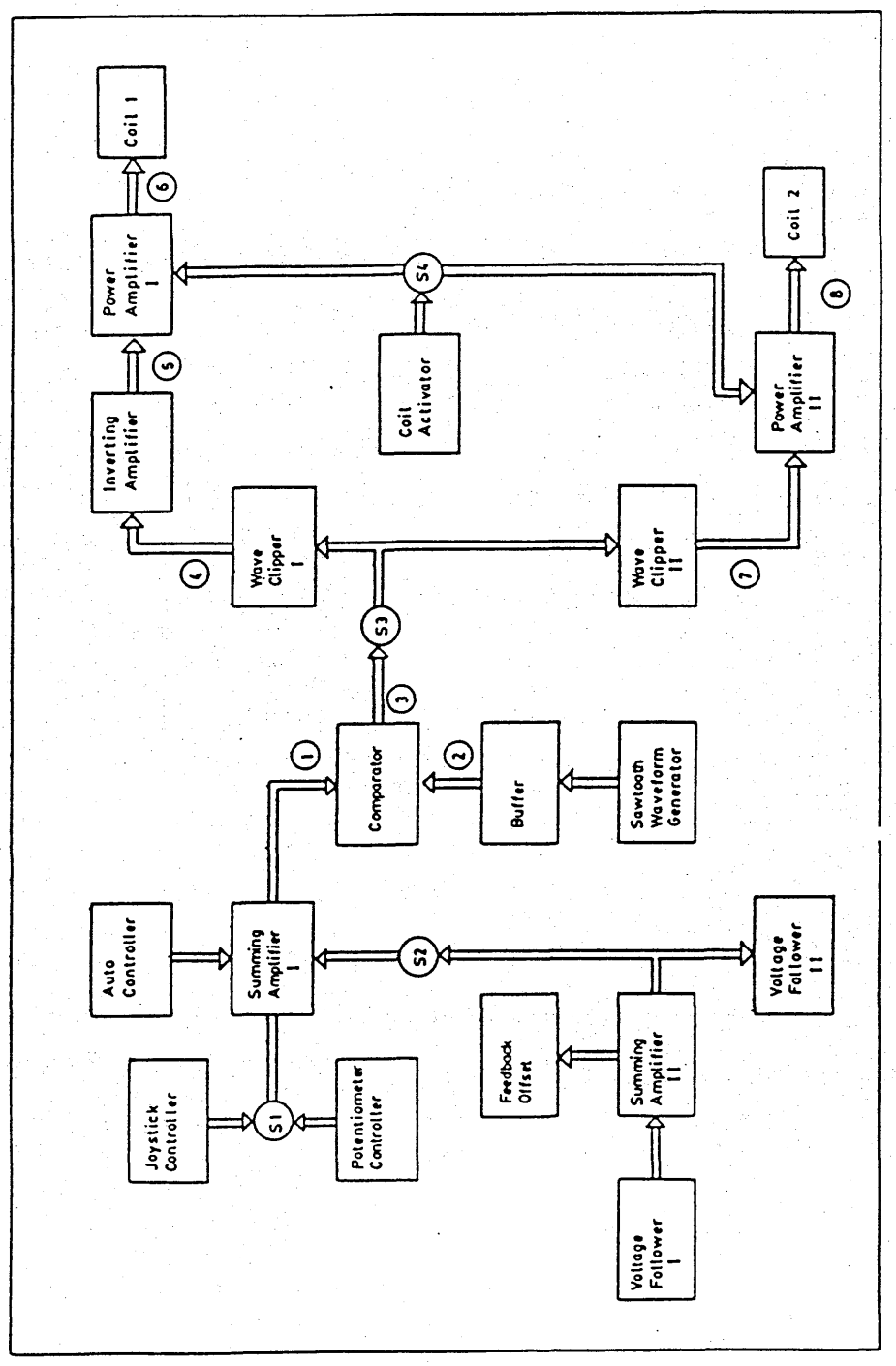

Fig. A5.9 A block diagram of the essential components of disc valve amplifier.

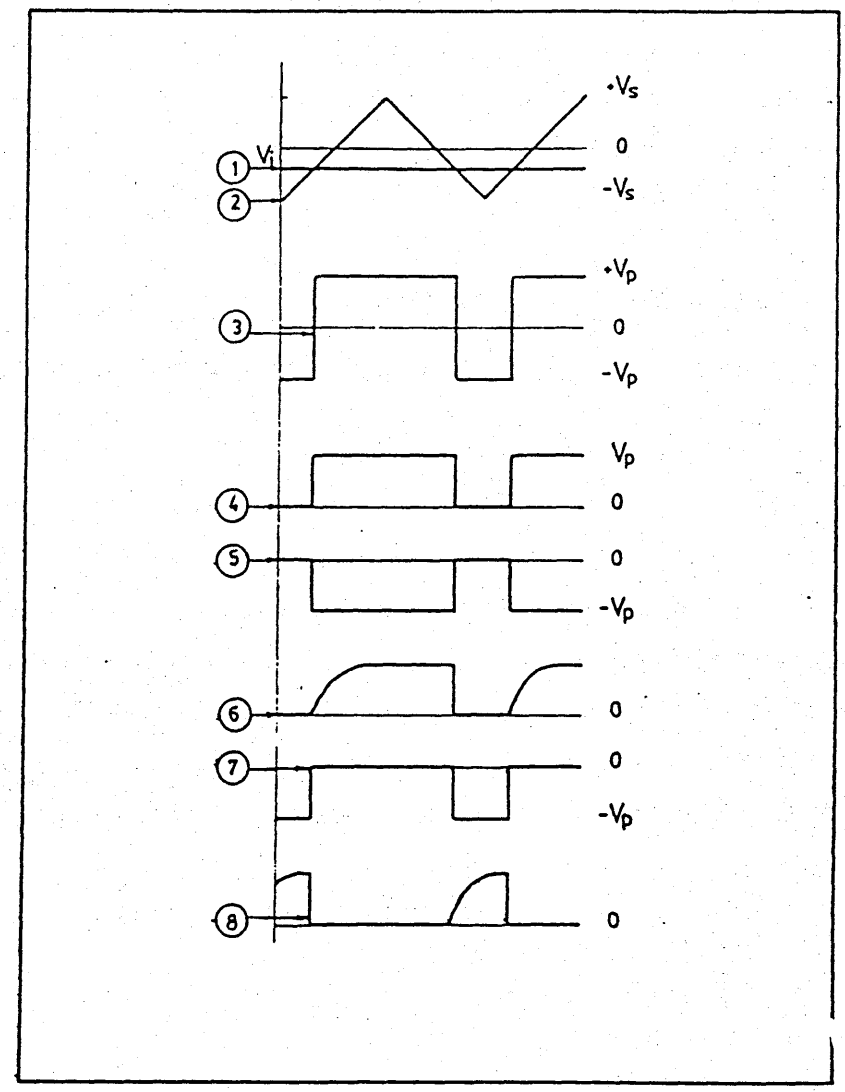

Fig. A5.10 Corresponding waveforms of various sections of disc valve amplifier.

APPENDIX A6

Digital pulse-width-modulator

A6: MICROPROCESSOR CONTROLLED DIGITAL PULSE-WIDTH-MODULATOR

A6-1 Introduction

The development of fast-acting, solenoid-actuated valves has made the direct control of hydraulic systems much more feasible, but it is still difficult to position loads accurately using these valves and conventional control techniques. The reason is that on-off controllers require sophisticated schemes to control load position to avoid overshoot, undershoot, and instability. If a microprocessor with appropriate control strategies is added to the valve control, these problems can be solved. It is for these reasons that a digital Pulse-Width-Modulator (PWM) is considered.

Pulses are short bursts of voltage, often of considerable amplitude, with intervals between pulses usually far greater than the duration of the pulse itself. Generally speaking, pulses are unidirectional in voltage and do not go alternatively positive and negative. The general shape is as shown in Fig. A6.1. An ideal pulse should be rectangular with rapid rise and fall and a flat top, indicating constant amplitude during the 'on' period. Pulses have a mark/space ratio, i.e. on/off ratio, which is often extremely small; in radar, for example, ratios of 1:1000 are common in the transmitter pulse. A Pulse-Width-Modulator changes the on-off ratio of a pulse train according to a control signal. In a digital Pulse-Width-Modulator, the control signal is a data word whose value determines the pulse width. The period of the modulated pulse train is constant and independent of pulse width.

Microprocessor control of a digital modulator is easily achieved. The microprocessor can supply a word to designate the pulse width at its output port, and the modulator can produce a train of pulses having the desired

width.

A6-2 Design approach

A digital PWM can be implemented in many different ways [73]. The one described here has the advantage of requiring a minimum number of components. Figure A6.2 shows a 12-bit PWM. In Fig. A6.2 , three LS 161 counter integrated circuits (ICS) form a free running divide-by-4096 counter whose output is constantly compared with the microprocessor output port value using the three cascade LS 85 comparators. When the counter output is less than the control word at the output port, the A>B comparator output stays high. When both inputs to the comparator are equal, the A>B output goes low, to zero, and remains low until the counter overflows. Then, A>B returns high and the process is repeated.

The period of the output waveform of a 12-bit modulator is

$$T_{out} = 4096\ T_{clk} \qquad (A6.1)$$

and the pulse width pw is

$$pw = cw\ T_{clk} \qquad (A6.2)$$

where cw is the control word value and T_{clk} is the clock period.

In general, the period of the output waveform of a n-bit modulator is

$$T_{out} = 2^n\ T_{clk} \qquad (A6.3)$$

and equation (A6.2) still hold for the pulse width.

With a zero control word, this circuit supplies a zero output level, and the device that it drives will remain fully off. However, with the maximum 2^n-1 (4095 for 12-bit) control word value, the output will not remain fully on, instead, it will drop low every 2^n-1 (4095) clock pulses and remain low for one clock period.

For n-bit modulator, the relationship between the clock frequency (f_{clk}) and the frequency (f_{out}) of the output of the PWM is

$$f_{clk} = 2^n f_{out} \quad (A6.4)$$

Therefore, for 12-bit modulator the relationship is

$$f_{clk} = 4096 f_{out} \quad (A6.5)$$

In other words, for n-bit modulator running at X Hz, the fundamental will lie around $X/2^n$ Hz. For example, with an 8-bit modulator running at 3.2768 MHz, the fundamental will lie around 12.8 KHz. For 12-bit accuracy, the fundamental drops to only 800 Hz. This show that for high accuracy and high bandwidth in a digital PWM demand a high clock frequency. In other words, the bandwidth of a digital PWM is limited.

In this design, a built-in clock was considered. This involved the use of a crystal and a dual-voltage controlled oscillator (LS 124) to generate the clock pulses. This approach gave a fixed clock frequency. To overcome this disadvantage, the output of the oscillator is fed through two counters (LS93) in cascade. The LS93 are 4-bit binary counter which means that there are now eight clock frequencies at user's disposal. The clock generating circuit is as shown in Fig. A6.3. For the 3.2768 MHz crystal used, the counter output frequency and the corresponding frequency of the PWM is as shown in Table A6.1.

Table A6.1 Counter frequency and PWM output frequency.

Counter frequency KHz	PWM frequency Hz
1638.4	400.000
819.2	200.000
409.6	100.000
204.8	50.000
102.4	25.000
51.2	12.500
25.6	6.250
12.8	3.125

The output frequencies of the LS93 counters are fed to the PWM via a rotary switch. The rotary switch is a one-pole six-way subminiature switch and

select the required clock frequency for the system. The 12.8 and 1638.4 KHz clock frequencies were not connected. Therefore, the PWM output frequencies available in this design in Hz are :- 6.25, 12.5, 25, 50, 100, and 200 in ascending order.

The description and functional block diagrams of LS85 (comparator), LS93 (counter), LS161 (counter) and LS124 (dual-voltage controlled oscillator) are given in [74,75].

A6-3 Spectral analysis

An understanding of the frequency domain characteristics of a Pulse-Width-Modulated signal is required for accurate use of a PWM. For a given pulse width, the signal spectrum can be found by performing a Fourier transformation on one period of the modulated output. Georgiou [73] pointed out that a graphical approach is faster and allow a feel for the spectral behaviour to develop. The spectrum is, of course, a line spectrum with non zero energy only at frequencies that are integer multiples of the fundamental frequency of $f_o = 1/T$, where T is the period of the output waveform (see Fig.A6.4).

The amplitude of the dc component in the spectrum [73], the average value of the time domain signal is given by:

$$v_{dc} = (pw\ v_p) / T \qquad (A6.6)$$

Substituting for pw/T from equation (A6.5) gives,

$$v_{dc} = (cw / 2^n)\ v_p \qquad (A6.7)$$

For 12-bit modulator,

$$v_{dc} = (cw / 4096)\ v_p \qquad (A6.8)$$

This equation shows that for a zero control word, the output of the PWM will remain zero. In other words, the amplitude of the amplitude of the dc component in the PWM spectrum is zero for zero control word.

For a given v_p (the amplitude of PWM), the dc component (i.e. the average value of the time domain signal) is proportional to control word (cw). On the other hand, if the PWM is used in a closed loop configuration, then the control word would be the error signal. Therefore,

$$v_{dc} = k\ ER \qquad (A6.9)$$

where k is the proportionality and ER is the error signal.

A6-4 Applications

The microprocessor controlled PWM has many uses. It can serve as a low cost digital to analogue converter (DAC) because the average or dc value of its output is proportional to the pulse width and, therefore, proportional to the value of the control word as shown in section A6-3. To operate a PWM as a DAC, it is important to filter its output of a frequency below the pulse repetition frequency. Because of its modulation method the DAC will be monotonic and will have excellent linearity.

An important advantage of PWM control is that power drivers will operate in the on-off mode with transistors fully saturated or fully off, minimising power dissipation in the driver. Another advantage of this PWM is that its fundamental frequency can be varied at will by simply changing the clock frequency via a rotary switch. The available fundamental frequencies in Hz are :- (3.125), 6.25, 12.5, 25, 50, 100, 200, and (400). Those enclosed in brackets are not available to user because they were not connected.

A6-4.1 Adaptation

The designed digital PWM is not directly compatible with switching amplifier constructed to control an electro-hydraulic Double-Disc valve. A switching amplifier requires a square wave input waveform to trigger on and off its output transistors. Hence an operational amplifier, 741, was wired

as a comparator to convert the output pulse train of a 12-bit digital PWM into a rectangular waveform. The mark/space ratio and the time domain of the rectangular waveform are the same as those of the pulse train. Figure A6.5 shows the converting circuit. The amplitude of the output can be varied via resistor R5. The block diagram of the modified digital PWM is shown in Fig. A6.6. A block diagram of a possible way of controlling the valve remotely using a microcomputer is shown in Fig. A6.7. The microprocessor receives the demand signal via a system console (VDU) and the feedback position signal from an analogue-to-digital converter (ADC). In a closed-loop application, the microprocessor performs the arithmetic subtraction through software to generate the control word (error signal) needed to trigger the digital PWM. Alternatively, for a digital feedback transducer, such as an encoder, the feedback signal is used directly without the ADC. With the aid of the microprocessor, sophisticated control strategies may be implemented, parameter changes may easily be monitored and proportional-integral-derivative (PID) controller or state-space control may also be incorporated. The microprocessor can monitor all the various stages of the control loop and as such it can also be used as a data acquisition system.

When a digital PWM is used in this manner, it is necessary to have a fundamental frequency which is significantly higher than the mechanical resonant frequency of the electro-hydraulic system so that the electro-hydraulic system acts as a mechanical low pass filter. On the other hand, if the fundamental frequency is too high, the electrical inductance of the electro-hydraulic system will filter out all the harmonics. Then, the time domain signal seen by the electro-hydraulic system will have dc characteristics.

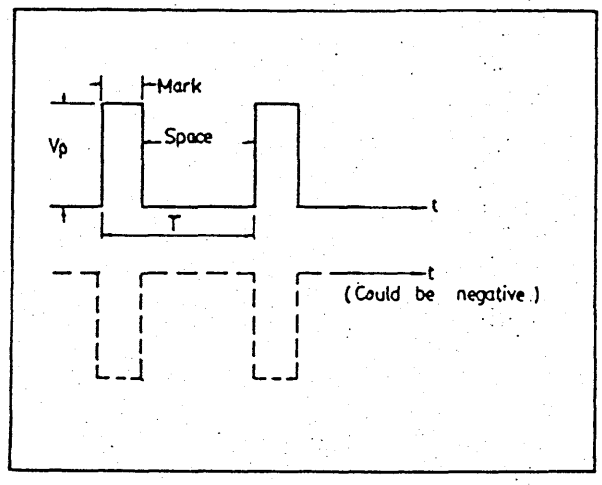

Fig. A6.1 Pulse waveform

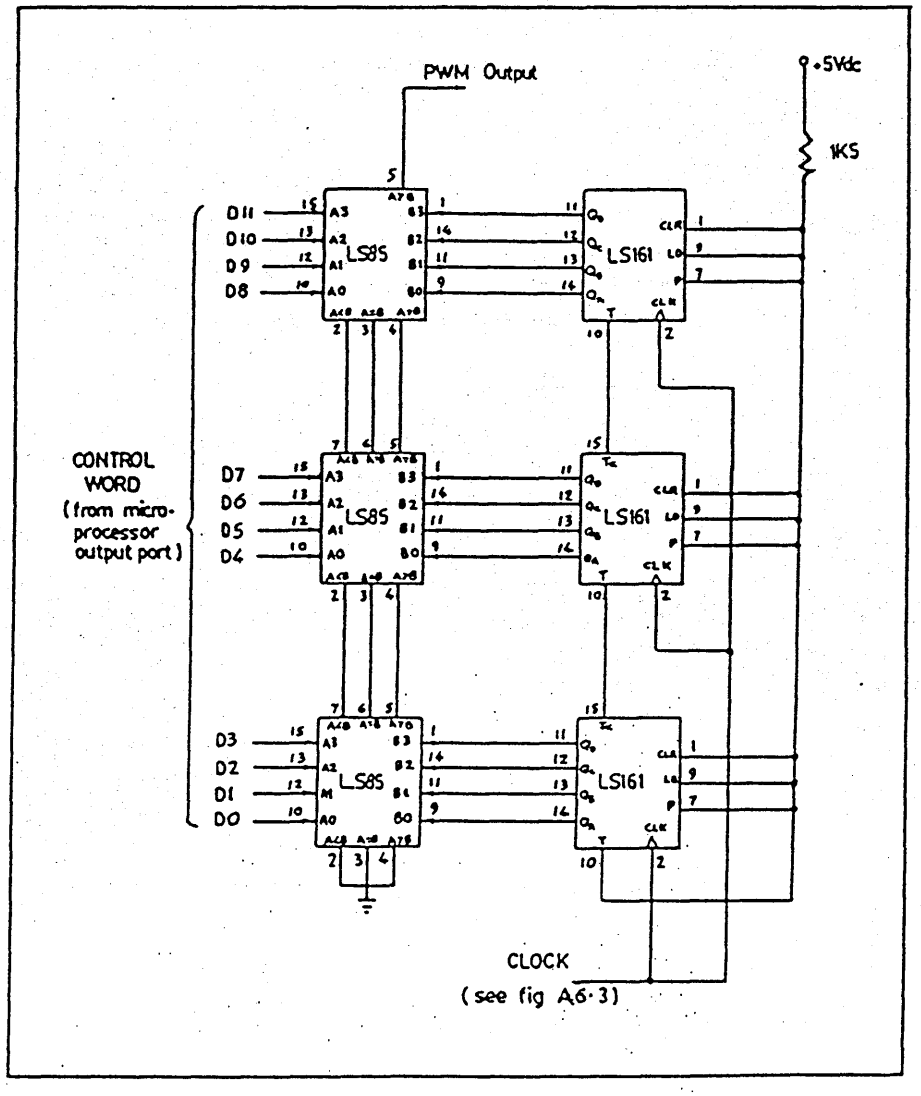

Fig. A6.2 PWM using free running counters and comparators.

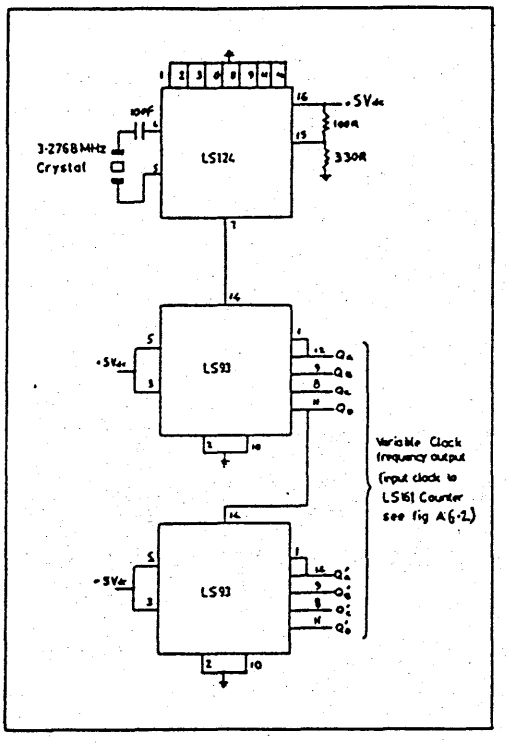

Fig. A6.3 Variable clock generating circuit using a 3.2768 MHz crystal, Dual voltage controlled oscillator (LS124), and two cascaded binary counters (LS93).

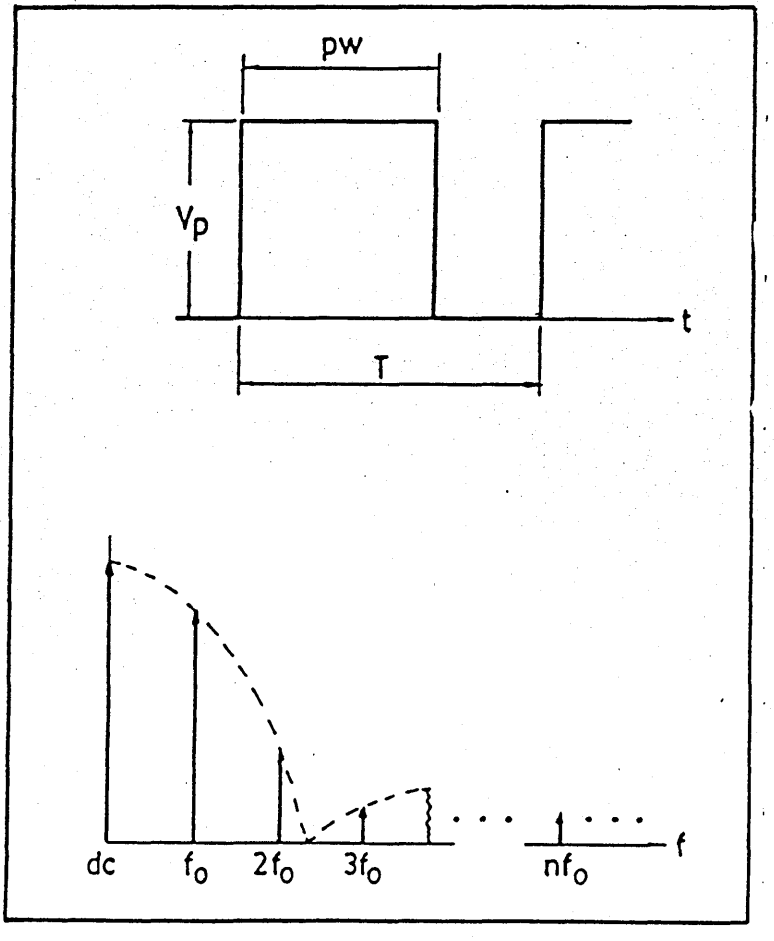

Fig. A6.4 Modulator output in time and frequency domain.

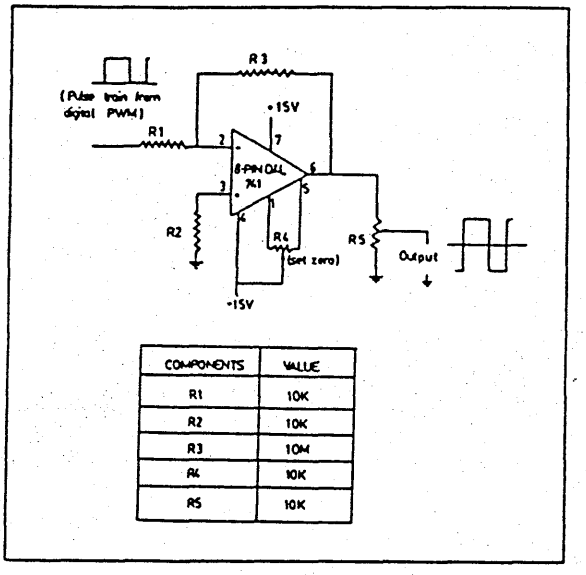

COMPONENTS	VALUE
R1	10K
R2	10K
R3	10M
R4	10K
R5	10K

Fig. A6.5 Circuit to convert output pulse train of a 12-BIT digital PWM into a rectangular waveform.

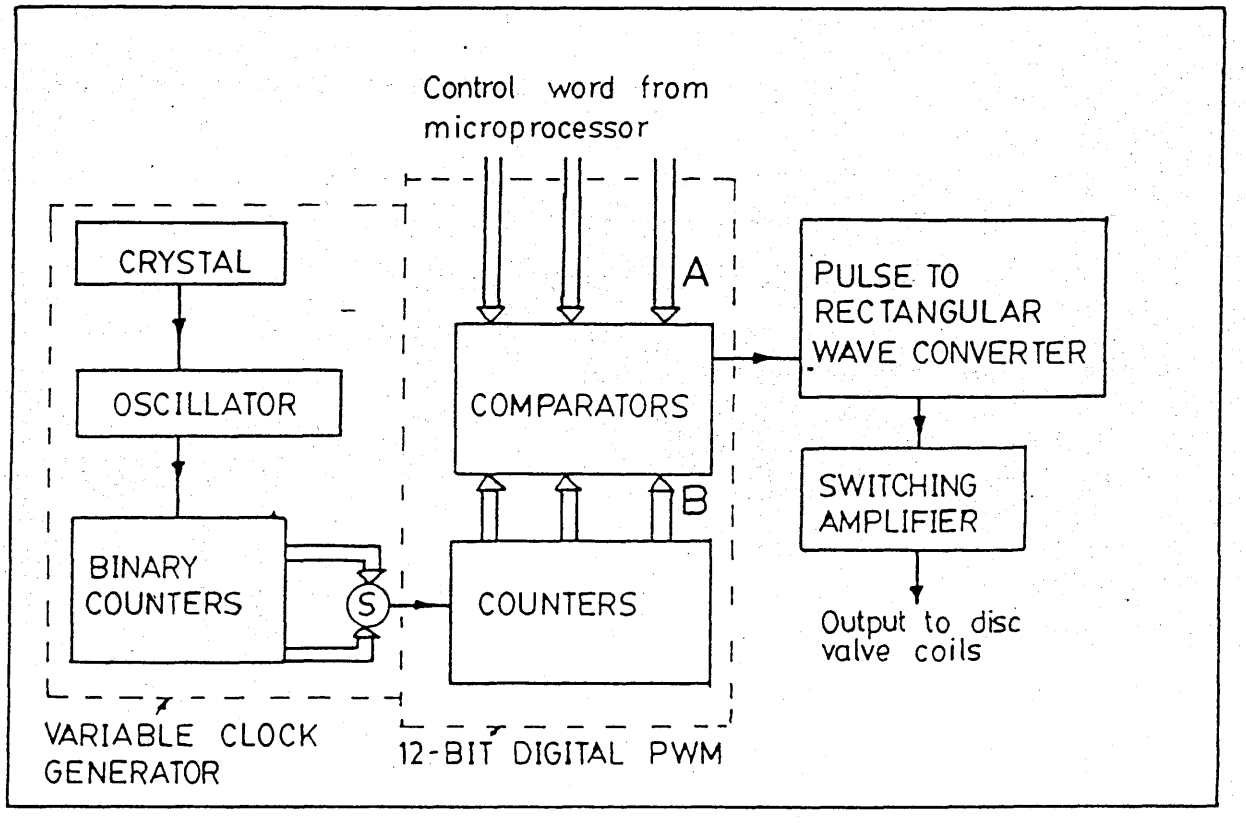

Fig. A6.6 Block diagram of a 12-BIT digital PWM adapted for use with a switching amplifier.

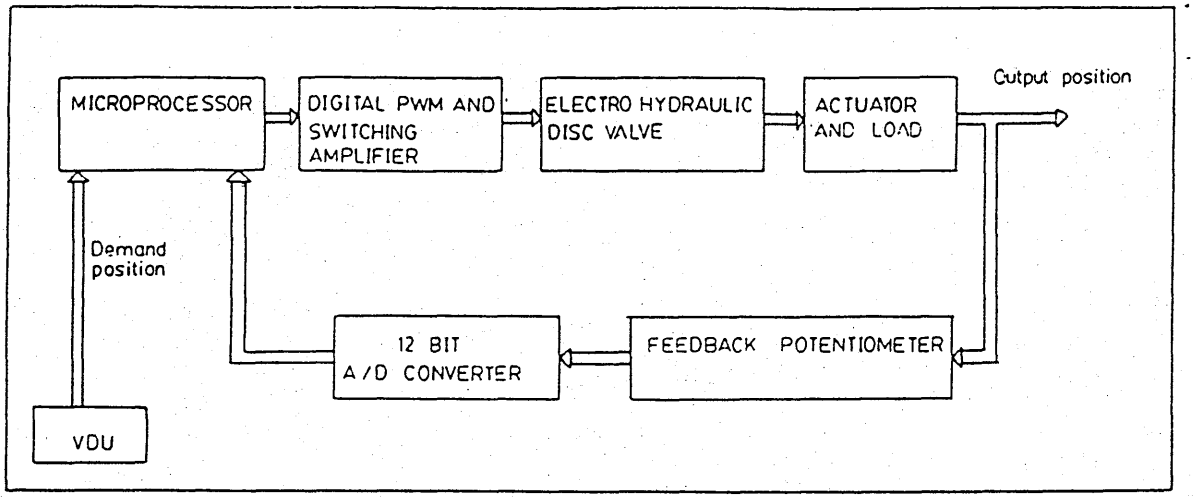

Fig. A6.7 A block diagram of a microprocessor manipulated electro-hydraulic position control system.

APPENDIX A7

Flow chart of steady-state fluid computer model

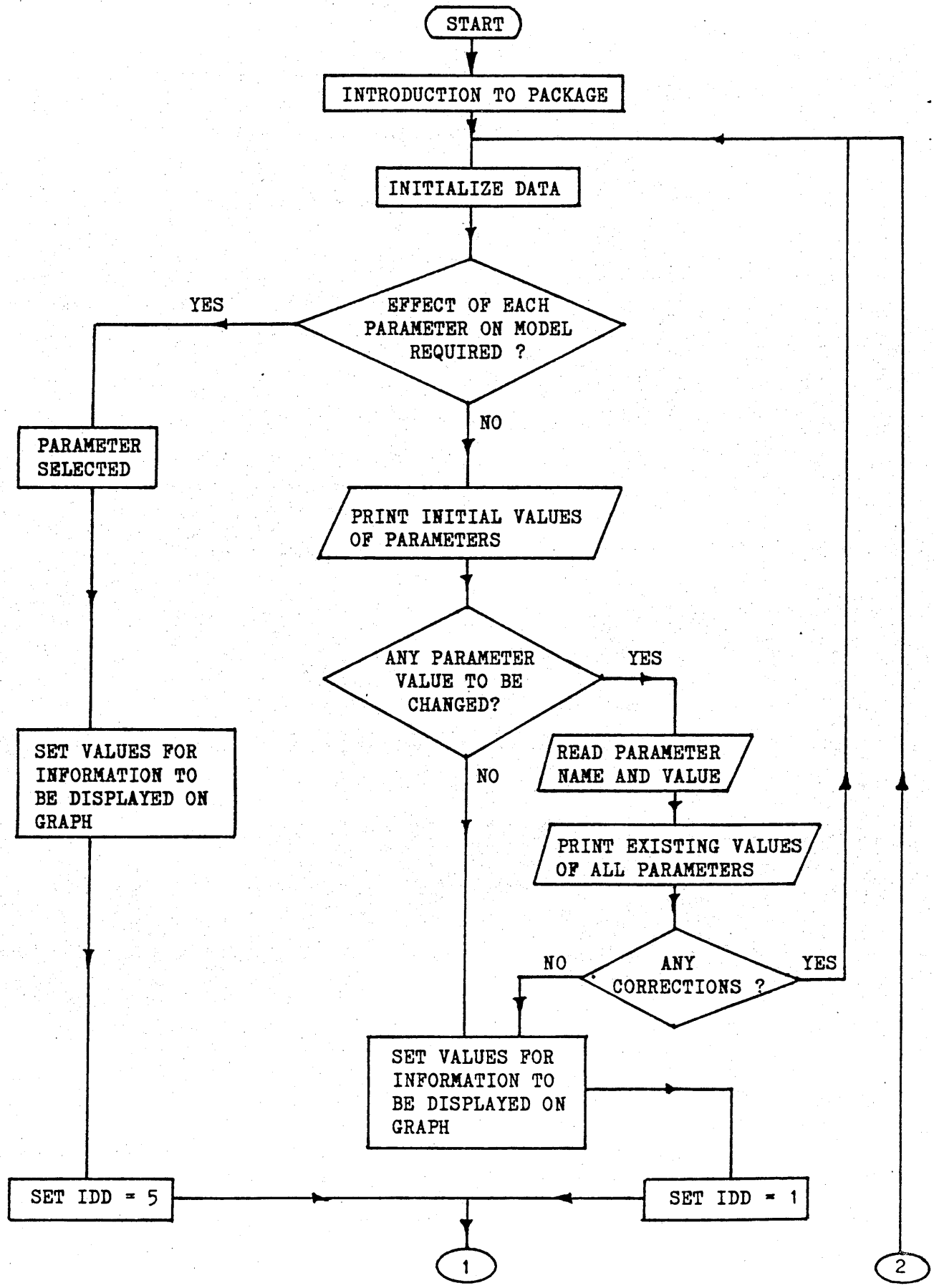
START
INTRODUCTION TO PACKAGE
INITIALIZE DATA
EFFECT OF EACH PARAMETER ON MODEL REQUIRED ?
YES
NO
PARAMETER SELECTED
PRINT INITIAL VALUES OF PARAMETERS
ANY PARAMETER VALUE TO BE CHANGED?
YES
NO
READ PARAMETER NAME AND VALUE
PRINT EXISTING VALUES OF ALL PARAMETERS
ANY CORRECTIONS ?
NO
YES
SET VALUES FOR INFORMATION TO BE DISPLAYED ON GRAPH
SET VALUES FOR INFORMATION TO BE DISPLAYED ON GRAPH
SET IDD = 5
SET IDD = 1
1
2

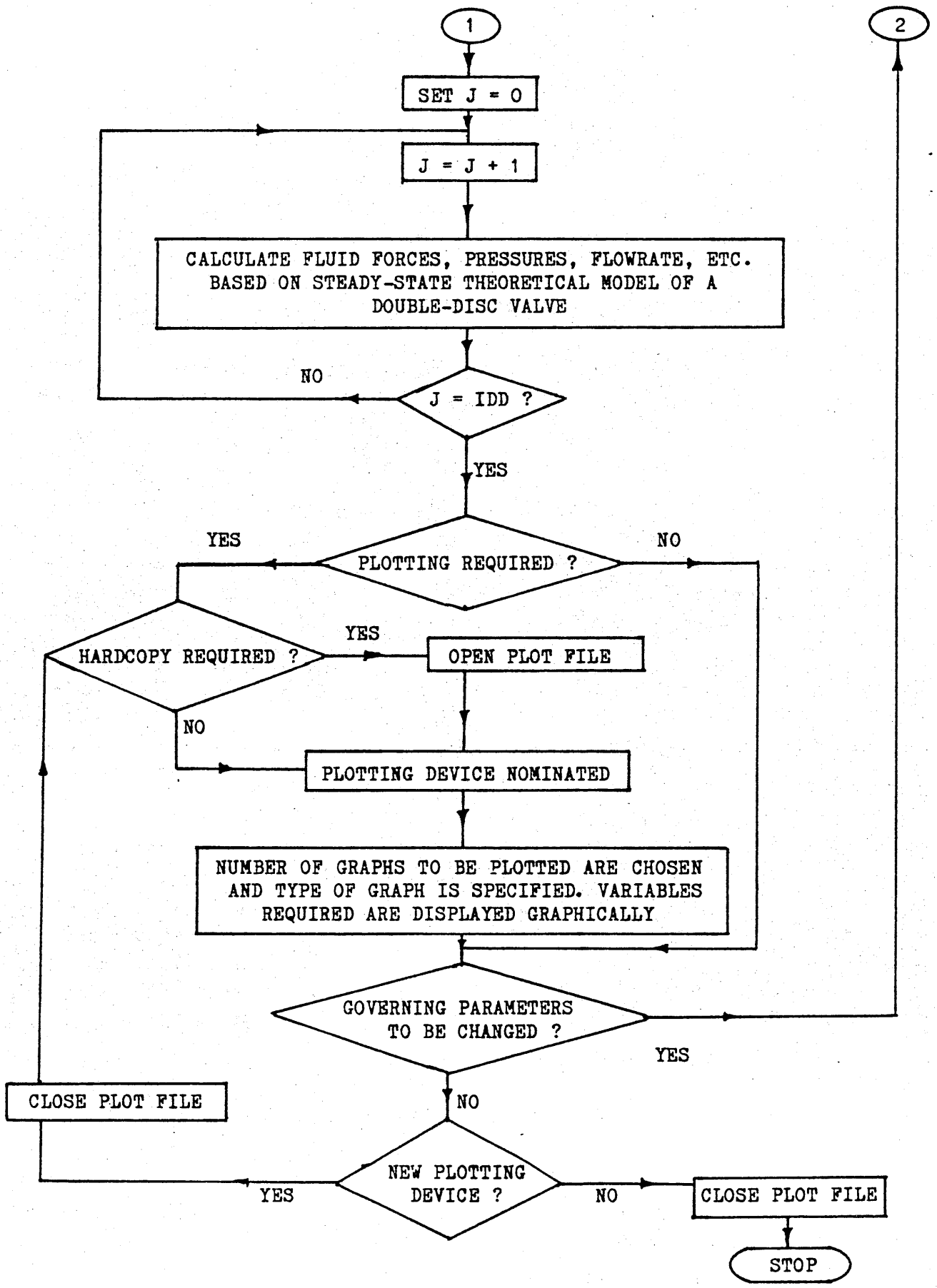
1
2
SET J = 0
J = J + 1
CALCULATE FLUID FORCES, PRESSURES, FLOWRATE, ETC. BASED ON STEADY-STATE THEORETICAL MODEL OF A DOUBLE-DISC VALVE
NO
J = IDD ?
YES
YES
PLOTTING REQUIRED ?
NO
YES
HARDCOPY REQUIRED ?
OPEN PLOT FILE
NO
PLOTTING DEVICE NOMINATED
NUMBER OF GRAPHS TO BE PLOTTED ARE CHOSEN AND TYPE OF GRAPH IS SPECIFIED. VARIABLES REQUIRED ARE DISPLAYED GRAPHICALLY
GOVERNING PARAMETERS TO BE CHANGED ?
YES
NO
CLOSE PLOT FILE
NEW PLOTTING DEVICE ?
YES
NO
CLOSE PLOT FILE
STOP

APPENDIX A8

Magnetisation curves (B-H) for REMKO magnetic iron

Hysteresis curves for soft-rolled Remko B

The tests were performed on ring specimens using the ballistic method.
The graph below shows the influence of heat treatment and decarburization on the appearance of the hysteresis curves in a closed magnetic circuit.

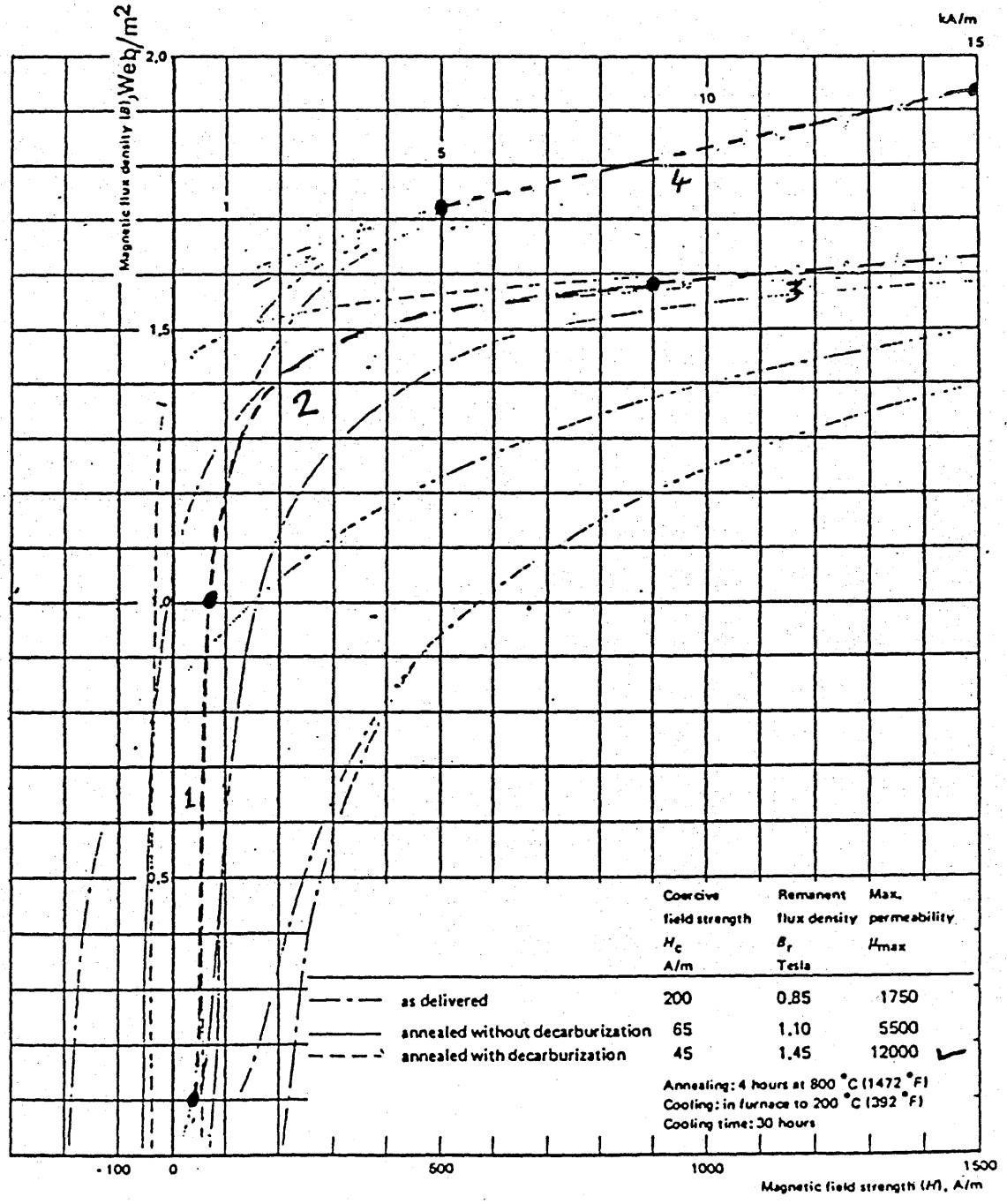

Fig. A8·1 Magnetisation curves (B–H) for REMKO magnetic iron.

APPENDIX A9

Flow chart of electro-magnetic circuit calculation

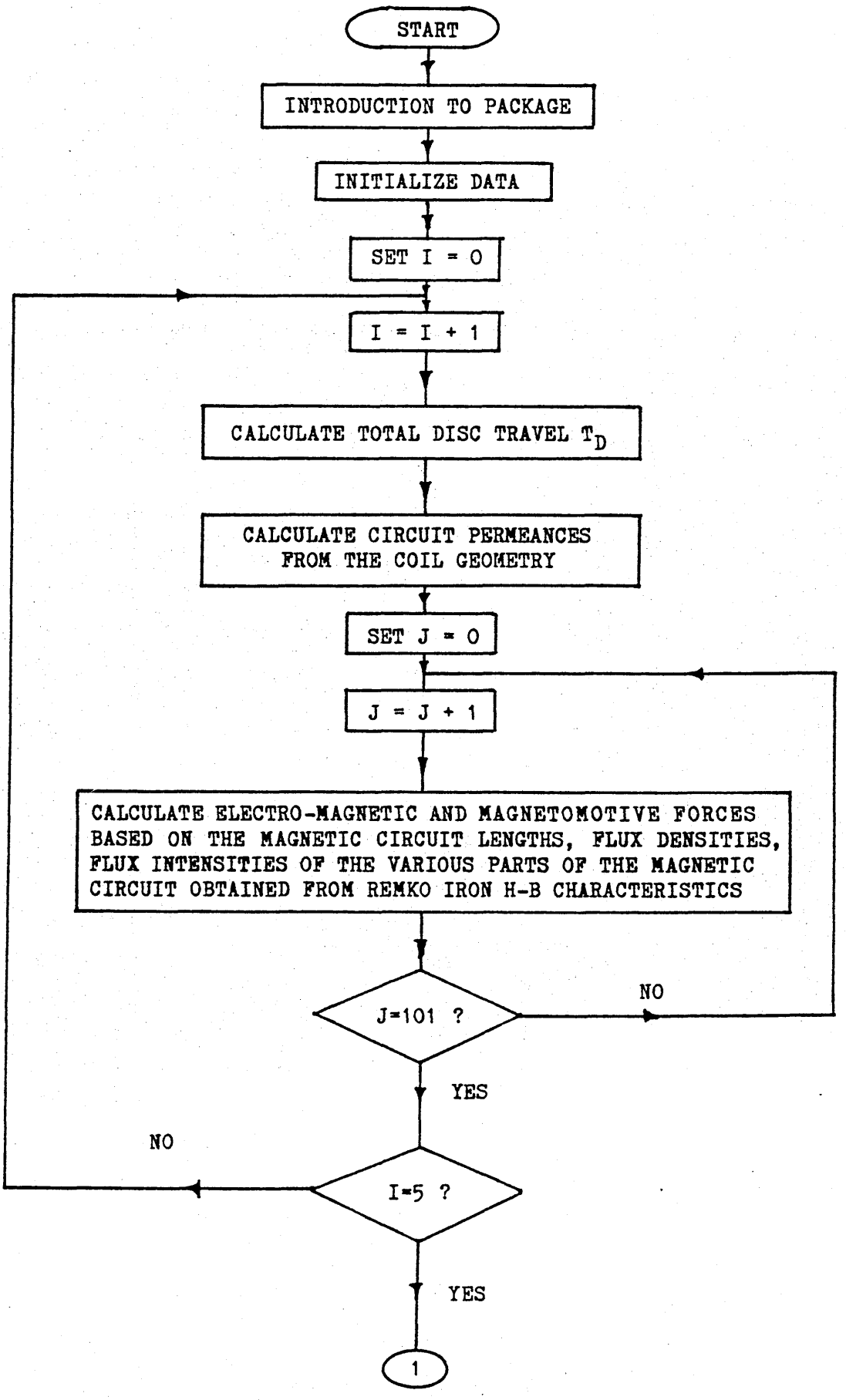
START
INTRODUCTION TO PACKAGE
INITIALIZE DATA
SET I = 0
I = I + 1
CALCULATE TOTAL DISC TRAVEL T_D
CALCULATE CIRCUIT PERMEANCES FROM THE COIL GEOMETRY
SET J = 0
J = J + 1
CALCULATE ELECTRO-MAGNETIC AND MAGNETOMOTIVE FORCES BASED ON THE MAGNETIC CIRCUIT LENGTHS, FLUX DENSITIES, FLUX INTENSITIES OF THE VARIOUS PARTS OF THE MAGNETIC CIRCUIT OBTAINED FROM REMKO IRON H-B CHARACTERISTICS
J=101 ?
NO
YES
I=5 ?
NO
YES
1

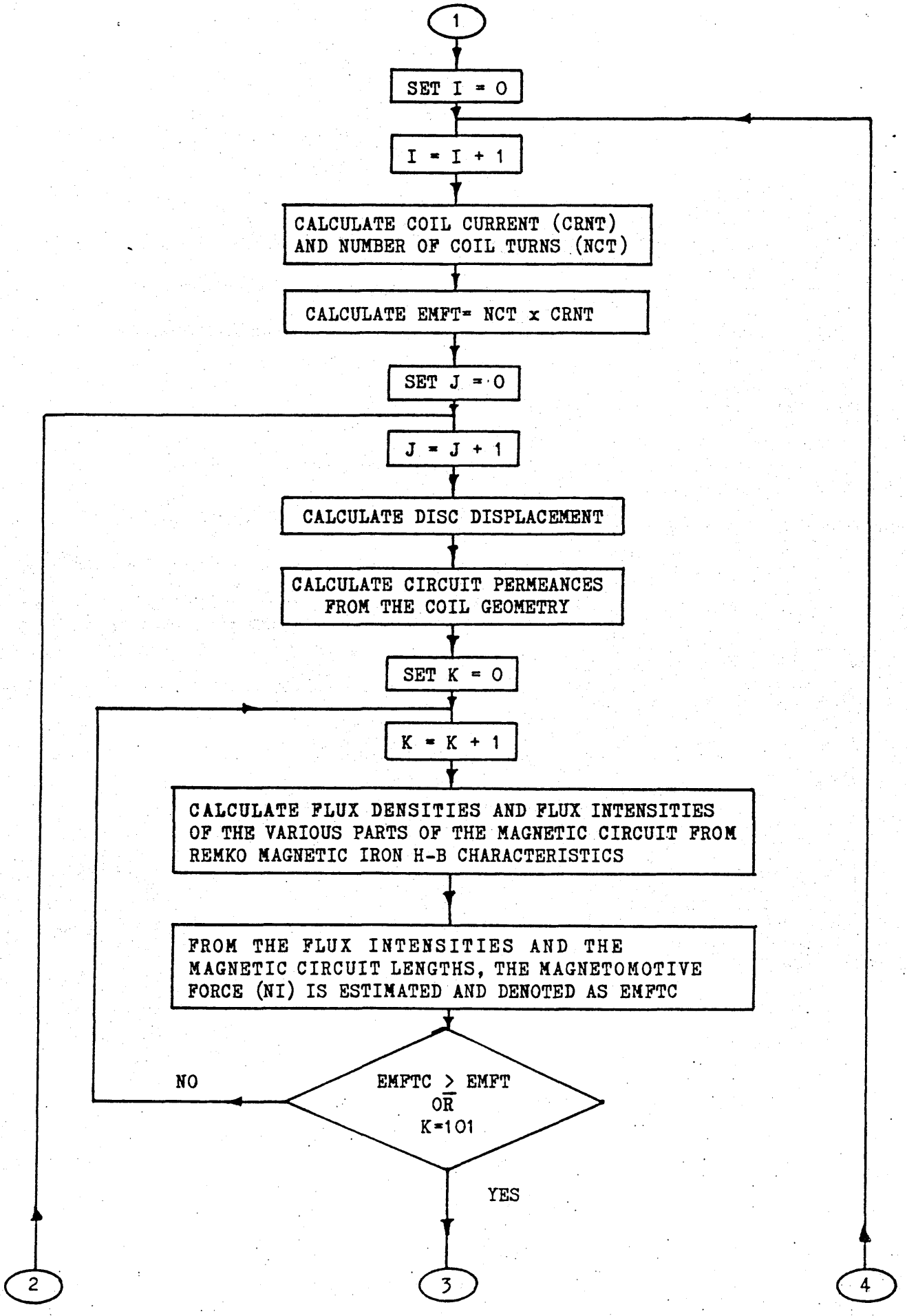
1
SET I = 0
I = I + 1
CALCULATE COIL CURRENT (CRNT) AND NUMBER OF COIL TURNS (NCT)
CALCULATE EMFT= NCT x CRNT
SET J = 0
J = J + 1
CALCULATE DISC DISPLACEMENT
CALCULATE CIRCUIT PERMEANCES FROM THE COIL GEOMETRY
SET K = 0
K = K + 1
CALCULATE FLUX DENSITIES AND FLUX INTENSITIES OF THE VARIOUS PARTS OF THE MAGNETIC CIRCUIT FROM REMKO MAGNETIC IRON H-B CHARACTERISTICS
FROM THE FLUX INTENSITIES AND THE MAGNETIC CIRCUIT LENGTHS, THE MAGNETOMOTIVE FORCE (NI) IS ESTIMATED AND DENOTED AS EMFTC
EMFTC > EMFT
OR
K=101
NO
YES
2
3
4

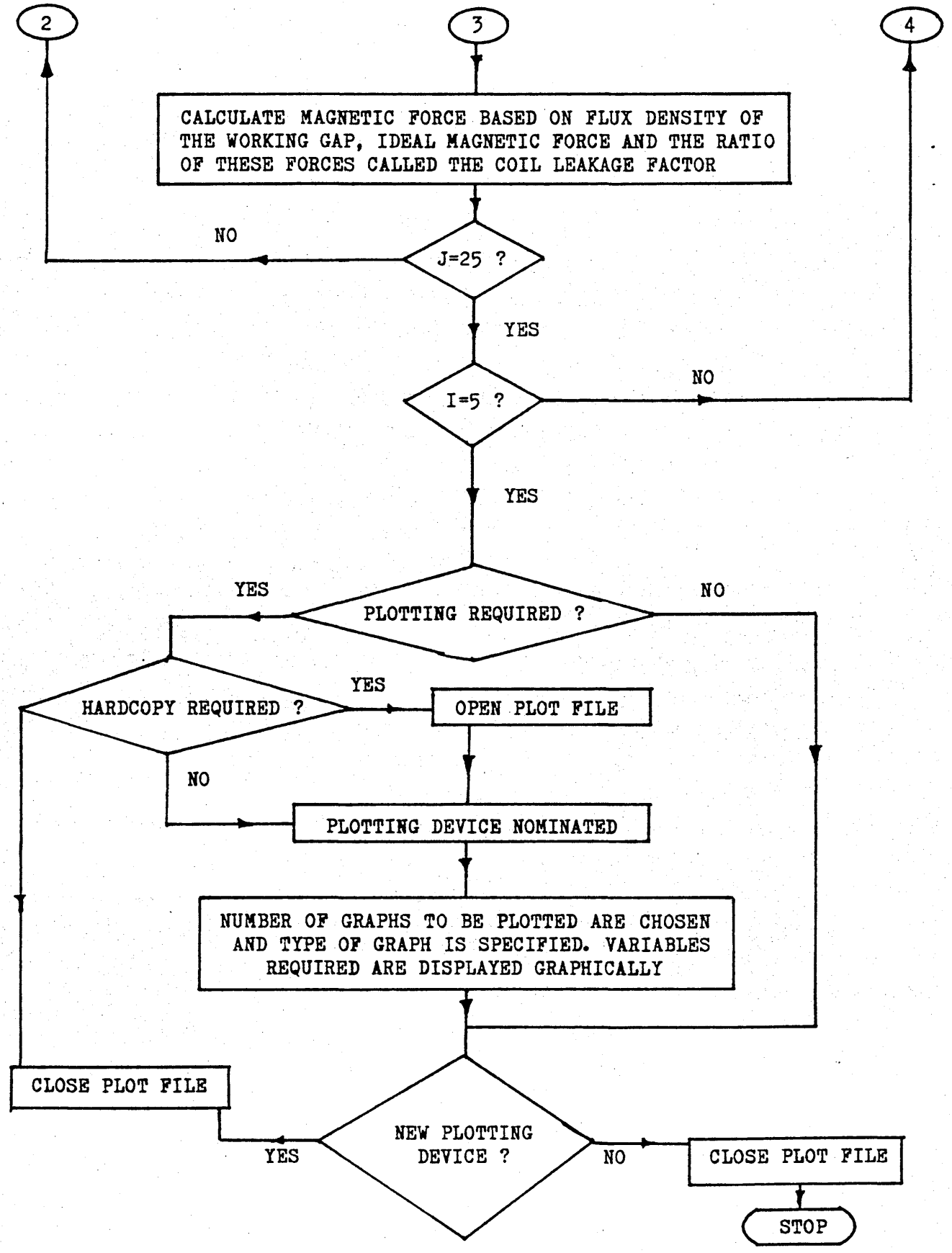
2
3
4
CALCULATE MAGNETIC FORCE BASED ON FLUX DENSITY OF THE WORKING GAP, IDEAL MAGNETIC FORCE AND THE RATIO OF THESE FORCES CALLED THE COIL LEAKAGE FACTOR
NO
J=25 ?
YES
I=5 ?
NO
YES
YES
PLOTTING REQUIRED ?
NO
HARDCOPY REQUIRED ?
YES
OPEN PLOT FILE
NO
PLOTTING DEVICE NOMINATED
NUMBER OF GRAPHS TO BE PLOTTED ARE CHOSEN AND TYPE OF GRAPH IS SPECIFIED. VARIABLES REQUIRED ARE DISPLAYED GRAPHICALLY
CLOSE PLOT FILE
NEW PLOTTING DEVICE ?
YES
NO
CLOSE PLOT FILE
STOP

APPENDIX A10

Selection of push rod diamensions

A10: SELECTION OF PUSH ROD DIMENSIONS

A10-1 Introduction

The two critical dimensions of a push rod are its length and diameter. The push rod form an annular passage for oil leaving the valve chambers to the drain. For a given drain nozzle, the radial clearance between the rod and the drain nozzle wall is dictated by the rod diameter. Clearly the rod diameter affect the drain flowrate, pressure sensitivity and valve stiffness. On the other hand, the length of the rod influence buckling action of the rod. From buckling point of view, a short rod would be better.

The rod used in the floating disc valve can be described as a pin-ended rod loaded by an axial compressive force at each end. The compressive forces are caused by the fluid forces acting on the valve discs. It is assumed that the line of action of the forces passes through the centroid of the cross-section of the rod. It is hoped that the critical load acting on the push rod to start buckling would be derived.

A10-2 Critical load

The critical load is defined to be that axial force which is enough to hold the bar in a slightly deformed configuration. Under the action of the load P the rod has the deflected shape shown in Figure A10.1

The bending moment at point A having coordinates (x,y) is given by

$$EI \frac{d^2y}{dx^2} = - Py \qquad (A10.1)$$

If we set

$$\frac{P}{EI} = K^2 \qquad (A10.2)$$

equation (A10.1) becomes

$$EI \frac{d^2y}{dx^2} + K^2y = 0 \qquad \text{(A10.3)}$$

The solution of equation (A10.3) is given by

$$y = C \sin Kx + D \cos Kx \qquad \text{(A10.4)}$$

A10-3 Boundary conditions

At the left end of the rod, y = 0 when x = 0. Substituting these values in (A10.4) we obtain

$D = 0$

At the right end of the rod, y = 0 when x = L. Substituting these values in (A10.4) with D = 0 we obtain

$0 = C \sin KL$

This implies that either C = 0 or sin KL = 0. But if C = 0 then y is everywhere zero and we have only trivial case of a straight rod which is the configuration before the occurrence of buckling. Since we are not interested in the solution, then we must take

$$\sin KL = 0 \qquad \text{(A10.5)}$$

For this to be true, we must have

$$KL = n\pi \text{ radians } (n = 1,2,3,\ldots) \qquad \text{(A10.6)}$$

Using equation (A10.2) in (A10.6) gives

$$P = n^2 \pi^2 EI / L^2 \qquad \text{(A10.7)}$$

The smallest value of this load P occurs when n = 1. Then we have the so-called first mode of buckling where the critical load is given by

$$P_{cr} = \pi^2 EI / L^2 \qquad \text{(A10.8)}$$

For a circular rod, the second moment of area I is given by

$$I = \pi D_R^4 / 64 \qquad \text{(A10.9)}$$

Substitute (A10.9) in (A10.8) to get

$$P_{cr} = \pi^3 E D_R^4 / 64L^2 \qquad \text{(A10.10)}$$

where E is the Young modulus of rod material. The rod is made of steel and therefore E = 200 GNm^{-2}. With this value equation (A10.10) becomes

$$P_{cr} = 9.68946 \times 10^{10} D_R^4 / L^2 \qquad (A10.11)$$

The critical buckling load as obtained from equation (A10.10) or (A10.11) gives an idea of the maximum supply pressure that a given disc valve size can withstand without any failure.

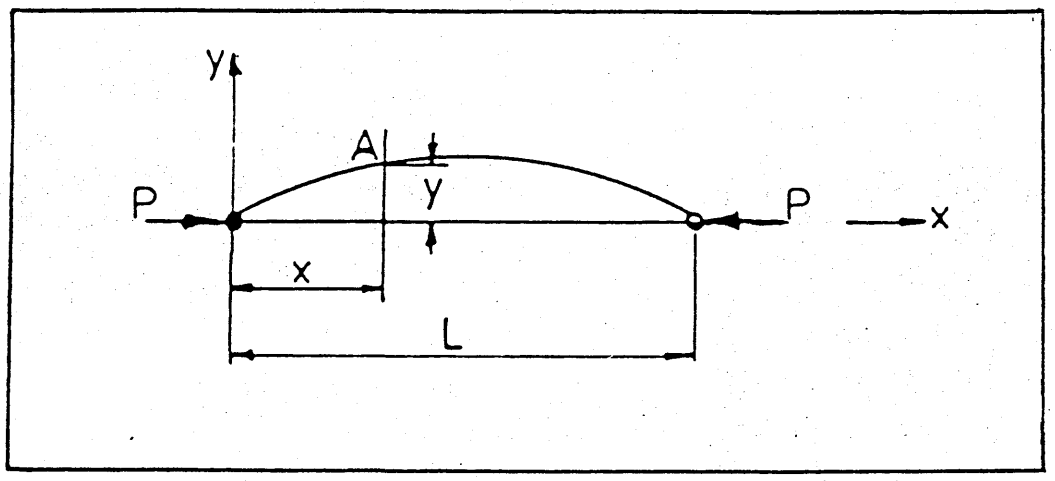

Fig. A10.1 Deflected shape of a push rod subjected to axial load P.

APPENDIX A11

Viscosity - temperature charts of Shell Tellus R oils

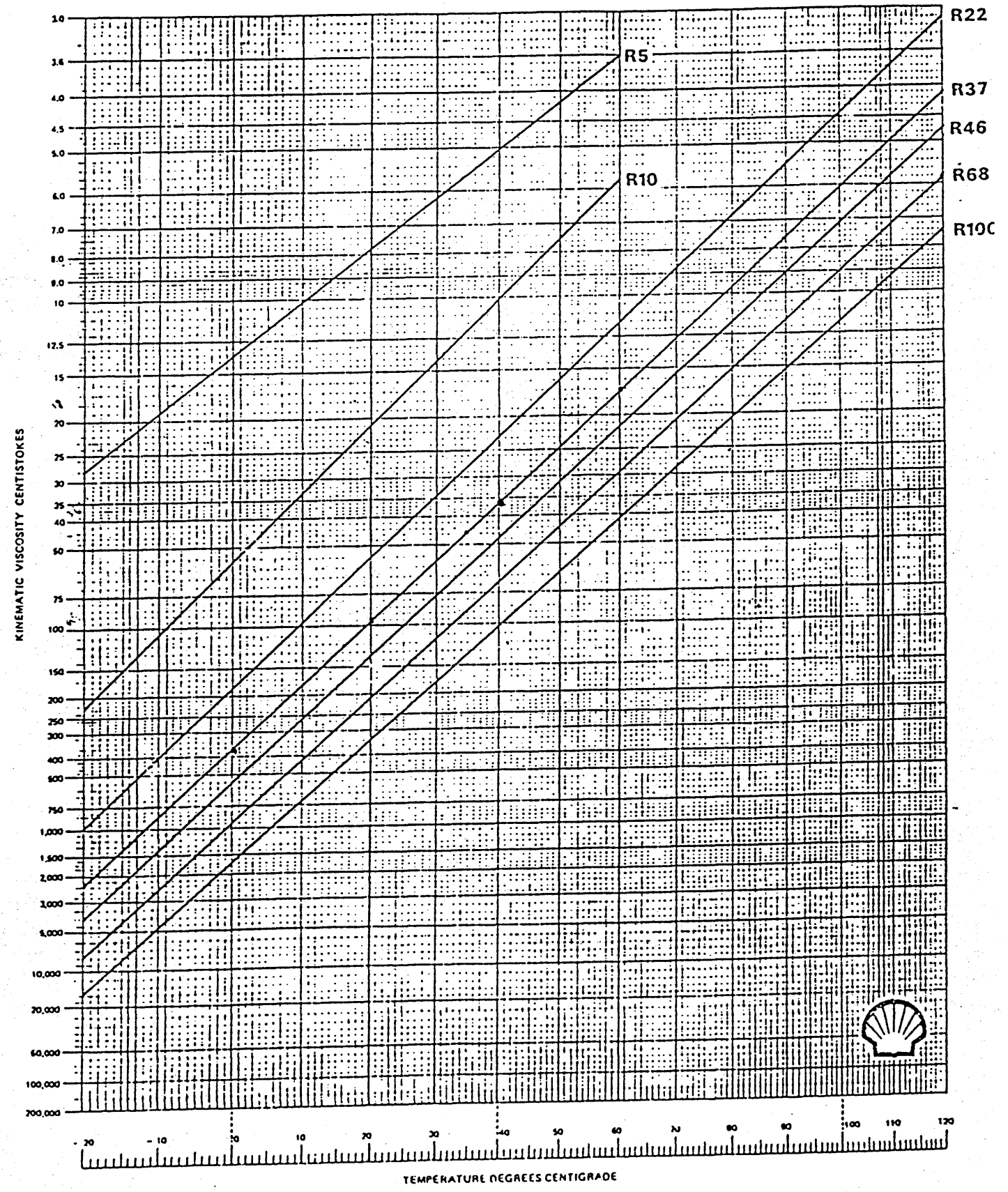

Fig. A11.1 Typical viscosity-temperature characteristics of Shell Tellus oils R.

APPENDIX A12

Transfer function of a servo-valve

A12: TRANSFER FUNCTION OF A SERVOVALVE

The transfer function of a servovalve is well treated in Chapter 7 of a Hydraulic Control System text book by Merritt [66]. For completeness the results are quoted in this appendix in order to define the symbols used. The transfer function of a servovalve alone is given by [66]

$$\frac{\Delta x_v}{\Delta v} = \frac{r K_o w_o^2}{(1 + s/w_r)\,[s^2 + (2 \zeta_o w_o)\, s + w_o^2]} \qquad \text{(A12.1)}$$

where

$K_o = \dfrac{2 K_t \mu}{(R_c + r_p)K_{at}(1 - K_m/K_a)}$ = static gain constant, rad/volts

r = radius arm of torque motor, in

$K_{at} = K_a + 0.43\, r^2\, W\, (P_s - P_{Lo})$ = total spring constant, in-lb/rad

$w_o = \sqrt{K_{at}/(J_a + r^2 M_v)}$ = total motor natural frequency, rad/sec

M_v = mass of spool, lb-sec^2/in

$w_r = (R_c + r_p)/2L_c$ = armature circuit break frequency for each coil.

$\zeta_o = K_m/2K_a$ = damping ratio

K_a = mechanical torsion spring constant of armature pivot, in-lb/rad.

J_a = inertia of armature and any attached load, in-ib-sec^2.

$K_m = (4.42\text{x}10^{-8})8(a/g)^2\, R_g\, \phi_g^2$ = magnetic spring constant of torque motor, in-lb/rad

$K_t = (4.42\text{x}10^{-8})4(a/g)\, N_c\, \phi_g$ = torque constant of the torque motor (i.e., for each coil), in-lb/amp.

a = radius of armature from pivot to centre of pole face, in.

$R_g = g/\mu_o A_g$ = reluctance of each air gap at neutral, amp-turns/in.

g = length of each air gap at neutral, in.

$\mu_o = 3.19$ = permeability of free space (air) used with English units.

A_g = pole face area at the air gaps, in^2.

$\phi_g = M_o/2R_g$ = flux in each of the four air gaps when the armature is at neutral.

R_c = resistance of each coil, ohms.

N_c = number of turns in each coil.

r_p = internal resistance (plate resistance) of amplifier in each coil circuit, ohm.

M_o = total mmf of all permanent magnets, amp-turns.

$L_c = (10^{-8})\ N_c^2/R_g$ = self-inductance of each coil, henrys.

APPENDIX A13

Description of a high pressure hydraulic rig

A13: Description of a high pressure hydraulic rig

The general layout of a high pressure rig used to supply hydraulic oil at constant pressure to a test bench is shown in Figure A13.1. In the Figure, the hydraulic oil (Shell Tellus R37) falls under gravity from a tank (1) to a boost pump (2). The boost pump is driven by a constant speed motor (M1) to supply oil to a main pump (5) at 7.7 bar. The oil from the boost pump flows through a 10-micron filter (3) and a pre-set pressure regulator (4) into a main pump (5) which is a swash plate. The main pump is driven by electric motor (M2). The filter (3) cleans the oil to prevent any damage to the relevant equipment. The relief valve (6) (adjustable spring type) controls the pressure to the main pump. At present this relief valve is set to 7.7 bar which gives about 126.0 bar main line pressure. If the boost pump pressure is increased, the line pressure will increase correspondingly. The boost pump pressure is registered by pressure gauge (7). The main pump is a variable swash plate axial piston type. The angle of the swash plate depends on the delivery. There would be no delivery when the swash plate is in vertical position (i.e. no demand).

The flow output from the main pump unit is controlled by a two-way manual lever-operated directional valve (10) and a pressure regulator/relief valve (11). The means of actuating the two pump units are situated on the main control panel. On the front of the test bench are the associated pressure gauges and relief valves to supply four channels. To increase the supply pressure, the pressure regulator knob is turned clockwise. The oil from the pressure regulator (11) then flows through another 10-micron filter into the test rig or test bench (14).

An accumulator (13) is fitted just upstream of the test rig. The pressurised accumulator (precharged to 2/3 of required working pressure with nitrogen), which has the same effect as a smoothing capacitor in a

d.c. supply, improves the pressure fluctuations and transient flow demands. The supply pressure is indicated by pressure gauge (12). The line pressure is indicated by (9) and oil temperature by gauge (8). The return flow, from the test rig, passes through a filter and oil cooler (16) into the tank (1). The return pressure is indicated by pressure gauge (15). The 10-micron oil filter in the main return line from the test rig prevent dirt from the test rig contaminating the main oil reservoir. Heating of the oil owing to pressure losses in the system can be severe problem, hence the oil cooler (16) maintain the oil temperature in the system at a given level.

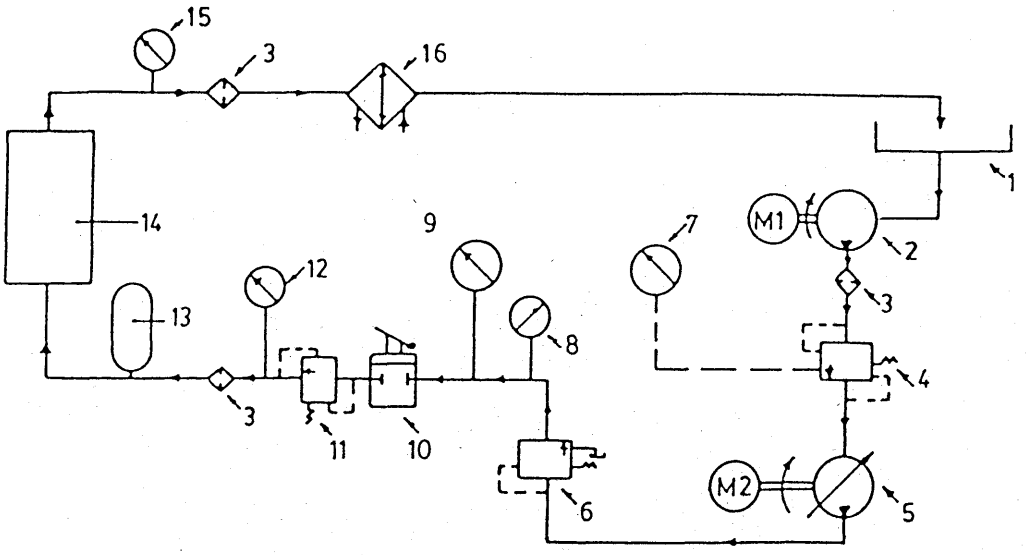

FIG. A13-1 HYDRAULIC CIRCUIT OF A HIGH PRESSURE HYDRAULIC RIG

KEY TO FIG. A13.1

(1) Tank - 60 gallon capacity.

(2) Boost pump (gear type)(LUCAS LTD.) Type GP.20111 motorised by a 5 hp at 1440 rpm foot & flange drip-proof type Newman electric motor - arranged for 400/440V 3-phase 50 cps.

(3) Filters (FAIREYS AVIATION LTD.) 10-micron cut-off type.

(4) Relief valve/Pressure regulator - preset to 110psi.

(5) Main pump (LUCAS LTD.) Type PM.500/(DB2)/MS/D4/M1 variable capacity pump unit with manual control- max. output 12 GPM at 3,000psi but limited to 10 GPM. Motorised by a 25 hp at 1440 rpm foot & flange, drip-proof electric motor - arranged for 400/440V 3 phase 50cps.

(6) Relief valve

(7) Boost pressure gauge (BOURDEN LTD.)

(8) Oil temperature gauge (BOURDEN LTD.)

(9) Main line pressure gauge (BOURDEN LTD.)

(10) Directional valve - lever control type (DENNISON LTD.)

(11) Relief valve/ pressure regulator

(12) Supply pressure gauge (BOURDEN LTD.)

(13) Accumulator (FAWCETT ENGINEERING LTD.)

(14) Test rig

(15) Return pressure gauge (BOURDEN LTD.)

(16) Oil coolant (SHELL LTD.)